

# **Remote sensing and bio-geo-optical properties of turbid, productive inland waters: a case study of Lake Balaton**

**Caitlin Anne Lyman Riddick**

UNIVERSITY of   
STIRLING

**Submitted to:**

**Biological and Environmental Sciences  
University of Stirling**

**May 2016**

**For the degree of Doctor of Philosophy**

**Supervisors:**

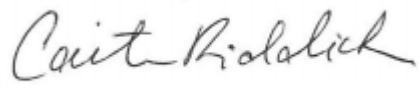
**Prof. Andrew N. Tyler  
Dr. Peter D. Hunter**



## **Statement of Originality**

I hereby confirm that this is an original piece of work conducted independently by the undersigned, and all work contained herein has not been submitted for any other degree. All research material has been duly acknowledged and cited.

Signature of Candidate:

A handwritten signature in cursive script that reads "Caitlin Riddick".

Caitlin Anne Lyman Riddick

Date: 24 May 2016

## Abstract

Algal blooms plague freshwaters across the globe, as increased nutrient loads lead to eutrophication of inland waters and the presence of potentially harmful cyanobacteria. In this context, remote sensing is a valuable approach to monitor water quality over broad temporal and spatial scales. However, there remain several challenges to the accurate retrieval of water quality parameters, and the research in this thesis investigates these in an optically complex lake (Lake Balaton, Hungary).

This study found that bulk and specific inherent optical properties [(S)IOPs] showed significant spatial variability over the trophic gradient in Lake Balaton. The relationships between (S)IOPs and biogeochemical parameters differed from those reported in ocean and coastal waters due to the high proportion of particulate inorganic matter (PIM). Furthermore, wind-driven resuspension of mineral sediments attributed a high proportion of total attenuation to particulate scattering and increased the mean refractive index ( $\bar{n}_p$ ) of the particle assemblage. Phytoplankton pigment concentrations [chlorophyll-*a* (Chl-*a*) and phycocyanin (PC)] were also accurately retrieved from a times series of satellite data over Lake Balaton using semi-analytical algorithms. Coincident (S)IOP data allowed for investigation of the errors within these algorithms, indicating overestimation of phytoplankton absorption [ $a_{ph}(665)$ ] and underestimation of the Chl-*a* specific absorption coefficient [ $a^*_{ph}(665)$ ]. Finally, Chl-*a* concentrations were accurately retrieved in a multiscale remote sensing study using the Normalized Difference Chlorophyll Index (NDCI), indicating hyperspectral data is not necessary to retrieve accurate pigment concentrations but does capture the subtle heterogeneity of phytoplankton spatial distribution.

The results of this thesis provide a positive outlook for the future of inland water remote sensing, particularly in light of contemporary satellite instruments with continued or improved radiometric, spectral, spatial and temporal coverage. Furthermore, the value of coincident (S)IOP data is highlighted and contributes towards the improvement of remote sensing pigment retrieval in optically complex waters.

## Acknowledgements

Without the combination of intellectual, technical, financial and familial support, this PhD would most certainly not have been possible. First and foremost, I would like to thank my supervisors at the University of Stirling, Prof. Andrew Tyler and Dr. Peter Hunter, for their endless guidance, patience and support throughout this PhD. Their efforts to accommodate me and my family throughout the last several years have ultimately made this PhD possible, and I am incredibly grateful for their commitment to my study.

I would also like to acknowledge the Centre for Ecology and Hydrology (CEH) for a desk to work at in Edinburgh and PhD training and support, particularly the phytoplankton knowledge provided by my CEH supervisor Dr. Laurence Carvalho. Thanks to Dr. Linda May, Dr. Bernie Dudley and Dr. Brian Spears for additional guidance and advice on lab and field work logistics.

Funding for this PhD was provided for by the University of Stirling Research Apprenticeship scheme and departmental funding from Biological and Environmental Sciences. The Lake Balaton field campaign was made possible by an equipment grant from the National Environmental Research Council (NERC) Field Spectroscopy Facility (FSF) and a grant from the NERC Airborne Research and Survey Facility (ARSF) (EU10-03). Specifically, the *in situ* optics equipment (AC-S, DH4 and ECO-BB3 (WET Labs Inc.), and the CTD (Sea-Bird Electronics) used for this work were provided by NERC Field Spectroscopy Facility (EU10-03). Funding for contributions from the Balaton Limnological Institute (BLI) were provided in part by the TÁMOP-4.2.2.A-11/1/KONV-2012-0038 project for evaluation and processing of field data. Travel to Lake Balaton and shipping funds were partially provided by the Carnegie Trust. Additional funding is acknowledged from the University of Stirling Article Processing Charge fund and Dr. Betsey Fuller for an award covering the substantial page fees to publish Chapter 3 in the *Journal of Geophysical Research – Oceans*.

I am grateful for field assistance on Lake Balaton provided by Eszter Zsigmond and Géza Dobos and lab assistance from Terézia Horváth and Erika Kozma (BLI). Valuable advice was appreciated from Attila Kovács, Hajnalka Horváth (BLI) and Tom Preston (Scottish Universities Environmental Research Centre). Additionally, wind speed data were measured by automatic stations established by predecessor in the title of Lake Balaton Development Coordination Agency and operated by the Central-

Transdanubian Water Directorate. In particular, I would like to acknowledge the late Mátyás Présing, who was a warm and welcoming host in Tihany, imparted much knowledge on Lake Balaton and was a valued colleague and friend.

From the University of Stirling, cell size data from Clare Neil is gratefully acknowledged, and valuable advice from Evangelos Spyrakos was provided on technical remote sensing queries. Other university staff were invaluable to this PhD, including Jon McArthur for GIS and ENVI technical support, Scott Jackson for IT solutions for my ancient MacBook, Bill Jamieson for production of the Balaton map for publication of Chapter 3, and Lynn, Rose and the Biological and Environmental Sciences office staff for their administrative support. Thank you especially to Rebecca Barclay for the printing and submission of this thesis.

Many thanks to Jose Antonio Dominguez-Gomez (Czech University of Life Sciences Prague) for providing SCAPE-M\_B2 corrected MERIS data for Chapter 5 and useful manuscript comments for the related manuscript submission to *Remote Sensing of Environment*.

The Plymouth Marine Laboratory (PML) is gratefully acknowledged for lab space and use of the dual beam spectrophotometer. Particular thanks go to Victor Martinez-Vicente for his guidance in all things related to IOPs, his infinite patience in the field and the lab, and the comments provided towards Chapters 3, 4 and 5. Also, thanks to Andrey Kurekin at PML for providing ATCOR-4 corrected AISA Eagle data for Chapter 6 and associated advice on working with this dataset.

I am grateful also for the additional field assistance provided by Stuart Bradley, Fiona Thompson, Shona McMillan and Stuart Riddick on Lochs Leven and Lomond, although this work is unfortunately not included in this thesis.

I cannot forget to thank my parents, Robert and Susan Lyman, who have provided incredible positivity and support throughout my PhD. They also gratefully offered Nona and Grandad's daycare, which allowed me invaluable time to work. My sister Sara also contributed master babysitting skills that were much appreciated. My parents in-law, John and Linda Riddick, are also gratefully acknowledged for their support and childcare in Scotland. Thank you as well to my grandparents, whose beach houses provided excellent writing havens.

Last but certainly not least, I would like to thank my wonderful husband Stuart, and our little ones Maxwell and Isabelle. It has been a long road, and I am so grateful to have such a patient and loving family to have shared this journey with.

# Table of Contents

Statement of Originality.....	3
Abstract.....	4
Acknowledgements.....	5
Table of Contents.....	7
List of Figures.....	12
List of Tables.....	19
List of Acronyms and Abbreviations.....	21
1 Introduction.....	24
1.1 Research context.....	24
1.1.1 Thesis aims and structure.....	27
1.1.2 Study site.....	28
2 Remote sensing of inland water quality.....	31
2.1 Phytoplankton and eutrophication.....	31
2.2 Importance of monitoring water quality.....	32
2.3 Remote sensing of inland waters.....	32
2.3.1 History of remote sensing application to lakes.....	33
2.3.2 Types of platform and sensors.....	34
2.4 Principles of light in water.....	36
2.4.1 Optically Active Constituents.....	37
2.4.2 Inherent and Apparent Optical Properties.....	38
2.5 Remote sensing algorithm types for extraction of in-water constituents.....	41
2.5.1 Empirical, semi-empirical and semi-analytical algorithms.....	42
2.5.2 Other algorithm approaches.....	43
2.5.3 Inversion of bio-optical models (analytical algorithms).....	43
2.6 Remote sensing of phytoplankton pigments.....	44
2.6.1 Phytoplankton pigments and optical discrimination.....	45
2.6.2 Remote sensing of chlorophyll- <i>a</i> .....	46
2.6.3 Remote sensing of phycocyanin.....	49
2.7 Considerations for the remote sensing of inland waters.....	50
2.7.1 Satellite mission capability.....	51
2.7.2 Geography of inland waters.....	51
2.7.3 Algorithms.....	52
2.7.4 <i>In situ</i> data.....	52
2.7.5 Atmospheric correction.....	52
2.7.6 Operational.....	53

2.8	Previous remote sensing studies of Lake Balaton .....	54
2.9	Summary and research priorities .....	56
2.9.1	Thesis in context .....	57
3	Spatial variability of absorption coefficients over a biogeochemical gradient in a large and optically complex shallow lake .....	59
3.1	Introduction .....	59
3.2	Methods .....	63
3.2.1	Study site .....	63
3.2.2	Water sampling .....	64
3.2.3	<i>In situ</i> optical measurements .....	66
3.2.4	Chlorophyll- <i>a</i> .....	67
3.2.5	Phycocyanin .....	67
3.2.6	Biomass and phytoplankton counts .....	67
3.2.7	Total suspended matter .....	68
3.2.8	Coloured dissolved organic matter absorption .....	68
3.2.9	Laboratory measurement of particulate absorption .....	68
3.3	Results .....	69
3.3.1	Comparison of <i>in situ</i> and laboratory measured absorption .....	69
3.3.2	Variability in optically active constituents .....	72
3.3.3	Variability in the inherent optical properties .....	80
3.4	Discussion .....	101
3.4.1	Contributions to the absorption budget .....	101
3.4.2	Variability in the IOPs .....	102
3.4.3	Relationships between $a_{ph}(\lambda)$ , Chl- <i>a</i> and phytoplankton biomass .....	103
3.4.4	Chl- <i>a</i> specific absorption .....	104
3.4.5	Phytoplankton and CDOM absorption in the UV .....	106
3.4.6	SIOPs and distance from the Zala River .....	106
3.4.7	$a_{NAP}(\lambda)$ and suspended matter .....	107
3.4.8	Effect of wind-driven resuspension .....	108
3.5	Conclusions .....	109
4	Scattering and backscattering of suspended matter in an optically complex, shallow lake .....	111
4.1	Introduction .....	111
4.2	Methods .....	115
4.2.1	Study area .....	115
4.2.2	Water sampling .....	118
4.2.3	<i>In situ</i> optical measurements .....	118

4.2.4	Chlorophyll- <i>a</i> .....	118
4.2.5	Phycocyanin.....	118
4.2.6	Biomass and phytoplankton counts .....	119
4.2.7	Total suspended matter and inorganic/organic fractions .....	119
4.2.8	Absorption by coloured dissolved organic matter .....	119
4.2.9	Particulate attenuation and scattering coefficients.....	120
4.2.10	Particulate backscattering coefficients.....	120
4.2.11	Bulk refractive index and particle size discrimination slope .....	122
4.3	Results .....	123
4.3.1	Nature of suspended particles across the basins .....	123
4.3.2	Relative contributions of absorption and scattering to total attenuation	126
4.3.3	Variability in scattering, backscattering and attenuation coefficients ....	127
4.3.4	Relationships between scattering coefficients and biogeochemical parameters.....	132
4.3.5	Backscattering ratio, bulk refractive index and particle size distribution	139
4.4	Discussion .....	140
4.4.1	Contributions to particulate attenuation.....	140
4.4.2	Variability in the scattering and backscattering properties, and relationships with optically active particles.....	141
4.4.3	Backscattering ratio, bulk refractive index and particle size distribution	142
4.5	Conclusions .....	146
5	Evaluation of algorithms for retrieval of cyanobacterial pigments in highly turbid, optically complex waters using MERIS data.....	147
5.1	Introduction .....	147
5.1.1	Satellite remote sensing of cyanobacteria blooms .....	148
5.1.2	MERIS phycocyanin algorithms.....	150
5.2	Methods.....	152
5.2.1	Study site.....	152
5.2.2	Routine monitoring programmes .....	155
5.2.3	MERIS validation campaign.....	156
5.2.4	MERIS data processing .....	159
5.3	Results .....	161
5.3.1	Pigment and cell counts .....	161
5.3.2	Validation of atmospheric correction .....	162
5.3.3	Algorithm performance.....	166
5.3.4	Chlorophyll- <i>a</i> retrieval .....	170

5.3.5	Phycocyanin retrieval.....	174
5.3.6	IOP retrievals .....	179
5.3.7	Time series analysis .....	181
5.4	Discussion .....	188
5.4.1	Algorithm performance for pigment retrievals at 1 day matchups .....	188
5.4.2	Ability to retrieve biomass using Simis05 and Gons05.....	189
5.4.3	Temporal windows for satellite validation .....	190
5.4.4	Impact of dataset used and sampling methods.....	191
5.4.5	Sources of error in the retrieval of (S)IOPs .....	191
5.4.6	Applicability of algorithms .....	194
5.5	Conclusions .....	195
6	Multiscale remote sensing observations of water quality in a large, turbid shallow lake 197	
6.1	Introduction .....	197
6.2	Methods.....	201
6.2.1	Study area – Lake Balaton .....	201
6.2.2	Water sampling .....	204
6.2.3	Chlorophyll- <i>a</i> pigment analysis.....	204
6.2.4	Phytoplankton biomass, total suspended matter and coloured dissolved organic matter .....	204
6.2.5	HyperSAS radiometry.....	204
6.2.6	Remote sensing datasets .....	205
6.2.7	Validation of atmospheric correction routines.....	209
6.2.8	The Normalized Difference Chlorophyll Index (NDCI) .....	209
6.2.9	Method for resampling resolution of Landsat 5 TM and AISA Eagle datasets 210	
6.3	Results .....	211
6.3.1	Summary of biogeochemical parameters and biomass .....	211
6.3.2	Validation of atmospheric corrections .....	212
6.3.3	Algorithm performance.....	219
6.3.4	Degradation of AISA Eagle and Landsat 5 TM datasets.....	222
6.4	Discussion .....	231
6.4.1	Atmospheric corrections .....	231
6.4.2	Chlorophyll- <i>a</i> retrieval with NDCI.....	232
6.4.3	Resampling of Landsat 5 TM and AISA Eagle datasets.....	232
6.5	Conclusions .....	235
7	Discussion, conclusions and future research .....	237
7.1	Contributions of this research .....	237

7.2	Summary of conclusions .....	239
7.3	The future of remote sensing for monitoring freshwater phytoplankton .....	244
8	Appendix – Supplementary Methods .....	251
8.1	August 2010 field campaign on Lake Balaton .....	251
8.1.1	Details of the campaign .....	251
8.1.2	Instrument specifications .....	251
8.2	Algorithms examined in Chapters 5 and 6 .....	254
8.2.1	Gons05 (Chlorophyll- <i>a</i> ) .....	254
8.2.2	Simis05 (Phycocyanin) .....	254
8.2.3	Mishra13 (Phycocyanin) .....	255
8.2.4	Li15 (Chlorophyll- <i>a</i> ) .....	257
8.2.5	Normalized Difference Chlorophyll Index, NDCI (Chlorophyll- <i>a</i> ) .....	259
8.3	Definitions of error metrics .....	260
9	References .....	261

## List of Figures

<b>Figure 1.1</b> Outline of the thesis structure. ....	28
<b>Figure 1.2</b> (a) Map of Lake Balaton and Kis-Balaton in western Hungary and (b) bathymetric map of Lake Balaton taken from Gallinaro et al. (2013). ....	29
<b>Figure 2.1</b> Particulate attenuation [ $c_p(660)$ ] as a function of Chl- <i>a</i> concentration in ocean waters (Loisel & Morel, 1998). ....	38
<b>Figure 2.2</b> Hyperspectral reflectance signatures of six phytoplankton genera examined in laboratory mesocosm experiments with broadly equivalent Chl- <i>a</i> concentrations. Reproduced from (Hunter et al., 2008b). ....	46
<b>Figure 2.3</b> Chl- <i>a</i> (top) and TSM (bottom) distribution maps for Lake Balaton in June 1988 as retrieved from simulated Landsat-MSS data. Reproduced from Gitelson et al. (1993b). ....	55
<b>Figure 3.1</b> Map of Lake Balaton and Kis-Balaton indicating the location of the basins and 38 sampling stations. ....	65
<b>Figure 3.2</b> Comparison of total non-water absorption [ $a(\lambda)=a_{ph}(\lambda)+a_{NAP}(\lambda)+a_{CDOM}(\lambda)$ ] from <i>in situ</i> (AC-S or AC-9) or laboratory methods at (a) 440, (b) 555 and (c) 676 nm. Axes are on logarithmic scale and dashed line represents the 1:1 line. ....	71
<b>Figure 3.3</b> Annual variation in chlorophyll- <i>a</i> (Chl- <i>a</i> ) concentrations (a-d) and total suspended matter (TSM) concentrations (e-h) for 2010 in Lake Balaton Basins 1-4. Solid dots are mean daily values measured during the August 2010 campaign, with error bars indicating standard deviation. Annual data provided by the routine monitoring at a single station in each basin by the Balaton Limnological Institute. ....	73
<b>Figure 3.4</b> Barplots of (a) the ratio of particulate inorganic matter (PIM:TSM) and particulate organic matter (POM:TSM), (b) chlorophyll- <i>a</i> (Chl- <i>a</i> ) and phycocyanin (PC) concentrations and (c) phytoplankton community composition (% total biomass) at all stations in order from west to east. ....	77
<b>Figure 3.5</b> Plots of (a) chlorophyll- <i>a</i> ( $\log[\text{Chl-}a \text{ (mg m}^{-3}\text{)}]$ ) and (b) phycocyanin ( $\log[\text{PC (mg m}^{-3}\text{)}]$ ) as a function of distance from the Zala River during the Lake Balaton sampling campaign. ....	78
<b>Figure 3.6</b> (a) Total suspended matter (TSM) as a function of chlorophyll- <i>a</i> (Chl- <i>a</i> ) and CDOM absorption at 440 nm [ $a_{CDOM}(440)$ ] as a function of (b) Chl- <i>a</i> and (c) TSM. Equations represent significant linear regressions on $\log(\text{data})$ . ....	79

- Figure 3.7** Plots of (a)  $\log(a_{ph}(440) [m^{-1}])$ , (b)  $\log(a_{NAP}(440) [m^{-1}])$  and (c)  $\log(a_{CDOM}(440) [m^{-1}])$  as a function of distance from the Zala River during the Lake Balaton sampling campaign. ....81
- Figure 3.8** Ternary plot indicating absorption by phytoplankton ( $a_{ph}$ ), non-algal particles ( $a_{NAP}$ ) and coloured dissolved organic matter ( $a_{CDOM}$ ) at (a) 440nm, (b) 555nm, (c) 620nm and (d) 675nm. Unique symbols indicate the basin and the sampling date 26 August is highlighted in red. Particulate absorption coefficients were measured in the laboratory by a dual beam spectrophotometer, and CDOM absorption was measured by spectrophotometry. ....83
- Figure 3.9** Spectra of absorption by colour dissolved organic matter [ $a_{CDOM}(\lambda)$ ] for all stations in Kis-Balaton and Lake Balaton by basin. Note the different y-axis scale for Kis-Balaton. ....84
- Figure 3.10** Plot of the slope of CDOM absorption coefficient ( $S_{CDOM}$ ) as a function of CDOM absorption at 440 nm [ $a_{CDOM}(440)$ ]. ....85
- Figure 3.11** Scatterplots of the phytoplankton absorption coefficient ( $a_{ph}$ ) at (a) 440 nm as a function of chlorophyll-*a* (Chl-*a*), (b) 675 nm as a function of Chl-*a*, (c) 620 nm as a function of phycocyanin (PC) and (d) 620 nm as a function of the summed pigments, PC + Chl-*a*. Chl-*a* results are by spectrophotometry and PC results are a selected average of the results by spectrophotometry. Absorption coefficients were measured in the lab by spectrophotometry. Note axes are on logarithmic scale. Solid line is a regression curve by least squares fit, and the dashed line in (a) is the fit from ocean waters in Bricaud et al. (1995). ....86
- Figure 3.12** Regression of (a) total biomass, (b) cyanobacterial biomass and (c) cyanobacteria and cryptophyte biomass against the absorption coefficient of phytoplankton ( $a_{ph}$ ) at (a) 675 nm and (b and c) 620 nm, respectively. Absorption coefficients were measured in the laboratory by a dual beam spectrophotometer. Solid lines represent regression curves by least squares fit. ....88
- Figure 3.13** Spectra of mass-specific absorption by phytoplankton [ $a^*_{ph}(\lambda)$ ] for all stations in Kis-Balaton and Lake Balaton by basin. ....90
- Figure 3.14** Variability of (a)  $a^*_{ph}(440)$  and (b)  $a^*_{ph}(675)$  over concentrations of chlorophyll-*a* (Chl-*a*) and (c)  $a^*_{ph}(620)$  as a function of phycocyanin (PC) concentrations. Specific absorption coefficients were measured in the

laboratory on a dual beam spectrophotometer, and PC and Chl- <i>a</i> results are from spectrophotometry. Note x-axes are on log scale. ....	92
<b>Figure 3.15</b> Spectra of absorption by non-algal particles [ $a_{NAP}(\lambda)$ ] for all stations in Kis-Balaton and Lake Balaton by basin. Note the different y-axis maximum for Kis-Balaton. ....	94
<b>Figure 3.16</b> Scatterplots of $S_{NAP}$ (the spectral slope of $a_{NAP}$ ) as a function of (a) the ratio of particulate inorganic to organic matter (PIM:POM) and (b) absorption by non-algal particles at 440 nm [ $a_{NAP}(440)$ ]. The linear regression in (b) is for $a_{NAP}(440) < 0.1 \text{ m}^{-1}$ only. ....	95
<b>Figure 3.17</b> Correlation between (a) total suspended matter (TSM) and absorption by non-algal particles [ $a_{NAP}(440)$ ] and (b) particulate inorganic matter (PIM) and the proportion of absorption by non-algal particles to absorption by particulate matter [ $a_{NAP}(440):a_p(440)$ ]. In plot (a), dashed line is a linear regression with null intercept indicating the relationship found across the range of TSM in coastal waters in Babin et al. (2003b) [ $a_{NAP}(440)=0.31*TSM$ ], and the solid line is a linear regression with null intercept for Kis-Balaton and Lake Balaton. The solid line in plot (b) is a linear regression. ....	96
<b>Figure 3.18</b> Variation of (a) $\log [a^*_{ph}(350)] (\text{m}^2 \text{ mg}^{-1})$ and (b) $\log (S_{CDOM}) (\text{nm}^{-1})$ over increasing distance from the Zala River inflow, and (c) relationship between $\log [a^*_{ph}(350)] (\text{m}^2 \text{ mg}^{-1})$ and $\log [a_{CDOM}(350)] (\text{m}^{-1})$ . ....	107
<b>Figure 4.1</b> Map of Lake Balaton indicating 4 basins and 35 station locations. ....	117
<b>Figure 4.2</b> Mean attenuation by basin due to particulate scattering, CDOM absorption and particulate absorption at (a) 440, (b) 555, (c) 620 and (d) 675 nm. The attenuation due to pure water absorption has been subtracted from the total attenuation and therefore not included in these graphs. The ratio axis is scaled to 0.2 for ease of viewing, however note that $b(p)$ continues to 1.0 in all plots. The abbreviations $b(p)$ , $a(CDOM)$ and $a(p)$ are used for $b_p(\lambda)$ , $a_{CDOM}(\lambda)$ and $a_p(\lambda)$ . ....	126
<b>Figure 4.3</b> Particulate attenuation at 660nm [ $c_p(660)$ ] plotted against (a) chlorophyll- <i>a</i> (Chl- <i>a</i> ), (b) total suspended matter (TSM), (c) particulate organic matter (POM) and (d) particulate inorganic matter (PIM). Solid lines and equations represent best-fit power functions. ....	127

<b>Figure 4.4</b> (a) The particulate backscattering ratio ( $\tilde{b}_{bp}$ ) for each station (n=29) over the three wavelengths at which <i>in situ</i> $b_{bp}$ was measured, and linear regression plots for $\tilde{b}_{bp}(532)$ as a function of (b) $\tilde{b}_{bp}(470)$ and (c) $\tilde{b}_{bp}(650)$ . .....	129
<b>Figure 4.5</b> Scatterplot of $b_p(531.3)$ and $b_{bp}(532)$ as measured by the AC-S and BB3, respectively. Solid line is a linear regression and vertical error bars are standard deviation of mean $b_{bp}(532)$ . .....	132
<b>Figure 4.6</b> Scatterplots of $b_p(531.3)$ , $b_{bp}(532)$ and $\tilde{b}_{bp}$ against concentrations of TSM (a, d, g), PIM (b, e, h) and POM (c, f, i). Solid lines and equations are for regression curves by least squares fit. ....	134
<b>Figure 4.7</b> Scatterplots of (a) $b_p(531.3)$ , (b) $b_{bp}(532)$ and (c) $\tilde{b}_{bp}$ as a function of Chl- <i>a</i> concentration. Solid lines and equations are for regression by least squares fit, with the exponential fit from Lake Taihu shown as a dashed line (Sun et al., 2009). ....	135
<b>Figure 4.8</b> Backscattering ratio ( $\tilde{b}_{bp}$ ) as a function of (a) total phytoplankton biomass, (b) cyanobacteria biomass and (c) ratio of cyanobacteria to total biomass. Solid lines are best-fit power functions. ....	137
<b>Figure 4.9</b> The mass-specific scattering coefficient ( $b^*_p(531.3)$ ; $m^2 g^{-1}$ ) as a function of (a) PIM:TSM , (b) POM:TSM, (c) Chl- <i>a</i> and (d) PC. Solid lines are best-fit linear regressions. Grey dashed line in (a) represents the linear relationship from 3 turbid Chinese lakes in Shi et al. (2014). ....	138
<b>Figure 4.10</b> Scatterplot of particulate backscattering ratio [ $\tilde{b}_{bp} = b_{bp}(532): b_p(531.3)$ ] against the PSD slope ( $\zeta$ ). Solid curves are overlaid to represent the refractive index contours ( $\bar{n}_p$ ) as calculated by Twardowski et al. (2001), ranging from 1.02 to 1.20 by increments of 0.02. ....	139
<b>Figure 5.1</b> Map of Lake Balaton, indicating the five regularly monitored stations (BLI) (Keszthely, Szigliget, Balatonszemes, Siófok and Tihany) and the 35 locations from the August 2010 field campaign. ....	154
<b>Figure 5.2.</b> Inter-annual variations in (a,b) chlorophyll- <i>a</i> , (c,d) phytoplankton biomass and (e,f) cyanobacteria biomass at Keszthely and Tihany stations (BLI data). 162	
<b>Figure 5.3.</b> Validation of MERIS data atmospherically corrected with SCAPE-M_B2 with <i>in situ</i> reflectance data, including scatter plots of $R_{rs}(\lambda)$ at each band. Scatterplots include all stations with <i>in situ</i> data (n=30), with same day matchups shown in red (n=7). Statistics correspond to the same day matchups only. ....	164

- Figure 5.4.** Validation MERIS data atmospherically corrected with SCAPE-M\_B2 with *in situ* HyperSAS reflectance data for stations 1-15. MERIS data is the mean of a 3x3 pixel window with error bars indicating standard deviation. HyperSAS radiometry is shown as a range of minimum to maximum recorded at each station..... 165
- Figure 5.5.** Validation MERIS data atmospherically corrected with SCAPE-M\_B2 with *in situ* HyperSAS reflectance data for stations 16-30. MERIS data is the mean of a 3x3 pixel window with error bars indicating standard deviation. HyperSAS radiometry is shown as a range of minimum to maximum recorded at each station. Same-day matchups include stations 16-22 only, shown in red (n=7). Note the different ranges for y-axis values..... 166
- Figure 5.6** Phycocyanin retrieval performance for a)Simis05, b)Mishra13 and c)Li15 algorithms using MERIS data from 2010-2011 (n=22). Matchups are within 1 day of *in situ* phycocyanin measurements. Mishra13 was applied using  $a^*_{pc}(620)=0.007 \text{ m}^2 \text{ mg}^{-1}$  from Simis et al. (2005) and  $a^*_{pc}(620)=0.0048 \text{ m}^2 \text{ mg}^{-1}$  from Mishra et al. (2013)..... 168
- Figure 5.7** Retrievals of Chl-*a* from MERIS at matchups with measured Chl-*a* within (a)  $\pm 1$  day, (b)  $\pm 3$  days and (c)  $\pm 7$  days. Retrievals shown are mean pixel values within 2 standard deviations. Linear regression results shown are for all data. Dashed line is 1:1..... 171
- Figure 5.8** Retrievals of Chl-*a* from MERIS at matchups with measured Chl-*a* within (a)  $\pm 1$  day, (b)  $\pm 3$  days and (c)  $\pm 7$  days, using only those matchups used for Simis05 retrievals of PC. Retrievals shown are mean pixel values within 2 standard deviations. Linear regression results shown are for all data. Dashed line is 1:1..... 172
- Figure 5.9** Retrievals of Chl-*a* from MERIS at matchups with measured phytoplankton biomass from (a)  $\pm 1$  day, (b)  $\pm 3$  days and (c)  $\pm 7$  days. Retrievals shown are mean pixel values within 2 standard deviations. Solid line is a linear regression for all data. .... 173
- Figure 5.10** Retrievals of PC from MERIS at matchups with measured PC from (a)  $\pm 1$  day, (b)  $\pm 3$  days and (c)  $\pm 7$  days. Retrievals shown are mean pixel values within 2 standard deviations. Linear regression results shown are for all data. Dashed line is 1:1..... 175

<b>Figure 5.11</b> Retrievals of PC from MERIS at matchups with measured cyanobacteria biomass from (a) $\pm 1$ day, (b) $\pm 3$ days and (c) $\pm 7$ days. Retrievals shown are mean pixel values within 2 standard deviations. Solid line is a linear regression for all data. ....	177
<b>Figure 5.12</b> Time series of estimated PC from MERIS (Simis05 algorithm) for May-September 2008. ....	178
<b>Figure 5.13</b> Retrieval of (a) $a_{ph}(665)$ and (b) $a_{ph}(620)$ using Simis05 for 22 August 2010 with matchups $\pm 7$ days (n=29).....	180
<b>Figure 5.14</b> (a) Spectra of backscattering at 3 wavelengths as measured by the ECO-BB3 during the August 2010 field campaign (n=35) and (b) linear regression of estimated $b_b(779)$ from Simis05 and measured $b_b(650)$ (n=29). ....	181
<b>Figure 5.15</b> MERIS retrieved concentrations of Chl- <i>a</i> (a-d) and PC (e-f) over the time series of <i>in situ</i> measurements of Chl- <i>a</i> (a-b), phytoplankton biomass (c-d) and cyanobacteria biomass (e-f) at Keszthely and Tihany. ....	182
<b>Figure 6.1</b> Map of Lake Balaton, indicating the 38 sampling stations. ....	203
<b>Figure 6.2</b> Validation of Landsat 5 TM atmospheric correction with <i>in situ</i> $R_{rs}$ at Landsat bands (a) 1 (450-520 nm), (b) 2 (520-600 nm) and (c) 3 (630-690 nm). <i>In situ</i> $R_{rs}$ was resampled to the respective Landsat 5 TM bands, using the Landsat 5 TM band center and full width half maximum, assuming a Gaussian distribution. Same-day matchups are presented for validation (red points), with equations and errors corresponding to these points only (n=7).....	214
<b>Figure 6.3</b> Validation of atmospheric correction of Landsat 5 TM with <i>in situ</i> $R_{rs}(\lambda)$ for same day matchups (n=7). <i>in situ</i> $R_{rs}(\lambda)$ is shown as two dashed grey lines, indicating the minimum and maximum $R_{rs}(\lambda)$ measured by HyperSAS radiometry. MERIS SCAPE-M_B2 $R_{rs}(\lambda)$ data also shown for comparison. Error bars indicate standard deviation. ....	215
<b>Figure 6.4</b> Validation of ATCOR4 atmospheric correction of AISA Eagle data with <i>in situ</i> $R_{rs}$ at (a) 442, (b) 620, (c) 665 and (d)708 nm. The <i>in situ</i> wavelength which was closest to the center of the respective AISA Eagle band was used for validation. Only same-day matchups are presented for validation (red points), with equations and errors corresponding to these points only (n=19).....	217
<b>Figure 6.5</b> Validation of ATCOR4 atmospheric correction of AISA Eagle data with <i>in situ</i> $R_{rs}(\lambda)$ for same day matchups (n=19). <i>in situ</i> $R_{rs}(\lambda)$ is shown as two dashed grey lines, indicating the minimum and maximum $R_{rs}(\lambda)$ measured by	

HyperSAS radiometry. MERIS SCAPE-M\_B2  $R_{rs}(\lambda)$  data also shown, with error bars indicating standard deviation. Note different y-axis ranges. ....218

**Figure 6.6** Scatterplots of retrieved Chl-*a* against measured Chl-*a* using the NDCI with (a) MERIS (b) Landsat 5 TM, (c) AISA Eagle and (d) HyperSAS datasets. Pixel window of 3x3 applied for each dataset. Statistics are for common dataset, shown in red, with any additional matchups shown as open circles. Determination coefficients ( $R^2$ ) represent linear regressions of common dataset. Dashed line represents 1:1 relationship. ....220

**Figure 6.7** Maps of Chl-*a* retrievals using the NDCI applied to the (a) MERIS (b) Landsat 5 TM and (c) AISA Eagle datasets. Pixel window of 3x3 applied for each dataset, i.e. maps shown at (a) 900 m, (b) 90 m and (c) 15 m resolutions. ....221

**Figure 6.8** Histograms of Chl-*a* concentrations ( $\text{mg m}^{-3}$ ) retrieved using the NDCI from (a) AISA Eagle, (b) Landsat 5 TM and (c) MERIS at variable spatial resolutions, as indicated. ....226

**Figure 6.9** Maps of Chl-*a* retrievals using the NDCI applied to the Landsat 5 TM data at (a) 30 m (1 pixel), (b) 90 m (3 x 3 pixel window) and (c) 330 m (11 x 11 pixel window) resolutions. ....227

**Figure 6.10** Maps of Chl-*a* retrievals using the NDCI applied to the AISA Eagle data at (a) 5 m (1 pixel), (b) 15 m (3 x 3 pixel window), (c) 35 m (7 x 7 pixel window) and (d) 305 m (61 x 61 pixel window) resolutions. ....229

**Figure 6.11** Maps of Chl-*a* retrievals using the NDCI applied to the AISA Eagle data for the Tihany peninsula at a) 5 m (1 pixel), (b) 15 m (3 x 3 pixel window), (c) 35 m (7 x 7 pixel window) and (d) 305 m (61 x 61 pixel window) resolutions. ....230

**Figure 6.12** Maps of Chl-*a* retrievals using the NDCI applied to (a) Landsat 5 TM data at the native 30 m resolution, (b) AISA Eagle data at 35 m resolution, (c) MERIS data at the native 300 m resolution and (d) AISA Eagle data at 305 m resolution for the Keszthely basin (Stations 16, 17 18). Data shown were acquired from 09:01-09:29 GMT on 22 August 2010. ....231

**Figure 6.13** True colour AISA Eagle images of the Tihany peninsula (Station 35) at (a) 5 m, (b) 15 m, (c) 35 m and (d) 305 m. ....233

**Figure 6.14** True colour Landsat 5 TM images of the Tihany peninsula (Station 35) at (a) 30 m, (b) 90 m, (c) 330 m. ....234

## List of Tables

<b>Table 3.1</b> Daily average wind speed over the sampling period at Basin 4 (Siófok, Lake Balaton).....	65
<b>Table 3.2</b> Mean Biogeochemical Parameters (Standard Deviation) for each basin and Kis-Balaton <sup>a</sup> .....	75
<b>Table 3.3</b> Absorption coefficients for the main basins of Lake Balaton only (n=35)....	97
<b>Table 3.4</b> Absorption coefficients for Kis-Balaton stations only (n=3).....	97
<b>Table 3.5</b> Mean absorption coefficients (standard deviation) by basin. ....	98
<b>Table 3.6</b> IOP and SIOPs from selected previous studies for comparison. ....	99
<b>Table 4.1</b> Mean ( $\pm$ standard deviation) biogeochemical parameters for each basin in Lake Balaton, including chlorophyll-a (Chl- <i>a</i> ), phycocyanin (PC), total suspended matter (TSM), particulate organic matter (POM), particulate inorganic matter (PIM), the ratio of PIM:TSM, phytoplankton biomass (Total Biomass) and cyanobacteria biomass (Cyano Biomass; mg m <sup>-3</sup> and % biomass) (table adapted from Table 3.2 in Chapter 3; Riddick et al., 2015). ....	125
<b>Table 4.2</b> Summary of scattering, backscattering and attenuation coefficients for Lake Balaton. ....	128
<b>Table 4.3</b> Mean $\pm$ standard deviation of backscattering and scattering coefficients in Lake Balaton by basin.....	131
<b>Table 4.4</b> Mean $\pm$ standard deviation of PIM ratios and refractive index ( $\bar{n}_p$ ) values, as calculated according to Twardowski et al. (2001). ....	140
<b>Table 4.5</b> Table of bulk and mass-specific scattering and backscattering coefficients and the backscattering ratio in other recent studies. ....	144
<b>Table 5.1</b> PC retrieval statistics for Simis05, Mishra13 and Li15 algorithms using MERIS data from 2010-2011 (n=22 unless specified otherwise). Matchups are within 1 day of <i>in situ</i> phycocyanin measurements.....	169
<b>Table 5.2</b> Least squares linear regression results ( $y=mx+b$ ) for Chl- <i>a</i> , PC, $a_{ph}$ and $b_b$ using Gons05 and Simis05 algorithms for all data, including integrated and surface samples. ....	183
<b>Table 5.3</b> Least squares linear regression results ( $y=mx+b$ ) for Chl- <i>a</i> , PC, $a_{ph}$ and $b_b$ retrievals using Gons05 or Simis05 algorithms, validated with surface samples only (August 2010 only). ....	184

<b>Table 5.4</b> Least squares linear regression results ( $y=mx+b$ ) for Chl- <i>a</i> and PC retrievals using Gons05 and Simis05 algorithms, respectively, validated with integrated samples only (BLI, 2007-2011). .....	186
<b>Table 5.5</b> Least squares linear regression results ( $y=mx+b$ ) for Chl- <i>a</i> retrievals using the Gons05 algorithm, validated with KdKVI surface samples only (2007-2011). .....	187
<b>Table 6.1</b> Date (XX August 2010) and acquisition time (GMT) of <i>in situ</i> and remote sensing datasets collected at each station. Same-day match-ups are shown in bold, and same-day matchups across all datasets are additionally highlighted in gray ( $n=7$ ). .....	206
<b>Table 6.2</b> Details of sensors investigated in this study. ....	211
<b>Table 6.3</b> Summary of biogeochemical parameters in August 2010 in Lake Balaton and Kis-Balaton, including Chlorophyll- <i>a</i> (Chl- <i>a</i> ), Total phytoplankton biomass, Total Suspended Matter (TSM), Particulate Inorganic Matter (PIM), Particulate Organic Matter (POM) and absorption of Coloured Dissolved Organic Matter at 440 nm [ $a_{CDOM}(440)$ ]. .....	212
<b>Table 6.4</b> Table of errors (Coefficient of Variation, %; Standard Deviation) within the resampled pixel windows for Chl- <i>a</i> retrieved by NDCI from AISA Eagle and Landsat 5 TM data. Sample size is for a common dataset ( $n=27$ ). .....	222
<b>Table 6.5</b> Comparison of errors for Chl- <i>a</i> retrievals from AISA Eagle, Landsat 5 TM and MERIS data using the NDCI. Sample size is for the common dataset ( $n=27$ ). .....	224
<b>Table 7.1</b> List of relevant recently launched or forthcoming satellite-based instruments for the remote sensing of inland waters [adapted from Tyler et al. (2016)]. Italicised entries indicate satellite instruments that are not yet launched. ....	246
<b>Table 8.1</b> Details of sensors investigated in this study. ....	253
<b>Table 8.2</b> Details of <i>in situ</i> optical sensors investigated in this study. ....	253

## List of Acronyms and Abbreviations

AVHRR 3	Advanced Very High Resolution Radiometer
AISA	Airborne Imaging Spectrometer for Applications
ATCOR4	Atmospheric and Topographic Correction model
BLI	Balaton Limnological Institute
Bias <sub>log</sub>	Bias calculated in log space
KdKVI	Central Transdanubian (Regional) Inspectorate for Environmental Protection, Nature Conservation and Water Management [Közép-dunántúli Környezetvédelmi, Természetvédelmi és Vízügyi Felügyelőség (KDT KTVF)]
Chl- <i>a</i>	Chlorophyll- <i>a</i>
CDOM	Coloured Dissolved Organic Matter
CDM	Combined CDOM and NAP
CHRIS	Compact High Resolution Imaging Spectrometer onboard Proba-1
ETM+	Enhanced Thematic Mapper Plus onboard Landsat 7
EnMAP	Environmental Mapping and Analysis Program
FLAASH	Fast Line-of-sight Atmospheric Analysis of Spectral Hypercubes
FLH	Fluorescence Line Height, an algorithm for Chl- <i>a</i> retrieval
GEO-CAPE	Geostationary Coastal and Air Pollution Events mission
HSI	Hyperspectral Imager onboard EnMAP
HypSIRI	Hyperspectral InfraRed Imager
HyperSAS	Hyperspectral Surface Acquisition System
ECO-BB3	<i>in situ</i> Environmental Characterization Optics series instrument measuring backscattering ( <i>b<sub>b</sub></i> ) at 3 wavelengths
AC-9	<i>in situ</i> spectrophotometer measuring absorption ( <i>a</i> ) and beam attenuation ( <i>c</i> ) at 9 wavelengths
AC-S	<i>in situ</i> spectrophotometer measuring absorption ( <i>a</i> ) and beam attenuation ( <i>c</i> ) spectra
IOPs	Inherent Optical Properties
LEDAPS	Landscape Ecosystem Disturbance Adaptive Processing System
MAPE	Mean Absolute Percentage Error
MERIS	Medium Resolution Imaging Spectrometer
MODIS	Moderate resolution Imaging Spectroradiometer
MODIS/6S	6S atmospheric correction routine developed for MODIS
MSI	MultiSpectral Imager, onboard Sentinel 2
MAAs	Mycosporine-like amino acids
NAP	Non-algal particles
NDCI	Normalized Difference Chlorophyll Index

OAC	Optically Active Constituent
OLCI	Ocean and Land Colour Instrument, onboard the Sentinel 3 satellite
OLI	Operational Land Imager onboard Landsat 8
PIM	Particulate Inorganic Matter
POM	Particulate Organic Matter
PC	Phycocyanin
PACE	Pre-Aerosols Clouds and ocean Ecosystems mission
RMSE	Root Mean Square Error
RMSE <sub>log</sub>	RMSE calculated in log space
SCAPE-M_B2	Self-Contained Atmospheric Parameters Estimation for MERIS data, following the implementation as in Domínguez et al. (2011)
(S)IOPs	SIOPs and IOPs
S <sub>CDOM</sub>	Slope of the CDOM absorption curve
S <sub>NAP</sub>	Slope of the NAP absorption curve
SIOPs	Specific Inherent Optical Properties
Landsat 5 TM	Thematic Mapper onboard Landsat 5
TSM	Total Suspended Matter
VIIRS	Visible Infrared Imaging Radiometer Suite
WFD	Water Framework Directive
$a(\lambda)$ or $a_T(\lambda)$	Total absorption coefficient (measured by the AC-S)
$a_{pg}(\lambda)$	Absorption of particulate (p) +dissolved (g)
$a_w(\lambda)$	Absorption coefficient of water
$a_p(\lambda)$	Particulate absorption coefficient
$a_{ph}(\lambda)$	Absorption coefficient of phytoplankton
$a_{chl}(\lambda)$	Chl- <i>a</i> absorption coefficient
$a_{pc}(\lambda)$	Phycocyanin absorption coefficient
$a^*_{ph}(\lambda)$ or $a^*_{chl}(\lambda)$	Chl- <i>a</i> specific absorption coefficient
$a^*_{pc}(\lambda)$	Phycocyanin specific absorption coefficient
$a_{CDOM}(\lambda)$	CDOM absorption coefficient
$a_{CDM}(\lambda)$	CDOM and detrital matter absorption coefficient
$a_{NAP}(\lambda)$	Absorption coefficient of non-algal particles (NAP)
$\beta_t(\lambda, 117^\circ)$	Total volume scattering function
$b_p(\lambda)$	Particulate scattering coefficient
$b_{bp}(\lambda)$	Particulate backscattering coefficient
$b_{bw}(\lambda)$	Backscattering coefficient of water
$b^*_p(\lambda)$	Specific particulate scattering coefficient

$b^*_{bp}(\lambda)$	Specific particulate backscattering coefficient
$\tilde{b}_{bp}(\lambda)$	Backscattering ratio at 532 nm [ $b_{bp}(\lambda):b_p(\lambda)$ ]
$c_p(\lambda)$	Particulate attenuation coefficient
$\bar{n}_p$	Bulk refractive index
$\xi$	Slope of the particulate size distribution
$\gamma$	Hyperbolic slope of the $c_p(\lambda)$ spectrum
$R_{rs}(\lambda)$	Remote sensing reflectance
$r_{rs}(\lambda)$	Subsurface remote sensing reflectance
$\rho_w(\lambda)$	Water-leaving reflectance, also known as MERIS reflectance
$E_s(\lambda)$	Downwelling irradiance
$L_t(\lambda)$	Water surface radiance
$L_{sky}(\lambda)$	Sky radiance
$L_w(\lambda)$	Water-leaving radiance
$u(\lambda)$	Ratio of the backscattering coefficient ( $b_b$ ) to the sum of total absorption ( $a$ ) and backscattering coefficients
$\rho_{sky}$	Air-sea interface reflection coefficient
$W$	Wind speed
$\lambda$	Wavelength
$\mu$	Mean
$\sigma$	Standard Deviation

# 1 Introduction

---

## 1.1 Research context

Freshwater lakes are important resources to the global biosphere, playing a vital role in biogeochemical cycling (McCusker et al., 1999), acting as conduits and reactors for carbon (Tranvik et al., 2009) and providing essential ecosystem services to society (Baron et al., 2002). Lakes are valuable sites for drinking water, fishing, agriculture, transport, recreation, tourism and simply add to the aesthetics of a landscape. However, the management of water quality is a major concern facing society today. To confront this challenge in Europe, the Water Framework Directive (WFD) was adopted for protection, improvement and sustainable use of Europe's freshwaters (European Commission, 2000). This directive (2000/60/EC) requires all Member States of the European Union to aim to achieve "good and non-deteriorating ecological status" in rivers, lakes, estuaries, coastal and groundwaters, ideally by 2015 and ultimately by 2027. Other relevant EU regulations include the Bathing Water Directive (2006/7/EC), which requires monitoring of all bathing waters for bacteria, cyanobacteria and microalgae to obtain a minimum of "sufficient" quality threshold (European Commission, 2006). The Habitats Directive (92/43/EEC) was implemented to protect Europe's most endangered, vulnerable, rare or endemic species, which also requires protected sites to be managed in accordance with ecological needs of the species (European Commission, 1992). Therefore, there is a great need to monitor the quality of European, and indeed, global freshwaters with efficient and accurate methods in order to establish and thus improve their ecological status.

The traditional method for monitoring lake water quality is a point-sampling technique, with water samples taken from discrete locations. However, this approach is vulnerable to influences from sampling bias, and may not adequately describe the true heterogeneity of the lake system. It is necessary to ensure adequate sampling frequency in both time and space in order to gain an unbiased understanding of regional differences and long-term trends, although sampling frequency is often inadequate, at best fortnightly, but more often conducted on a monthly, quarterly or only annual basis (Rantajarvi et al., 1998). More recently, monitoring buoy installations are available to monitor water depth, meteorological conditions, water quality parameters, and even

sondes to measure fluorescence (e.g. chlorophyll). However, while these can provide high temporal resolution they still only provide very limited data spatially. Furthermore, the large number of lakes monitored globally, or even nationally, presents a substantial cost as well as a sheer logistical challenge to acquire monitoring data using traditional *in situ* methods. In fact, it was recently estimated that there are as many as 117 million lakes, comprising ~3.7% of the Earth's surface (Verpoorter et al., 2014).

In this context, remote sensing can provide a more efficient means of monitoring lake water quality. Remote sensing is a tool that provides a broad spatial and temporal context for point-based measurements (Rainey et al., 2003, Tyler et al., 2006). Such technology includes the use of satellite, airborne or handheld spectrometry to measure the radiometric properties of the water surface. Recent advancements have enabled the possibility of extracting biophysical information from remotely sensed data, including satellite and airborne platforms (Aplin, 2005).

Remote sensing has been widely applied to open ocean waters to extract information on their biogeochemical properties. However, progress has been limited on the remote sensing of inland or coastal waters. Remote sensing of inland waters is more complex due to greater contributions from optically active constituents (OACs) other than phytoplankton, including mineral particles, organic detritus and coloured dissolved organic matter (CDOM). Specifically, the OACs in inland waters typically do not co-vary over space and time, and their optical properties tend to be highly variable between and within water bodies (Palmer et al., 2015a). In contrast, the dominant OAC in ocean waters is phytoplankton and their associated by-products. Thus, the additional contributions from minerals, detritus and CDOM in inland waters present a challenge when retrieving the parameter of interest from remotely sensed imagery.

Previous studies have applied remote sensing to estimate chlorophyll-*a* concentration in lakes, a widely accepted proxy for phytoplankton biomass, and developed algorithms for this purpose (Mittenzwey et al., 1992, Dekker, 1993, Gons, 1999, George & Malthus, 2001, Ammenberg et al., 2002, Gons et al., 2002, Kutser, 2004, Gons et al., 2005, Tyler et al., 2006, Hunter et al., 2008a, Hunter et al., 2010). However, the use of remote sensing for inland waters in the past has been restricted because of the spatial and spectral constraints posed by the lake setting. Space-borne instruments that have been designed for ocean colour remote sensing tend to have coarse resolutions (0.3-1.1 km), which may only suit the largest lakes. However, terrestrial observation satellites often have bands that are not optimally positioned and

resolution that is too coarse to allow isolation of features such as phytoplankton pigment absorption (Lindell et al., 1999, Tyler et al., 2006). Therefore, it is pertinent to test and develop algorithms for the retrieval of biogeochemical data from lakes using hyperspectral technology, such as *in situ* and airborne remote sensing, which provide high resolution data over a flexible time series. Such data can provide a useful framework with which to model the capabilities of satellite based sensors and inform the design of future systems.

Advancement of the remote sensing of lakes also requires a detailed understanding of the bio-optical properties of the OACs. With knowledge of the inherent optical properties (IOPs) of the water column, including absorption, scattering and backscattering, it has been recognised that the accuracy of bio-optical models for inland waters should greatly improve (Binding et al., 2008). In fact, a recent review article identified a need for investigation of the variability of biogeochemical properties and IOPs in lakes, and their relationships (Mouw et al., 2015). However, the IOPs of lakes have been little studied, and there is a lack of understanding about how they vary with biogeochemical composition. Some studies also suggest marked seasonal variability in the optical properties of ocean water (Sathyendranath et al., 1999), coastal and shelf seas (Binding et al., 2005) and lake waters (Paavel et al., 2008, Zhang et al., 2010). However, further observations of IOPs are required to improve the accuracy of remote sensing products in optically complex waters, and to understand the implications of this variability on retrieved biogeochemical parameters (Binding et al., 2008).

It is further widely acknowledged that chlorophyll-*a* algorithms applied to standard ocean colour satellites perform poorly over inland waters (IOCCG, 2000, Darecki & Stramski, 2004, Reinart & Kutser, 2006, Ruiz-Verdu et al., 2008). Algorithm development for inland waters has been designated a priority area of research by the International Colour Coordinating Group and European Science Foundation (IOCCG, 2000). Additionally, a recent review has acknowledged the challenges to remote sensing of inland and coastal waters, highlighting outstanding issues including limited satellite mission capability and a lack of *in situ* observations, algorithm development and processing capability (Mouw et al., 2015). Mouw et al. (2015) identified a present lack of transferability for inland water algorithms, and suggested a coordinated comparison of algorithms is needed to identify the strengths and limitations of these.

Broadly, there remains need for further research to ultimately refine the approach for the application of remote sensing to lakes. There is a lack of understanding about the within-lake variability in the IOPs, and how these vary with or are related to the biogeochemistry of the water column. Furthermore, it is vital to test and improve the robustness of current algorithms for constituent retrieval with the goal of increased utility and transferability of algorithms for inland waters. An increased knowledge of these areas would greatly improve progress towards the ultimate aim of operational use of remote sensing for inland waters.

### **1.1.1 Thesis aims and structure**

The aim of this thesis is to explore *in situ* bio-geo-optical properties of and applications of remote sensing at a range of spatial, spectral and temporal scales in optically complex inland waters. More specifically, this thesis aims to: (i) increase the present understanding of the within-lake variations in bio-geo-optical properties over a trophic gradient; (ii) investigate the use of satellite remote sensing for retrieval of phytoplankton and cyanobacterial pigments in highly turbid waters; and (iii) conduct an inter-comparison of coincident remote sensing datasets over a range of spectral and spatial resolutions for the retrieval of phytoplankton biomass. Ultimately, this thesis is meant to provide an in-depth case study of an optically complex lake with a view to understand how the variability in optical properties may affect retrievals of phytoplankton pigments using presently available algorithms. This case study can provide an example of a large shallow lake with a wide range of biogeochemical and optical properties, which may inform remote sensing applications to similarly complex water bodies.

This thesis is presented as a series of seven chapters (Figure 1.1). The first two chapters introduce and provide a context for the field of remote sensing of inland waters, highlighting knowledge gaps and outlining thesis aims. This is followed by two results chapters that focus on the variability of absorption coefficients [Chapter 3; (Riddick et al., 2015)] and scattering and backscattering coefficients (Chapter 4), and the relationships of these with biogeochemical parameters in Lake Balaton. Chapter 5 evaluates semi-analytical and bio-optical algorithms for the retrieval of cyanobacteria pigments using MERIS (MEdium Resolution Imaging Spectrometer) data, and investigates the sources of error using knowledge of the inherent optical properties (Riddick et al., in review). The final results chapter combines four coincident remote

sensing datasets, including satellite, airborne and *in situ* observations, to assess the accuracy of chlorophyll-*a* retrieval and quantify within pixel variability (Chapter 6). Finally, the thesis concludes with Chapter 7, which provides a summary of the key conclusions from this work and identifies possibilities for future research.

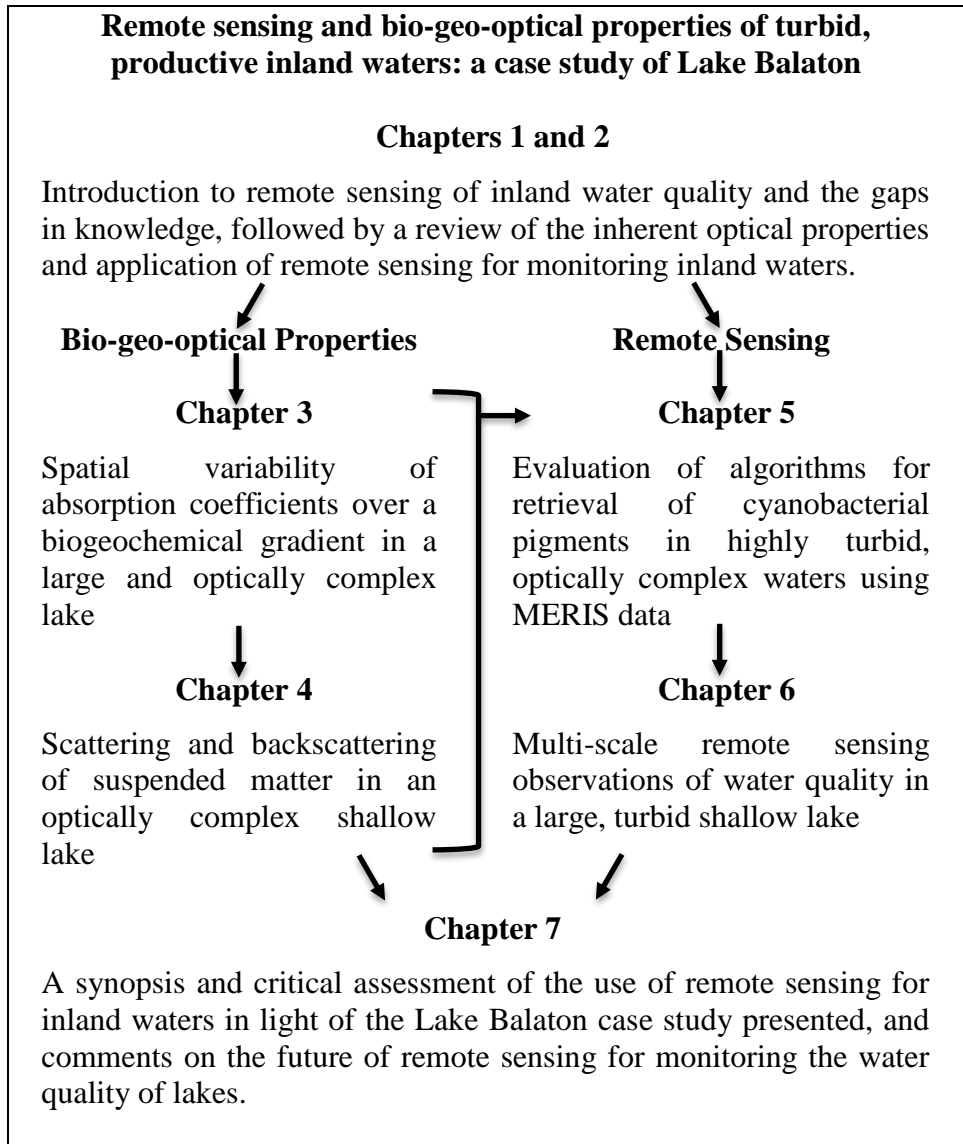


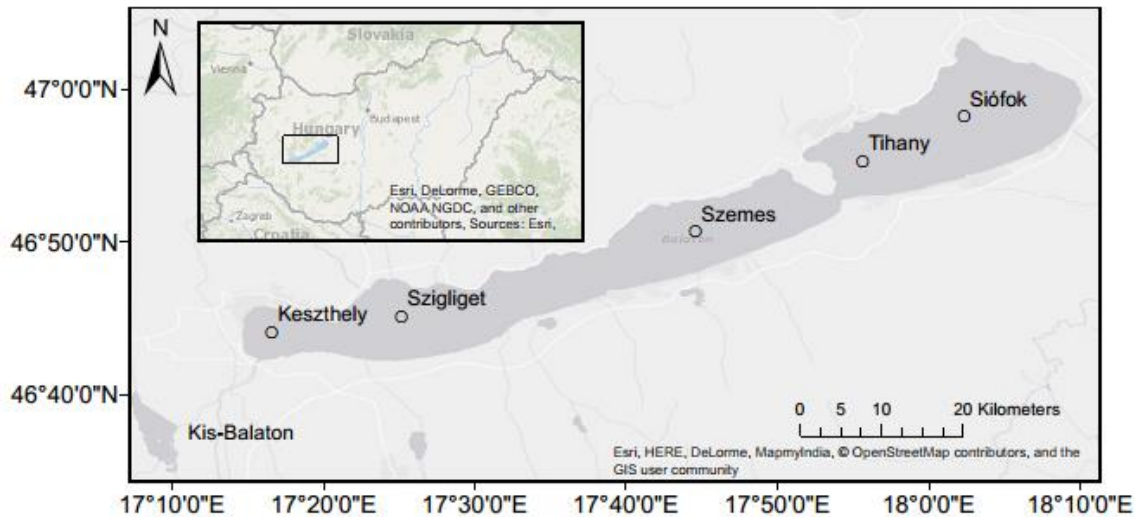
**Figure 1.1** Outline of the thesis structure.

### 1.1.2 Study site

Lake Balaton, Hungary (46° 51' 3" N, 17° 45' 58" E; Figure 1.2) provides an ideal study site for the research conducted in this thesis. Located in western Hungary, Lake Balaton is the largest freshwater lake in central Europe by surface area (595 km<sup>2</sup>) and has a mean depth of approximately 3 m (Herodek, 1986, Présing et al., 2001, Tyler

et al., 2006). The lake is comprised of four basins, with a wetland system in the west (Kis-Balaton Water Protection System), which was engineered in the mid-1980s to early 1990s (Dömötörfy et al., 2003, Tyler et al., 2006). The Zala River in the west is the main inflow to the lake, which typically produces a pronounced nutrient and trophic gradient across the lake. The only outflow is a highly regulated channel in the east at Siófok.

(a)



(b)

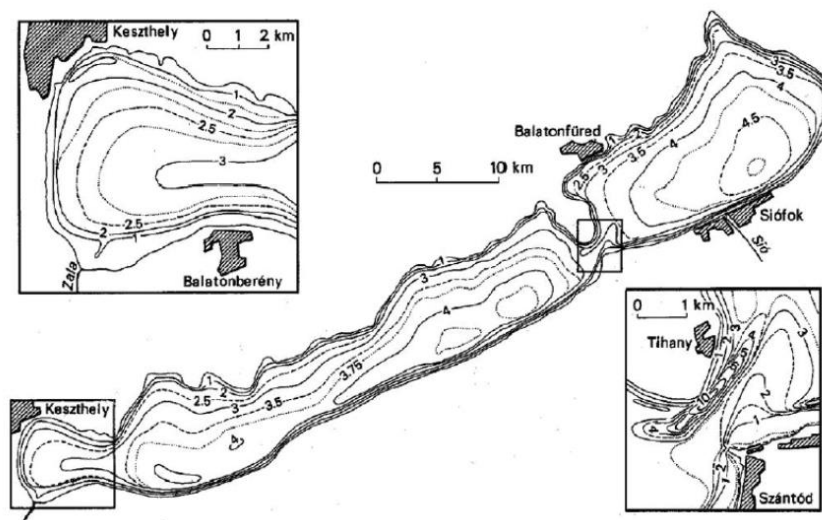


**Figure 1.2** (a) Map of Lake Balaton and Kis-Balaton in western Hungary and (b) bathymetric map of Lake Balaton taken from Gallinaro et al. (2013).

Lake Balaton has exhibited a history of eutrophication, and at its worst experienced hypereutrophic conditions in its westerly basins and eutrophic conditions in eastern basins due to increased nutrient loads in the 1970s (Herodek, 1986, Herodek et

al., 1995). Blooms of filamentous cyanobacteria (*Cylindrospermopsis raciborskii*) dominated the plankton community in the 1980s and 1990s (Présing et al., 1996). Since then, extensive waste water treatment and diversion schemes, the introduction of Kis-Balaton wetlands, closure of nearby farms in 1987 and reduction of fertilizer use have all substantially reduced nutrient loading to Lake Balaton, resulting in lower algal biomass and improved water quality (Somlyódy et al., 1997, Présing et al., 2001).

Prior to the research presented in this thesis, the optical properties of Lake Balaton have been not been studied. Additionally, only limited applications of remote sensing for assessment of water quality have been presented (Buttner et al., 1987, Gitelson et al., 1993b, Svab et al., 2005, Tyler et al., 2006, Palmer et al., 2015c). Thus, the research presented in this thesis presents: (i) a novel study of the bio-geo-optical properties of Lake Balaton and their spatial variability; and (ii) an investigation of remote sensing of phytoplankton over a range of temporal, spatial and spectral scales, expanding upon the emergent base of literature for the remote sensing of inland waters more broadly and of Lake Balaton, specifically.

## 2 Remote sensing of inland water quality

---

### 2.1 Phytoplankton and eutrophication

Phytoplankton are the basis of the pelagic food web and important regulators of biogeochemical cycling in lakes. They comprise a diverse group of eukaryotic and some prokaryotic algae that tend to be dominated in freshwaters by six major groups, including chlorophytes (green algae), bacillariophytes (diatoms), chrysophytes (golden algae), cryptophytes (cryptomonads), dinophytes (dinoflagellates) and cyanophytes (cyanobacteria) (Schmid et al., 1998, Reynolds, 2006). Other phyla such as haptophytes, xanthophytes, euglenophytes and raphidophytes are more rarely dominant, but can bloom in low alkalinity waters.

Phytoplankton are considered highly sensitive indicators of environmental change and can provide evidence as to the ecological health of a lake. For instance, when high nutrient loads (particularly nitrogen and phosphorus) are sustained for a period of time, the lake can change from a ‘desirable’ clear-water system, often dominated by macrophytes, to an ‘undesirable’ turbid system with elevated phytoplankton biomass (Scheffer, 2001). This phenomenon is called eutrophication, and is generally associated with an increased frequency of harmful algal blooms (Downing, 2001, Smith, 2003, Glibert et al., 2005a, Glibert et al., 2005b, Ptacnik et al., 2008). There are about 300 bloom-forming species of phytoplankton, and about 60-80 of these produce toxins (*Alexandrium* spp., *Gymnodinium* spp., *Dinophysis* spp., *Pseudo-nitzschia* spp., *Nodularia* spp., etc.) (Smayda, 1997, Landsberg, 2002, Kutser, 2009). Cyanobacteria blooms are of particular concern, as there are several known toxin-producing genera, including *Microcystis*, *Anabaena*, *Anabaenopsis*, *Planktothrix*, *Aphanizomenon*, *Cylindrospermopsis*, *Raphidiopsis* and *Nodularia* (Codd et al., 2005a).

In addition to producing toxins, phytoplankton blooms can have other damaging effects to lake systems. High phytoplankton biomass can reduce penetration of sunlight, and severely limit the growth of submerged vegetation (Kutser, 2009). Furthermore, decaying blooms can cause oxygen depletion in the water column, leading to mortality of animals (Anderson et al., 2002). Particular environmental conditions favour the growth of potentially toxic cyanobacteria blooms, with specific risk factors including high nutrient concentrations, high phytoplankton biomass (chlorophyll-*a* > 10 µg l<sup>-1</sup>), low water colour and high alkalinity (Dokulil & Teubner, 2000, Wagner &

Adrian, 2009, Carvalho et al., 2011). However, the long-term dominance of cyanobacteria is typically due to multiple factors, including nutrient concentrations, lake morphometry, water temperature, underwater light availability, mixing and food-web structure (Dokulil & Teubner, 2000). Thus, it is vital to ensure the quality of freshwater resources by reducing the likelihood of conditions likely to promote the growth of nuisance cyanobacteria blooms.

## **2.2 Importance of monitoring water quality**

Some studies suggest that lakes are highly sensitive indicators for climate change (Adrian et al., 2009, Schindler, 2009). Recent climate warming, in conjunction with other factors such as rainfall and flushing, may exacerbate poor water quality conditions in freshwater ecosystems, encouraging the development of harmful cyanobacteria blooms (Paerl & Huisman, 2008, Johnk et al., 2008). Furthermore, the need for improved risk management to protect water resources, economies and human health has been recognised by national and international bodies (Scottish Executive, 2002, WHO, 2003, WHO, 2004, Codd et al., 2005b). Instances of dog and cattle deaths have been attributed to cyanobacterial blooms in lakes, and a well-documented case of several human fatalities at a dialysis centre in Brazil were attributed to cyanotoxins (microcystins) in the water supply (Carmichael et al., 2001). Even though reported health effects may be relatively uncommon, many less severe or chronic effects may be unreported or unknown, and the threat of cyanobacterial blooms can significantly limit the use and access to freshwaters across Europe (and globally) to avoid these recognised health effects. It is therefore a priority to improve monitoring methods and develop quick response and alert systems for algal blooms, in order to prevent health impacts and limit their exposure to the public, pets and livestock. In this way, remote sensing may prove to provide real-time monitoring of inland waters for the benefit of human health. Additionally, remote sensing may also support the collection of water body status for lakes, as required by the Water Framework Directive (2000/60/EC) and Bathing Waters Directive (2006/7/EC) (European Commission, 2000; 2006).

## **2.3 Remote sensing of inland waters**

Remote sensing is generally defined as an observation of the Earth's surface (land or water) by means of reflected or emitted electromagnetic energy (Campbell, 2006). Remote sensing is a valuable tool because it offers a wide range of spatial and

temporal scales with which to investigate a landscape. The benefit to lake ecological studies is that remote sensing provides a much more complete investigation than the traditional point sampling methods.

Remote sensing can be divided into passive and active methods. Active methods send a known signal from the sensor to the water and the return signal is detected and quantified based on the time delay and the known speed of light. This approach is commonly referred to as Light Detection and Ranging, or LiDAR. For instance, laser-induced fluorescence can be used to detect chlorophyll, coloured dissolved organic matter or pollutants (Mobley et al., 2016). A pulse of UV light is sent to the water surface, and the spectral character and strength of the induced fluorescence provides information about the location, type and concentration of fluorescing substances present. The use of ship-mounted ultraviolet fluorescence LiDAR (UFL) was investigated for retrieval of water quality parameters in Lake Balaton in a recent PhD thesis, Palmer (2015). Another example of active remote sensing is LiDAR bathymetry, where pulsed lasers (water-penetrating green wavelengths) are reflected off the water surface and sea or lake bottom in order to generate a bathymetry map of the water body. Surface water salinity can also be deduced using spaceborne L-band radar (Burrage et al., 2008, Klemas, 2011, Tyler et al., 2016).

Passive remote sensing methods involve detection of the light that is naturally emitted or reflected by the water body. This includes optical and thermal remote sensing, which is detection of ambient light in the visible and infrared portions of the spectrum, respectively. Thermal remote sensing can provide estimates of water surface temperature, using measurements of the thermal infrared between 8-14  $\mu\text{m}$  (MacCallum & Merchant, 2012, Politi et al., 2012). Most commonly, passive remote sensing involves the detection of sunlight that was backscattered in the water and returned to the sensor (Mobley et al., 2016). Passive optical remote sensing can be used to acquire biogeochemical parameters indicative of water quality, including phytoplankton pigments, total suspended matter, turbidity and coloured dissolved organic matter, and this remote sensing method is the focus of the research in this thesis.

### **2.3.1 History of remote sensing application to lakes**

Over four decades ago, airborne and satellite remote sensing were proved functional for the detection of phytoplankton blooms (Wrigley & Horne, 1974, Ostrom, 1976). Since then, remote sensing has been applied to various limnology studies,

including the compilation of lake inventories (Finlayson & Vandervalk, 1995, Verpoorter et al., 2014), monitoring of water resource use (Beeri & Phillips, 2007) and hazard assessment (McKillop & Clague, 2007, Quincey et al., 2007). Most commonly, however, remote sensing is applied to extract water quality parameters in order to provide information on lake ecological status. These include lake surface temperature (George, 1993, Kay et al., 2005, Politi et al., 2012, Grim et al., 2013), secchi disc depth (Harrington et al., 1992, Baban, 1993, Nellis et al., 1998, Torbick et al., 2013, Binding et al., 2015), coloured dissolved organic matter (Kutser et al., 2005a, Kutser et al., 2005b, Zhang et al., 2007), lake carbon fractions (Kutser et al., 2015), suspended sediments (Lathrop et al., 1991, Choubey & Subramanian, 1992, Schiebe et al., 1992, Binding et al., 2010, Song et al., 2014), and phytoplankton pigments such as chlorophyll-*a* (Mittenzwey et al., 1992, George & Malthus, 2001, Ammenberg et al., 2002, Gons et al., 2002, Koponen et al., 2002, Kutser, 2004, Gons et al., 2005, Tyler et al., 2006, Doerffer & Schiller, 2007, Gitelson et al., 2008, Gilerson et al., 2010, Matthews et al., 2012, Mishra & Mishra, 2012) and phycocyanin (Schalles & Yacobi, 2000, Vincent et al., 2004, Simis et al., 2005, Simis et al., 2007, Mishra et al., 2009, Hunter et al., 2010, Mishra et al., 2013, Ogashawara et al., 2013, Mishra & Mishra, 2014, Li et al., 2015).

### **2.3.2 Types of platform and sensors**

Remote sensing applied to freshwater studies, can include the use of spaceborne or airborne instruments. Spaceborne (i.e. satellite-mounted) instruments have been widely applied to terrestrial and marine environments. However, satellite instruments often have larger spatial resolutions and/or broad spectral resolutions, which are less suitable for lake environments. Satellite instruments can offer large scale regional coverage with recurring data acquisition, and some now provide hyperspectral resolution as well. For instance, ocean colour satellite sensors have been used for inland waters, including MODIS (MODERate resolution Imaging Spectroradiometer), SeaWiFS (Sea-viewing Wide Field-of-view Sensor) and MERIS (Medium Resolution Imaging Spectrometer). MODIS was a 12-bit sensor onboard the Terra and Aqua satellites that measured over a broad spectral range (405-14,385 nm) and provided complete coverage of the Earth every 1-2 days, however the spatial resolution is low (250-1000 m), particularly over the bands for retrieval of phytoplankton pigments (1000 m for bands 8-16). MODIS is succeeded by the Visible Infrared Imaging Radiometer

Suite (VIIRS), a sensor with a 12-bit radiometric resolution, 1 day revisit cycle and 750 m spatial resolution over the spectral range 402-11,800 (22 bands). Another commonly used ocean colour satellite was WiFS onboard SeaWiFS, a 10-bit sensor which measured over the spectral range of 402-885 nm (8 bands) with a 2 day temporal resolution, however spatial resolution was poor (1000 m). MERIS was perhaps the most commonly applied ocean colour satellite to inland waters because it had an appropriate spectral range (390-1040 nm) with bands centred at phytoplankton pigment absorption peaks, and a 3-day revisit cycle with high radiometric sensitivity (16-bit). MERIS spatial resolution (300 m) still limits its use to larger water bodies.

However, there are satellite-based instruments with improved spatial resolutions, though many of these data are only available for a fee. For example, the 11-bit sensor onboard Digital Globe's Worldview-3 satellite can provide excellent spatial (1.24 m visible and near-infrared) and temporal (1 day) resolution of multispectral data (400-1040 nm; 8 bands). Satellite instruments with hyperspectral resolution also presently exist. For instance, HICO is a 14-bit sensor that measures 87 spectral bands from 300-1000 nm, although it is geostationary (onboard the international space station). Polar-orbiting satellites with hyperspectral capabilities include the Hyperion sensor onboard EO-1, which measures 220 bands from 400-2500 nm with a spatial resolution of 30m, however the revisit time of 16 days (or <16 days with off-nadir viewing capabilities) may not be adequate to capture freshwater phytoplankton dynamics. Other sensors specifically developed for land applications can be used over inland waters, e.g. Enhanced Thematic Mapper (ETM+) onboard Landsat 7 and the Operational Land Imager (OLI) onboard Landsat 8, which have lower radiometric resolutions (8- or 12-bit) but higher spatial resolutions than the ocean colour satellite instruments (30 m). There exists a great range of temporal, radiometric and spatial resolutions among earth observation sensors that have been used or are presently available for assessing inland water quality, and a recent list can be found in Tyler et al. (2016). A list of historic, current and future ocean colour sensors is available on the International Ocean Colour Coordinating Group (IOCCG) website ([http://www.ioccg.org/sensors\\_ioccg.html](http://www.ioccg.org/sensors_ioccg.html)). However, note that some of these instruments are not optimised for measuring water-leaving reflectance over inland or coastal waters (Mouw et al., 2015).

In contrast, airborne instruments can provide high spatial resolution and can offer hyperspectral technology applied over a flexible time span. In this way, airborne

instruments can often provide a more detailed “snapshot” of the water body. Recent airborne sensors include the Compact Airborne Spectrographic Imager (CASI-2), which was used by Hunter et al. (2008a) to achieve 2.5 m spatial resolution multispectral (13 bands, 412-820 nm) imagery to capture a cyanobacteria bloom in Barton Broad. The AISA Eagle spectrometer is a 12-bit hyperspectral (400-970 nm) sensor that can achieve high spatial resolution imagery of up to ~ 2 m, e.g. over Esthwaite Water and Loch Leven in Hunter et al. (2010). The tandem AISA Hawk is a 14-bit hyperspectral sensor that measures over the spectral range 970-2450 nm and achieved up to 3.6 m spatial resolution in Hunter et al (2010). The AISA Eagle and Hawk sensors were also used for the research in this thesis (Chapter 6), where 5 m spatial resolution data were collected over Kis-Balaton and Lake Balaton. The AISA Fenix is a dual sensor which collects hyperspectral data in both the visible and SWIR wavelengths (380-2500 nm) and will succeed the AISA Eagle and Hawk sensors onboard the NERC Airborne Research and Survey Facility (ARSF) airplane (for further details see <http://arsf.nerc.ac.uk/instruments/aisafenix.asp>).

The specifications for the sensors employed in this study and justification for the use of these particular instruments is provided in detail in Chapter 8 (Appendix – Supplementary Methods). Table 7.1 in Chapter 7 also summarises relevant recently launched or forthcoming instruments for the remote sensing of inland waters.

## **2.4 Principles of light in water**

The spectral characteristics of water bodies are determined by a combination of factors, including the radiation incident to the water surface, water surface roughness, air-water interface, in-water optical properties, and the angle of observation and illumination, with bottom reflectance an additional consideration in shallow waters (Campbell, 2006). The spectral properties, or colour, of the water body are determined largely by scattered and reflected radiation within the water itself, and this is known as volume reflection (Campbell, 2006). Water colour is also a result of wavelength-dependent absorption, while the signals measured by remote sensing are derived from the backscattered photons that exit the water column. More formally, when light penetrates the water column as downwelling irradiance ( $E_d$ ), it is influenced by the absorption ( $a$ ,  $m^{-1}$ ) and scattering ( $b$ ,  $m^{-1}$ ) processes of pure water itself. Additionally, absorption, scattering, reflection and diffraction of  $E_d$  occurs by the optically active constituents in the water (i.e. suspended and dissolved particulate matter) (Mobley,

1994, Kirk, 1994). The interaction of these processes in the first “penetration depth” or upper layer of the water column is the focus of remote sensing (Gordon et al., 1975).

#### **2.4.1 Optically Active Constituents**

The optically active constituents (OACs) vary depending on the water body. For instance, in open ocean waters (often termed “Case 1” waters), the primary OACs are pure water itself and phytoplankton (and associated by-products). However, in inland and coastal waters (often termed “Case 2” waters), the water is more optically complex with the primary OACs including pure water, phytoplankton, CDOM (also known as humic substances, yellow substance or Gelbstoff) and tripton (minerals and detritus). Therefore, the optical properties of ocean waters, by definition, primarily depend on, and are related to, the corresponding chlorophyll concentration in the water (Morel & Maritorena, 2001). For example, the following well-documented relationship between particulate attenuation at 660 nm [ $c_p(660)$ ] and Chl-*a* concentrations in ocean waters is shown in Figure 2.1 (Loisel & Morel, 1998). This linear relationship emphasises that the optically active particles in oceans are primarily comprised of phytoplankton (Chl-*a*), and therefore that light attenuation is almost entirely related to variations in the size, abundance, pigmentation and composition of phytoplankton. It is thus relatively straightforward to develop remote sensing models for ocean waters that relate optical properties (e.g., scattering, absorption or reflectance) to Chl-*a*. Due to their more complex nature, it is acknowledged that inland waters have more demanding requirements for water constituent retrieval algorithms (IOCCG, 2000). In fact, it has been acknowledged that many single band Chl-*a* retrieval algorithms for inland waters do not enable distinction between phytoplankton-rich and sediment-rich waters, and many misinterpret CDOM as Chl-*a* (Kutser, 2009).

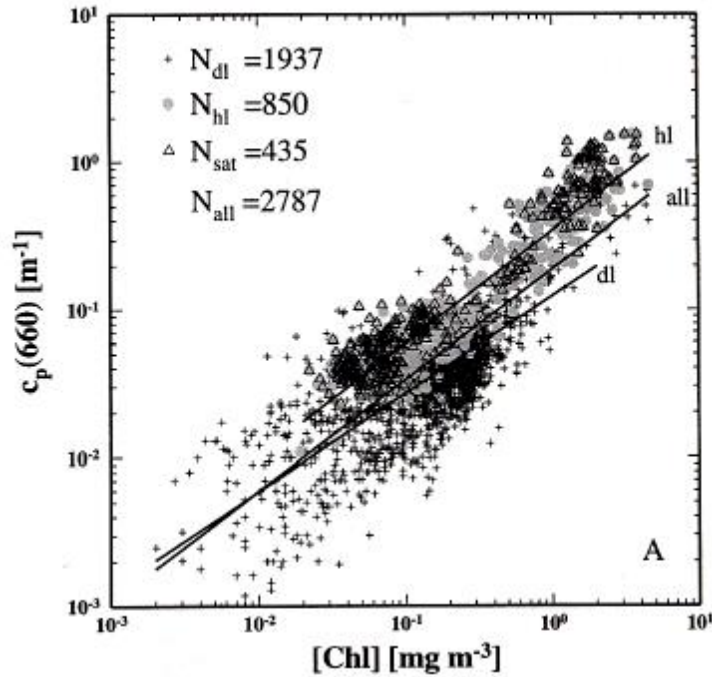


**Figure 2.1** Particulate attenuation [ $c_p(660)$ ] as a function of Chl-*a* concentration in ocean waters (Loisel & Morel, 1998).

#### 2.4.2 Inherent and Apparent Optical Properties

The inherent optical properties (IOPs) of the in-water constituents fundamentally include the absorption coefficient [ $a(\lambda)$ ,  $\text{m}^{-1}$ ] and volume scattering function [ $\beta(\theta)$ ,  $\text{m}^{-1}\text{sr}^{-1}$ ]. Other IOPs, including the scattering coefficient [ $b(\lambda)$ ,  $\text{m}^{-1}$ ], backscattering coefficient [ $b_b(\lambda)$ ,  $\text{m}^{-1}$ ] and the coefficient of beam attenuation [ $c(\lambda)$ ,  $\text{m}^{-1}$ ], provide useful information about the underwater light climate and can be defined in terms of  $a(\lambda)$  and  $\beta(\theta)$ . By definition, the IOPs are the optical properties of water that are independent of the ambient light field (Preisendorfer, 1976). When light enters the water column photons are removed from its path by absorption, whereby the photon energy is converted to another form such as heat or the energy contained in a chemical bond (Mobley, 1994). Total  $a(\lambda)$  is defined as the sum of absorption by particulate and dissolved constituents and water itself. Light is also scattered by suspended particles, whereby the photon changes its direction and/or energy (Mobley, 1994). Scattering is described by the volume scattering function (VSF),  $\beta(\theta)$ , or the angular dependence,  $(\theta)$ , of scattered light from an incident unpolarised beam (Sullivan et al., 2013). The scattering coefficient [ $b(\lambda)$ ] is commonly defined as a measure of the total magnitude of scattered light (without regard to its angular distribution), while  $b_b(\lambda)$  is defined as the

total light scattered in the backwards direction. More specifically, the scattering coefficient,  $b(\lambda)$ , is the integrated VSF from 0 to  $\pi$  radians ( $0^\circ$  to  $180^\circ$ ):

$$b(\lambda) = 2\pi \int_0^\pi \sin(\theta)\beta(\theta)d\theta \quad (2.1)$$

Likewise, the backscattering coefficient,  $b_b(\lambda)$ , is the integral of the VSF in the backwards direction from  $\pi/2$  to  $\pi$  ( $90^\circ$  to  $180^\circ$ ):

$$b_b(\lambda) = 2\pi \int_{\pi/2}^\pi \sin(\theta)\beta(\theta)d\theta \quad (2.2)$$

The absorption and backscattering processes are wavelength dependent, and according to Beer's Law, these properties can be expressed as a function of each OAC in the water column:

$$a(\lambda) = a_w(\lambda) + a_{ph}(\lambda) + a_{NAP}(\lambda) + a_{CDOM}(\lambda) \quad (2.3)$$

$$b_b(\lambda) = b_{b,w}(\lambda) + b_{b,ph}(\lambda) + b_{b,NAP}(\lambda) \quad (2.4)$$

where  $a_w(\lambda)$  is absorption by pure water,  $a_{ph}(\lambda)$  is absorption by phytoplankton,  $a_{NAP}(\lambda)$  is absorption by non-algal particles (tripton) and  $a_{CDOM}(\lambda)$  is the absorption by CDOM. Likewise,  $b_{b,w}(\lambda)$  is backscattering by pure water,  $b_{b,ph}(\lambda)$  is backscattering by phytoplankton and  $b_{b,NAP}(\lambda)$  is backscattering by non-algal particles (tripton). It is generally assumed that CDOM is a non-scattering component.

The sum of  $a(\lambda)$  and  $b(\lambda)$  is the beam attenuation coefficient [ $c(\lambda)$ ], or the total light attenuated in the water column, via the following equation:

$$a(\lambda) + b(\lambda) = c(\lambda) \quad (2.5)$$

The mass-specific representations, or specific inherent optical properties (SIOPs), are essentially the IOP per unit of constituent, and can be derived from measured values of IOPs and the measured concentrations of water constituents. The most commonly applied SIOPs for the purposes of remote sensing constituent retrievals and bio-optical models include  $a^*_{ph}(\lambda)$  (Chl-*a* specific absorption coefficient,  $m^2 \text{ mg}^{-1}$ ),  $b^*_p(\lambda)$  (specific particulate scattering coefficient,  $m^2 \text{ g}^{-1}$ ) and  $b^*_{bp}(\lambda)$  (specific particulate backscattering coefficient,  $m^2 \text{ g}^{-1}$ ), and these are derived from Chl-*a* and total suspended matter (TSM) concentrations ( $\text{mg m}^{-3}$  and  $\text{mg L}^{-1}$ , respectively) as follows:

$$a^*_{ph}(\lambda) = a_{ph}(\lambda)/[Chl - a] \quad (2.6)$$

$$b^*_p(\lambda) = b_p(\lambda)/[TSM] \quad (2.7)$$

$$b_{bp}^*(\lambda) = b_{bp}(\lambda)/[TSM] \quad (2.8)$$

Absorption and scattering by dissolved and particulate matter are key processes that influence the spectral shape and magnitude of the water-leaving reflectance signal measured by Earth-observing satellites (Morel & Prieur, 1977, Kirk, 1994, Mobley, 1994). Therefore, knowledge of the IOPs is of great importance towards furthering radiative transfer studies and the development of analytically-based inversion algorithms for aquatic remote sensing. More specifically,  $R_{rs}(0+, \lambda)$  can be related to the IOPs via the following relationship, where  $f$  is an experimental constant dependent on the light field and volume scattering function and  $Q$  is a parameter accounting for geometrical attenuation of light exiting the water column (Gordon et al., 1975, Morel & Gentili, 1991, Dall'Olmo & Gitelson, 2005):

$$R_{rs}(0+, \lambda) \propto \frac{f}{Q} \frac{b_b(\lambda)}{a(\lambda) + b_b(\lambda)} \quad (2.9)$$

Variability in  $R_{rs}(\lambda)$  is also controlled by the particulate backscattering ratio ( $\tilde{b}_{bp}$ ):

$$\tilde{b}_{bp} = b_{bp}(\lambda)/b_p(\lambda) \quad (2.10)$$

where  $b_{bp}$  and  $b_p$  are the particulate scattering and backscattering coefficients, respectively (Mobley et al., 2002, Lubac & Loisel, 2007).  $\tilde{b}_{bp}$  is generally calculated using  $b_{bp}$  and  $b_p$  at 532 nm, however research in a range of waters (inland, coastal and ocean) has determined that this ratio should be constant at all wavelengths (i.e. no spectral dependence) (Whitmire et al., 2007). The  $\tilde{b}_{bp}$  is defined as the proportion of light scattered in the backwards direction, which can also provide information on the bulk refractive index and particle size and composition of the suspended particulate material (Boss et al., 2004).

In contrast to the IOPs, the apparent optical properties (AOPs) are dependent on the ambient light field. AOPs are measurements provided by remote sensing instruments, whereas IOPs can be either measured *in situ* or in the lab (Lindell et al., 1999). The AOPs of interest to aquatic remote sensing typically include spectral irradiance reflectance [ $R(z, \lambda)$ ], remote sensing reflectance [ $R_{rs}(0+, \lambda)$ , sr<sup>-1</sup>] and water-leaving reflectance [ $\rho_w(\lambda)$ , sr<sup>-1</sup>]. Spectral irradiance reflectance was most commonly used in early ocean colour remote sensing, and is defined as the ratio of spectral upwelling [ $E_u(z, \lambda)$ ] to downwelling [ $E_d(z, \lambda)$ ] plane irradiances (Mobley, 1994):

$$R(z, \lambda) = \frac{E_u(z, \lambda)}{E_d(z, \lambda)} \quad (2.11)$$

However,  $R_{rs}$  is more commonly applied in recent literature to ocean and inland water remote sensing, as it is less sensitive than  $R$  to environmental conditions (e.g. sun angle or sky conditions) (Mobley, 1994). Spectral remote sensing reflectance can be derived as the ratio between the water-leaving or upwelling radiance from the water surface ( $L_w$ ) to downwelling solar irradiance ( $E_d$ ) (Mobley, 1994, Lindell et al., 1999, Mueller et al., 2003):

$$R_{rs}(0+, \lambda, \theta \in \Omega_{FOV}; \theta_o) = \frac{L_w(0+, \lambda, \theta, \phi \in \Omega_{FOV}; \theta_o)}{E_d(0+, \lambda; \theta_o)} \quad (2.12)$$

where  $\lambda$  is wavelength,  $\theta$  is the zenith angle,  $\theta_o$  is the solar zenith angle,  $\phi$  is the azimuth angle (where the sun's azimuth is  $\phi_o=0$ ), and  $\Omega_{FOV}$  is the solid-angle field of view (FOV) of the radiometer. The strict definition of  $R_{rs}$  may also include the subtraction of reflected skylight, and is measured with adherence to a defined geometry where ( $\theta \approx 45^\circ$  and  $\phi = 135-225^\circ$  solar azimuth) (Pers. Comm. Hunter, P.D.). The reflected skylight error term assumes the water to be totally absorbing ("black") at  $\lambda = 750$  nm, and if it is further assumed that this term is not wavelength dependent (i.e. "white") then a simple offset correction can be described by (Mueller et al., 2003):

$$R_{rs}(0+, \lambda, \theta \in \Omega_{FOV}; \theta_o) = R'_{rs}(0+, \lambda, \theta \in \Omega_{FOV}; \theta_o) - R'_{rs}(0+, 750, \theta \in \Omega_{FOV}; \theta_o) \quad (2.13)$$

Especially over turbid waters, sun glint and cloud radiance can contribute a non-zero value to  $R_{rs}(0+, 750, \theta \in \Omega_{FOV}; \theta_o)$ . However, this simple white-offset correction is presently not recommended for general use by the NASA Ocean Optics Protocols (Mueller et al., 2003).

Water-leaving reflectance can then be related to remote sensing reflectance by a simple factor of pi:

$$R_{rs}(\lambda) = \rho_w(\lambda)/\pi \quad (2.14)$$

Other AOPs include the remote-sensing ratio ( $RSR$ ), diffuse attenuation coefficients ( $K$  functions) and mean cosines ( $\bar{\mu}$ ) (Mobley, 1994).

## 2.5 Remote sensing algorithm types for extraction of in-water constituents

The retrieval of in-water constituents from radiometric measurements is achieved through the use of a model (or algorithm) that empirically relates or physically inverts the measured radiances or reflectances to derive IOPs and/or constituent

concentrations. In general, there are two main approaches for algorithms that extract concentrations of in-water constituents from remotely sensed data: empirical (and semi-empirical) and semi-analytical (or analytical), and these are described in further detail below. A summary of empirical procedures for retrieval of biogeochemical parameters in inland and coastal waters is provided in Matthews (2011), and a review of retrieval algorithms for optically deep and complex waters (2006-2011) can be found in Odermatt et al. (2012).

### 2.5.1 Empirical, semi-empirical and semi-analytical algorithms

The most straightforward empirical method is to correlate the value of a single spectral band with the measured parameter of interest, deriving an algorithm by simple regression. However, single channel algorithms tend to be less effective in inland waters, where the same band may be used to retrieve more than one parameter (e.g. phytoplankton pigments and suspended sediments) (Kutser, 2009).

Another common empirical approach is the band-ratio, where a ratio of two reflectance bands ( $R_i$ ) are used to estimate a parameter,  $p$ , where  $\alpha$ ,  $\beta$  and  $\gamma$  are regression coefficients (IOCCG, 2000):

$$p = \alpha \frac{R_1^\beta}{R_2} + \gamma \quad (2.15)$$

A band-ratio algorithm employing  $R_1=665$  and  $R_2=709$  has proved effective for retrieval of Chl-*a* concentrations in eutrophic inland waters (Mittenzwey et al., 1992, Dekker, 1993, Gons et al., 2002, Gurlin et al., 2011). Empirical algorithms have been widely used and are relatively simple to derive and apply, generally producing robust results for the particular lake studied. In fact, on occasion they have been found to be more robust than complex analytical models, e.g. (Ogashawara et al., 2013).

Semi-empirical or semi-analytical models are a variation which employ prior knowledge of the optical properties of the parameter(s) of interest to optimise empirical models. Empirical and semi-empirical algorithms do not require detailed information on the IOPs, which is often not available or not measured *in situ*. For instance, the Ocean Chlorophyll 4 (OC4) algorithm and its predecessors developed for SeaWiFS can be considered semi-empirical because they do not involve any knowledge or assumptions about the IOPs, but the choice of wavelengths used for the maximum band ratio is based on physics rather than statistics (O'Reilly et al., 1998). An example of a semi-analytical algorithm is the Chl-*a* retrieval algorithm developed by Gons et al. (Gons, 1999, Gons et al., 2002, Gons et al., 2005), which has been further adapted by

Simis et al. (2005) for the retrieval of PC in inland waters. The Gons et al. (2005) semi-analytical algorithm is a band ratio approach, but it employs knowledge of the relationship between IOPs and  $R_{rs}(\lambda)$ , and estimates  $a_{ph}(665)$  rather than Chl-*a* directly. Pigment concentration is then calculated using knowledge of the Chl-*a* specific absorption coefficient.

### 2.5.2 Other algorithm approaches

Other algorithms for the retrieval of Chl-*a* concentrations have focused on using peaks in the spectrum caused by chlorophyll fluorescence or phytoplankton scattering (Matthews, 2011). Examples of these have included the Maximum Peak Height algorithm (MPH) (Matthews et al., 2012, Matthews & Odermatt, 2015), Maximum Chlorophyll Index (MCI) (Gower et al., 2005), Fluorescence Line Height (FLH) (Gower et al., 1999) and the Reflectance Line Height (RLH) or Scattered Line Height (SLH) algorithms (Dierberg & Carriker, 1994, Yacobi et al., 1995, Schalles et al., 1998). The FLH algorithm, for example, measures height of the peak at 685 nm from a linear baseline between points on either side of the peak (Dierberg & Carriker, 1994, Giardino et al., 2005).

More recently, artificial neural network type approaches have been investigated for coastal and inland waters [e.g. Case 2 Regional (Doerffer & Schiller, 2007), Free Universität Berlin (FUB/WeW) (Schroeder et al., 2007), Eutrophic Lake and Boreal Lake (Doerffer & Schiller, 2008), CoastColour (Brockmann Consult, 2014), Regional neural network for rias Babcas (NNRB) (Gonzalez Vilas et al., 2011, Spyrakos et al., 2011) and multilayer perceptron neural network (MLPN) (Ioannou et al., 2013) processors]. Neural network type algorithms typically require a large training set of IOPs and AOPs as input and provide IOPs and/or concentrations as the output (Doerffer & Schiller, 2007, Schroeder et al., 2007, Doerffer & Schiller, 2008). Some of these are now available as plug-ins in the widely used BEAM software (Brockmann Consult), providing ease and accessibility of these more complex algorithms. However, these approaches have not been trained using data from lakes, therefore their utility in inland waters might be limited as a result.

### 2.5.3 Inversion of bio-optical models (analytical algorithms)

It is important to have knowledge of the variability of spectral characteristics of lakes in order to parameterise bio-optical models, which is another method of extracting water quality parameters from satellite or airborne water reflectance signatures. Bio-

optical models can be used to model the AOPs as a function of the IOPs, thus generating a synthetic dataset from which algorithms can be derived to extract the water quality parameter(s) of interest (either semi-empirically, semi-analytically or analytically) (Kirk, 1994). The semi-analytical (or analytical) approach models the water-leaving reflectance [ $\rho(0^+, \lambda)$ ] or remote sensing reflectance [ $R_{rs}(0^+, \lambda)$ ] in terms of the IOPs through radiative transfer modelling (Dekker et al., 2001, Matthews, 2011). The so-called ‘forward’ model derives  $\rho(0^+, \lambda)$  from the IOPs using an approximation of the radiative transfer equation (RTE), called the reflectance approximation (Morel & Prieur, 1977, Zaneveld, 1995), or through direct solution of the RTE using models such as Hydrolight (Mobley, 1994). The ‘inverse’ model conversely solves for the IOPs and concentrations of in-water OACs from  $\rho(0^+, \lambda)$  measured by satellite, airborne or *in situ* methods. Inverse bio-optical models can be solved via optimisation or multiple nonlinear regression procedures to produce semi-analytical or inversion algorithms (IOCCG, 2000). Inversion models have been commonly developed for Chl-*a* retrievals in ocean and coastal waters, e.g. the Quasi-Analytical Algorithm (QAA) (Lee et al., 2002), Garver–Siegel–Maritorena Model (GSM) (Maritorena et al., 2002) and the adaptive Linear Matrix Inversion Method (aLMI) (Brando et al., 2012). However, inversion methods have also been applied to inland waters, e.g. Modular Image Processing system (MIP) (Heege & Fischer, 2004). In general, the applicability of physics-based analytical approaches is reliant on appropriate parameterisation, and this requires *a priori* knowledge of the SIOPs for the optical water type of interest.

## 2.6 Remote sensing of phytoplankton pigments

Several previous studies have applied remote sensing to estimate bulk phytoplankton biomass (chlorophyll-*a* concentration) in lakes, using various algorithms and sensor types. The phytoplankton pigment Chl-*a* is the most commonly derived parameter in remote sensing of lakes, as it provides a proxy for bulk phytoplankton biomass. Apart from Chl-*a*, there is an increasing body of literature interested in the remote sensing of phycocyanin (PC) as a bio-marker pigment for cyanobacteria. Although PC is found in other phytoplankton phyla (e.g. cryptophytes), there is increasing evidence that PC can be a proxy for cyanobacteria biomass [e.g. (Horváth et al., 2013a)]. An overview of literature on the remote sensing retrieval of phytoplankton pigments Chl-*a* and PC is provided below.

### **2.6.1 Phytoplankton pigments and optical discrimination**

The primary pigment used as a general proxy for phytoplankton biomass is chlorophyll-*a* (Chl-*a*). This is a light-harvesting pigment that is common to nearly all taxonomic groups, therefore it is a bulk signal unable to discriminate between phytoplankton taxa. However, phytoplankton contain a range of accessory pigments in addition to Chl-*a*, including carotenoids and phycobiliproteins, and many of these are specific to certain algal taxa (Rowan, 1989, Richardson, 1996). For example, peridinin (dinoflagellates), alloxanthin (cryptophytes), fucoxanthin and diadinoxanthin (diatoms), and zeaxanthin and phycobiliproteins (cyanobacteria) are potential biomarker pigments for the respective phytoplankton functional groups (Jeffrey et al., 1997). A study by Hunter et al. (2008b) was able to discriminate four phytoplankton groups (brown, green, blue-green and red) in laboratory experiments after measuring their spectral reflectance signatures, and the spectral signatures of 6 freshwater phytoplankton groups are shown in Figure 2.2. In ocean waters, the phytoplankton absorption spectra has been found to vary in magnitude and spectral shape depending on pigment composition (Sathyendranath et al., 1987, Hoepffner & Sathyendranath, 1991) and cell size (Ciotti et al., 2002). In light of these findings, for example, Sathyendranath et al. (2004) developed a bio-optical algorithm for distinguishing diatom populations in the North West Atlantic Ocean, although similar research has yet to be done for lakes.

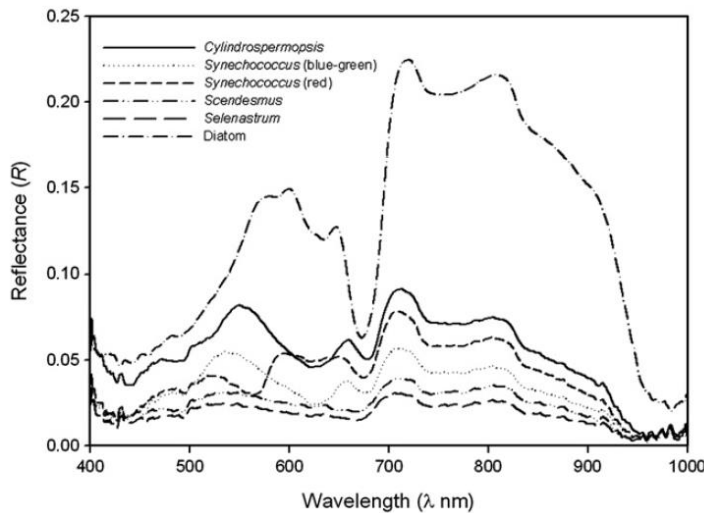


**Figure 2.2** Hyperspectral reflectance signatures of six phytoplankton genera examined in laboratory mesocosm experiments with broadly equivalent Chl-*a* concentrations. Reproduced from (Hunter et al., 2008b).

However, apart from Chl-*a*, phycocyanin (PC) is the most commonly retrieved pigment by remote sensing, and has proved effective in distinguishing potentially toxic cyanobacteria in inland waters (Dekker, 1993, Schalles & Yacobi, 2000, Vincent et al., 2004, Simis et al., 2005, Simis et al., 2007, Hunter et al., 2008a, Mishra et al., 2009, Hunter et al., 2010, Mishra et al., 2013, Ogashawara et al., 2013, Mishra & Mishra, 2014). Phycocyanin is a phycobiliprotein, which is a pigment-protein, amino acid storage complex common to cyanobacteria, Rhodophyta and some cryptophytes (Williams et al., 1980, Horváth et al., 2013a). A reflectance “trough” at approximately 620 nm distinguishes this pigment, and is a result of strong absorption by PC at this wavelength. An overview of remote sensing of cyanobacteria and other intense phytoplankton blooms in inland waters is also provided by Kutser (2009).

The benefit of distinguishing phytoplankton functional groups by their optical properties is that taxa-specific bio-optical models can then be developed for application to remotely sensed data for mapping and quantifying both phytoplankton abundance and composition (Gege, 1998, Matthews, 2011). In terms of lake water quality and management, this would clearly be beneficial if blooms of known potentially toxic cyanobacteria genera could be discriminated from non-toxic phytoplankton blooms.

### 2.6.2 Remote sensing of chlorophyll-*a*

Single band Chl-*a* algorithms for satellite sensors [e.g. Landsat and AVHRR (Advanced Very High Resolution Radiometer)] have proven to work in inland waters

when there have been very high concentrations of phytoplankton (Galat & Verdin, 1989, Kahru et al., 1993, Kahru & Mitchell, 2000). In such situations where cyanobacteria are in sufficiently high concentrations, the optical properties of the water are almost completely determined by phytoplankton at all wavelengths of the visible and near infrared (NIR) portions of the spectrum (Kutser, 2009). Thus, in these cases a single band Chl-*a* retrieval algorithm may be sufficient.

However, band ratio algorithms for Chl-*a* tend to be more robust than single band algorithms. Band ratio algorithms are less sensitive to interference from other optically active constituents in the water column and artefacts resulting from the incomplete atmospheric correction (assuming such artefacts are spectrally neutral over the wavelengths used in the ratio). Blue-green band ratios are operationally employed for Chl-*a* retrieval from ocean colour satellite instruments (e.g. MODIS/MERIS OC3/4 algorithms), however these have had limited success in inland waters (George & Malthus, 2001, Kutser, 2009). The ratio of reflectance at approximately 700 nm to 670 nm has been more widely used to estimate Chl-*a* concentrations for inland waters, with some studies showing especially strong correlations between modelled and measured Chl-*a* concentrations (Mittenzwey et al., 1992, Gitelson et al., 1993b, Dierberg & Carriker, 1994, Gons, 1999, Flink et al., 2001, Harma et al., 2001, Kallio et al., 2001, Ammenberg et al., 2002, Gons et al., 2002, Koponen et al., 2002, Kallio et al., 2003, Gons et al., 2005, Jiao et al., 2006, Menken & Brezonik, 2006, Duan et al., 2007, Hunter et al., 2008a, Hunter et al., 2009, Hunter et al., 2010).

Additionally, various three-band or multiple-band ratio approaches (Mittenzwey et al., 1991, Gitelson et al., 1993b, Harma et al., 2001, Koponen et al., 2002, Dall'Olmo et al., 2003, Dall'Olmo & Gitelson, 2005, Zimba & Gitelson, 2006, Gitelson et al., 2008, Gitelson et al., 2009, Moses et al., 2009, Le et al., 2009b) have proved effective for estimating Chl-*a* concentration in coastal and inland waters. In particular, indices using band differences have retrieved accurate concentrations of Chl-*a* in turbid productive coastal waters, e.g. the Normalized Difference Chlorophyll Index (NDCI) (Mishra & Mishra, 2012). These band difference indices build on similar widely-applied algorithms for detection of terrestrial vegetation [e.g. NDVI (Normalized Difference Vegetation Index)]. The NDCI is explored in Chapter 6 and further detail on this algorithm is supplied in Chapter 8 (Appendix – Supplementary Methods).

Another technique presented in the literature includes using the first derivative of reflectance at a specified wavelength to estimate Chl-*a* concentrations. Derivative

transformations of reflectance spectra have been applied to inland waters in several studies, using wavelengths of 620, 638 and 661 nm (Malthus & Dekker, 1995), 690 nm (Rundquist et al., 1996, Han & Rundquist, 1997) and 429 and 695 nm (Fraser, 1998) and 670 nm (Hunter et al., 2008b).

Supervised classification methods have also been employed for Chl-*a* retrieval (Koponen et al., 2002, Subramaniam et al., 2002, Huang et al., 2014a). Classification methods have been based on, for example, the magnitude of the 490-channel reflectance and the spectral shape of  $R_{rs}$  at 443, 490 and 555 nm (Subramaniam et al., 2002) or more operational water classification schemes such as the Water Quality Classification of Inland Waters in Finland and the Organisation for Economic Cooperation and Development Lake Classification Scheme (Koponen et al., 2002).

More complex neural network type algorithms (Schiller & Doerffer, 1999, Huang & Lou, 2003, Pozdnyakov et al., 2005, Doerffer & Schiller, 2007, Doerffer & Schiller, 2008) have been further used to map and quantify Chl-*a*. One of the most common types of neural networks for remote sensing is the Multi-Layer Perceptron (MLP), which might consist of layers including radiances at certain wavelengths, an internal layer and a layer indicating the number of parameters (Pozdnyakov et al., 2005). Each neuron in a network is connected to all neurons in the other layers and assigned an associated weight. The MERIS Case 2 coastal water algorithm is based on a neural network which relates the bi-directional water leaving radiance reflectances with IOPs (Doerffer & Schiller, 2007). The neural network is trained with simulated reflectances based on a large dataset from European waters.

Bio-optical modelling approaches, where reflectance spectra are simulated from measurements of the IOPs and OACs, are an increasingly common analytical method applied to remote sensing of phytoplankton. Such models are described in detail by Pierson and Stromback (2001), however there have been many recent advances particularly with bio-optical inversion algorithms. For instance, a well-cited algorithm was developed for Chl-*a* retrieval in ocean waters called the Quasi-Analytical Algorithm (QAA) (Lee et al., 2002). Since its development, the QAA has been validated in inland waters as well, including Lake Taihu (Le et al., 2009a), Lake Poyang (Huang et al., 2014b) and Mississippi aquaculture ponds (Mishra et al., 2014). A similar bio-optical inversion algorithm has been proposed for lakes called the IOP Inversion Model of Inland Waters (IIMIW), which retrieved Chl-*a* with a mean relative error of 22% in Indiana Reservoirs (Li et al., 2013). In general, however, there remains

very limited validation of inland water bio-optical algorithms with independent datasets.

### 2.6.3 Remote sensing of phycocyanin

While limited in comparison to Chl-*a*, PC retrieval algorithms are of increasing interest to inland water remote sensing for the monitoring of potentially toxic cyanobacteria blooms. A recent performance review of empirical PC algorithms is presented in Ogashawara et al. (2013).

As for Chl-*a*, reflectance band-ratios or band differences have proven effective for PC retrieval in lakes. One of the earliest approaches for estimating PC concentrations in lakes was conducted by Dekker (1993) using a semi-empirical baseline algorithm relating  $R_{rs}$  at 600, 648 and 624 nm. Schalles and Yacobi (2000) developed a band-ratio algorithm for the hypereutrophic Carter Lake, where a ratio of reflectance for the peak at 650 nm and trough at 625 nm was an effective predictor of phycocyanin concentration. Vincent et al. (2004) applied a spectral ratio model for the retrieval of phycocyanin in the western basin of Lake Erie. Mishra et al. (2009) adapted the spectral band ratio algorithm by using reflectance at the wavelengths 700 and 600 nm, in order to reduce sensitivity of the algorithm to chlorophyll absorption. This band ratio was further modified in Ogashawara et al. (2013), using  $R_{rs}$  at 724 and 600 nm. In Lac des Allemands, Dash et al. (2011) developed an empirical inversion algorithm to estimate PC concentration from  $R_{rs}$  at 510.6 and 556.4 nm using the Oceansat-1 satellite Ocean Colour Monitor (OCM).

Building on the band-ratio approach and the Gons et al. (2002, 2005) algorithm for Chl-*a* retrieval, Simis et al. (2005) developed a semi-analytical algorithm for PC retrieval for the band settings of MERIS. This algorithm is tested in Chapter 5 and presented in detail in Chapter 8 (Appendix – Supplementary Methods). Again, this algorithm combines the empirical and analytical approaches, through using the band ratio (709:620 nm) and knowledge of the (specific) inherent optical properties.

A study on the Laurentian Great Lakes used the change in spectral shape at 681 nm was to distinguish cyanobacteria blooms (Wynne et al., 2008). Several studies have also employed various three-band empirical algorithms for PC retrieval (Hunter et al., 2008b, Hunter et al., 2010, Song et al., 2013, Mishra & Mishra, 2014). For example, Hunter et al. (2010) used the difference between the inverse of  $R_{rs}$  at 615 and 600 nm, multiplied by  $R_{rs}$  at 725 nm, which is an approach based on the medium-independent

model for pigment retrieval developed by Dall’Olmo (2003). Other approaches for PC retrieval have included a four-band semi-analytical algorithm (Le et al., 2011), and a three-band and baseline algorithm (Li et al., 2012). More recently, a PC Index (PCI) algorithm was developed by Qi et al. (2014), which uses  $R_{rs}(620)$  normalised against a linear baseline between  $R_{rs}(560)$  and  $R_{rs}(665)$ .

The QAA algorithm for Chl-*a* retrieval developed by Lee et al. (2002) has also been adapted to estimate PC concentrations. Becker et al. (2009) used non-negative least squares fitting to total absorption calculated from the QAA and published PC absorption spectra to estimate PC concentrations in Lakes Erie and Ontario. Mishra et al. (2013) also extended the QAA to retrieve PC absorption at 620 nm, based on the assumptions that  $a_{ph}(620)$  is approximately equal to the sum of Chl-*a* and PC at this wavelength and that  $a_{ph}(665)$  is predominately due to Chl-*a*. An alternative bio-optical inversion model that was developed for estimation of Chl-*a* concentration (IIMIW) (Li et al. 2013) was also further adapted for PC retrieval by Li et al. (2015). The adaptations to the IIMIW partitioned non-water absorption into contributions from phytoplankton, CDOM and PC, and this model in particular was found to be a good predictor for low PC concentrations in central Indiana reservoirs ( $\leq 50 \text{ mg m}^{-3}$ ) (Li et al., 2015). However, these bio-optical inversion methods for PC retrieval have received little to no validation with independent datasets, therefore it is unknown how transferable these algorithms are to other inland water types. The bio-optical inversion models by Mishra et al. (2013) and Li et al. (2015) are tested in Chapter 5 and outlined in further detail in Chapter 8 (Appendix – Supplementary Methods).

## **2.7 Considerations for the remote sensing of inland waters**

In addition to the optical complexity of inland waters, several other factors present obstacles towards the progression of remote sensing of inland waters. These are mainly to do with either the inherent nature of inland water bodies or limitations of instrument capability and processing. A recent review of the challenges and recommendations for coastal and inland water colour remote sensing is presented by Mouw et al. (2015). Similarly, Palmer et al. (2015b) presents an editorial for a special issue in Remote Sensing of Environment, which outlines the challenges and progress to date for the remote sensing of inland waters.

### **2.7.1 Satellite mission capability**

The size and shape of lakes is frequently too small for the use of currently available satellite sensors. Many satellite-based instruments were developed for ocean colour monitoring (e.g. MERIS and MODIS), therefore the spatial resolution is often too coarse (>300 m). Alternatively, satellite instruments developed for terrestrial applications (e.g. Landsat) may retrieve turbidity/total suspended matter, but have insufficient spectral and radiometric resolution for retrieval of phytoplankton pigments in inland waters. With the exception of MERIS and MODIS, most past and current satellite sensors do not measure over a large spectral region between 555 and 670 nm, which also does not capture the PC absorption peak at ~620 nm (Mouw et al., 2015). Many instruments on satellite platforms also lack sufficient revisit frequency to capture the ephemeral dynamics of inland waters. An airborne survey over Barton Broad (Norfolk, UK) demonstrated the marked variability in cyanobacteria spatial distribution over a matter of mere hours (Hunter et al., 2008a). However, with the exception of geostationary satellites, few instruments are available with a frequent revisit time in order to capture these dynamics in lakes. Furthermore, the balance between instrument radiometric sensitivity and dynamic range is a challenge to inland water remote sensing. Even instruments with high signal-to-noise ratios (SNR) tend to saturate over highly turbid waters (Mouw et al., 2015).

### **2.7.2 Geography of inland waters**

Another factor affecting inland water remote sensing is the proximity of land, which is also linked to lake size and shape. Firstly, the pixel may include both water, land and/or emerging vegetation (i.e. pixel contamination or mixed pixels), especially for coarse resolution data. Secondly, the adjacency effect may mask pixels adjacent to land or clouds. Pixels adjacent to land or clouds are affected by stray light contamination from these “bright” features, which can present difficulty for atmospheric correction of these pixels (Santer & Schmechtig, 2000, Meister & McClain, 2010). Recent studies have focused on developing approaches to correct for or minimise the adjacency effect [e.g. (Kiselev et al., 2015, Sterckx et al., 2015)].

In shallow waters, the contribution of bottom reflectance is an additional consideration for aquatic colour remote sensing (Lee et al., 1994, Maritorena et al., 1994, Lee et al., 1998). Therefore, algorithms developed for optically deep waters are typically not suitable for shallow waters (Mouw et al., 2015). Bottom properties are

typically heterogeneous within inland waters, which adds further complexity to quantifying the contribution from bottom reflectance.

### **2.7.3 Algorithms**

It is widely acknowledged that the retrieval algorithms for biogeochemical parameters from ocean waters break down over coastal and inland waters (IOCCG, 2000). The recent algorithm developments for inland waters are lacking in reproducibility, with multiple approaches and typically limited validation of algorithms with independent datasets. Algorithms tend to be dataset-, region- or sensor-specific, however further intercomparison exercises have been recommended to evaluate the applicability of current algorithms to certain water types and conditions (Mouw et al., 2015).

### **2.7.4 *In situ* data**

*In situ* data is required in order to develop or validate algorithms for retrieval of water quality parameters. In order to advance inland water remote sensing, it is therefore paramount to have coincident (S)IOP and biogeochemical data alongside collection of AOP data. However, such *in situ* datasets are scarce, and few adequately characterise the large range of inland water body types in order to provide independent validation of current in-water algorithms. Specifically, there is a present lack of information about variations in (S)IOPs, in terms of both seasonal, spatial and regional differences in these properties. These variations result in a degree of uncertainty in the retrieved water quality products. Therefore it has been recommended that efforts continue to characterise SIOPs, in particular, in optically complex waters (Mouw et al., 2015). This deficiency may be addressed in part by advances in *in situ* technology for measuring water column optical properties, with instruments that more accurately and reliably measure IOPs. Additionally, coincident *in situ* AOP data and aerosol vertical distribution measurements are required for the development and validation of atmospheric correction algorithms. The accuracy of satellite- or airborne- measured  $R_{rs}(\lambda)$  largely depends on improved atmospheric correction (Hu et al., 2013), therefore these *in situ* data are fundamental towards improving inland water remote sensing.

### **2.7.5 Atmospheric correction**

As over 90% of the light that reaches a satellite sensor over water derives from the atmosphere, the largest potential source of error and uncertainty in remote sensing

from airborne and spaceborne instruments is the residual error from atmospheric correction (IOCCG, 2010, Mouw et al., 2015). Ocean colour instruments may be atmospherically corrected using a variation of the “black-pixel” assumption, which is that  $R_{rs}$  in the NIR is negligible (i.e. water absorption is high) and therefore any NIR reflectance measured is atmosphere-derived (Gordon & Wang, 1994). However, inland waters have high concentrations of scattering materials, especially suspended particulate matter, which can contribute to  $R_{rs}$  in the NIR and therefore results in overcorrection (Siegel et al., 2000). As the short wave infrared (SWIR) wavelengths have a higher absorption coefficient than the NIR, SWIR bands have been proposed as an alternative for atmospheric correction (Wang & Shi, 2007, Aurin et al., 2013).

Furthermore, atmospheric correction is complicated by nearshore or inland concentrations of absorbing aerosols and gaseous emissions (Gordon, 1997). There is a lack of measurement of anthropogenic emissions, and these can vary significantly during a day (Tzortziou et al., 2015). Stray light contamination from nearby bright pixels (i.e. land or clouds) is another challenge to accurate atmospheric correction over inland water bodies (Santer & Schmechtig, 2000, Meister & McClain, 2010). The collection of *in situ* observations coincident with remote sensing data will provide a necessary step towards improvements in atmospheric correction, e.g. the Aerosol Robotic NETwork-Ocean Colour (AERONET-OC) series of photometers for incident surface measurements for SeaWiFS ocean colour data (Zibordi et al., 2009, Mouw et al., 2015).

### **2.7.6 Operational**

Lastly, Mouw et al. (2015) have recently identified that existing remote sensing capacity building efforts are still needed to better link data users and data providers. Presently, there is limited access to satellite data, with tailored products available for some regions, but further data and product access is required to advance inland water remote sensing. Several international organizations presently exist to further the use of remote sensing for management and observation of inland and coastal waters [see Table 5 in Mouw et al. (2015)]. However, with the aim of ultimately applying remote sensing towards operational water quality monitoring, increased data access, expanded user outreach and training and implementation of a more user-driven community are still needed.

## 2.8 Previous remote sensing studies of Lake Balaton

There have been relatively few remote sensing studies conducted on Lake Balaton to date. The earliest published use of satellite data on the lake was conducted by Buttner et al. (1987). This study used Landsat MSS data to retrieve Chl-*a* and suspended matter via simple empirical relationships between satellite-measured radiances and *in situ* water quality data. Other early studies were conducted using biogeochemical and *in situ* spectral irradiance measurements from Lake Balaton (1985, 1986 and 1988) in combination with various inland and coastal waters in the former USSR, Hungary, Bulgaria and Germany (Gitelson, 1993, Gitelson et al., 1993a, Gitelson et al., 1993b). Gitelson et al. (1993b) developed reflectance band ratio and empirical algorithms for retrieval of Chl-*a*, TSM and dissolved organic matter (DOM) concentrations in these waters, and used simulated Landsat-MSS data to test the accuracy of derived concentrations. This work provided some of the first maps of Chl-*a* and TSM spatial distribution over the Keszthely basin of Lake Balaton (Figure 2.3). These early results indicate the utility a trophic gradient for algorithm testing, as algorithms performed differently depending on trophic state. However, these studies by Gitelson et al. (1993) only used *in situ* reflectance and simulated satellite data, and serve as a basis for future studies using satellite-based platforms.

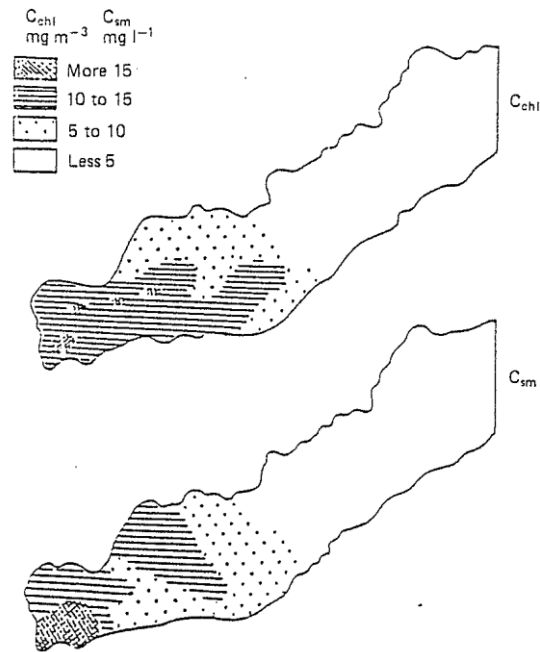


**Figure 2.3** Chl-*a* (top) and TSM (bottom) distribution maps for Lake Balaton in June 1988 as retrieved from simulated Landsat-MSS data. Reproduced from Gitelson et al. (1993b).

Subsequently, Sváb et al. (2005) used principal component analysis (PCA) to identify spectrally unique end-members, finding that spectral linear mixture modelling combined with multivariate regression analysis can estimate phytoplankton biomass. This study used coincident phytoplankton biomass and *in situ* and laboratory reflectance measurements, from which they simulated Landsat TM and Enhanced Thematic Mapper Plus (ETM+) data. Tyler et al. (2006) took this research the step further and derived estimates of Chl-*a* concentrations from Landsat TM imagery using a linear mixture modelling approach. These studies provided a foundation for using Landsat TM data to retrieve Chl-*a* concentrations in the context of high suspended sediment concentrations.

Additional remote sensing on Lake Balaton has included a recent meta-study by MacCallum and Merchant (2012), which used Lake Balaton as one of 258 large lakes to retrieve surface water temperatures from (Advanced) Along-track Scanning Radiometers (ATSR-2 and AATSR) imagery between 1995 and 2009.

Most recently, Palmer et al. (2015c) retrieved Chl-*a* concentrations in Lake Balaton using a 5-year time series of MERIS data. In this study, the Fluorescence Line Height (FLH) algorithm retrieved the most accurate Chl-*a* concentrations of the 6

algorithms tested. Using the FLH algorithm, Palmer et al. (2015a) undertook a study of phytoplankton phenology using 10 years of MERIS data to examine phytoplankton seasonality metrics. These papers formed part of a PhD thesis by Stephanie Palmer (Palmer, 2015), which further investigated atmospheric correction of MERIS data and the use of Ultraviolet Fluorescence Light detection and ranging measurements of water quality in Lake Balaton.

Lake Balaton is also now part of several ongoing European and global initiatives to further the remote sensing of inland waters, including Globolakes ([globolakes.stir.ac.uk](http://globolakes.stir.ac.uk)), Diversity 2 ([diversity2.info](http://diversity2.info)) and INFORM ([copernicus-inform.edu](http://copernicus-inform.edu)) projects.

These studies on Lake Balaton form the context to the August 2010 field campaign on Lake Balaton, which is the fundamental dataset used for the case study presented in this thesis. Further detail on this campaign is provided in Chapter 8 (Appendix – Supplementary Methods). Prior to this thesis, the optical properties of Lake Balaton have not been characterised. Thus, this thesis presents a novel study of the bio-geo-optical properties of Lake Balaton and their spatial variability and relationships. Secondly, this thesis provides an investigation of remote sensing of phytoplankton over a range of temporal, spatial and spectral scales, expanding upon the emergent base of literature for remote sensing of this optically complex shallow lake. Additionally, no prior testing of PC retrieval algorithms has been conducted on Lake Balaton, despite the ongoing prevalence of significant summer blooms of nitrogen-fixing cyanobacteria.

## **2.9 Summary and research priorities**

Recent advances have shown that remote sensing can be a valuable tool for the monitoring of inland water quality, providing information over vast temporal and spatial scales. However, there remain many challenges in obtaining useful information from remotely sensed imagery over shallow, optically complex waters. Firstly, little is known about the within lake spatial variability of in-water bio-geo-optical properties and how the relationships between (S)IOPs and biogeochemical parameters differ from those reported in ocean and coastal waters. Further study of the nature of (S)IOPs in turbid waters will provide context for algorithm validation studies and support algorithm parameterisation, e.g. for a “menu” of inland water algorithm types, as suggested in Mouw et al. (2015).

Secondly, there remains a dearth of validation studies which assess retrieval of phytoplankton pigments using independent datasets collected from inland waters. There is a need to extend validation exercises to a larger range of lake optical water types in order to determine the uncertainties and limits of applicability for current algorithms, particularly those for the retrieval of parameters such as phycocyanin that have received less attention in the literature. Existing retrieval algorithms lack transferability amongst inland waters (i.e. are generally either site- or instrument-specific), and further testing of these alongside knowledge of the (S)IOPs in optically complex waters may elucidate the mechanisms behind algorithm success or failure.

Finally, the current use of satellite-based remote sensing instruments remains limited by the available technology, which is typically directed towards the needs of ocean colour or terrestrial applications. Thus, to achieve operational real-time monitoring of inland waters, further research is needed to understand algorithm transferability between sensors with different capabilities and how this influences the efficacy of the retrieved products (e.g. for water resource management).

### **2.9.1 Thesis in context**

With regard to the current state of the science, this PhD thesis attempts to address some of the present shortcomings in the field of remote sensing of inland waters. In particular, this thesis aims to contribute towards the knowledge of the variability of bio-geo-optical properties and the application of a range of remote sensing methods for assessment of phytoplankton in optically complex shallow lakes. Specific objectives for each results chapter are outlined as follows:

*Chapter 3* – To investigate if and how bulk and specific absorption coefficients vary spatially across a trophic gradient in Lake Balaton and the relationships with biogeochemical properties in comparison to other published studies in ocean, coastal and inland waters.

*Chapter 4* – To examine the spatial variability of scattering and backscattering properties (bulk and specific) within an optically complex lake, with particular investigation of the relative contributions to particulate attenuation in the water column.

*Chapter 5* – To evaluate the performance of existing PC retrieval algorithms in an optically complex shallow lake using a time series of MERIS data, provide a detailed assessment of a semi-analytical PC retrieval algorithm and its sources of error using knowledge of the (S)IOPs, and to investigate the change in algorithm performance over a range of temporal matchup windows.

*Chapter 6* – To assess the remote sensing of phytoplankton blooms using a novel coincident dataset of satellite (MERIS and Landsat 5 TM), airborne (AISA Eagle) and *in situ* water-leaving reflectance, with a focus on the ability to retrieve Chl-*a* concentrations at different spatial scales using the Normalized Difference Chlorophyll Index (NDCI).

Using these results, this thesis will critically evaluate the use of remote sensing for monitoring phytoplankton populations in shallow and optically complex inland waters.

### **3 Spatial variability of absorption coefficients over a biogeochemical gradient in a large and optically complex shallow lake**

*This chapter is based on the following publication:*

Riddick, C.A.L., Hunter, P.D., Tyler, A.N., Martinez-Vicente, V., Horváth, H., Kovács, A.W., Vörös, L., Preston, T. and Présing, M. (2015) Spatial variability of absorption coefficients over a biogeochemical gradient in a large and optically complex shallow lake. *Journal of Geophysical Research – Oceans*, 120: 7040-7066. doi: 10.1002/2015JC011202.

---

#### **3.1 Introduction**

Understanding the sources and magnitude of variability in light absorption in lakes and reservoirs is fundamentally important to studies concerned with photochemistry (Moran & Zepp, 1997, Bertilsson & Tranvik, 2000), photosynthesis (Blache et al., 2011), primary production (Tilstone et al., 2005, Lee et al., 2011), heat and energy transfers (Jolliff et al., 2008, Dera & Wozniak, 2010) and biogeochemical models (Ciavatta et al., 2014). The absorption and scattering of light (termed inherent optical properties, IOPs) are also key processes influencing the magnitude and spectral distribution of the water-leaving reflectance signal measured by Earth-observing satellites (Mobley, 1994, Kirk, 1994). Remote sensing has allowed for characterization of water bodies at improved spatial and temporal scales with the aim of monitoring water quality operationally in ocean, coastal and, more recently, inland waters. However, remote sensing algorithms developed for retrieval of physical and biogeochemical properties in open ocean waters are often inaccurate when applied to more turbid and optically complex inland waters (Sathyendranath et al., 1999, IOCCG, 2000, Binding et al., 2008). Inland waters typically have higher concentrations of phytoplankton biomass, detritus, inorganic particulates and colour dissolved organic matter (CDOM), and large percentages of suspended particulates can be land-derived. Moreover, the biogeochemical properties of inland waters do not co-vary over space and time, resulting in potentially large variability in the IOPs of the optically active constituents (OACs) (Binding et al., 2008, Palmer et al., 2015b). In order to improve the performance of algorithms for the retrieval of biogeochemical parameters in lakes it

is vital that we develop a better understanding of the variability in the absorption and backscattering coefficients ( $a(\lambda)$  and  $b_b(\lambda)$ ;  $\text{m}^{-1}$ ) of the main OACs in lakes [i.e., phytoplankton, non-algal particles (NAP) and coloured dissolved organic matter (CDOM)] and their mass-specific representations [ $a^*(\lambda)$  and  $b_b^*(\lambda)$ ;  $\text{m}^2 \text{mg}^{-1}$ ]. When light enters the water column photons are removed from its path by absorption, and  $a(\lambda)$  is defined as the sum of absorption by particulate and dissolved constituents and water itself. Light is also scattered by suspended particles, and the scattering coefficient [ $b(\lambda)$ ] is commonly defined as a measure of the total magnitude of scattered light (without regard to its angular distribution).  $b_b(\lambda)$  can therefore be defined as the total light scattered in the backwards direction. The sum of  $a(\lambda)$  and  $b(\lambda)$  is the beam attenuation coefficient [ $c(\lambda)$ ], or the total light attenuated in the water column. Knowledge of the IOPs is particularly important for radiative transfer studies and the development of analytically-based inversion algorithms. The bio-optical properties of open ocean (Morel & Maritorena, 2001) and coastal waters (Babin et al., 2003b) have been extensively studied over the last four decades, but our knowledge of these properties in lakes and other inland waters remains comparatively poor (Luis Perez et al., 2011, Zhang et al., 2011), particularly for highly turbid and productive water bodies.

In spite of the fact that lakes represent only ~3.7% of the Earth's total non-glaciated land surface (Verpoorter et al., 2014), the variability in their absorption and scattering coefficients is likely to be far greater than that encountered in the oceans, shelf seas and coastal waters due to the close proximity of land. Surface run-off from land exerts a strong influence on the composition and concentration of dissolved and particulate matter in lakes. In turn, absorption and scattering by dissolved and particulate materials affect the spectral shape and magnitude of the remote sensing reflectance [ $R_{rs}(\lambda)$ ] measured by satellite sensors (Morel & Prieur, 1977, Kirk, 1994). Knowledge of the variability of mass-specific inherent optical properties (SIOPs) is thus necessary for the interpretation of water-leaving reflectance signals. More formally,  $R_{rs}$  can be related to  $a(\lambda)$  and  $b_b(\lambda)$ , where  $f$  is an experimental constant dependent on the light field and volume scattering function and  $Q$  is a parameter accounting for geometrical attenuation of light exiting the water column (Gordon et al., 1975, Morel & Gentili, 1991, Dall'Olmo & Gitelson, 2005):

$$R_{rs}(0^+, \lambda) \propto \frac{f}{Q} \frac{b_b(\lambda)}{a(\lambda) + b_b(\lambda)} \quad (3.1)$$

The absorption and backscattering coefficients can be further partitioned into the contributions from each optically active constituent:

$$a(\lambda) = a_{ph}(\lambda) + a_{\text{NAP}}(\lambda) + a_{\text{CDOM}}(\lambda) + a_w(\lambda) \quad (3.2)$$

$$b_b(\lambda) = b_{b,ph}(\lambda) + b_{b,\text{NAP}}(\lambda) + b_{b,w}(\lambda) \quad (3.3)$$

where  $a_{ph}(\lambda)$ ,  $a_{\text{NAP}}(\lambda)$ ,  $a_{\text{CDOM}}(\lambda)$  and  $a_w(\lambda)$  represent the absorption coefficients for phytoplankton, NAP, CDOM and water, and  $b_{b,ph}(\lambda)$ ,  $b_{b,\text{NAP}}(\lambda)$  and  $b_{b,w}(\lambda)$  represent the backscattering coefficients for phytoplankton, NAP and pure water respectively. It is generally assumed that CDOM is non-scattering.

The relative contribution of the dissolved and particulate constituents to absorption and backscattering budgets varies significantly between different water types. Moreover, changes in size and composition of the constituents can result in marked changes in the SIOPs. For instance, the mass-specific particulate scattering coefficient [ $b^*_p(555)$ ] was reported to vary in ocean and coastal waters based on the proportion of organic versus mineral particles, and particle water content, apparent density and refractive index (Babin et al., 2003a). The variability of SIOPs is a major source of uncertainty in the interpretation of water-leaving reflectance signals, in the retrieval of biogeochemical properties and in estimates of primary production (Dall'Olmo & Gitelson, 2005, Gilerson et al., 2010, Tilstone et al., 2012). The improved parameterisation of remote sensing algorithms for turbid lakes and other optically complex waters thus relies on a comprehensive knowledge of the mass-specific absorption and scattering coefficients of lake water constituents and on an understanding of the sources and magnitude of their variability across different lake types. In particular, knowledge of the absorption properties at the wavelengths of ~440, 620 and 675 nm have direct implications for the remote sensing retrievals of phytoplankton pigments, including chlorophyll-*a* (Chl-*a*) and phycocyanin (PC), in order to distinguish potentially harmful cyanobacteria blooms in lakes (Simis et al., 2005, Kutser et al., 2006, Hunter et al., 2010, Mishra et al., 2013).

The (S)IOPs of inland waters have been relatively poorly studied, but the limited research to date suggests that they exhibit significant variability. Luis Perez et al. (2011) found that the absorption and mass-specific absorption coefficients of particulate matter in Laguna Chascomús, Argentina show significant seasonal variability. In Lake Taihu, China both spatial and seasonal differences were found in the absorption

coefficients of phytoplankton, with significantly lower  $a_{ph}(440)$  and  $a_{ph}(665)$  recorded in the winter (Zhang et al., 2010). While no spatial differences were found in the Chl-*a* specific absorption coefficient,  $a^*_{ph}(440)$  was significantly higher in spring, and  $a^*_{ph}(665)$  was highest in spring and summer in Lake Taihu (Zhang et al., 2010). Seasonal variations in  $a^*_{ph}(\lambda)$  in Lake Taihu have also been associated with the seasonal changes in community composition, and  $a^*_{ph}(\lambda)$  increased with the succession from chlorophytes to cyanophytes (Zhang et al., 2012). In contrast, in Lake Onondaga, USA mean annual  $a^*_{ph}(676)$  remained nearly uniform over a five-year study period (Perkins et al., 2014).  $a^*_{ph}(440)$  was observed to decline during a particular interval where diatoms dominated, however no statistically significant or recurring trends in  $a^*_{ph}(\lambda)$  were reported in this study (Perkins et al., 2014). Some evidence for regional differences in SIOPs has also been reported in studies where multiple water bodies were investigated. For instance, in several eutrophic turbid inland waters in China there were large regional differences in  $a^*_{ph}(675)$  and  $a^*_{NAP}(440)$ , with variations in  $a^*_{ph}(675)$  ranging from 0.002-0.285 m<sup>2</sup> mg<sup>-1</sup> (Shi et al., 2013). Another study on three productive reservoirs in South Africa found differences in  $a^*_{ph}(440)$  related to trophic class and the presence of monospecific cyanobacteria blooms (Matthews & Bernard, 2013). Spatial differences in optical properties within a single water body have also been reported, although chiefly with regard to IOPs rather than SIOPs. Following a wind event in western Lake Erie, spectral variations in  $a(\lambda)$  and its contributing components was reported, and more modest wavelength dependencies for  $b_p(\lambda)$  and  $b_{bp}(\lambda)$  which were consistent with observations reported for coastal systems (O'Donnell et al., 2010). Similarly, spatial heterogeneity in IOPs and apparent optical properties (AOPs) has been reported in Lake Champlain, with uncoupled variation between absorption and biogeochemical parameters (O'Donnell et al., 2013). A study by Effler et al. (2012) demonstrated both spatial and temporal differences in the IOPs in Oneida Lake, NY, with the sum of  $a_{NAP}$ ,  $a_{CDOM}$  and  $a_{ph}$  at 440 nm ranging from 0.9-2.0 m<sup>-1</sup> over the summer months (June-August). This study further found a high contribution from CDOM to  $a(440)$ , however variations in NAP and phytoplankton ultimately drove absorption dynamics. Thus, while it has been widely documented in previous studies that IOPs and AOPs are variable in both time and space along with variations in the optically active constituents (OACs), further knowledge is required to characterise the relationships between IOPs and OACs in other systems, given the wide range of biogeochemical composition in inland waters. In particular, there are few

measurements of the mass-specific IOPs (SIOPs) in inland waters. Therefore, the focus of this study is to characterise the extent and cause of the spatial variability of the SIOPs within a large turbid freshwater system.

In particular, the main aims of this study are: (1) to improve our quantitative knowledge of the absorption coefficients of dissolved and particulate matter in highly productive and turbid lake systems; and (2) to determine the magnitude and sources of spatial variability in the absorption coefficients of the in-water constituents across biogeochemical gradients. This study builds on previous research on the bio-optical properties of lakes by extending measurements into highly minerogenic waters with marked variability in both phytoplankton biomass and terrestrial inputs of CDOM. It is anticipated this work will progress our understanding of the underwater light field and water-leaving radiative signals in lakes and inform the parameterisation and selection of remote sensing algorithms for the retrieval of biogeochemical parameters in different lake optical types. This additionally includes an understanding of the uncertainties and biases on the resulting products.

## **3.2 Methods**

### **3.2.1 Study site**

Lake Balaton is the largest freshwater lake in central Europe by surface area (596 km<sup>2</sup>) and one of the most intensively studied. The lake is very shallow with a mean depth of approximately 3 m and, as such, bottom sediments are frequently resuspended in the water column (Herodek, 1986, Présing et al., 2001, Tyler et al., 2006). This results in high concentrations of suspended mineral particles that can readily exceed 50 mg L<sup>-1</sup> from resuspension during strong wind events. The lake is comprised of four basins and an adjoining a wetland system (Kis-Balaton) to the west. The main inflow into the lake is the Zala River on the western shore, and the only outflow is a highly regulated channel at Siófok in the east. Nutrient inputs from the Zala River typically produce a pronounced trophic gradient from west to east. Whilst the hydrobiology and hydroecology have been comprehensively studied, there is presently no published information on the optical properties of Lake Balaton.

At its worst, Lake Balaton experienced hypereutrophic conditions in its westerly basins and eutrophic conditions in eastern basins because of increased nutrient loads in the 1970s (Herodek, 1986). Blooms of filamentous cyanobacteria (*Cylindrospermopsis*

*raciborskii* (Wołoszynska) Seenayya and Subba Raju) dominated the summer plankton community in the 1980s and 1990s (Présing et al., 1996). Since then, extensive waste water treatment and diversion schemes, the introduction of Kis-Balaton wetlands, closure of nearby farms in 1987 and reduction of fertilizer use have all substantially reduced nutrient loading to Lake Balaton, resulting in lower phytoplankton biomass and improved water quality (Somlyódy et al., 1997).

### **3.2.2 Water sampling**

Field measurements in Lake Balaton and Kis-Balaton were conducted at 38 stations over a one-week period in August 2010 (Figure 3.1), with the aim of collecting data on the spatial variability in the light absorption budget over a gradient from the highly productive, high phytoplankton biomass waters in western basins and Kis-Balaton to the low chlorophyll, low CDOM waters in the eastern basins. Daily average wind speed was also measured during each sampling occasion at automatic stations in order to investigate variations in the IOPs during resuspension events (Table 3.1; Central-Transdanubian Water Directorate). At each station, a surface water sample was divided into subsamples for subsequent filtration or preservation. Subsamples for the determination of pigment concentrations and laboratory measurements of particulate absorption were filtered on the boat immediately after sample collection under low vacuum pressure through 25 mm GF/F filter papers (Whatman, nominal pore size 0.7  $\mu\text{m}$ ). Depending on the turbidity, between 20 and 70 mL of water was filtered. Filter papers were flash frozen in liquid nitrogen for <12 hours and stored in a -80°C freezer until analysis (no more than 6 months). Further subsamples for CDOM and total suspended matter (TSM) were kept cool and in the dark on the boat and processed in the laboratory within 24 hours. Finally, one subsample was collected for phytoplankton enumeration and preserved in Lugol's solution immediately after collection.

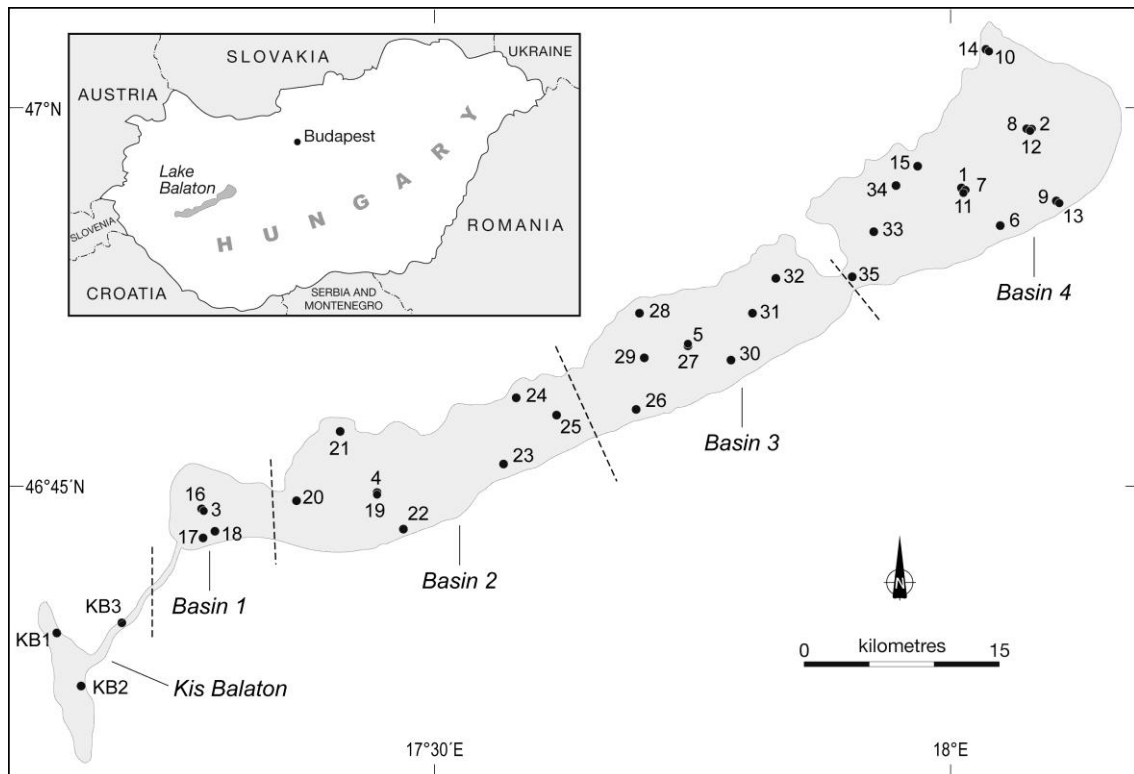


**Figure 3.1** Map of Lake Balaton and Kis-Balaton indicating the location of the basins and 38 sampling stations.

**Table 3.1** Daily average wind speed over the sampling period at Basin 4 (Siófok, Lake Balaton).

<b>Date</b>	<b>Average Wind Speed (m s<sup>-1</sup>)<sup>a</sup></b>	<b>Daily Maximum Wind Speed (m s<sup>-1</sup>)</b>
17-Aug	3.2	7.6
18-Aug	2.4	7.7
19-Aug	2.5	5.7
20-Aug	2.9	7.0
21-Aug	1.8	3.1
22-Aug	1.4	3.3
23-Aug	2.4	5.1
24-Aug	2.7	9.2
25-Aug	5.6	13.6
26-Aug	3.6	5.1
All dates	2.9	13.6

<sup>a</sup> Average of hourly wind speed measurements at Basin 4.

### 3.2.3 *In situ* optical measurements

To measure the IOPs *in situ* two optical instrument packages were deployed. The first consisted of an AC-S (WET Labs Inc.) *in situ* spectrophotometer interfaced with a CTD (Sea-Bird Electronics) recording temperature, salinity and pressure (depth). This package also included an ECO-BB3 (WET Labs Inc.) backscatter meter. These instruments were mounted in a black metal cage and deployed over a beam, which extended the cage approximately 1.5 m away from the boat. Simultaneously, an AC-9 (WET Labs Inc.) *in situ* spectrophotometer was deployed with and without a 0.2 $\mu$ m AcroPak filter (Pall Corporation) for separation of dissolved and particulate contributions to absorption. Because Lake Balaton is highly turbid and very well mixed, all measurements were made just below the water surface within the first optical depth. Prior to data collection, the AC-S and AC-9 were flushed and debubbled for 5 minutes. Five-minute casts were subsequently executed at each station with the data recorded to a DH4 data logger (WET Labs Inc.).

An AC-S and AC-9 (WET Labs Inc.) were deployed to collect absorption (*a*) and attenuation (*c*) measurements. The AC-S collected hyperspectral spectra over 84 wavelengths, from 401-755 nm at ~4 nm resolution, while the AC-9 collected data at 9 wavelengths only (412, 440, 488, 510, 532, 555, 650, 676 and 715 nm). The AC-S was only utilised in Basins 1-4, while AC-9 data was collected in Kis-Balaton as well. The AC-S or AC-9 raw data was corrected for the time lag associated with the flow rate for the instrument, then was merged with the CTD data for temperature, salinity and pressure. Using the CTD data, the effects of temperature and salinity on pure water absorption and attenuation were removed with wavelength-dependent corrections according to Pegau et al.(1997). To correct for instrument drift, a pure water calibration was subtracted from both attenuation and absorption data. The proportional scattering correction of Zaneveld et al. (1994) was applied to absorption data to account for inefficient collection of the scattered light within the AC-S or AC-9 reflecting tube. The proportional scattering correction is used here to be consistent with recent studies (Leymarie et al., 2010, Slade et al., 2010, Astoreca et al., 2012). All AC-S and AC-9 data were also screened for any data out with two standard deviations in order to eliminate any error from bubbles or large particles.

### **3.2.4 Chlorophyll-*a***

Frozen GF/F filter papers were thawed from -80°C in the dark prior to analysis for pigments and particulate absorption. Chlorophyll-*a* (Chl-*a*) was measured in triplicate via spectrophotometry (Shimadzu UV-1601) after a hot 90% methanol extraction following Iwamura et al.(1970). The hot methanol method was used here because it has been previously found to provide the most complete extraction of Chl-*a* for the phytoplankton types found in Lake Balaton (M. Présing, pers. comm.).

The spectrophotometric method was also validated against samples analyzed using high-performance liquid chromatography (HPLC). Pigments were extracted in acetone containing an internal standard (apo-carotenoate) after Martinez-Vicente et al. (2010) and separated using a reverse-phase Hypersil 3 mm C8 MOS-2 column on Thermo-separations© and Agilent© instruments with photodiode array detection (Barlow et al., 1997, Llewellyn et al., 2005). Pigments were quantified against commercial phytoplankton pigment standards (DHI Lab Products, Denmark). The spectrophotometric Chl-*a* data showed strong agreement with Chl-*a* results determined using HPLC methods ( $R^2=0.987$ ,  $p<0.001$ ). Results presented hereafter are based on the Chl-*a* data from spectrophotometry because the HPLC measurements were not replicated.

### **3.2.5 Phycocyanin**

Phycocyanin was extracted in a solution of 15 ml 0.05M phosphate buffer (pH=6.8). The solution was then subjected to sonication over ice for 15 seconds (Ultrasonic Homogenizer 4710 Series with micro-tip and 50% duty cycle, Cole-Parmer Instrument Co., USA) as in Horváth et al. (2013a). The extracts were clarified by filtration (Whatman GF/C filter) and the absorption was measured on a spectrophotometer (Shimadzu UV-1601, Shimadzu Corp., Japan). Phycocyanin concentrations were calculated using the equations of Siegelman and Kycia (1978). Clear outlying values were discarded so the PC concentrations were the mean of (minimum) two replicates.

### **3.2.6 Biomass and phytoplankton counts**

Phytoplankton species were enumerated with an inverted plankton microscope (Utermöhl, 1958). The wet weight of each species was calculated from cell volumes (Németh & Vörös, 1986). At least 25 cells (or filaments) of each species were measured to determine biomass and at least 400 were counted.

### 3.2.7 Total suspended matter

TSM was obtained by gravimetric analysis. 500-1500 ml of water was filtered under low-vacuum pressure (<700mbar, -50kpa) through a pre-ashed (furnace at 450°C) and pre-weighed 47 mm GF/C filter paper (Whatman). Following filtration, filter papers were dried for 24 hours in a clean oven at 60°C and subsequently weighed to obtain TSM. Filters were then placed in a furnace at 450°C overnight and subsequently weighed to obtain particulate inorganic matter (PIM). Particulate organic matter (POM) was calculated as the difference between TSM and PIM.

### 3.2.8 Coloured dissolved organic matter absorption

Water samples were filtered into clean glassware through 0.2 µm nucleopore membrane filters (Whatman) and measured according to Tilstone et al. (2002) within 24 hours of collection. Absorption of the filtrate was determined on a spectrophotometer (Shimadzu UV-1601) with a 5 cm quartz glass cuvette over the range of 350-800 nm, using MilliQ water as a reference. The absorption coefficient of CDOM ( $a_{\text{CDOM}}$ ) was calculated using the following equation:

$$a_{\text{CDOM}}(\lambda) = 2.303D(\lambda)/r \quad (3.4)$$

where  $D(\lambda)$  is the measured absorption at a given wavelength and  $r$  is the cuvette path length in meters. A baseline correction was applied by subtracting the mean value of  $a_{\text{CDOM}}(\lambda)$  in 5 nm interval around 685 nm (Babin et al., 2003b). This wavelength was used because there is negligible  $a_{\text{CDOM}}$  at 685 nm and the effects of temperature and salinity on water absorption are small (Pegau et al., 1997). The spectral slope of the CDOM absorption curve ( $S_{\text{CDOM}}$ ) was calculated over the wavelength range of 400-500 nm using an exponential function fitted by non-linear regression (Twardowski et al., 2004, Perkins et al., 2009).

### 3.2.9 Laboratory measurement of particulate absorption

The absorbance of the material on the filter was measured from 350-750 nm according to the ‘transmittance-reflectance’ method of Tassan and Ferrari (1998) using a dual beam spectrophotometer (Lambda 2, PerkinElmer Inc.) retro-fitted with a spectralon coated integrating sphere. Absorption was measured before and after bleaching with a 1% solution of NaClO to obtain total particulate absorption [ $a_p^{\text{spec}}(\lambda)$ ] and absorption by non-algal particles [ $a_{\text{NAP}}(\lambda)$ ], respectively. The pathlength

amplification correction of Tassan and Ferrari (1998) was applied, and absorption by phytoplankton [ $a_{ph}(\lambda)$ ] was calculated as the difference between  $a_p^{spec}(\lambda)$  and  $a_{NAP}(\lambda)$ . Chlorophyll-specific absorption coefficients [ $a_{*ph}(\lambda)$ ] were obtained by dividing  $a_{ph}(\lambda)$  by the respective Chl-*a* concentration. An exponential function was fitted by nonlinear regression to the  $a_{NAP}(\lambda)$  spectra, and the spectral slope of  $a_{NAP}(\lambda)$  ( $S_{NAP}$ ) was obtained. Wavelengths 350-750 nm were used in fitting the exponential function, disregarding the ranges 400-480 nm and 620-710 nm to avoid any residual pigment absorption, as in Babin et al. (2003b). The data from three stations (26, 27 and 30) were discarded for the purposes of  $S_{NAP}$  calculation due to extremely low values of  $a_{NAP}(440)$ .

### 3.3 Results

#### 3.3.1 Comparison of *in situ* and laboratory measured absorption

Bulk absorption coefficients [ $a(\lambda)$ ,  $m^{-1}$ ] measured *in situ* were compared with summed laboratory measurements of particulate and CDOM absorption [ $a(\lambda) = a_p(\lambda) + a_{CDOM}(\lambda)$ ]. Linear regressions of laboratory and *in situ* total absorption measurements at three wavelengths (440, 555 and 676 nm) are shown in Figure 3.2. There was some agreement between *in situ* and lab measurements, with roughly the same distribution but some differences in absolute values. *In situ* measurements generally correlated well with laboratory measurements, with  $R^2$  values of 0.743-0.843 ( $p < 0.001$ ) for the AC-S and 0.871-0.967 ( $p < 0.001$ ) for the AC-9. However, there was a particular lack of sensitivity in the AC-9 and, to a lesser extent, the AC-S data to variations in absorption at 555 nm. Additionally, *in situ* measurements over-estimated laboratory total absorption at these wavelengths by a factor of 1.1-2.1 (AC-S) and 1.5-2.5 (AC-9), with improved agreement in the red portion of the spectrum (676 nm) (Figure 3.2). In contrast, a previous study by Leymarie et al. (2010) found measured  $a(\lambda) + a_w(\lambda)$  (total non-water and water absorption) to be underestimated when using the proportional scattering correction, with the errors highest in the red portion of the spectrum. In the present study, it is expected that the overestimate of absorption is due to the scattering errors in the AC-9 and AC-S measurements which were not resolved by the proportional scattering correction (Mckee et al., 2008). Scattering increases at shorter wavelengths, thus a smaller difference (i.e. better agreement) would exist between the *in situ* and laboratory absorption measurements at longer wavelengths. Furthermore, there was a marked discrepancy between the two datasets of *in situ* absorption

coefficients (at 440nm, absolute error = 0.041-0.31 m<sup>-1</sup>). In general, the lab data more accurately reflected the spatial variability in absorption and had greater sensitivity, particularly in waters with low absorption. Thus, for the purpose of this study, laboratory measured absorption and specific absorption coefficients will be considered only, and *in situ* results are solely presented in the methods for comparison.

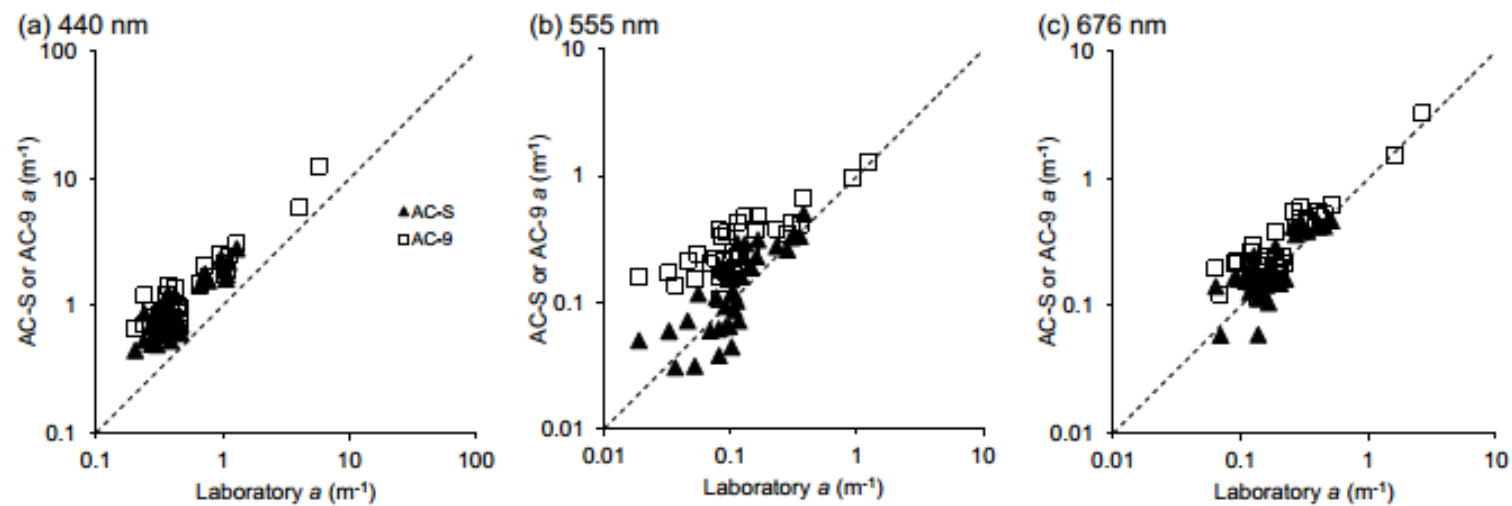


**Figure 3.2** Comparison of total non-water absorption [ $a(\lambda)=a_{ph}(\lambda)+a_{NAP}(\lambda)+a_{CDOM}(\lambda)$ ] from *in situ* (AC-S or AC-9) or laboratory methods at (a) 440, (b) 555 and (c) 676 nm. Axes are on logarithmic scale and dashed line represents the 1:1 line.

### 3.3.2 Variability in optically active constituents

The Chl-*a* and TSM data collected during the sampling campaign are shown in Figure 3.3 in relation to the annual cycle for these parameters. In all four basins, Chl-*a* concentrations peaked in early August immediately prior to the sampling campaign due to the development of a cyanobacterial bloom over much of the lake and remained high during the sampling campaign in three of the four basins. TSM concentrations were more variable over the year, with a marked peak in early summer in all basins and a winter peak in Basin 1 due to wind-driven resuspension. The sampling campaign was undertaken during a period with TSM concentrations mostly slightly lower than the annual mean ( $22 \pm 21 \text{ mg L}^{-1}$ ) but these were not atypical for Lake Balaton.

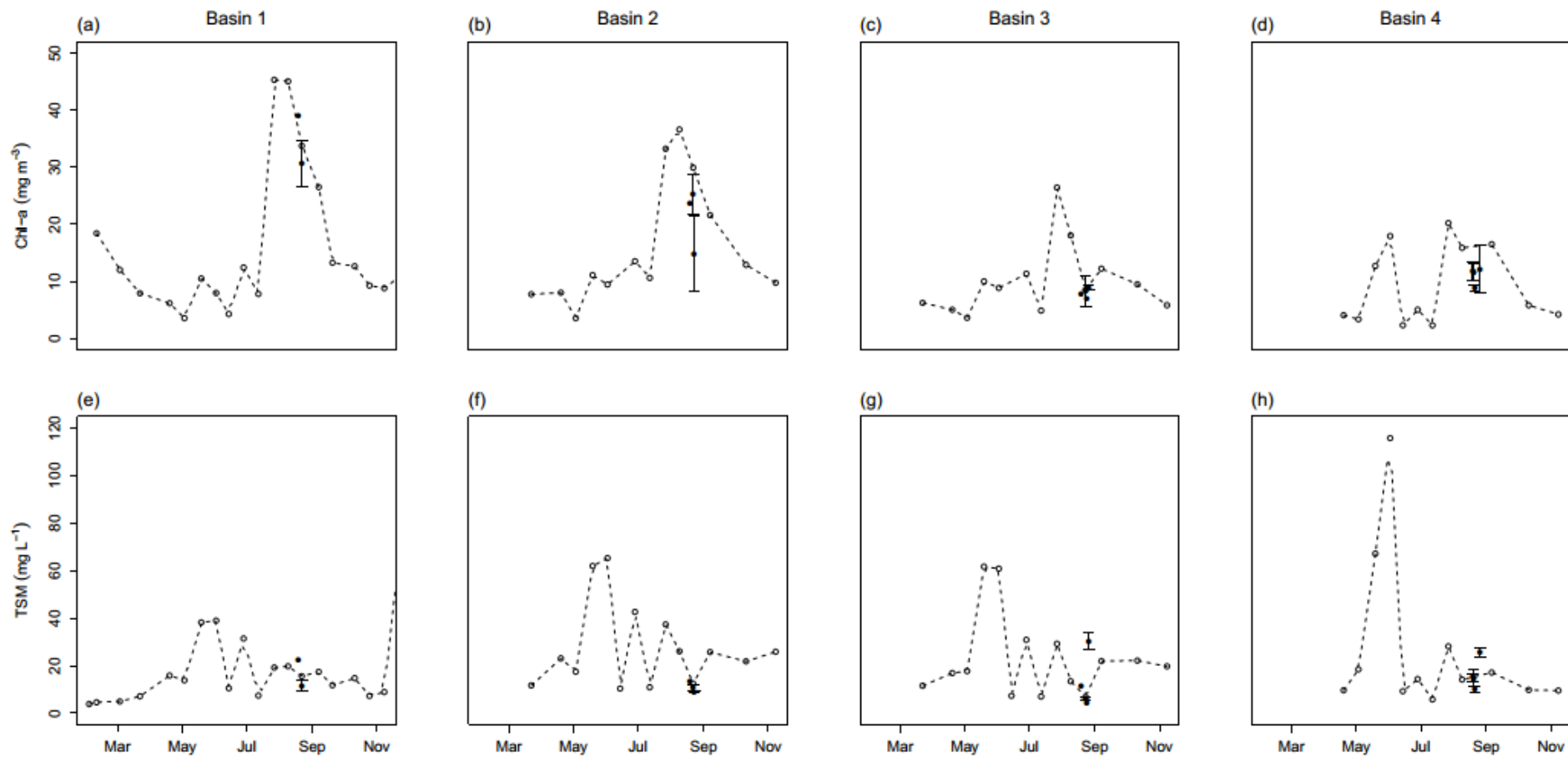


**Figure 3.3** Annual variation in chlorophyll-*a* (Chl-*a*) concentrations (a-d) and total suspended matter (TSM) concentrations (e-h) for 2010 in Lake Balaton Basins 1-4. Solid dots are mean daily values measured during the August 2010 campaign, with error bars indicating standard deviation. Annual data provided by the routine monitoring at a single station in each basin by the Balaton Limnological Institute.

The stations sampled in Lake Balaton and Kis-Balaton during summer 2010 demonstrated significant variability in the concentration of optically active constituents (Table 3.2). Mean Chl-*a* concentrations ranged from ~160 mg m<sup>-3</sup> in Kis-Balaton to ~10 mg m<sup>-3</sup> in Basin 4, and phytoplankton biomass ranged from ~70,000 to ~2,800 mg m<sup>-3</sup>, over the trophic gradient from west to east across the system. TSM ranged from ~40 mg L<sup>-1</sup> in Kis-Balaton to 13 mg L<sup>-1</sup> in Basin 4, with POM comprising the majority of TSM in Kis-Balaton (67%) and PIM comprising the majority of TSM in Basins 1-4. The greatest contribution of PIM to TSM (81%) was observed in Basin 3. Chl-*a* was strongly linearly correlated with POM ( $R^2=0.97$ ,  $p<0.001$ ,  $n=38$ ) with mean Chl-*a*:POM =  $0.00395\pm 0.00110$ . Total phytoplankton biomass was also linearly correlated with POM ( $R^2=0.88$ ,  $p<0.001$ ,  $n=38$ ) with mean total biomass:POM =  $0.998\pm 0.583$ . The mean PC:POM ratio for all basins is  $0.00321\pm 0.00145$  ( $R^2=0.75$ ,  $p<0.001$ ,  $n=38$ ), although this linear relationship had more dispersion than that for Chl-*a* or total biomass with POM. Stations in the east of Basin 3 and west of Basin 4 had markedly higher concentrations of TSM because wind-driven resuspension of bottom material was more prevalent in these basins during sampling than elsewhere. Chl-*a*, PC and ratios of POM and PIM at each station are shown in Figure 3.4, while the gradients in Chl-*a* and PC concentrations over distance from the Zala River are presented in Figure 3.5.

**Table 3.2** Mean Biogeochemical Parameters (Standard Deviation) for each basin and Kis-Balaton <sup>a</sup>

	<b>Kis-Balaton (n=3)</b>		<b>Basin 1 (n=4)</b>		<b>Basin 2 (n=8)</b>		<b>Basin 3 (n=8)</b>		<b>Basin 4 (n=15)</b>		<b>Lake Mean<sup>f</sup> (n=35)</b>		<b>Units</b>
Chl- <i>a</i>	166.51	(83.15)	32.74 <sup>cde</sup>	(5.40)	21.12 <sup>bde</sup>	(6.71)	8.24 <sup>bc</sup>	(1.91)	10.80 <sup>bc</sup>	(2.30)	15.08	(8.90)	mg m <sup>-3</sup>
PC	156.27	(176.68)	22.33 <sup>de</sup>	(7.41)	15.62 <sup>d</sup>	(4.56)	6.19 <sup>bc</sup>	(2.05)	9.95 <sup>b</sup>	(2.67)	11.80	(6.19)	mg m <sup>-3</sup>
TSM	40.98	(13.28)	14.41 <sup>-</sup>	(5.82)	10.36 <sup>-</sup>	(1.78)	12.55 <sup>-</sup>	(11.23)	15.37 <sup>-</sup>	(6.11)	13.47	(7.01)	mg L <sup>-1</sup>
POM	27.53	(8.63)	6.09 <sup>de</sup>	(1.23)	4.71 <sup>de</sup>	(1.41)	2.41 <sup>bc</sup>	(0.53)	3.41 <sup>bc</sup>	(0.49)	3.78	(1.43)	mg L <sup>-1</sup>
PIM	13.44	(11.54)	8.32 <sup>-</sup>	(4.79)	5.65 <sup>-</sup>	(1.63)	10.14 <sup>-</sup>	(10.96)	11.97 <sup>-</sup>	(6.04)	9.69	(6.98)	mg L <sup>-1</sup>
Total Biomass	70839	(53637)	7062 <sup>cde</sup>	(1780)	3916 <sup>bd</sup>	(1376)	1854 <sup>bc</sup>	(603)	2851 <sup>b</sup>	(821)	3348	(1832)	mg m <sup>-3</sup>
Cyano Biomass	55876	(58954)	5756 <sup>cde</sup>	(1810)	3456 <sup>bd</sup>	(1163)	1232 <sup>bc</sup>	(759)	2134 <sup>b</sup>	(671)	2644	(1658)	mg m <sup>-3</sup>
Cyano Biomass	57	(50)	81 <sup>-</sup>	(8)	88 <sup>-</sup>	(6)	64 <sup>-</sup>	(27)	74 <sup>-</sup>	(17)	76	(19)	%

<sup>a</sup> Chl-*a*, chlorophyll-*a* measured by spectrophotometry; PC, phycocyanin; TSM, total suspended matter; POM, particulate organic matter; PIM, particulate inorganic matter; Total Biomass, all phytoplankton biomass; Cyano Biomass, cyanobacteria biomass only.

<sup>b,c,d,e</sup> Numerical superscripts designate statistically significant differences between the respective parameter in Basins 1-4 using Tukey's Honest Significant Difference method ( $p < 0.01$ , adjusted for multiple comparisons), where superscript <sup>b</sup>=significantly different to Basin 1, <sup>c</sup>=significantly different to Basin 2, <sup>d</sup>=significantly different to Basin 3, <sup>e</sup>=significantly different from Basin 4, <sup>-</sup>=not significantly different from any basin.

<sup>f</sup> Lake Mean includes the 35 stations in the main basin only (not including Kis-Balaton).

Cyanobacteria biomass was found to correlate strongly with measured PC concentrations ( $R^2=0.97$ ,  $p<0.001$ ,  $n=38$ ), and total biomass showed a strong linear relationship with Chl-*a* ( $R^2=0.96$ ,  $p<0.001$ ,  $n=38$ ). PC concentrations were highest in Kis-Balaton ( $156 \text{ mg m}^{-3}$ ) with decreasing concentrations from Basins 1 to 3 (22 to  $6 \text{ mg m}^{-3}$ ) and a slight increase in Basin 4 ( $10 \text{ mg m}^{-3}$ ), which corresponds to the abundance of nitrogen fixing cyanobacteria (Figure 3.4). In almost all stations, cyanobacteria comprised the majority of the phytoplankton (up to 96%) with the most abundant species being *Cylindrospermopsis raciborskii*, which typically comprised over 50% of the cyanobacterial biomass in the lake. Phytoplankton composition at each station is shown in Figure 3.4c, indicating the dominance of cyanobacteria, with an increasing presence of cryptophytes, chlorophytes, dinophytes and heterokontophytes in Basins 3 and 4.

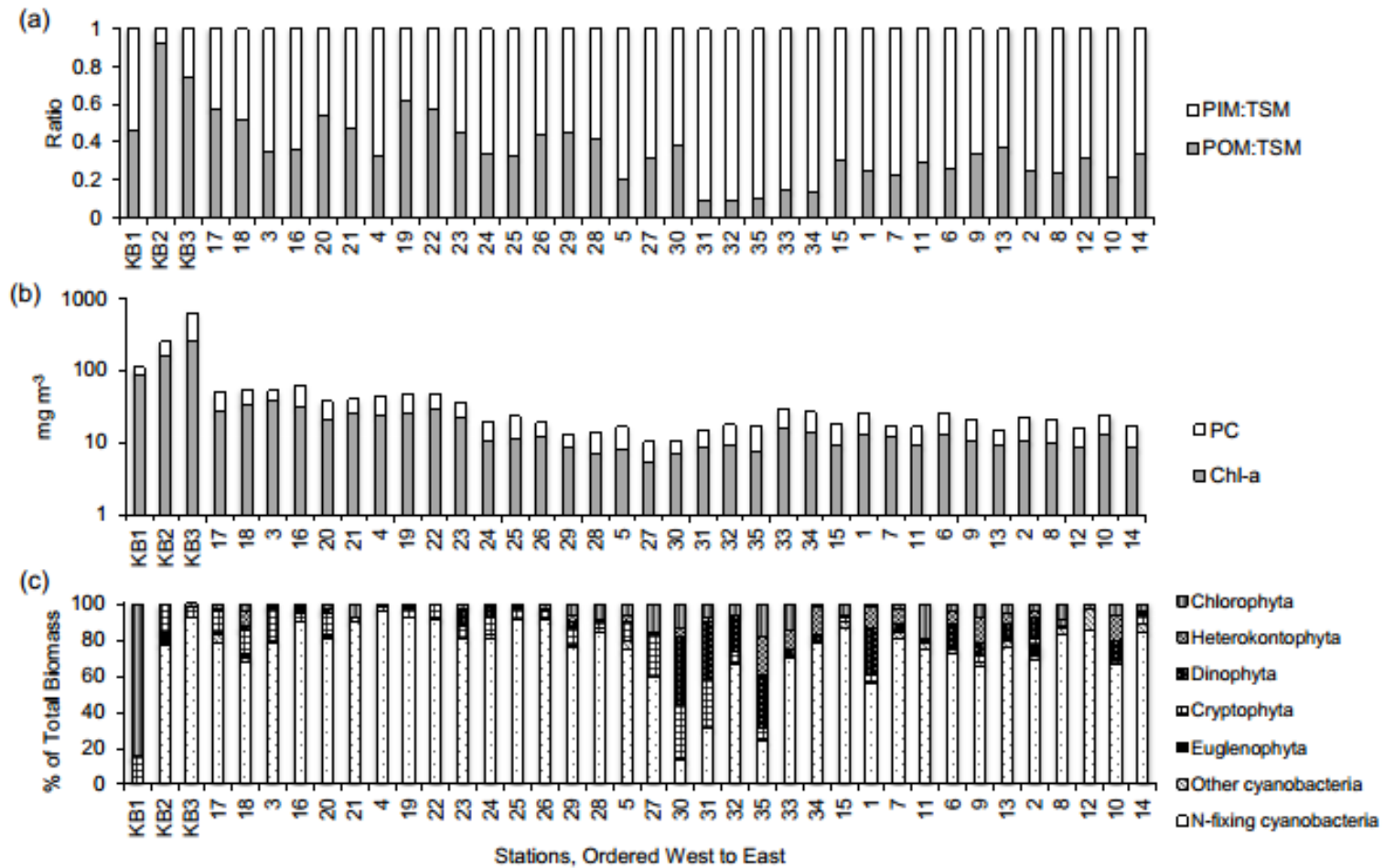


**Figure 3.4** Barplots of (a) the ratio of particulate inorganic matter (PIM:TSM) and particulate organic matter (POM:TSM), (b) chlorophyll-*a* (Chl-*a*) and phycocyanin (PC) concentrations and (c) phytoplankton community composition (% total biomass) at all stations in order from west to east.

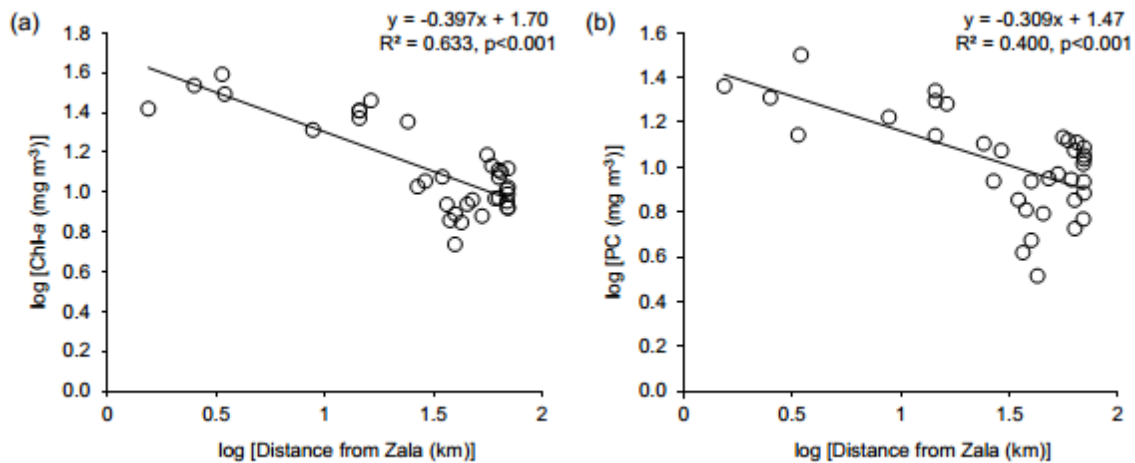


**Figure 3.5** Plots of (a) chlorophyll-*a* ( $\log[\text{Chl-}a \text{ (mg m}^{-3}\text{)}]$ ) and (b) phycocyanin ( $\log[\text{PC (mg m}^{-3}\text{)}]$ ) as a function of distance from the Zala River during the Lake Balaton sampling campaign.

Unusual stations to note include KB1, 30, 31 and 35. KB1 is nearest to the inflow from the Zala River and this area typically has lower biomass than the rest of Kis-Balaton, and generally has lower cyanobacteria biomass as well. In 2010, the inflow was high, therefore high turbidity and turnover prevented the development of cyanobacterial blooms (M. Présing, pers. comm.). Stations 30, 31 and 35 had low percentages of N-fixing cyanobacteria and larger communities of cryptophytes and dinophytes present, although total cell biomass was relatively low ( $<2,100 \text{ mg m}^{-3}$ ). These three stations were sampled on 24 and 26 August 2010, when high wind speeds caused increased turbulent mixing (Table 3.1), potentially encouraging the dominance of larger phytoplankton cells (e.g. dinoflagellates) at the surface.

Chl-*a*, CDOM and TSM were plotted against each other in order to investigate the relationships between these OACs (Figure 3.6). A weak but significant linear relationship was found between  $\log(\text{TSM})$  and  $\log(\text{Chl-}a)$  ( $R^2=0.306$ ,  $p<0.001$ ,  $n=38$ ; Figure 3.6a), similar to that reported for Lake Taihu (Zhang et al., 2010) and European coastal waters (Babin et al., 2003b). However, the increased scatter around this relationship in Lake Balaton is likely attributed to the large proportion of minerals in the suspended matter.  $\log[a_{\text{CDOM}(440)}]$  and  $\log(\text{Chl-}a)$  also co-varied linearly (Figure 3.6b;  $R^2=0.714$ ,  $p<0.001$ ,  $n=38$ ), a relationship that has been reported in a range of coastal waters (Babin et al., 2003b). In Lake Balaton, this is likely due to the fact that both CDOM and Chl-*a* decrease with increasing distance from the Zala River.

However, this relationship broke down in Kis-Balaton and Basin 1, which are closest to the river inflow. No significant linear relationship was reported between  $\log[a_{\text{CDOM}(440)}]$  and  $\log(\text{TSM})$  ( $R^2=0.132$ ,  $p=0.025$ ,  $n=38$ ; Figure 3.6c). Again, in Lake Balaton much of the TSM was comprised of PIM due to resuspension, thus a strong relationship with CDOM was not expected.

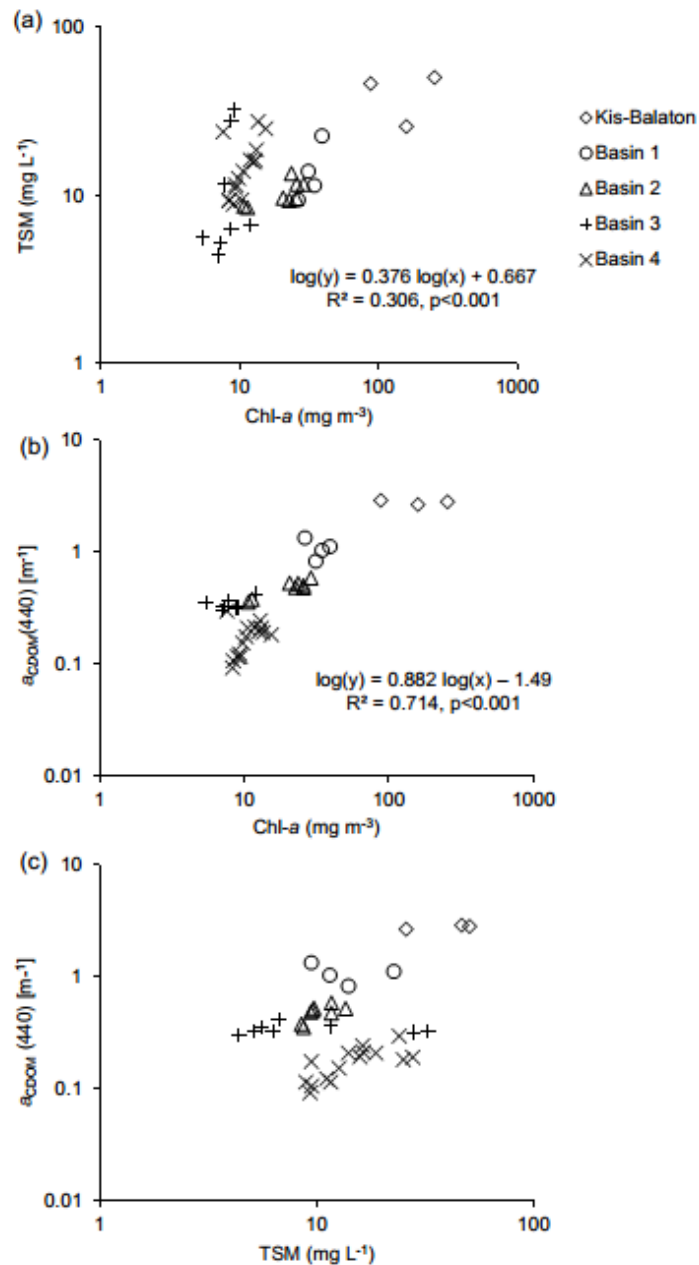


**Figure 3.6** (a) Total suspended matter (TSM) as a function of chlorophyll-*a* (Chl-*a*) and CDOM absorption at 440 nm [ $a_{\text{CDOM}(440)}$ ] as a function of (b) Chl-*a* and (c) TSM. Equations represent significant linear regressions on  $\log(\text{data})$ .

As the campaign was conducted over several days, any effect of sampling date on the measured concentrations was assessed using a generalised linear model, and the only significant relationship was observed for PIM ( $p < 0.001$ ). This was likely due to differences in the wind-driven resuspension of mineral particles from the lake bottom. Thus, most of the variability observed in the biogeochemical constituents can be assumed to be due to local differences in fluvial input, biological productivity and in-lake processing of particulate and dissolved material.

### **3.3.3 Variability in the inherent optical properties**

In general, the IOPs were variable across the system, with the most distinctly different properties exhibited in the westernmost portion, Kis-Balaton (Table 3.4). As with biogeochemical parameters, the measured (S)IOPs were tested for the effect of sampling date using a generalised linear model.  $a_p(440)$  was the only parameter with a significant relationship with sampling date ( $p < 0.001$ ). Figure 3.7 illustrates the gradients of  $a_{ph}(440)$ ,  $a_{NAP}(440)$  and  $a_{CDOM}(440)$  across the lake over increasing distance from the Zala River. Table 3.3, Table 3.4 and Table 3.5 summarise the bulk and specific IOPs and statistics for the four basins and Kis-Balaton, and Table 3.6 provides a summary of the optical properties of other large lakes from selected previous studies for comparison.

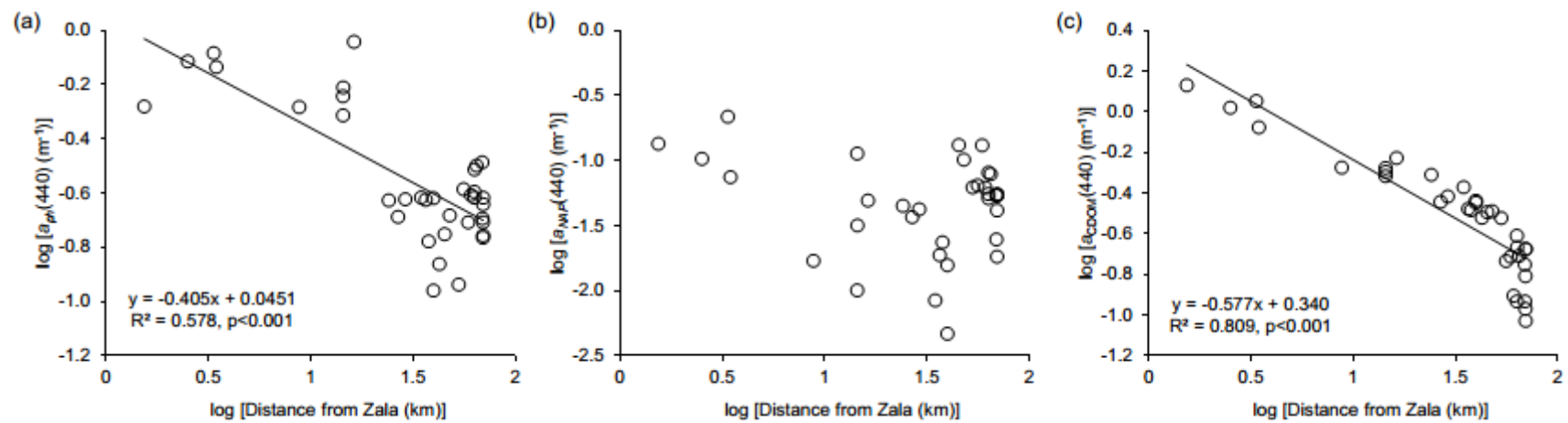


**Figure 3.7** Plots of (a)  $\log(a_{ph}(440)) [m^{-1}]$ , (b)  $\log(a_{NAP}(440)) [m^{-1}]$  and (c)  $\log(a_{CDOM}(440)) [m^{-1}]$  as a function of distance from the Zala River during the Lake Balaton sampling campaign.

The relative contributions of optically active substances to total absorption for the 38 stations sampled on Lake Balaton is shown in Figure 3.8 for selected wavelengths. At all wavelengths (440, 555, 620 and 675 nm),  $a_{\text{NAP}}(\lambda)$  was the smallest contributor, consistently making up less than 35% of the total absorption. At 440 nm,  $a_{\text{CDOM}}$  comprised between 33-76% and  $a_{\text{ph}}$  between 23-62% of absorption, while at 555 nm there was a wider range of composition with no clear trend by basin. Absorption at 620 nm included a higher percentage of absorption by phytoplankton (39-95%), although up to 48% and 32% were attributed to  $a_{\text{CDOM}}$  and  $a_{\text{NAP}}$ , respectively. At 675 nm over 70% of absorption was due to  $a_{\text{ph}}$  at all sites, with less than 10% due to  $a_{\text{CDOM}}$  and up to 23% due to  $a_{\text{NAP}}$ , although it was noted that CDOM and NAP had a greater contribution at 620 nm as compared to 675 nm. Thus,  $a_{\text{NAP}}$  and  $a_{\text{CDOM}}$  can contribute markedly to absorption at the wavelengths where PC and Chl-*a* absorb strongly (620 and 675 nm).

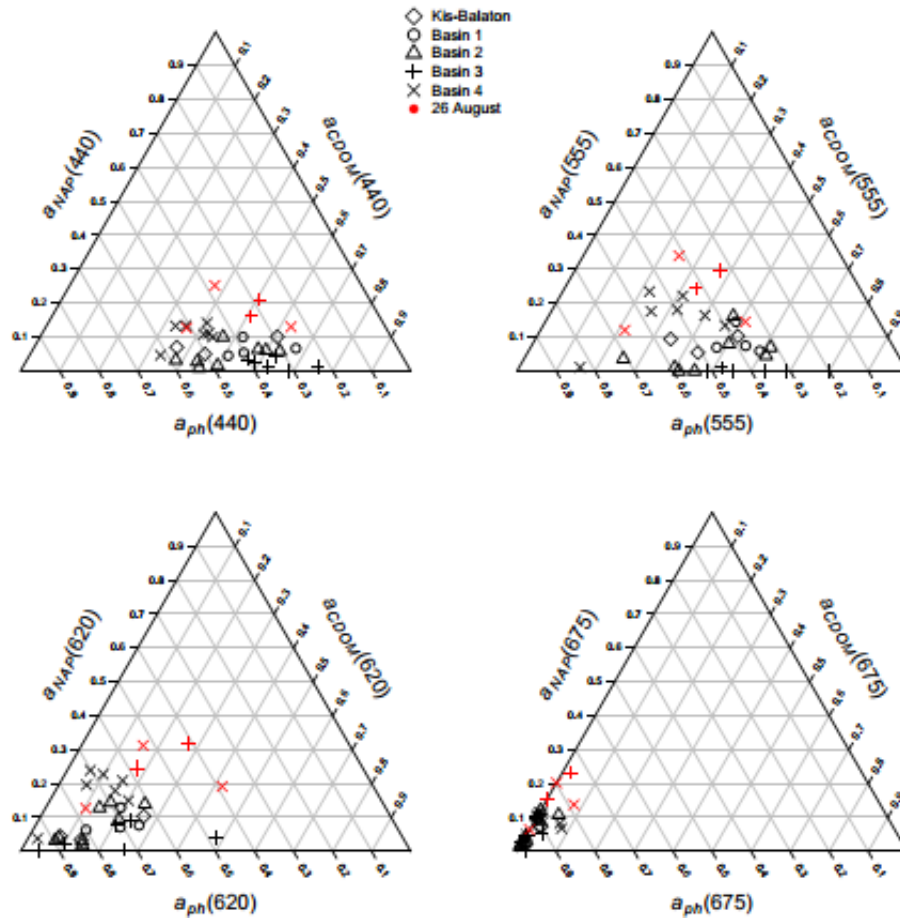


**Figure 3.8** Ternary plot indicating absorption by phytoplankton ( $a_{ph}$ ), non-algal particles ( $a_{NAP}$ ) and coloured dissolved organic matter ( $a_{CDOM}$ ) at (a) 440nm, (b) 555nm, (c) 620nm and (d) 675nm. Unique symbols indicate the basin and the sampling date 26 August is highlighted in red. Particulate absorption coefficients were measured in the laboratory by a dual beam spectrophotometer, and CDOM absorption was measured by spectrophotometry.

### 3.3.3.1 CDOM absorption

CDOM absorption at 440 nm in Lake Balaton ranged from 0.093-2.93  $m^{-1}$ . There was a gradient of  $a_{CDOM}(\lambda)$  across the lake (Figure 3.9), with  $a_{CDOM}(440)$  highest in the west (Kis-Balaton, 2.82  $m^{-1}$ ) where the Zala River enters and lowest in the east (Basin 4, 0.18  $m^{-1}$ ). Additionally, the difference in  $a_{CDOM}(440)$  was statistically significant between the four basins (Table 3.5). The mean value for the spectral slope of CDOM ( $S_{CDOM}$ ) was 0.018  $nm^{-1}$  in Kis-Balaton and 0.020  $nm^{-1}$  in the Lake Balaton.

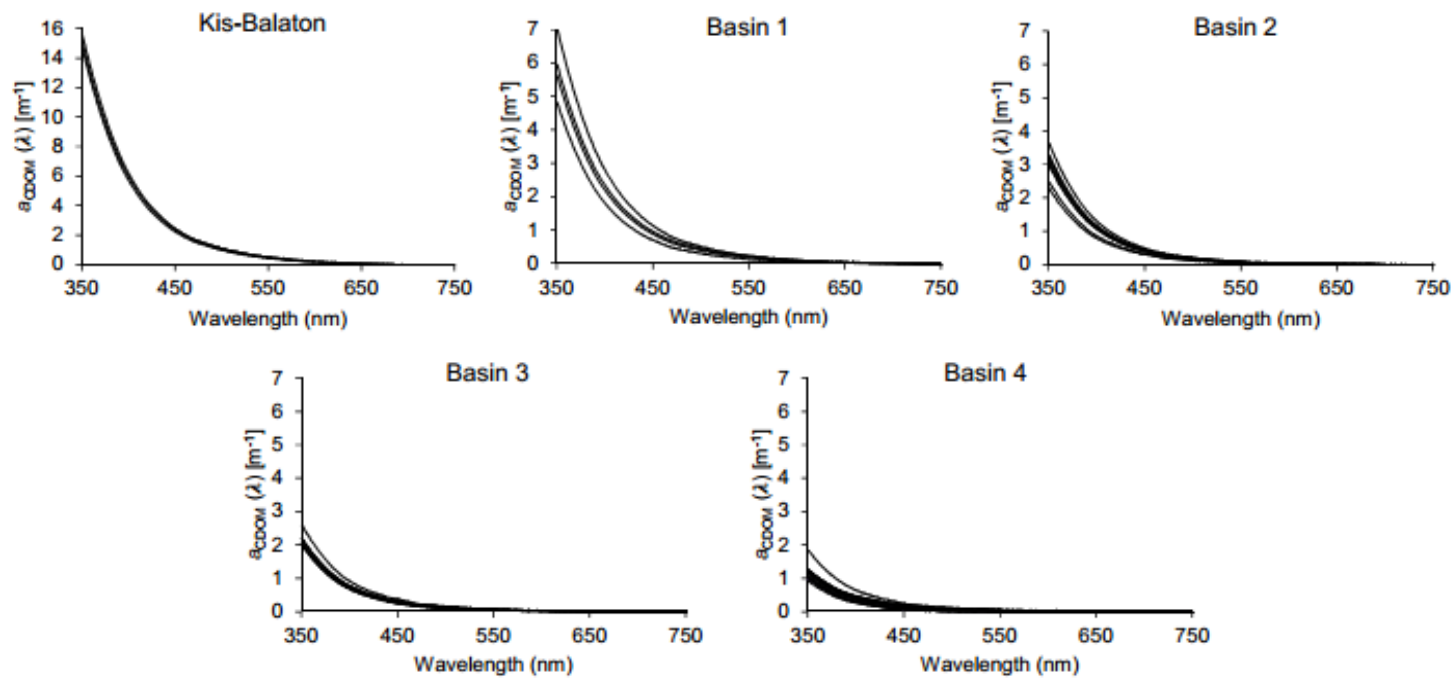


**Figure 3.9** Spectra of absorption by colour dissolved organic matter [ $a_{\text{CDOM}}(\lambda)$ ] for all stations in Kis-Balaton and Lake Balaton by basin. Note the different y-axis scale for Kis-Balaton.

$S_{\text{CDOM}}$  was found to decrease exponentially with increasing  $a_{\text{CDOM}}(440)$  ( $p < 0.001$ ,  $n = 38$ ; Figure 3.10). However, this relationship is driven by the larger range of  $S_{\text{CDOM}}$  values in Basin 4, and the mean  $S_{\text{CDOM}}$  excluding Basin 4 varied over a much narrower range ( $0.0183 \pm 0.000822$ ). There was no significant difference in  $S_{\text{CDOM}}$  values across the four basins (ANOVA  $p > 0.01$ ). Stations in Basin 4 had the greatest range in  $S_{\text{CDOM}}$  ( $0.015$  to  $0.041 \text{ nm}^{-1}$ ), whereas the  $S_{\text{CDOM}}$  values in the western basins and Kis-Balaton had much less variation (Table 3.5). This is likely due to the large influence of the Zala River on CDOM concentrations in the west of Lake Balaton, while complex interactions between localised fluvial inputs and increased contributions from autochthonous sources (phytoplankton decomposition) may play a larger role in the more variable CDOM concentrations observed in the east of the lake.

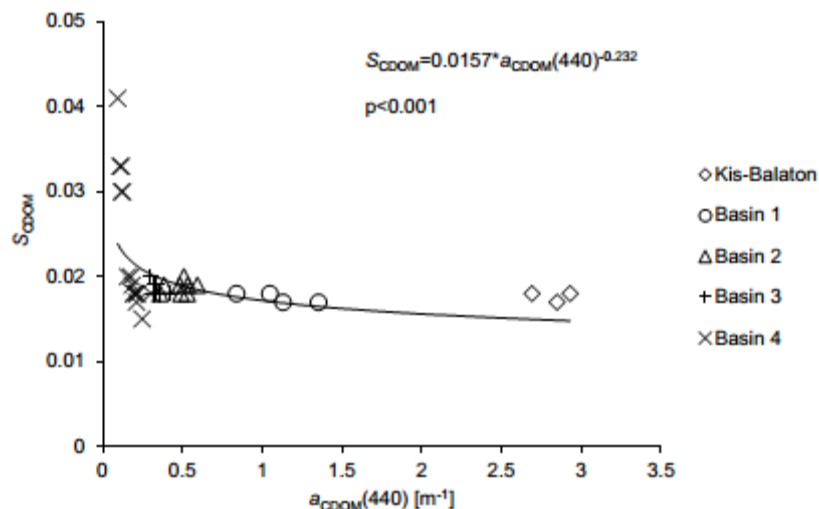
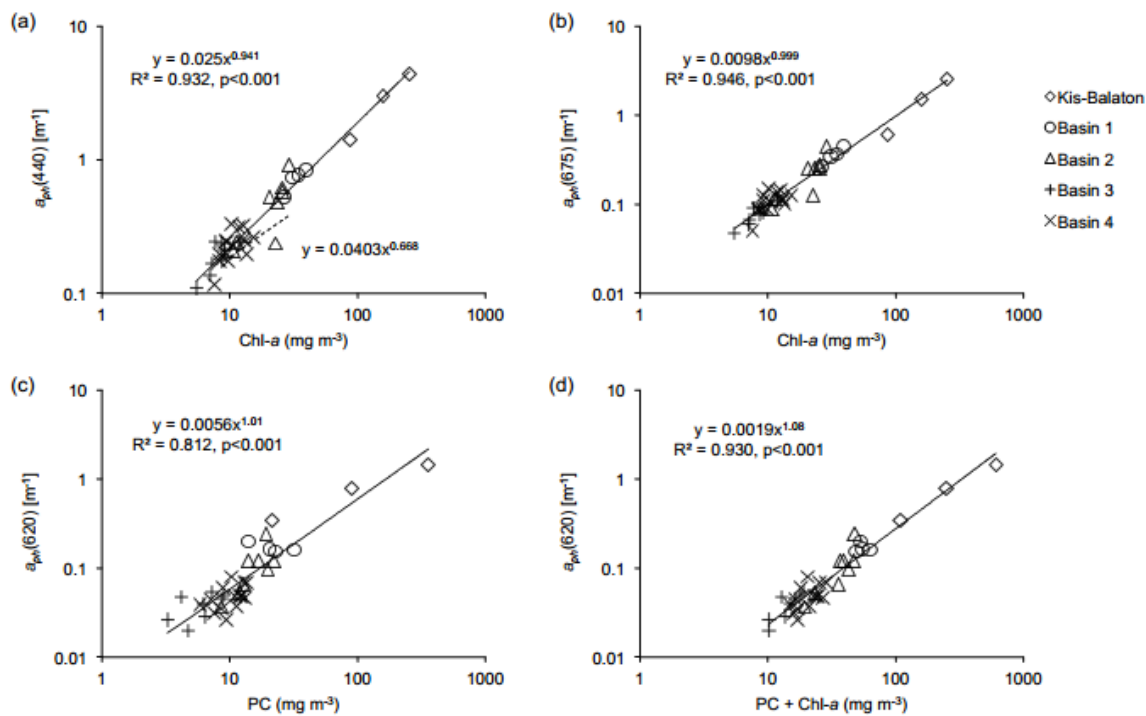


**Figure 3.10** Plot of the slope of CDOM absorption coefficient ( $S_{\text{CDOM}}$ ) as a function of CDOM absorption at 440 nm [ $a_{\text{CDOM}}(440)$ ].

### 3.3.3.2 Phytoplankton absorption

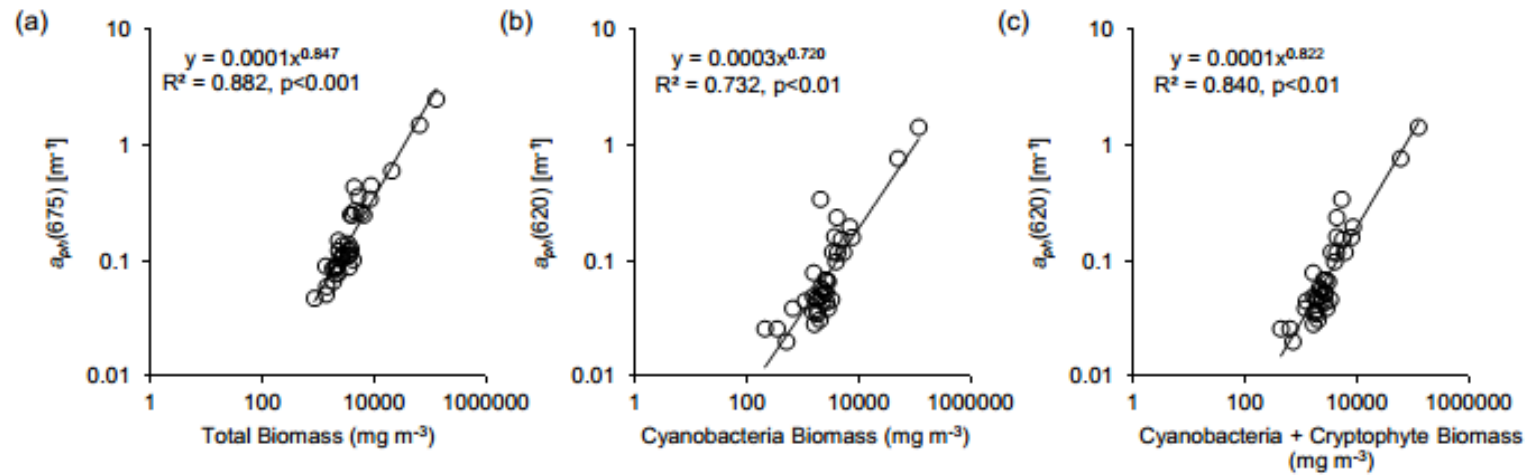
Particulate absorption at 440 [ $a_p(440)$ ] was generally dominated by phytoplankton, with  $a_{ph}(440)$  contributing up to 90% of the total particulate absorption (Basin 2). Phytoplankton absorption coefficients at 620 and 675 nm exhibited a decreasing gradient from west to east, with the lowest  $a_{ph}$  at both wavelengths in Basin 3. Mean  $a_{ph}(675)$  ranged from  $0.078 \text{ m}^{-1}$  (Basin 3) to  $1.55 \text{ m}^{-1}$  (Kis-Balaton), and  $a_{ph}(620)$  ranged from  $0.038 \text{ m}^{-1}$  (Basin 3) to  $0.85 \text{ m}^{-1}$  (Kis-Balaton) (Table 3.5).

Chl-*a* concentration showed a strong relationship with  $a_{ph}(440)$  ( $R^2=0.93$ ,  $p<0.001$ ,  $n=38$ ; Figure 3.11a), although a greater amount of scatter was noted around 10  $\text{mg m}^{-3}$  Chl-*a* with a slightly steeper slope than that found for oceans (Bricaud et al., 1995). Chl-*a* was also related to  $a_{ph}(675)$ , with a coefficient of determination of 0.95 for a fit by least squares ( $p<0.001$ ,  $n=38$ ; Figure 3.11b). Similarly, phycocyanin concentrations were positively correlated with phytoplankton absorption at 620 nm, but phycocyanin itself only explained 81% of the variability in  $a_{ph}(620)$  (Figure 3.11c). However, when Chl-*a* and PC were summed, 93% of the variability in  $a_{ph}(620)$  was explained, which reflects the contribution of Chl-*a* to phytoplankton absorption at 620 nm (Figure 3.11d).



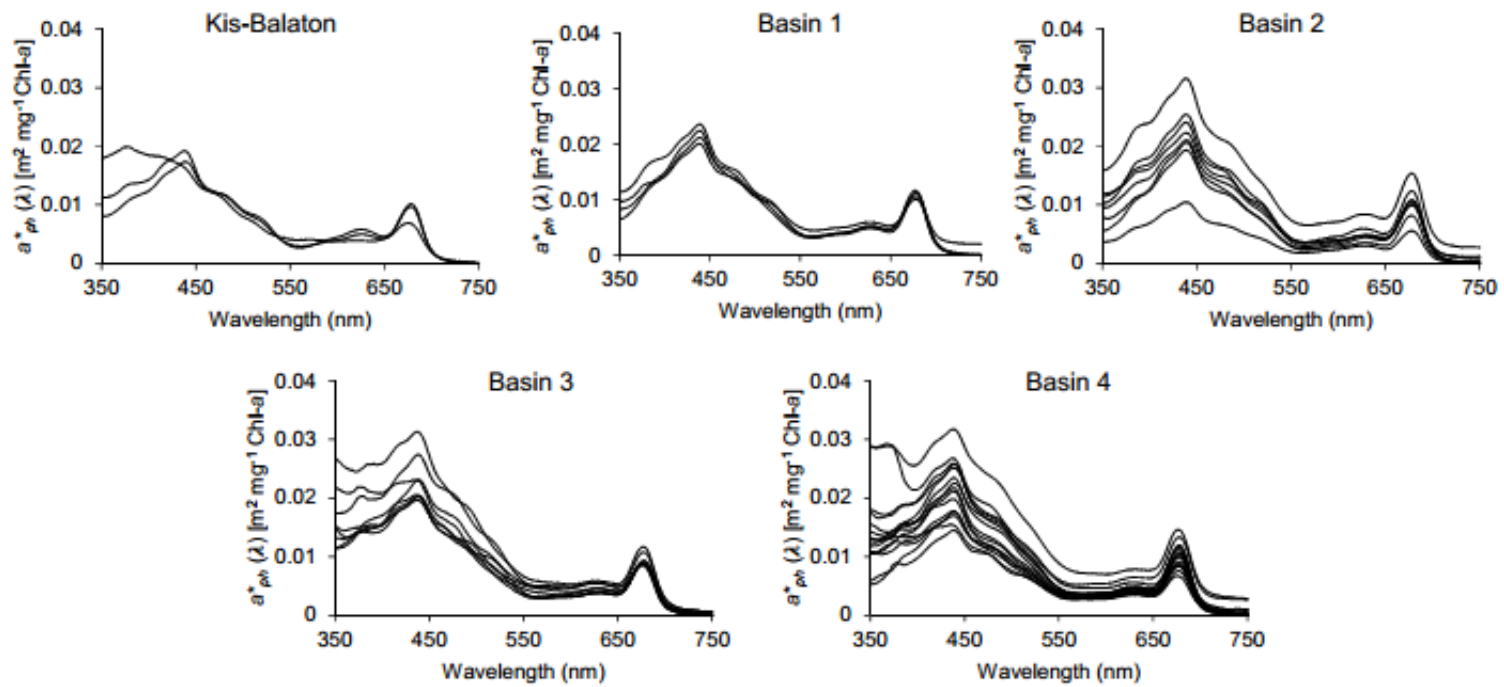
**Figure 3.11** Scatterplots of the phytoplankton absorption coefficient ( $a_{ph}$ ) at (a) 440 nm as a function of chlorophyll-*a* (Chl-*a*), (b) 675 nm as a function of Chl-*a*, (c) 620 nm as a function of phycocyanin (PC) and (d) 620 nm as a function of the summed pigments, PC + Chl-*a*. Chl-*a* results are by spectrophotometry and PC results are a selected average of the results by spectrophotometry. Absorption coefficients were measured in the lab by spectrophotometry. Note axes are on logarithmic scale. Solid line is a regression curve by least squares fit, and the dashed line in (a) is the fit from ocean waters in Bricaud et al. (1995).

Phytoplankton absorption coefficients were also strongly related to phytoplankton biomass. Using nonlinear regression by least squares fit, 88% of the variability in  $a_{ph}(675)$  was explained by total phytoplankton biomass, while 73% of that in  $a_{ph}(620)$  was explained by cyanobacteria biomass. However, using a sum of cyanobacteria and cryptophyte biomass, a higher percentage of variability in  $a_{ph}(620)$  was explained (84%). Higher  $a_{ph}(675)$  and  $a_{ph}(620)$  values corresponded with increased total phytoplankton and cyanobacteria biomass, respectively (Figure 3.12).



**Figure 3.12** Regression of (a) total biomass, (b) cyanobacterial biomass and (c) cyanobacteria and cryptophyte biomass against the absorption coefficient of phytoplankton ( $a_{ph}$ ) at (a) 675 nm and (b and c) 620 nm, respectively. Absorption coefficients were measured in the laboratory by a dual beam spectrophotometer. Solid lines represent regression curves by least squares fit.

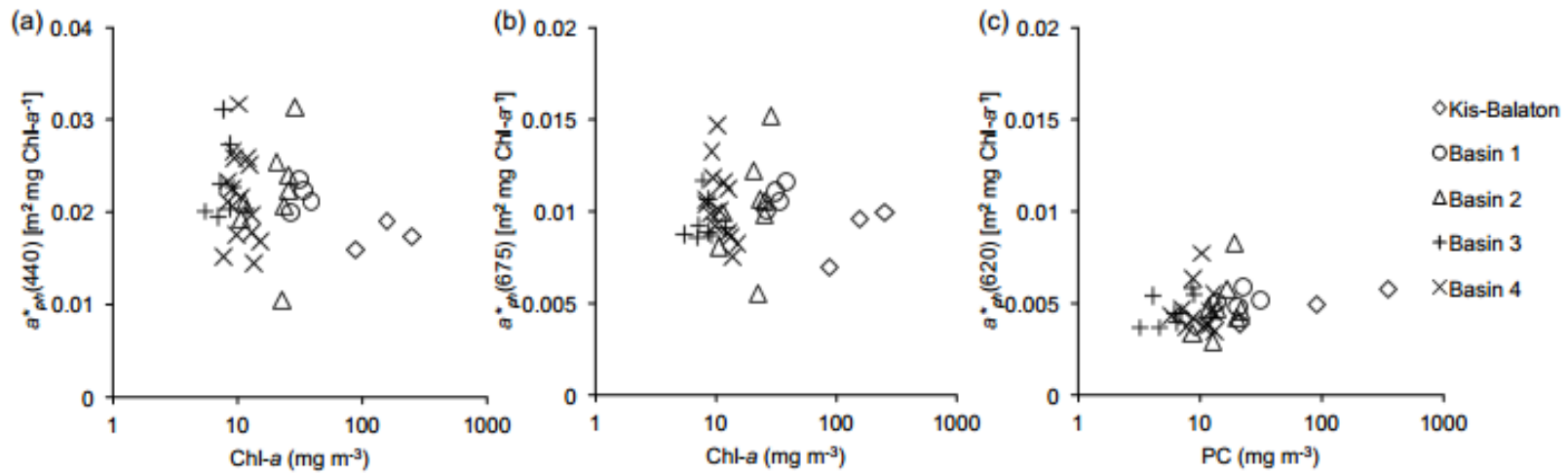
Mass-specific phytoplankton absorption spectra are shown for the four basins and Kis-Balaton in Figure 3.13. All stations show the distinctive Chl-*a* absorption maxima peaks at c.a. 440 nm and 675 nm, and all stations (except for KB1) demonstrate a smaller absorption peak at c.a. 620 nm due to the presence of phycocyanin. Stations in Basins 3 and 4 also had distinct peaks in the UV portion of the spectrum at approximately 360 nm, which were not visible in the spectra for Kis-Balaton and Basins 1 and 2.



**Figure 3.13** Spectra of mass-specific absorption by phytoplankton [ $a^*_{ph}(\lambda)$ ] for all stations in Kis-Balaton and Lake Balaton by basin.

The mean Chl-*a* specific absorption coefficient at 440 nm [ $a^*_{ph}(440)$ ] was 0.022 m<sup>2</sup> mg<sup>-1</sup> in Lake Balaton and 0.017 m<sup>2</sup> mg<sup>-1</sup> in Kis-Balaton (Table 3.3 and Table 3.4). There was greater variation in mean  $a^*_{ph}(440)$  across the basins and Kis-Balaton than observed for mean  $a^*_{ph}(675)$ , ranging from 0.017-0.023 m<sup>2</sup> mg<sup>-1</sup> (Table 3.4 and Table 3.5). The mean  $a^*_{ph}(675)$  for the four lake basins was 0.010 m<sup>2</sup> mg<sup>-1</sup> (Table 3.3) and was slightly lower in Kis-Balaton (0.0088 m<sup>2</sup> mg<sup>-1</sup>; Table 3.4). Mean values for  $a^*_{ph}(675)$  showed little variation across the basins and Kis-Balaton, with a narrow range of 0.0088 – 0.011 m<sup>2</sup> mg<sup>-1</sup> (Table 3.4 and Table 3.5).

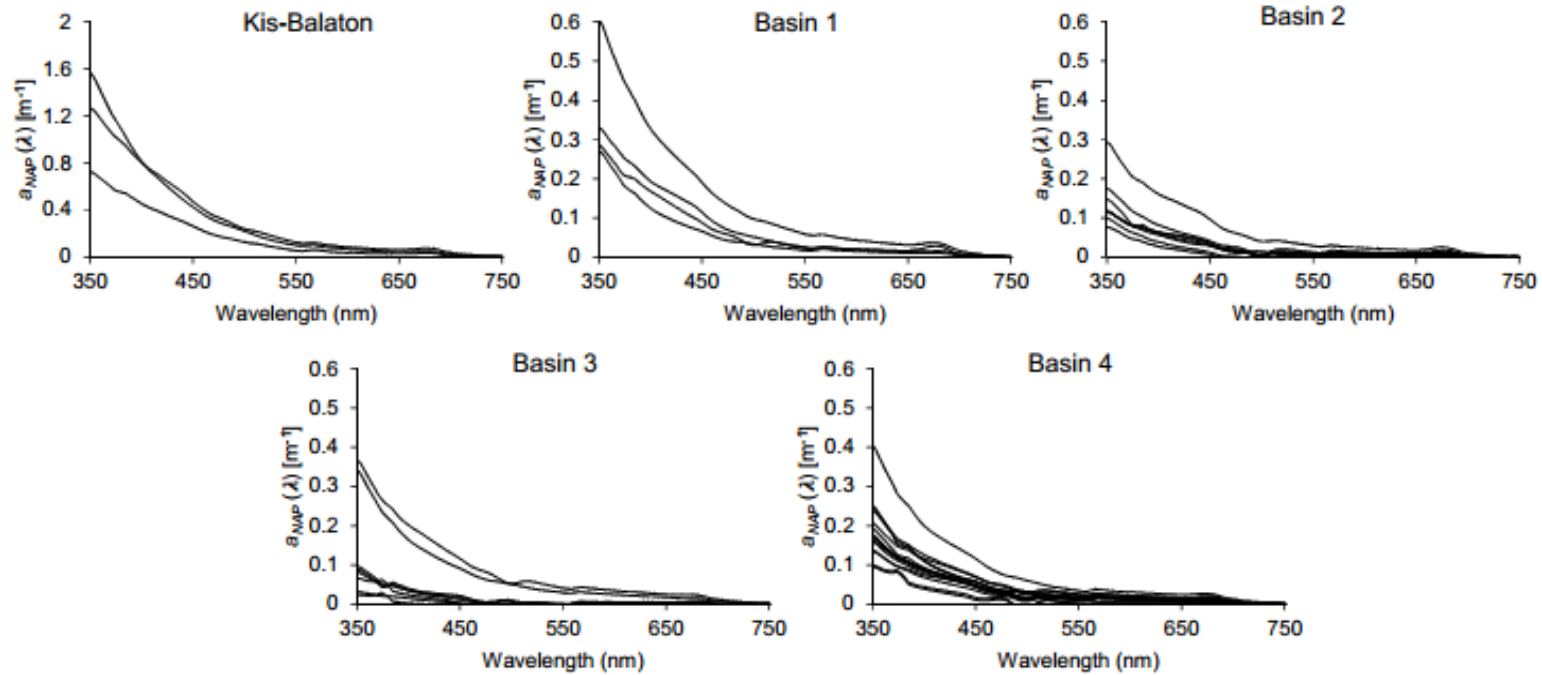
The specific absorption coefficient of phytoplankton showed variability across pigment concentrations (Figure 3.14).  $a^*_{ph}(440)$  and  $a^*_{ph}(675)$  varied by ~200% and ~150%, respectively, within the same basin on the same sampling date (i.e. Basin 2; Figure 3.14a and b), while  $a^*_{ph}(620)$  showed less variability and a slight positive trend over increasing phycocyanin concentrations (Figure 3.14c). Previous studies in ocean waters have found  $a^*_{ph}(\lambda)$  to decrease across increasing Chl-*a* concentrations, due to variations in pigment composition and pigment packaging (Bricaud et al., 1995, Bricaud, 2004). Although similar patterns were evident in Lake Balaton at 440 nm and 675 nm (Figure 3.14a and b), the relationships were not significant.



**Figure 3.14** Variability of (a)  $a^*_{ph}(440)$  and (b)  $a^*_{ph}(675)$  over concentrations of chlorophyll-*a* (Chl-*a*) and (c)  $a^*_{ph}(620)$  as a function of phycocyanin (PC) concentrations. Specific absorption coefficients were measured in the laboratory on a dual beam spectrophotometer, and PC and Chl-*a* results are from spectrophotometry. Note x-axes are on log scale.

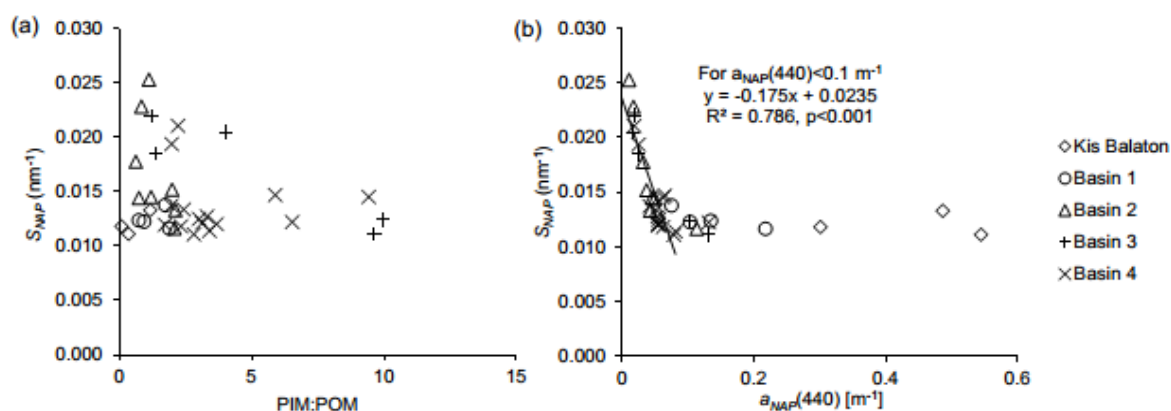
### 3.3.3.3 *NAP absorption*

Figure 3.15 shows the absorption spectra for non-algal particles for each basin and Kis-Balaton.  $a_{\text{NAP}}(440)$  was 2 to 3 times higher in Kis-Balaton than in the lake basins, and was also significantly different between Basin 1 and Basins 2, 3 and 4 (Table 3.5). In general, marked variability was reported across the lake, with  $a_{\text{NAP}}(350)$  ranging from up to  $1.6 \text{ m}^{-1}$  in Kis-Balaton to  $<0.1 \text{ m}^{-1}$  in Basins 3 and 4 (Figure 3.15). Note that a small amount of residual pigment absorption can occasionally be observed in the spectra in the region of Chl-*a* absorption ( $\sim 675 \text{ nm}$ ), due to incomplete bleaching. Residual pigment absorption in the  $a_{\text{NAP}}$  spectra propagated to an error of up to 5% in the calculated values of  $a_{\text{ph}}(675)$ , therefore this effect on  $a_{\text{ph}}(\lambda)$  was considered minimal.



**Figure 3.15** Spectra of absorption by non-algal particles [ $a_{NAP}(\lambda)$ ] for all stations in Kis-Balaton and Lake Balaton by basin. Note the different y-axis maximum for Kis-Balaton.

$a_{\text{NAP}}(\lambda)$  spectra followed a decreasing exponential shape, with a mean slope ( $S_{\text{NAP}}$ ) of  $0.0146 \text{ nm}^{-1}$  (coefficient of variation = 26%), ranging from  $0.011 - 0.025 \text{ nm}^{-1}$  across all basins (Table 3.3). There were no significant differences in  $S_{\text{NAP}}$  found between the basins (Table 3.5).  $S_{\text{NAP}}$  generally declined with an increasing ratio of inorganic particulates, although the linear relationship was not significant ( $R^2 = 0.0507$ ,  $p > 0.1$ ,  $n = 35$ ), with the greatest variability in  $S_{\text{NAP}}$  at lower ratios of PIM:POM (Figure 3.16a).  $S_{\text{NAP}}$  was negatively correlated to  $a_{\text{NAP}}(440)$  for  $a_{\text{NAP}}(440) < 0.1 \text{ m}^{-1}$  (Figure 3.16b). At TSM greater than  $\sim 10 \text{ mg L}^{-1}$  and  $a_{\text{NAP}}(440)$  greater than  $\sim 0.1 \text{ m}^{-1}$ ,  $S_{\text{NAP}}$  remained relatively constant ( $\sim 0.01 \text{ nm}^{-1}$ ).



**Figure 3.16** Scatterplots of  $S_{\text{NAP}}$  (the spectral slope of  $a_{\text{NAP}}$ ) as a function of (a) the ratio of particulate inorganic to organic matter (PIM:POM) and (b) absorption by non-algal particles at 440 nm [ $a_{\text{NAP}}(440)$ ]. The linear regression in (b) is for  $a_{\text{NAP}}(440) < 0.1 \text{ m}^{-1}$  only.

Scatterplots of  $a_{\text{NAP}}(440)$  as a function of TSM and PIM are shown in Figure 3.17. When applying a linear regression with a null intercept to  $a_{\text{NAP}}(440)$  as a function of TSM, a significantly lower slope (0.0069) exists than that previously found in coastal waters (0.031) by Babin et al. (2003b) (Figure 3.17a) and thus presumably lower  $a_{\text{NAP}}^*(440)$ . The proportion of  $a_{\text{NAP}}(440)$  to particulate absorption [ $a_p(440)$ ] is additionally correlated with PIM (Figure 3.17b), indicating the strong influence by the mineral component of TSM towards non-algal particle absorption.

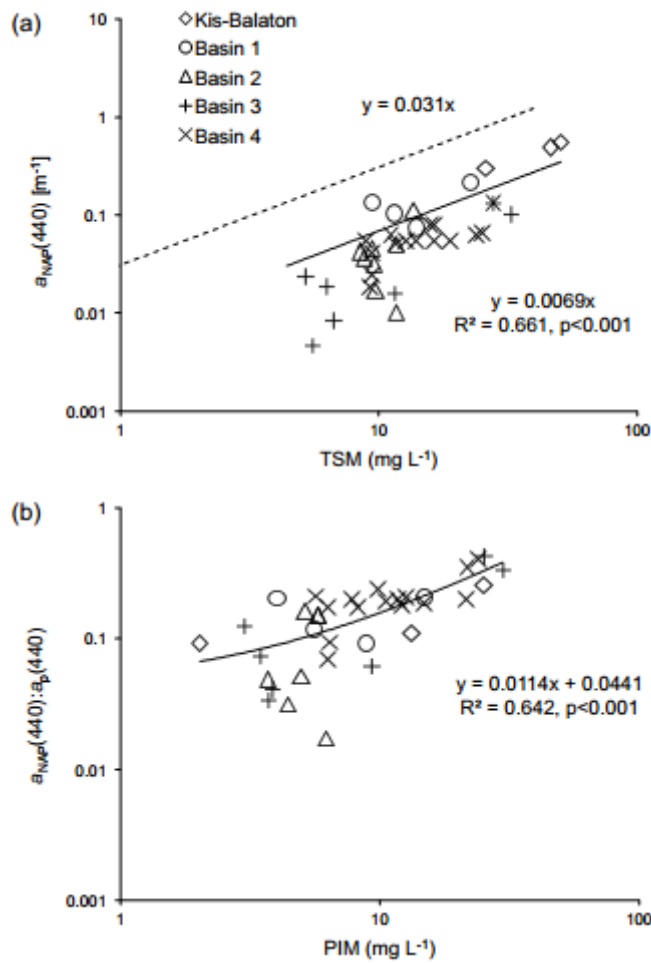


**Figure 3.17** Correlation between (a) total suspended matter (TSM) and absorption by non-algal particles  $[a_{\text{NAP}}(440)]$  and (b) particulate inorganic matter (PIM) and the proportion of absorption by non-algal particles to absorption by particulate matter  $[a_{\text{NAP}}(440):a_p(440)]$ . In plot (a), dashed line is a linear regression with null intercept indicating the relationship found across the range of TSM in coastal waters in Babin et al. (2003b)  $[a_{\text{NAP}}(440)=0.31*\text{TSM}]$ , and the solid line is a linear regression with null intercept for Kis-Balaton and Lake Balaton. The solid line in plot (b) is a linear regression.

**Table 3.3** Absorption coefficients for the main basins of Lake Balaton only (n=35).

<b>IOP</b>	<b>Min</b>	<b>Median</b>	<b>Max</b>	<b>Mean</b>	<b>St Dev</b>	<b>Units</b>
$a_{\text{CDOM}}(440)$	0.093	0.32	1.35	0.39	0.30	$\text{m}^{-1}$
$S_{\text{CDOM}}(400-500)$	0.015	0.018	0.041	0.020	0.0057	$\text{nm}^{-1}$
$a_p(440)$	0.11	0.31	1.04	0.39	0.24	$\text{m}^{-1}$
$a_p(675)$	0.050	0.12	0.49	0.17	0.11	$\text{m}^{-1}$
$a_{\text{NAP}}(440)$	0.00	0.054	0.22	0.059	0.046	$\text{m}^{-1}$
$S_{\text{NAP}}^a$	0.011	0.013	0.025	0.015	0.0039	$\text{nm}^{-1}$
$a_{ph}(350)$	0.057	0.15	0.46	0.18	0.094	$\text{m}^{-1}$
$a_{ph}(440)$	0.11	0.24	0.91	0.33	0.22	$\text{m}^{-1}$
$a_{ph}(620)$	0.020	0.049	0.24	0.073	0.053	$\text{m}^{-1}$
$a_{ph}(675)$	0.048	0.11	0.45	0.16	0.11	$\text{m}^{-1}$
$a^*_{ph}(350)$	0.0036	0.012	0.029	0.013	0.0061	$\text{m}^2 \text{mg}^{-1}$
$a^*_{ph}(440)$	0.010	0.022	0.032	0.022	0.0046	$\text{m}^2 \text{mg}^{-1}$
$a^*_{ph}(620)$	0.0029	0.0045	0.0083	0.0047	0.0011	$\text{m}^2 \text{mg}^{-1}$
$a^*_{ph}(675)$	0.0055	0.0095	0.010	0.010	0.0020	$\text{m}^2 \text{mg}^{-1}$

<sup>a</sup> Results for  $S_{\text{NAP}}$  disregard stations 26, 27 and 30 (n=32).

**Table 3.4** Absorption coefficients for Kis-Balaton stations only (n=3).

<b>IOP</b>	<b>Min</b>	<b>Median</b>	<b>Max</b>	<b>Mean</b>	<b>St Dev</b>	<b>Units</b>
$a_{\text{CDOM}}(440)$	2.69	2.85	2.93	2.82	0.12	$\text{m}^{-1}$
$S_{\text{CDOM}}(400-500)$	0.017	0.018	0.018	0.018	0.00058	$\text{nm}^{-1}$
$a_p(440)$	1.89	3.32	4.94	3.38	1.52	$\text{m}^{-1}$
$a_{\text{NAP}}(440)$	0.30	0.49	0.54	0.44	0.13	$\text{m}^{-1}$
$S_{\text{NAP}}$	0.011	0.012	0.013	0.012	0.0011	$\text{nm}^{-1}$
$a_{ph}(350)$	1.58	1.79	2.02	1.80	0.22	$\text{m}^{-1}$
$a_{ph}(440)$	1.40	3.02	4.39	2.94	1.50	$\text{m}^{-1}$
$a_{ph}(620)$	0.34	0.77	1.44	0.85	0.55	$\text{m}^{-1}$
$a_{ph}(675)$	0.60	1.51	2.52	1.55	0.96	$\text{m}^{-1}$
$a^*_{ph}(350)$	0.0080	0.011	0.018	0.012	0.0051	$\text{m}^2 \text{mg}^{-1}$
$a^*_{ph}(440)$	0.016	0.017	0.019	0.017	0.0015	$\text{m}^2 \text{mg}^{-1}$
$a^*_{ph}(620)$	0.0039	0.0049	0.0057	0.0048	0.00089	$\text{m}^2 \text{mg}^{-1}$
$a^*_{ph}(675)$	0.0069	0.0095	0.0099	0.0088	0.0017	$\text{m}^2 \text{mg}^{-1}$

**Table 3.5** Mean absorption coefficients (standard deviation) by basin.

<b>IOP</b>	<b>Basin 1 (n=4)</b>		<b>Basin 2 (n=8)</b>		<b>Basin 3 (n= 8)</b>		<b>Basin 4 (n=15)</b>		<b>Units</b>
$a_{CDOM}(440)$	1.09 <sup>bcd</sup>	(0.21)	0.48 <sup>ad</sup>	(0.077)	0.34 <sup>ad</sup>	(0.038)	0.18 <sup>abc</sup>	(0.058)	m <sup>-1</sup>
$S_{CDOM}(400-500)$	0.018 <sup>-</sup>	(0.00058)	0.018 <sup>-</sup>	(0.00071)	0.019 <sup>-</sup>	(0.00076)	0.023 <sup>-</sup>	(0.0079)	nm <sup>-1</sup>
$a_p(440)$	0.85 <sup>bcd</sup>	(0.16)	0.52 <sup>acd</sup>	(0.24)	0.23 <sup>ab</sup>	(0.074)	0.29 <sup>ab</sup>	(0.064)	m <sup>-1</sup>
$a_{NAP}(440)$	0.13 <sup>bcd</sup>	(0.062)	0.043 <sup>a</sup>	(0.031)	0.037 <sup>a</sup>	(0.050)	0.059 <sup>a</sup>	(0.026)	m <sup>-1</sup>
$S_{NAP}$	0.013 <sup>-</sup>	(0.00090)	0.017 <sup>-</sup>	(0.0048)	0.017 <sup>-</sup>	(0.0048)	0.014 <sup>-</sup>	(0.0029)	nm <sup>-1</sup>
$a_{ph}(350)$	0.29 <sup>-</sup>	(0.048)	0.21 <sup>-</sup>	(0.13)	0.14 <sup>-</sup>	(0.049)	0.15 <sup>-</sup>	(0.073)	m <sup>-1</sup>
$a_{ph}(440)$	0.71 <sup>cd</sup>	(0.13)	0.47 <sup>cd</sup>	(0.24)	0.19 <sup>ab</sup>	(0.050)	0.23 <sup>ab</sup>	(0.058)	m <sup>-1</sup>
$a_{ph}(620)$	0.17 <sup>cd</sup>	(0.019)	0.11 <sup>cd</sup>	(0.062)	0.038 <sup>ab</sup>	(0.012)	0.049 <sup>ab</sup>	(0.015)	m <sup>-1</sup>
$a_{ph}(675)$	0.36 <sup>bcd</sup>	(0.078)	0.22 <sup>acd</sup>	(0.11)	0.078 <sup>ab</sup>	(0.020)	0.11 <sup>ab</sup>	(0.026)	m <sup>-1</sup>
$a^*_{ph}(350)$	0.0092 <sup>-</sup>	(0.0020)	0.0096 <sup>-</sup>	(0.0039)	0.016 <sup>-</sup>	(0.0051)	0.014 <sup>-</sup>	(0.0067)	m <sup>2</sup> mg <sup>-1</sup>
$a^*_{ph}(440)$	0.022 <sup>-</sup>	(0.0060)	0.022 <sup>-</sup>	(0.0041)	0.023 <sup>-</sup>	(0.0048)	0.022 <sup>-</sup>	(0.0015)	m <sup>2</sup> mg <sup>-1</sup>
$a^*_{ph}(620)$	0.0052 <sup>-</sup>	(0.00047)	0.0048 <sup>-</sup>	(0.0016)	0.0046 <sup>-</sup>	(0.00083)	0.0045 <sup>-</sup>	(0.0012)	m <sup>2</sup> mg <sup>-1</sup>
$a^*_{ph}(675)$	0.011 <sup>-</sup>	(0.00067)	0.010 <sup>-</sup>	(0.0028)	0.0094 <sup>-</sup>	(0.0011)	0.010 <sup>-</sup>	(0.0021)	m <sup>2</sup> mg <sup>-1</sup>

<sup>a,b,c,d</sup> Numerical superscripts designate statistically significant differences between the respective parameter in Basins 1-4 using Tukey's Honest Significant Difference method ( $p < 0.01$ , adjusted for multiple comparisons), where superscript <sup>a</sup>=significantly different to Basin 1, <sup>b</sup>=significantly different to Basin 2, <sup>c</sup>=significantly different to Basin 3, <sup>d</sup>=significantly different from Basin 4 and <sup>-</sup>=no significant differences between basins.

**Table 3.6** IOP and SIOPs from selected previous studies for comparison.

<b>(S)IOP</b>	<b>Min</b>	<b>Max</b>	<b>Mean</b>	<b>StDev</b>	<b>Units</b>	<b>Location</b>	<b>Source</b>
$a_{CDOM}(440)$	0.33	45.89	7.99	7.93	$m^{-1}$	Chagan Lake	Wang et al. (2011)
$a_{CDOM}(440)$	0.11	2.00			$m^{-1}$	Western Lake Erie	O'Donnell et al. (2010)
$a_{CDOM}(440)$	0.073	0.234	0.145	0.049	$m^{-1}$	Lake Superior	Effler et al. (2010)
	0.105	1.607	0.186	0.439			
$a_{CDOM}(440)$	0.27-0.46	1.52- 2.36	0.71-0.91	0.20-0.35	$m^{-1}$	Lake Taihu	Zhang et al. (2010)
$a_{CDOM}(440)$	0.08	0.75	0.23		$m^{-1}$	Lake Erie	Binding et al. (2008)
$a_{CDOM}(440)$	0.27-0.38	1.52-2.36	0.71-0.98	0.26-0.22	$m^{-1}$	Lake Taihu	Zhang et al. (2007)
$a_{CDOM}(442)$	0.43	14.5	2.65		$m^{-1}$	15 boreal lakes	Ylöstalo et al. (2014)
$S_{CDOM}(400-500)$			0.0165		$nm^{-1}$	Lake Erie	O'Donnell et al. (2010)
$S_{CDOM}(400-500)$	0.0090-	0.0139-	0.0107-	0.0016-	$nm^{-1}$	Lake Superior	Effler et al. (2010)
	0.0111	0.0169	0.0134	0.002			
$S_{CDOM}(350-500)$	0.011	0.025	0.0176	0.0020	$nm^{-1}$	European coastal waters	Babin et al. (2003b)
$S_{CDOM}(400-500)$	0.0178	0.0190	0.0186		$nm^{-1}$	Oneida Lake	Effler et al. (2012)
$S_{CDOM}(350-700)$	0.0155	0.020	0.0182		$nm^{-1}$	15 boreal lakes	Ylöstalo et al. (2014)
$S_{NAP}(482-618,712-750)$	0.0113	0.0145	0.0128		$nm^{-1}$	Oneida Lake	Effler et al. (2012)
$S_{NAP}(380-400,480-620,710-730)$	0.0089	0.0178	0.0123	0.0013	$nm^{-1}$	European coastal waters	Babin et al. (2003b)
$S_{NAP}(482-618,712-730)$			0.013		$nm^{-1}$	Western Lake Erie	Peng and Effler (2013)
$a^*_{ph}(440)$	0.005	0.084	0.018-0.056	0.007-0.021	$m^2 mg^{-1}$	3 small reservoirs	Matthews and Bernard (2013)
$a^*_{ph}(440)$			0.026	0.008	$m^2 mg^{-1}$	Lake Kasumigaura	Yoshimura et al. (2012)
$a^*_{ph}(440)$	0.013	0.505	0.086		$m^2 mg^{-1}$	Lake Erie	Binding et al. (2008)
$a^*_{ph}(440)$			0.033		$m^2 mg^{-1}$	Laurentian Great	Perkins et al. (2013)

(S)IOP	Min	Max	Mean	StDev	Units	Location	Source
$a^*_{ph}(440)$			0.035		$m^2 mg^{-1}$	Lakes Onondaga Lake	Perkins et al. (2014)
$a^*_{ph}(440)$			0.048-	0.012-	$m^2 mg^{-1}$	Lake Taihu	Huang et al. (2015)
			0.083	0.021			
$a^*_{ph}(443)^{\wedge}$	~0.008	~0.095			$m^2 mg^{-1}$	European coastal waters	Babin et al. (2003b)
$a^*_{ph}(675)$			0.0199-		$m^2 mg^{-1}$	Lake Chascomus	Luis Perez et al. (2011)
			0.0274				
$a^*_{ph}(675)$			0.0288		$m^2 mg^{-1}$	Lake Taihu	Sun et al. (2010)
$a^*_{ph}(675)$			0.018	0.005	$m^2 mg^{-1}$	Lake Kasumigaura	Yoshimura et al. (2012)
$a^*_{ph}(676)$	0.002	0.042		0.009	$m^2 mg^{-1}$	Long Island Sound	Aurin et al. (2010)
$a^*_{ph}(676)$	0.008	0.020	0.014		$m^2 mg^{-1}$	15 boreal lakes	Ylöstalo et al. (2014)
$a^*_{ph}(670)$	0.007	0.157	0.040		$m^2 mg^{-1}$	Lake Erie	Binding et al. (2008)
$a^*_{ph}(676)$			0.0171		$m^2 mg^{-1}$	Onondaga Lake	Perkins et al. (2014)
$a^*_{ph}(676)^{\wedge}$	~0.004	~0.035			$m^2 mg^{-1}$	European coastal waters	Babin et al. (2003b)

<sup>^</sup> Estimated from Figure 6 in Babin et al. (2003b).

## 3.4 Discussion

### 3.4.1 Contributions to the absorption budget

Using the ternary approach proposed by Prieur and Sathyendranath (1981), the relative contributions to the absorption budget were characterised in this study. At 675 nm at least 70% of absorption is attributed to phytoplankton, with up to 30% of absorption accounted for by NAP and CDOM (Figure 3.8). However, relative contributions were more variable in the blue portion of the spectrum (440 nm), where phytoplankton comprised between 20-70%, CDOM between 30-80% and NAP up to 30% of the absorption budget (Figure 3.8). In contrast, in coastal waters it has been reported that NAP can form an even greater percentage of up to 80% of the non-water absorption at 442 nm, although a similar contribution was observed from CDOM (Babin et al., 2003b, Tilstone et al., 2012). In ocean waters, an approximately equal contribution to non-water absorption has been measured from CDOM (40-50%) and phytoplankton (30-60%) at 440 nm (Bricaud et al., 2010), although varying over a much narrower range than found in Lake Balaton. This indicates greater variations in the contributions to non-water absorption than that reported for ocean waters, suggesting that inland waters may indeed exhibit more variability in optical properties than oceans. It is also important to note that the contribution of NAP to non-water absorption in Lake Balaton is higher than that reported in ocean waters (e.g. up to 20% and typically below 10% at 440 nm in the South Pacific) (Bricaud et al., 2010). Contributions of CDOM and NAP were also relatively high at 620 nm (up to 48% and 32%, respectively) and 675 nm (up to 10% and 23%, respectively), wavelengths of particular interest for remote sensing retrievals of PC and Chl-*a* pigments. Similar instances were reported in some European coastal waters, where up to 60% of total absorption at the PC (620 nm) and Chl-*a* (665 nm) absorption peaks was due to particulate detritus, and  $a_{\text{CDOM}}$  occasionally contributed over 80% of absorption at 620 nm (Babin et al., 2003b). Similar findings were also reported in three South African reservoirs, where up to 60% and 30% of absorption was attributed to CDOM, while NAP contributed up to >90% and 60% at 620 and 675 nm, respectively (Matthews & Bernard, 2013). The high contribution of NAP and CDOM at these wavelengths therefore must be considered in bio-optical models for pigment retrieval at these wavelengths.

### 3.4.2 Variability in the IOPs

A distinct gradient in optical properties was also observed along the trophic gradient of Lake Balaton. Basin 1 is phytoplankton-dominated water, while Basin 4 is mineral-dominated water, as shown by a decrease in the organic fraction of TSM from west to east, paralleled with a decrease in total phytoplankton biomass (Table 3.2). Total non-water absorption [ $a_p(\lambda)$  and  $a_{\text{CDOM}}(\lambda)$ ] generally decreases from Basin 1 to 4 as the water progresses from phytoplankton-dominated to mineral-dominated. The significance of this is that phytoplankton particles have different absorption properties than mineral particles. Phytoplankton pigments absorb strongly in the blue and red portion of the spectrum (Mobley, 1994), while inorganic particles have the highest absorption in the blue portion of the spectrum and near exponential decrease in absorption across the spectrum (Babin et al., 2003b). Therefore, this gradient in CDOM, phytoplankton and mineral particles creates differences in both the quantity and quality of the underwater light field across Lake Balaton.

The IOPs in Lake Balaton generally show marked variability across the basins from the eutrophic western portion where biological particles dominate to the oligotrophic eastern basins with greater relative influence of minerogenic particles. As expected, Kis-Balaton and Lake Balaton had higher CDOM absorption than coastal ( $a_{\text{CDOM}}(443) < 1 \text{ m}^{-1}$ ) (Babin et al., 2003b) or marine waters ( $a_{\text{CDOM}}(375) = 0.06\text{--}4.2 \text{ m}^{-1}$ , although values  $> 1 \text{ m}^{-1}$  are rare) (Bricaud et al., 1981), with levels markedly higher than hyperoligotrophic ocean waters [ $a_{\text{CDOM}}(370)$  typically  $< 0.04 \text{ m}^{-1}$  (Morel et al., 2007)]. However, mean CDOM absorption in Lake Balaton ( $a_{\text{CDOM}}(440) = 0.58 \text{ m}^{-1}$ ) was comparable with other shallow inland waters, with absorption coefficients higher than the oligotrophic Lake Superior (Effler et al., 2010) or Lake Erie (Binding et al., 2008), but lower than organic rich lakes such as Lake Taihu and Chagan Lake in China (Zhang et al., 2007, Zhang et al., 2010, Wang et al., 2011).

Comparisons of  $S_{\text{CDOM}}$  should be viewed cautiously because there is no commonly agreed standard wavelength range or method for calculating its value and approaches vary greatly in the literature. However, compared to studies with similar methods of calculation, mean  $S_{\text{CDOM}}$  for Lake Balaton ( $0.020 \text{ nm}^{-1}$ ) is generally higher than reported values for marine ( $0.014 \pm 0.0032 \text{ nm}^{-1}$ ) (Bricaud et al., 1981), European coastal waters ( $0.0176 \pm 0.0020 \text{ nm}^{-1}$ ) (Babin et al., 2003b) and the oligotrophic Lake Superior ( $0.0107\text{--}0.0134 \text{ nm}^{-1}$ ) (Effler et al., 2010), but comparable to that reported for the shallow and eutrophic Oneida Lake ( $0.0186 \text{ nm}^{-1}$ ) (Effler et al., 2012). Fichot and

Benner (2012) have shown that  $S_{CDOM}$  is a sensitive tracer of terrigenous dissolved organic carbon (DOC) in river-influenced ocean margins with lower values observed in more terrestrially-influenced waters. The pool of DOC in Lake Balaton is likely to be dominated by allochthonous material, certainly in the western parts of the lake closer to the inflow of the Zala River where mean  $S_{CDOM}$  was lower ( $0.018 \text{ nm}^{-1}$ ).

### 3.4.3 Relationships between $a_{ph}(\lambda)$ , Chl-*a* and phytoplankton biomass

This study also found  $a_{ph}(675)$  to correlate linearly with the Chl-*a* concentration (Figure 3.11b), although large variability existed in the  $a_{ph}(\lambda)$  parameter, especially at stations with higher concentrations of Chl-*a*.  $a_{ph}(675)$  was further related to total phytoplankton biomass (Figure 3.12a), while  $a_{ph}(620)$  varied linearly with the sum of cyanobacteria and cryptophyte biomass (Figure 3.12b and c).  $a_{ph}(620)$  has not been specifically investigated in previous studies, and here we show a good relationship with PC concentrations, although a stronger correlation exists at this wavelength with summed PC and Chl-*a* pigments (Figure 3.11d). This wavelength (620 nm) is of importance in order to distinguish potentially harmful cyanobacteria blooms, and the correlation shown here for Lake Balaton is evidence for its future application to remote sensing algorithms for phycocyanin retrieval.

It is important to note that although there was a strong positive dependency of  $a_{ph}(\lambda)$  on Chl-*a* (Figure 3.11a and b), this relationship was different from that observed in ocean waters, particularly at the 440 nm peak (Bricaud et al., 1995). In Lake Balaton, there was greater absorption by phytoplankton at 440 nm per unit Chl-*a* than found in ocean waters in Bricaud et al. (1995), and this has also been reported in the English Channel (Babin et al., 2003b) and more recently, Lake Onondaga (Perkins et al., 2014) and three South African reservoirs (Matthews & Bernard, 2013). However, the contrary was found in the North Sea and Western English Channel coastal waters, with slightly lower  $a_{ph}(442)$  per unit Chl-*a* (Tilstone et al., 2012). Given that the Bricaud et al. (1995) relationship was established over a narrower range of Chl-*a* ( $<30 \text{ mg m}^{-3}$ ), it is unsurprising that this relationship is different over the wider range of Chl-*a* concentrations found in Lake Balaton ( $\sim 5\text{-}250 \text{ mg m}^{-3}$ ). It was suggested by Babin et al. (2003b) that the deviance from the Bricaud et al. (1995) relationship was likely a result of differences in phytoplankton cell size, given the widely accepted observation that oligotrophic waters are typically picoplankton-dominated while eutrophic waters are typically microplankton-dominated. In Lake Balaton, the dominant phytoplankton

group (N-fixing cyanobacteria) was comprised of mainly *Cylindrospermopsis raciborskii*, with *Aphanizomenon flos-aquae*, *Aphanizomenon issatschenkoi*, *Anabaena aphanizomenoides* and *Planktothrix agardhii* also present. The cell size of these dominant cyanobacteria species was in the region of 100-200  $\mu\text{m}$ , classifying this phytoplankton group as microplankton. Other large species were present in smaller numbers, including dinophytes (e.g. *Ceratium hirundinella*; 25-100  $\mu\text{m}$  = microplankton) and large colonial diatoms (e.g. *Melosira granulate*, 1200  $\mu\text{m}$  = microplankton), and the presence of these microplankton may account for the greater  $a_{ph}(440)$  observed in Lake Balaton as compared to ocean waters.

The increased scatter found in the relationship between  $a_{ph}(440)$  and Chl-*a* in Lake Balaton at  $\sim 10 \text{ mg m}^{-3}$  Chl-*a* (Figure 3.11a) is also evident in coastal waters from the study by Babin et al. (2003b) (see Figure 7f therein), where it appears there is increased scatter in  $a_{ph}(443)$  from  $\sim 0.3\text{-}10 \text{ mg m}^{-3}$  Chl-*a*. In Lake Balaton, the greatest variation in  $a_{ph}(440)$  was observed in Basins 3 and 4, and it is expected that this increased scatter is a result of variations in the phytoplankton community. Indeed, the eastern basins (Basins 3 and 4) comprised a more diverse phytoplankton community, with generally a greater range of community composition between the stations as compared to the western basins where N-fixing cyanobacteria composed anywhere from 14-86% of the total biomass (Figure 3.4). This increased phytoplankton diversity, and thus increased variations in cell size, in the eastern basins would account for the greater variations in  $a_{ph}(440)$  per unit Chl-*a* that were observed in this portion of Lake Balaton.

#### 3.4.4 Chl-*a* specific absorption

The Chl-*a* specific absorption coefficient [ $a^*_{ph}(\lambda)$ ] has been identified as a major source of uncertainty in accurately retrieving Chl-*a* in turbid productive waters (Dall'Olmo & Gitelson, 2006). The mean  $a^*_{ph}(440)$  ranged from 0.017-0.023  $\text{m}^2 \text{mg}^{-1}$  across Kis-Balaton and the four lake basins. In comparison,  $a^*_{ph}(443)$  varies over a much broader range in ocean [ $\sim 0.01\text{-}0.18 \text{ m}^2 \text{mg}^{-1}$ ; from Figure 1 in (Bricaud et al., 1995)] and coastal waters [ $\sim 0.008\text{-}0.10 \text{ m}^2 \text{mg}^{-1}$ ; from Figure 6 in (Babin et al., 2003b)]. However, measured  $a^*_{ph}(440)$  in Lake Balaton is within the range measured in three small oligotrophic to hypereutrophic reservoirs (0.005-0.084  $\text{m}^2 \text{mg}^{-1}$ ) (Matthews & Bernard, 2013). Comparable  $a^*_{ph}(440)$  were also reported in Lake Kasumigaura (0.026  $\text{m}^2 \text{mg}^{-1}$ ) (Yoshimura et al., 2012), while higher coefficients were reported in Lake Erie

(0.086 m<sup>2</sup> mg<sup>-1</sup>) (Binding et al., 2008) and Onondaga Lake, New York, USA (0.035 m<sup>2</sup> mg<sup>-1</sup>) (Perkins et al., 2014). Mean  $a^*_{ph}(675)$  values varied over a narrow range across the four basins and Kis-Balaton (0.0088 – 0.011 m<sup>2</sup> mg<sup>-1</sup>). The mean  $a^*_{ph}(675)$  in Balaton is at the lower end of the range reported for ocean waters (~0.005-0.06 m<sup>2</sup> mg<sup>-1</sup>) (Bricaud et al., 1995), and most similar to the coastal waters in the Baltic and Adriatic Seas (Babin et al., 2003b) or Long Island Sound (median  $a^*_{ph}(676)$ =0.010 m<sup>2</sup> mg<sup>-1</sup>) (Aurin et al., 2010). While  $a^*_{ph}(675)$  in Lake Balaton falls on the low end of the range for highly turbid lakes such as the hypereutrophic Lake Chascomus, Argentina ( $a^*_{ph}(675)$ =0.0199-0.0274 m<sup>2</sup> mg<sup>-1</sup>) (Luis Perez et al., 2011) and eutrophic Lake Taihu, China (mean  $a^*_{ph}(675)$ =0.0288 m<sup>2</sup> mg<sup>-1</sup>) (Sun et al., 2010), it was similar to the alkaline hypereutrophic to mesotrophic conditions in Onondaga Lake (mean  $a^*_{ph}(676)$ =0.0171 m<sup>2</sup> mg<sup>-1</sup>) (Perkins et al., 2014).

Previous studies document that  $a^*_{ph}(\lambda)$  decreases from oligotrophic to eutrophic waters, due to the ‘pigment package effect’ and changes in species composition and thus pigmentation (Bricaud et al., 1995). However, in Lake Balaton, there was no clear trend of decreasing  $a^*_{ph}(440)$  or  $a^*_{ph}(675)$  across increasing concentrations of Chl-*a* (Figure 3.14ab), although any trend in  $a^*_{ph}(\lambda)$  may be unclear in this study simply due to the relatively small sample size of 38 stations or the relatively small Chl-*a* gradient in Lake Balaton. Similarly,  $a^*_{ph}(620)$  showed a narrow range across the basins (~0.002-0.008 m<sup>2</sup> mg<sup>-1</sup>), and a general trend of increasing  $a^*_{ph}(620)$  across increasing phycocyanin concentrations (Figure 3.14b). It has recently been suggested that  $a^*_{ph}(\lambda)$  varies greatly with phytoplankton species composition; for example, in Lake Taihu  $a^*_{ph}(\lambda)$  increased with the succession from chlorophytes to cyanophytes (Zhang et al., 2012). Lake Balaton was dominated by cyanobacteria during the sampling period, which is possibly why no significant changes in  $a^*_{ph}(\lambda)$  were observed between basins. However, there were variations in phytoplankton community composition within the non-dominant functional groups, including a greater percentage of chlorophytes, dinophytes and diatoms (heterokontophytes) in Basins 3 and 4 (Figure 3.4). In particular, the slightly greater abundance of microplankton in Basin 3 (96%, compared to 87-95% in Basins 1, 2 and 4), including dinoflagellates (*Gymnodinium* sp., 25 µm), diatoms (*Synedra acus* v. rad, 110 µm) and chlorophytes (*Schroederia robusta*, 80 µm; *Staurastrum paradoxum*, 40 µm), may explain the low mean  $a^*_{ph}(675)$  measured in this basin (0.0094 m<sup>2</sup> mg<sup>-1</sup>). Larger cells are subject to a greater package effect and thus decreased absorption efficiency. Thus, the observed variations in  $a^*_{ph}(\lambda)$  may be a

result of changes in pigment packaging within the different cell types due to variations in cell size with the change in phytoplankton community composition.

### 3.4.5 Phytoplankton and CDOM absorption in the UV

The phytoplankton absorption peak in the UV in Basins 3 and 4 corresponds with decreased CDOM absorption in these eastern basins [mean  $a_{\text{CDOM}(440)}$  0.34 and 0.18  $\text{m}^{-1}$ , respectively], compared with the CDOM absorption in the western basins [mean  $a_{\text{CDOM}(440)}$  ranges from 0.48-2.82  $\text{m}^{-1}$ ]. As CDOM absorbs strongly in the lower wavelengths (see Figure 3.9), it may serve as a UV protectant for phytoplankton and other organisms. It is possible that the cyanobacteria in the eastern basins of Lake Balaton are compensating for this decrease in CDOM by producing a pigment to absorb harmful UV rays. In a recent study on the Florida Keys, phytoplankton were found to produce mycosporine-like amino acids (MAAs) to absorb ultra-violet (UV) light, with a peak in  $a_{ph}$  at ~315-360 nm, to compensate for low CDOM absorption (Ayoub et al., 2012). There are inconclusive results of MAA production by *Cylindrospermopsis raciborskii* in Lake Balaton [A.W. Kovács, pers. comm.], and many marine cyanobacteria species have been documented to produce MAAs (Sinha et al., 2007). An earlier study also details the presence of UV-screening compounds in terrestrial cyanobacteria mats, including MAAs and scytonemin (Cockell & Knowland, 1999). In freshwater lakes the literature is scarce, with *Microcystis aeruginosa* as the only documented cyanobacteria species found to produce MAAs (Liu et al., 2004). It is therefore possible that one of the most dominant cyanobacteria in Lake Balaton are producing MAAs or similar photo-protective pigments in response to UV stress in the eastern basins where there are lower concentrations of CDOM.

### 3.4.6 SIOPs and distance from the Zala River

The SIOPs varied greatly from west to east across Lake Balaton, principally based on the distance from the main source of nutrients and organic matter, the Zala River. Each station was assigned a distance from the Zala River, and significant differences ( $p < 0.05$ ) were found where none were previously observed using the four basin designations (Figure 3.18).  $a^*_{ph}(350)$  was found to increase with increasing distance from the Zala River over a decreasing CDOM gradient (Figure 3.18ac). Given that a single species comprised the dominant phytoplankton over the study period, it is theorised that the change in  $a^*_{ph}$  in the UV portion of the spectrum is linked to the variable production of photoprotective pigments. Additionally, a significant change in

$S_{\text{CDOM}}$  was measured with increasing distance from the Zala River (Figure 3.18b). The western basins have a larger terrestrial input to CDOM, given the proximity to the river, and this is reflected in the lower values of  $S_{\text{CDOM}}$ . It is important to note that this positive correlation is driven by a small number of stations >60 km from the Zala River, and a subsequent in-depth spatial investigation of  $S_{\text{CDOM}}$  would clarify this relationship. In bio-optical models for retrieval of IOPs and pigments from remote sensing, the  $a_{\text{CDOM}}(\lambda)$  absorption spectrum is often derived from an assumed or estimated  $S_{\text{CDOM}}$  (Lee et al., 2002, Mishra et al., 2013, Li et al., 2013, Li et al., 2015). As such,  $S_{\text{CDOM}}$  may be a prime source of error in the parameterisation of analytical models, with further propagation of errors to retrieved pigment concentrations.

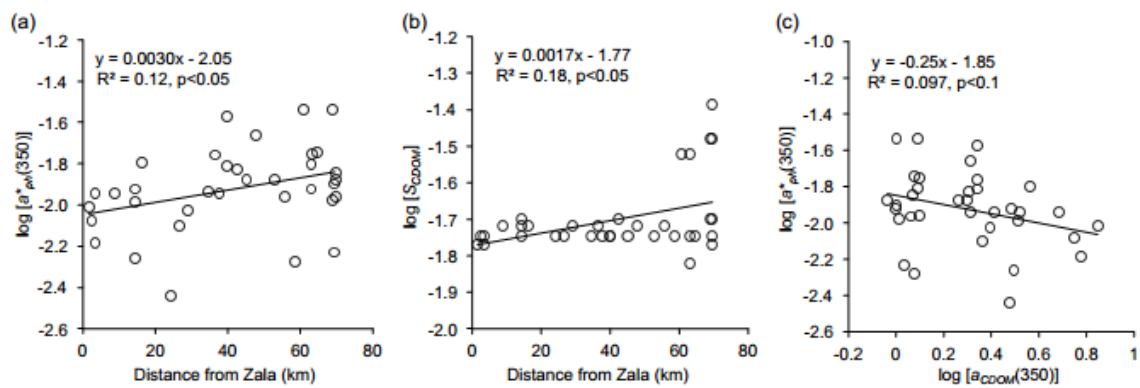


**Figure 3.18** Variation of (a)  $\log [a^*_{ph}(350)]$  ( $\text{m}^2 \text{mg}^{-1}$ ) and (b)  $\log (S_{\text{CDOM}})$  ( $\text{nm}^{-1}$ ) over increasing distance from the Zala River inflow, and (c) relationship between  $\log [a^*_{ph}(350)]$  ( $\text{m}^2 \text{mg}^{-1}$ ) and  $\log [a_{\text{CDOM}}(350)]$  ( $\text{m}^{-1}$ ).

### 3.4.7 $a_{\text{NAP}}(\lambda)$ and suspended matter

Lake Balaton is often characterised by high and heterogeneous concentrations of suspended minerals due to the wind-induced resuspension of dolomite limestone bottom sediments (Tyler et al., 2006), with lake mean PIM concentrations comprising over 70% of TSM. Most of the variability in TSM concentrations in this study was explained by PIM (57%), and significantly more so if the 3 Kis-Balaton stations are excluded (96%) (Kis-Balaton is dominated by phytoplankton, with POM comprising up to 92% of the TSM at station KB2). The proportion of  $a_{\text{NAP}}(\lambda)$  was also significantly correlated with PIM, demonstrating the large contribution from inorganic matter to non-algal particulate absorption (Figure 3.17). A study on mineral absorption found that mineral absorption in the Irish Sea decreases from blue to red, with a slight increase

between 450 and 550 nm (Bowers & Binding, 2006). This does not seem to be the case in Lake Balaton, and in fact, the spectra sometimes show a slight dip in this wavelength range. This can largely be explained by the difference in sediment types, specifically the siliceous sediments of the Irish Sea (Bryant et al., 1996) contrasting with the dolomitic sediments of Lake Balaton (Tyler et al., 2006).

The slope of the  $a_{\text{NAP}}(\lambda)$  curve ( $S_{\text{NAP}}$ ) was similar across all basins, with a mean value of  $0.015 \pm 0.004 \text{ nm}^{-1}$ . Other studies have reported similarly narrow ranges of  $S_{\text{NAP}}$ , however mean  $S_{\text{NAP}}$  in Lake Balaton was distinctly higher than that reported in ocean [ $0.0094 \pm 0.0018$  (Bricaud et al., 2010) and  $0.011 \pm 0.0025$  (Bricaud et al., 1998)] or coastal waters (Babin et al., 2003b, Bowers & Binding, 2006). Comparable values were reported for the turbid waters of western Lake Erie (Peng & Effler, 2013), although maximum  $S_{\text{NAP}}$  values in Lake Balaton were higher. Babin et al. (2003b) hypothesized that the observed variations in  $S_{\text{NAP}}$  in coastal waters were a result of the differences in the proportion of mineral versus organic matter. Differences related to NAP composition were found in this study, with lower mean  $S_{\text{NAP}}$  reported in Kis-Balaton where the highest proportion of organic matter was measured (46-92% POM), while higher mean values were reported in Basins 2 and 3 where PIM comprised up to 90% of TSM (Basin 3).  $S_{\text{NAP}}$  also generally declined with an increasing ratio of inorganic particulates, but followed a distinctly linear decreasing pattern with  $a_{\text{NAP}}(440)$  for values of  $a_{\text{NAP}}(440) < 0.1 \text{ m}^{-1}$  (Figure 3.16). Bricaud et al. (2010) also found a decrease in  $S_{\text{NAP}}$  over a low range of  $a_{\text{NAP}}(440)$  in ocean waters ( $< 0.05 \text{ m}^{-1}$ ), which they attributed to the variable abundance and nature of organic particles comprising the NAP pool (e.g. weakly coloured versus coloured particles). It is likely that the differing nature of organic particles which make up the NAP in Lake Balaton also contributes to the observed variations in  $S_{\text{NAP}}$ , particularly for low levels of TSM ( $< 10 \text{ mg L}^{-1}$ ) and  $a_{\text{NAP}}(440)$  ( $< 0.1 \text{ m}^{-1}$ ).

### **3.4.8 Effect of wind-driven resuspension**

Another potential source of variability in the optical properties of Lake Balaton is the change in the composition and size distribution of particles, as often occurs during resuspension events. The absorption measured at stations sampled on 26 August 2010 in this study indicated a marked difference in contributions from phytoplankton, non-algal particles and CDOM to total absorption (Figure 3.8). The mean wind speed on 26 August at Siófok was  $3.6 \text{ m s}^{-1}$ , which is higher than the daily averages from the

other 7 sampling dates (Table 3.1). Additionally, the maximum wind speed on the previous day (25 August) was  $13.6 \text{ m s}^{-1}$ . As the generally accepted threshold for turbulent mixing in shallow lakes is  $4 \text{ m s}^{-1}$  (Hunter et al., 2008a), it is likely that the water column was affected by substantial resuspension of sediments on 26 August. This difference in sampling conditions may explain some of the variability in the (S)IOPs seen in this study, as wind-driven resuspension of sediments has been shown to cause significant increases in light absorption, scattering and attenuation particularly in shallow inland or coastal waters (Zhang et al., 2006, Verspecht & Pattiaratchi, 2010, Liu et al., 2014). Due to highly variable winds across Lake Balaton, both temporally and spatially, future study should include anemometer readings taken alongside the optical measurements at each station in order to investigate this effect further. There is also a lag time effect from weather conditions from the previous day, which should be considered when interpreting the effect on optical properties.

### 3.5 Conclusions

In summary, the IOPs in Lake Balaton show distinct spatial variability, with decreasing absorption coefficients across a decreasing trophic gradient of Chl-*a* and phytoplankton biomass.  $a_{\text{NAP}}$  was significantly correlated with PIM, which indicates the strong influence of mineral particles on non-water absorption in Lake Balaton. Specific phytoplankton absorption [ $a_{\text{ph}}^*(675)$ ] was variable across Chl-*a* concentrations, with no clear trend across the basins, likely due to the dominance of one cyanobacteria species across the lake (*Cylindrospermopsis raciborskii*). However, significant differences were reported in  $a_{\text{ph}}^*(350)$  and  $S_{\text{CDOM}}$  over increasing distance from the Zala River and a decreasing CDOM gradient. This is likely to be linked to the variable production of photoprotective pigments (i.e. MAAs), as opposed to variations in the phytoplankton community composition. While this study was suitable for demonstrating the spatial variability in (S)IOPs in Lake Balaton, further investigation into seasonal variations is pertinent. With regard to the wider implications for remote sensing, bio-optical models for inversion of constituents such as Chl-*a* must consider the full range of values for (S)IOPs in that water body in order to avoid significant uncertainties in the retrieved values. This has implications for algorithm applications in large shallow lakes with variable biogeochemistry across basins, such as Lake Balaton, and calls into question whether a single algorithm for constituent extraction is suitable across the entire lake. Large lakes with variable biogeochemistry may require basin-

specific remote sensing algorithms for accurate parameter retrieval [e.g. (Campbell et al., 2011)] This research will furthermore contribute towards progressing bio-optical models using absorption and scattering measurements to improve remote sensing retrieval in optically complex waters.

## 4 Scattering and backscattering of suspended matter in an optically complex, shallow lake

---

### 4.1 Introduction

Scattering is quantified as the volume scattering function (VSF),  $\beta(\theta)$ , or the angular dependence,  $(\theta)$ , of scattered light from an incident unpolarised beam (Sullivan et al., 2013). The scattering coefficient,  $b(\lambda)$ , is the integrated VSF from 0 to  $\pi$  radians ( $0^\circ$  to  $180^\circ$ ):

$$b(\lambda) = 2\pi \int_0^\pi \sin(\theta)\beta(\theta)d\theta \quad (4.1)$$

and the backscattering coefficient,  $b_b(\lambda)$ , is the integral of the VSF in the backwards direction from  $\pi/2$  to  $\pi$  ( $90^\circ$  to  $180^\circ$ ):

$$b_b(\lambda) = 2\pi \int_{\pi/2}^\pi \sin(\theta)\beta(\theta)d\theta \quad (4.2)$$

Knowledge of the scattering properties of the water column can provide pertinent information on underwater radiative transfer processes, as well as the nature and dynamics of the optically active constituents (OACs) in the water itself (Sullivan et al., 2013). Optical scattering is an inherent optical property (IOP) and is therefore independent of ambient light (Loisel et al., 2006). However, the magnitude and spectral pattern of particulate scattering is generally affected by the concentration, size distribution, composition and shape of the suspended particles (Peng & Effler, 2016). Particularly in turbid waters, high concentrations of total suspended matter (TSM) and variable composition of inorganic and organic fractions (PIM and POM, respectively) can result in significant variations in scattering properties. Scattering by the OACs alters the underwater light climate in lakes, and can thus affect the emergent light reflected from the water surface and detected by remote sensing systems (Snyder et al., 2008). Therefore, it is vital to understand the variability of scattering properties in inland waters to minimise the uncertainty of retrieved parameters from remote sensing instruments.

More specifically, particle concentration and composition have an effect on backscattering (Mobley, 1994, Twardowski et al., 2001, Jonasz & Fournier, 2007), therefore characterization of the  $b_b(\lambda)$  coefficient can inform studies of particle dynamics, biogeochemical cycling and remote sensing (Ulloa et al., 1994, Twardowski et al., 2001, Boss et al., 2004, Sullivan et al., 2005, Loisel et al., 2007, Stramski et al.,

2008, Sun et al., 2009, Dall'Olmo et al., 2009, Twardowski et al., 2012). For example, optical measurements of attenuation or backscattering have been used to infer the concentration (e.g. Jerlov, 1976) or bulk composition (Twardowski et al., 2001, Boss et al., 2004, Loisel et al., 2007, Peng et al., 2009) of suspended particles. In ocean waters, the particulate backscattering coefficient [ $b_{bp}(\lambda)$ ] has also been suggested as a proxy for estimates of phytoplankton biomass, due to the significant contribution of large phytoplankton to particulate backscattering (Dall'Olmo et al., 2009). Particulate scattering and backscattering coefficients have also been widely used as proxies for TSM concentration in coastal waters (Babin et al., 2003a, Boss et al., 2009). Use of light scattering metrics as proxies for water quality parameters provides information on the temporal and spatial dynamics of these parameters through the use of *in situ* optical instruments. *In situ* optical instruments could provide increased temporal frequency of water quality measurements, as compared to traditional water sampling and laboratory analysis methods. Therefore, knowledge of the scattering properties in the water column is of importance to understanding the dynamic in-water particle concentrations and compositions.

Knowledge of the backscattering coefficient is also particularly of use in semi-analytical and analytical inversion algorithms, which estimate  $b_{bp}(\lambda)$  for the retrieval of in-water constituents from remote sensing systems. These algorithms are based on the radiative transfer theory that specifies remote sensing reflectance,  $R_{rs}(\lambda)$ , is proportional to  $b_b/(a+b_b)$ , where  $a$  is the absorption coefficient (Gordon et al., 1975). Given this relationship, the sum of particulate backscattering [ $b_{bp}(\lambda)$ ] and the backscattering coefficient of pure water  $b_{bw}(\lambda)$  can contribute greatly to variability in the spectral shape of  $R_{rs}(\lambda)$  in the upper layer of the water column, and therefore retrievals of biogeochemical parameters from  $R_{rs}(\lambda)$  (e.g. chlorophyll-*a* (Chl-*a*) or TSM concentration). It has recently been shown that changes in particle composition and thus scattering properties have an impact on  $R_{rs}(\lambda)$  in the near infrared, affecting the remote sensing retrieval of Chl-*a* in turbid inland (Qi et al., 2015) and coastal waters (Gilerson et al., 2007, Mckee et al., 2007). Variations in scattering properties in inland waters thus impact the accuracy of remote sensing to retrieve water quality parameters, therefore it is vital to better quantify this variability and reduce errors in retrieved concentrations.

Variability in  $R_{rs}(\lambda)$  is also controlled by the particulate backscattering ratio,  $\tilde{b}_{bp}$ , which is defined as:

$$\tilde{b}_{bp} = b_{bp}(\lambda)/b_p(\lambda) \quad (4.3)$$

where  $b_{bp}(\lambda)$  and  $b_p(\lambda)$  are the particulate scattering and backscattering coefficients, respectively (Mobley et al., 2002, Lubac & Loisel, 2007).  $\tilde{b}_{bp}$  is generally calculated using  $b_{bp}$  and  $b_p$  at 532 nm, and research in a range of inland, coastal and ocean waters indicates that this ratio should be constant at all wavelengths (i.e. no spectral dependence) (Whitmire et al., 2007). The  $\tilde{b}_{bp}$  is the proportion of light scattered in the backwards direction, also known as the backscattering efficiency, and it can provide information on the bulk refractive index and particle size and composition of the suspended particulate material (Boss et al., 2004).

It has generally been reported that particulate attenuation, scattering and backscattering coefficients increase with greater concentrations of total suspended matter, while the mass-specific coefficients vary with the nature of particles (i.e. size, shape, structure, refractive index and composition) (Neukermans et al., 2012). However, the relationship between suspended particles and light scattering has been mainly studied in ocean and coastal waters to date (Twardowski et al., 2001, Babin et al., 2003a, Boss et al., 2009, Martinez-Vicente et al., 2010, Xi, 2015), while there is little information available on inland waters (Sun et al., 2009, Shi et al., 2014, Lyu Heng et al., 2015). Recent studies of scattering properties in lakes have included the shallow eutrophic Lake Taihu, where scattering parameters were closely related to particulate inorganic matter (PIM) as opposed to particulate organic matter (POM) or Chl-*a*, and there was a wider range in  $b^*_p$  than reported for coastal waters (Sun et al., 2009). In Poyang Lake,  $b^*_p(700)$  declined exponentially with increasing TSM concentration (Wu et al., 2013). Shi et al (2014) studied scattering in three eutrophic Chinese lakes, finding that  $b^*_p(532)$  was positively correlated with the ratio of PIM:TSM. Lyu et al. (2016) confirmed distinctive relationships between  $\tilde{b}_{bp}$  and water quality parameters in these same three Chinese lakes, attributed to the differing concentrations of OACs in each lake and thus differing relative contributions of organic and inorganic particles to scattering and backscattering. Other studies on American lakes have measured scattering properties for the purpose of parameterizing bio-optical models (Peng & Effler, 2016) or optical closure (O'Donnell et al., 2010, Peng & Effler, 2012, O'Donnell et al., 2013). Recent studies on the relationships between scattering properties and OACs in inland waters have been geographically limited and focused on primarily eutrophic lakes (e.g. Lake Taihu, Lake Chaohu, Lake Dianchi). There is

generally a lack of information on optical scattering and backscattering properties in European lakes, and particularly large shallow lakes with a trophic gradient and a high concentration of inorganic particulates.

There is a broad range of biogeochemical composition comprising inland waters, therefore scattering is expected to vary greatly from ocean waters. For example, it has been suggested that minerogenic particles play a more dominant role in scattering in coastal (Stramski et al., 2001, Loisel et al., 2007) and inland waters (Peng et al., 2007, Peng & Effler, 2016). Minerogenic particles have a higher scattering efficiency than phytoplankton, and PIM is considered to have the greatest mass-specific backscattering coefficient of the particulates (Stramski et al., 2001). For example, Babin et al. (2003a) reported a significantly higher value of mass-specific particulate scattering [ $b_p^*(550)$ ] for ocean waters as compared to coastal waters, which was attributed to the dominance of organic or inorganic (minerogenic) particles, respectively. Particles in inland waters are also likely to demonstrate greater spatial and temporal variability than in oceans, particularly in shallow dynamic lacustrine systems with frequent resuspension of sediments. Frequent resuspension may also change the particle size distribution and thus scattering properties, with greater concentrations of larger particles present in the water column. Stramski et al. (2007) found increases in  $b_p^*(\lambda)$  for terrigenous minerogenic sediment samples following settling (preferential loss of larger particles). Therefore it may be expected that changes in the particle size due to variable resuspension may also alter the scattering properties in lakes. Additionally, point-source delivery (e.g. river input) of nutrients and total suspended matter, as well as highly dynamic surface algal blooms may generate variability on much smaller spatial scales than for most open ocean waters (Mouw et al., 2015). For instance, some inland or coastal phytoplankton species have the ability to develop a bloom or substantially expand bloom size in a matter of hours (Hunter et al., 2008a, Hu & Feng, 2014). River flow rate and runoff events may further affect scattering properties in inland waters. Peng and Effler (2012) found that abrupt increases in flow rate and total suspended matter caused corresponding substantial increases in  $b_p(660)$  and decreases in  $b_p^*(660)$  in Esopus Creek. Thus, preliminary work indicates that scattering properties in inland and coastal waters may be distinct from those in ocean waters, and are affected by the dynamic processes inherent in these systems.

Therefore, this study aims to quantify the variability of the scattering and backscattering properties in a large and optically complex shallow lake, and how optical scattering is related to the biogeochemistry of a dynamic minerogenic-dominated system. Additionally, Chapter 3 found the bulk and specific absorption properties of Lake Balaton to vary significantly, with differing relationships to those reported in ocean waters (Riddick et al., 2015), therefore the present study provides a complementary investigation of the corresponding differences in bulk and specific scattering properties. In this chapter, relationships between scattering properties and the concentration and composition of total suspended matter will be qualified and placed in context of other inland, coastal and marine studies, with the aim of determining the drivers of the optical scattering properties in a large, turbid lake. Lake Balaton serves as a case study of a lake with a trophic gradient and a high concentration of particulate inorganic matter, therefore providing an example of a complex optical scenario.

## **4.2 Methods**

### **4.2.1 Study area**

Lake Balaton is a large shallow freshwater lake in Europe, with a mean surface area of 596 km<sup>2</sup> and mean depth of approximately 3 m (Herodek, 1986, Présing et al., 2001, Tyler et al., 2006). The lake is subdivided into four basins (Figure 4.1), with an engineered wetland system in the west (Kis-Balaton) constructed in the mid-1980s to early 1990s (Tyler et al., 2006). The sediments are predominantly comprised of dolomite limestone, rich in fine particles of calcium and magnesium (Svab et al., 2005, Tyler et al., 2006). Lake Balaton is shallow, and as such, the sediments are frequently resuspended in the water column due to wind-driven mixing.

Lake Balaton is by nature subject to substantial variations in the particle assemblage. Seasonal variations in the phytoplankton population are well documented, with small blooms in winter/spring and more severe blooms of nitrogen-fixing cyanobacteria occurring in the late summer months (Mozes et al., 2006, Hajnal & Padisak, 2008, Palmer et al., 2015a). The relative contributions to the particle assemblage in Lake Balaton also vary spatially across the lake, with waters dominated by biological particles in the west and a greater proportion of mineral particles in the eastern basins (up to 81% PIM in Basin 3; Chapter 3) (Riddick et al., 2015). Lake

Balaton is further subject to episodic changes due to resuspension driven by wind or storm events, resulting in highly heterogeneous distribution of total suspended matter (typically  $\sim 3\text{-}300 \text{ mg L}^{-1}$ ) (Tyler et al., 2006).

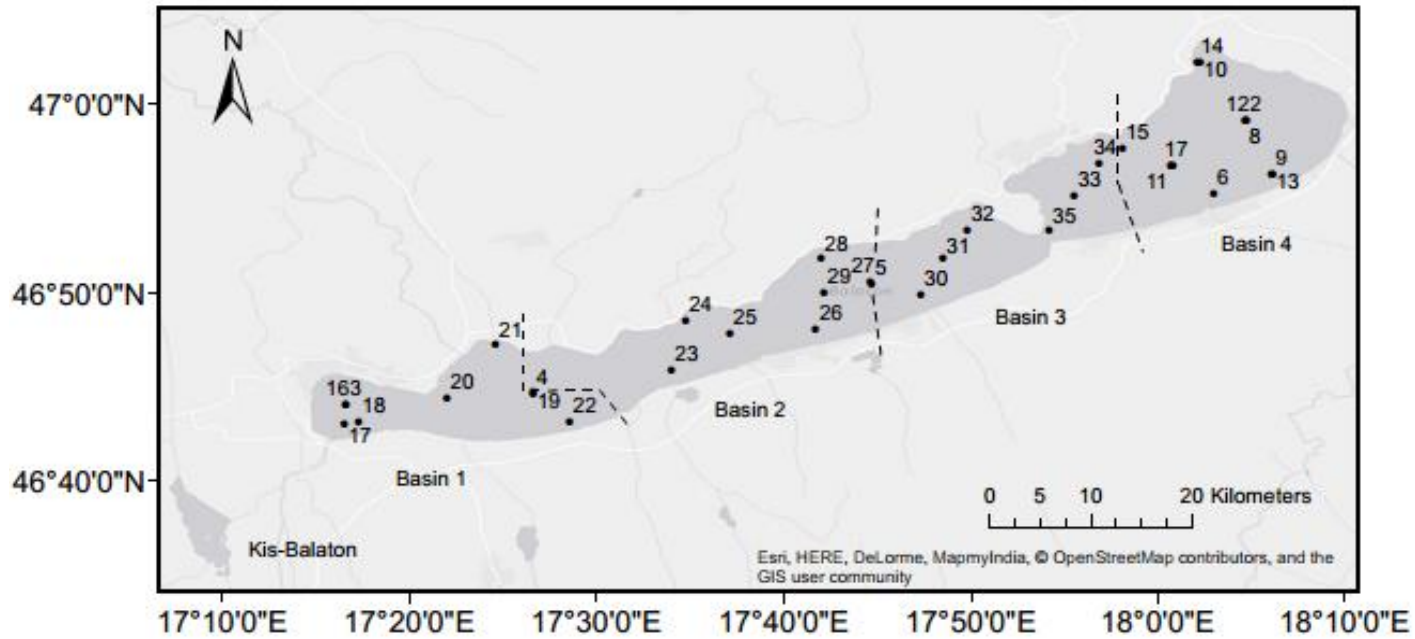


**Figure 4.1** Map of Lake Balaton indicating 4 basins and 35 station locations.

#### 4.2.2 Water sampling

Field measurements in Lake Balaton were conducted at 35 stations between 19<sup>th</sup> and 26<sup>th</sup> August 2010 (Figure 4.1). Surface water samples were collected and filtered on the boat under low vacuum pressure through GF/F (Whatman) filter papers. Depending on water clarity between 20 and 70 mL of sample water was filtered, and filter papers were flash frozen in liquid nitrogen for <12 hours. Samples were stored in a -80°C freezer and analyzed within 6 months.

#### 4.2.3 *In situ* optical measurements

The instruments deployed *in situ* consisted of a WET Labs AC-S and ECO-BB3, along with a Seabird CTD to record the temperature, salinity and pressure (depth). These were deployed in a black metal cage over a beam that extended the cage approximately 1.5 m from the boat hull. A WET Labs AC-9 was concurrently deployed at the same location. The instruments were submerged just below the water surface and de-bubbled for at least five minutes before measurements commenced. Five-minute casts were subsequently recorded to a data logger at each station with the data from the AC-S monitored in real-time for quality assurance.

#### 4.2.4 Chlorophyll-*a*

Frozen GF/F filter papers were thawed from -80°C and chlorophyll-*a* (Chl-*a*) was measured spectrophotometrically (Shimadzu UV-1601) after a hot 90% methanol extraction, as in Iwamura *et al.* (1970). Three replicates were analysed for Chl-*a* from each station. The concentration ( $\text{mg m}^{-3}$ ) of Chl-*a* was determined according to the following formula, where  $A_{665}$  is the measured absorbance at 665 nm:

$$[\text{Chl} - a] = 13.9 \times A_{665}. \quad (4.4)$$

#### 4.2.5 Phycocyanin

Frozen GF/F filter papers were thawed from -80°C and the pigment was extracted in a solution of 15 ml 0.05M phosphate buffer (pH=6.8). A minimum of two replicates were analyzed for measurement of phycocyanin (PC) concentration, with outlying values discarded. Following the method of Horváth *et al.* (2013a), samples in the buffer solution were subjected to sonication over ice for 15 seconds (*Ultrasonic Homogenizer 4710 Series* with micro-tip and 50% of duty cycle, Cole-Palmer Instrument Co., USA). The solution was clarified by filtration (Whatman GF/C), and extract absorption was measured on a spectrophotometer (Shimadzu UV-1601,

Shimadzu Co., Japan). Phycocyanin concentrations ( $\text{mg m}^{-3}$ ) were calculated using the following equation of Siegelman and Kycia (1978):

$$[PC] = (A_{615} - 0.474 \times A_{652})/5.34 \quad (4.5)$$

where  $A_x$  is the measured absorbance at  $x$  wavelength (nm).

#### 4.2.6 Biomass and phytoplankton counts

Phytoplankton samples were preserved in Lugol's solution immediately after collection. Algal species were enumerated with an inverted plankton microscope (Utermöhl, 1958). The wet weight of each species was calculated from cell volumes (Németh & Vörös, 1986). At least 25 cells (or filaments) of each species were measured to determine biomass and at least 400 were counted.

#### 4.2.7 Total suspended matter and inorganic/organic fractions

Total suspended matter (TSM) was measured by filtration and gravimetric analysis. 500-1500 ml of the water sample was filtered under low-vacuum pressure ( $<700\text{mbar}$ ) through a pre-ashed (furnace at  $450^\circ\text{C}$ ) and pre-weighed GF/C filter paper. Following filtration, filter papers were dried overnight in a clean oven at  $60^\circ\text{C}$  and subsequently weighed to obtain TSM. Filters were then placed in a furnace at  $450^\circ\text{C}$  overnight and subsequently weighed to obtain particulate inorganic matter (PIM). Particulate organic matter (POM) was then calculated by simple subtraction.

#### 4.2.8 Absorption by coloured dissolved organic matter

Water samples were filtered into clean glassware through  $0.22 \mu\text{m}$  nucleopore membrane filters (Whatman) within 24 hours of sample collection, according to REVAMP and IESCA protocols (Tilstone et al., 2002, Tilstone & Martinez-Vicente, 2012). Absorption of the filtrate was determined on a spectrophotometer with a 4 or 5 cm cuvette over the range of 350-800 nm, using filtered MilliQ as a reference blank. The absorption coefficient of CDOM ( $a_{CDOM}$ ) was calculated using the following equation:

$$a_{CDOM}(\lambda) = 2.303 D(\lambda)/r \quad (4.6)$$

where  $D(\lambda)$  is the measured absorption at a given wavelength and  $r$  is the cuvette path length in meters. A baseline correction was applied by subtracting the mean value of  $a_{CDOM}$  in a 5 nm interval around 685 nm (Babin et al., 2003b). This wavelength was

applied because there is negligible  $a_{CDOM}$  at 685 nm and small effects of temperature and salinity on water absorption (Pegau et al., 1997).

#### 4.2.9 Particulate attenuation and scattering coefficients

An AC-S (WET Labs) collected hyperspectral absorption ( $a$ ) and attenuation ( $c$ ) measurements over 84 wavelengths, from 401-755 nm at ~4 nm resolution. Simultaneously, an AC-9 collected  $a$  and  $c$  data at 9 wavelengths (412, 440, 488, 510, 532, 555, 650, 676 and 715 nm). The AC-S and AC-9 raw data were corrected for the time lag associated with the flow rate for the instrument, and then merged with the CTD data for temperature, salinity and pressure. Using the CTD data, the effects of temperature and salinity on pure water absorption and attenuation were removed with wavelength-dependent corrections. To correct for instrument drift, a pure water calibration was applied to both attenuation and absorption data. The proportional scattering correction of Zaneveld et al. (1994) was applied to absorption data to account for inefficient collection of the scattered light within the AC-S reflecting tube. While other scattering corrections exist, the proportional scattering correction is used here for consistency with previous work on Lake Balaton (Chapter 3; Riddick et al., 2015) and comparable studies elsewhere (Leymarie et al., 2010, Slade et al., 2010, Astoreca et al., 2012). The AC-S data for each station were screened for any outliers ( $\pm 2 \sigma$ ) in order to eliminate measurements adversely affected by bubbles. Particulate attenuation [ $c_p(\lambda)$ ] was calculated by subtraction of  $a_{CDOM}(\lambda)$  from the total attenuation coefficient [ $c_p(\lambda) = c_{pg}(\lambda) - a_{CDOM}(\lambda)$ ]. The particulate scattering coefficient [ $b_p(\lambda)$ ] was then calculated by subtracting the AC-S measured absorption from attenuation [ $b_p(\lambda) = c_p(\lambda) - a_{pg}(\lambda)$ ]. It was assumed that scattering of the dissolved fraction (i.e. CDOM) is negligible, i.e.  $b_{pg}(\lambda) = b_p(\lambda)$ .

#### 4.2.10 Particulate backscattering coefficients

Particle backscattering coefficients [ $b_{bp}(\lambda)$ ] were derived from measurements collected with an ECO-BB3 backscatter meter (WET Labs). The calibration was performed by the manufacturer immediately prior to sampling, and it was assumed that there was no drift in the calibration coefficients and/or dark counts. The ECO-BB3 measures the total volume scattering function [ $\beta_t(\lambda, 124^\circ)$ ] from a centroid angle of scattering ( $124^\circ$ ) at 3 wavelengths ( $\lambda = 470, 532$  and  $650$  nm). The transformation of the

raw counts into  $b_{bp}(\lambda)$  was done following the manufacturer's user guide (WET Labs, 2010) and the methods as in Slade and Boss (2015).

Firstly, the instrument raw counts were converted into an uncorrected value of the volume scattering function,  $[\beta_u(\lambda, 124^\circ)]$ :

$$\beta_u(\lambda, 124^\circ) = s(\lambda)[raw(\lambda) - d(\lambda)] \quad (4.7)$$

Where  $s$  and  $d$  are scaling and dark counts factors, respectively, with values supplied by the manufacturer. The scaling factors change with time at a typical rate of 10%, 4% and 3% per year for blue, green and red wavelengths, respectively (Sullivan et al., 2013). As this sampling campaign was conducted over 10 days, the expected maximum change over time is about 0.3% of the signal, and retrospective laboratory tracking from 2013-2015 of the scaling factor on this ECO-BB3 has corroborated this assumption (Martinez-Vicente, pers. comm.).

Secondly,  $\beta_u(\lambda, 124^\circ)$  was corrected to account for the light attenuation within the instrument path length using an attenuation factor,  $K(\lambda)$ :

$$K(\lambda) = \exp\left(La_{pg}(\lambda)\right) \quad (4.8)$$

Where  $L$  is the effective pathlength (0.015 m) and  $a_{pg}(\lambda)$  is the absorption due to particulate and dissolved matter.  $a_{pg}(\lambda)$  was simultaneously measured by the AC-9, and these data were processed using the temperature *proportional*<sup>e</sup> scattering correction from Roettgers et al. (2013) and pure water calibrations measured before and after the campaign. In each case, the nearest wavelengths to the ECO-BB3 wavelengths were applied (i.e. 488, 532 and 660).  $\beta_t(\lambda, 124^\circ)$  is then calculated as:

$$\beta_t(\lambda, 124^\circ) = \beta_u(\lambda, 124^\circ) \times K(\lambda) \quad (4.9)$$

Thirdly, the value of the volume scattering function of water was subtracted from  $\beta_t(\lambda, 124^\circ)$  using the model by Zhang et al. (2009) with fixed temperature and salinity values of 24.0 °C and 0.4 psu, respectively.

Finally, the volume scattering function of the particles at 124° was extrapolated to the backwards direction using a conversion factor of  $\chi_p(124^\circ)=1.08$  as in Sullivan et al. (2013):

$$b_{bp}(\lambda) = 2\pi\chi_p(124^\circ) \times [\beta_t(\lambda, 124^\circ) - \beta_w(\lambda, 124^\circ)] \quad (4.10)$$

Mean  $b_{bp}(\lambda)$  values were calculated over 1-5 min measurement periods.

The specific backscattering coefficient [ $b_{bp}^*(532)$ ] was calculated by dividing  $b_{bp}(532)$  by the respective concentration of TSM. The particulate backscattering ratio ( $\tilde{b}_{bp}$ ) was calculated as the ratio of particulate backscattering at 532 nm, as measured by the ECO-BB3, to particulate scattering at 531.3 nm, as measured by the AC-S:

$$\tilde{b}_{bp} = b_{bp}(532) / b_p(531.3) \quad (4.11)$$

This ratio represents the fraction of light scattered in the backwards direction (Neukermans et al., 2012).

It was noted that the BB3 saturated at approximately  $b_{bp}(532) = 0.22 \text{ m}^{-1}$ , and this occurred at stations with high concentrations of TSM. This has been similarly reported in other lacustrine studies using *in situ* optical instruments for measurement of backscattering (Gallegos et al., 2008, O'Donnell et al., 2010). Saturation occurred at six stations (3, 31-35), and with the exception of Station 3 these stations are located in Basin 3. As Basin 3 (including Stations 31-35) was sampled on August 26<sup>th</sup> during and after windy conditions, there were high concentrations of suspended sediments as a result of wind-driven resuspension (see Chapter 3; Riddick et al., 2015). Therefore, these stations have been excluded from analysis and only unsaturated stations are considered.

#### 4.2.11 Bulk refractive index and particle size discrimination slope

The  $c_p(\lambda)$  spectra measured by the AC-S can be described by a hyperbolic equation as follows (Twardowski et al., 2001):

$$c_p(\lambda) = A\lambda^{-\gamma} \quad (4.12)$$

where  $\gamma$  is the hyperbolic slope of the  $c_p(\lambda)$  spectrum and  $A$  is the amplitude.  $\gamma$  is related to the shape of the particle size distribution (PSD) or Junge exponent,  $\xi$ , most simply by (Boss et al., 2001):

$$\xi = \gamma + 3 \quad (4.13)$$

For more general cases of PSDs with finite limits,  $\xi$  can be related to  $\gamma$  according to a nonlinear fit (Boss et al., 2001):

$$\xi = \gamma + 3 - 0.5\exp(-6\gamma) \quad (4.14)$$

In this study, both relationships were used to estimate  $\xi$ .

The bulk refractive index,  $\bar{n}_p$ , was estimated using the model by Twardowski et al. (2001), a method which has been previously employed in inland waters (Sun et al., 2009).  $\bar{n}_p$  was estimated according to the following equation:

$$\bar{n}_p = 1 + \tilde{b}_{bp}^{0.5377+0.4867(\xi-3)^2} [1.4676 + 2.2950(\xi - 3)^2 + 2.3113(\xi - 3)^4] \quad (4.15)$$

## 4.3 Results

### 4.3.1 Nature of suspended particles across the basins

The four basins sampled in Lake Balaton during summer 2010 demonstrated marked variability in biogeochemical composition (Table 4.1). Total suspended matter concentrations ranged from ~4 to 50 mg L<sup>-1</sup>, with the highest mean concentration in Basin 4 (~15 mg L<sup>-1</sup>). There was a gradient in PIM from east to west, with PIM comprising ~55% of TSM in Basins 1 and 2, and up to 75% of suspended particles in Basin 4. Basin 3 had notably high mean concentrations of TSM and PIM with high standard deviation (Mean 13 ± 11 mg L<sup>-1</sup> and 10 ± 11 mg L<sup>-1</sup>, respectively) due to wind-driven resuspension on the sampling date for this basin [see Table 3.1 in Chapter 3; Riddick et al. (2015)].

This gradient in TSM composition is also driven by variability in phytoplankton abundance across the lake. Mean Chl-*a* concentrations ranged from ~33 mg m<sup>-3</sup> in the most westerly basin (Basin 1) to ~8 mg m<sup>-3</sup> in the east (Basin 3). Similarly, total phytoplankton biomass ranged from ~1854 to ~7062 mg m<sup>-3</sup> from east to west, confirming a trophic gradient across the lake during this study (Riddick et al., 2015). The most abundant species in all basins was the nitrogen-fixing cyanobacteria *Cylindrospermopsis raciborskii*, which has been noted to dominate summer algal blooms in Lake Balaton in recent years. However, an increasing presence of other phytoplankton groups was noted from west to east, with a greater abundance of cryptophytes, chlorophytes, dinophytes and heterokontophytes in Basins 3 and 4 [see Figure 3.4c in Chapter 3; Riddick et al. (2015)].

Variations in the material inputs from the Zala River are an additional mechanism behind the observed biogeochemical gradient in Lake Balaton, as the river is the main inflow, providing a major input of nutrients and dissolved and particulate matter to the western shore. This results in the pronounced gradient in phytoplankton abundance, with the highest mean phytoplankton biomass in the Keszthely basin (Basin 1; 7062 mg m<sup>-3</sup>). The Zala River also generates a gradient in CDOM, with the highest

$a_{\text{CDOM}}(440)$  in Kis-Balaton ( $2.82 \text{ m}^{-1}$ ) to the lowest in Basin 4 ( $0.18 \text{ m}^{-1}$ ) (Chapter 3; Riddick et al., 2015).

**Table 4.1** Mean ( $\pm$  standard deviation) biogeochemical parameters for each basin in Lake Balaton, including chlorophyll-a (Chl-*a*), phycocyanin (PC), total suspended matter (TSM), particulate organic matter (POM), particulate inorganic matter (PIM), the ratio of PIM:TSM, phytoplankton biomass (Total Biomass) and cyanobacteria biomass (Cyano Biomass;  $\text{mg m}^{-3}$  and % biomass) (table adapted from Table 3.2 in Chapter 3; Riddick et al., 2015).

	<b>Basin 1 (n=4)</b>		<b>Basin 2 (n=8)</b>		<b>Basin 3 (n=8)</b>		<b>Basin 4 (n=15)</b>		<b>Lake Mean (n=35)</b>		<b>Units</b>
Chl- <i>a</i>	32.74	$\pm 5.40$	21.12	$\pm 6.71$	8.24	$\pm 1.91$	10.8	$\pm 2.30$	15.08	$\pm 8.90$	$\text{mg m}^{-3}$
PC	22.33	$\pm 7.41$	15.62	$\pm 4.56$	6.19	$\pm 2.05$	9.95	$\pm 2.67$	11.80	$\pm 6.19$	$\text{mg m}^{-3}$
TSM	14.41	$\pm 5.82$	10.36	$\pm 1.78$	12.55	$\pm 11.23$	15.37	$\pm 6.11$	13.47	$\pm 7.01$	$\text{mg L}^{-1}$
POM	6.09	$\pm 1.23$	4.71	$\pm 1.41$	2.41	$\pm 0.53$	3.41	$\pm 0.49$	3.78	$\pm 1.43$	$\text{mg L}^{-1}$
PIM	8.32	$\pm 4.79$	5.65	$\pm 1.63$	10.14	$\pm 10.96$	11.97	$\pm 6.04$	9.69	$\pm 6.98$	$\text{mg L}^{-1}$
PIM:TSM	0.55	$\pm 0.11$	0.55	$\pm 0.12$	0.70	$\pm 0.15$	0.75	$\pm 0.08$	0.67	$\pm 0.14$	-
Total Biomass	7062	$\pm 1780$	3916	$\pm 1376$	1854	$\pm 603$	2851	$\pm 821$	3348	$\pm 1832$	$\text{mg m}^{-3}$
Cyano Biomass	5756	$\pm 1810$	3456	$\pm 3456$	1232	$\pm 759$	2134	$\pm 671$	2644	$\pm 1658$	$\text{mg m}^{-3}$
Cyano Biomass	81	$\pm 8$	88	$\pm 6$	64	$\pm 27$	74	$\pm 17$	76	$\pm 19$	%

### 4.3.2 Relative contributions of absorption and scattering to total attenuation

Attenuation due to particulate and dissolved matter in Lake Balaton is mostly due to particulate scattering (Figure 4.2). In this study,  $b_p(\lambda)$  accounts for up to 85-99% of attenuation, however a study of four Finnish lakes found it only comprised 38-84% of total attenuation (when absorption of pure water is included) (Paavel & Arst, 2009). There also exists a clear absorption gradient across the basins, with the highest proportion of attenuation due to absorption [ $a_p(\lambda) + a_{CDOM}(\lambda)$ ] in Basin 1 (Figure 4.2).

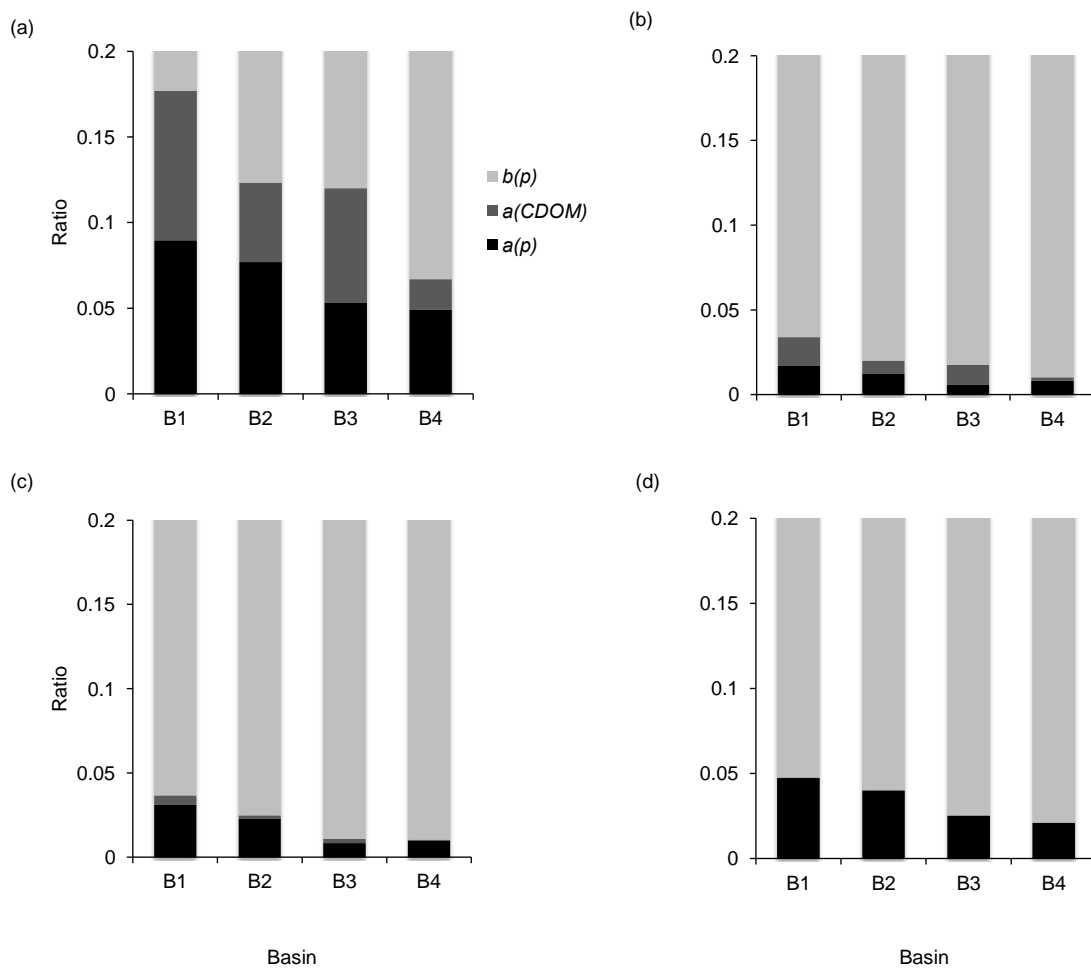


**Figure 4.2** Mean attenuation by basin due to particulate scattering, CDOM absorption and particulate absorption at (a) 440, (b) 555, (c) 620 and (d) 675 nm. The attenuation due to pure water absorption has been subtracted from the total attenuation and therefore not included in these graphs. The ratio axis is scaled to 0.2 for ease of viewing, however note that  $b(p)$  continues to 1.0 in all plots. The abbreviations  $b(p)$ ,  $a(CDOM)$  and  $a(p)$  are used for  $b_p(\lambda)$ ,  $a_{CDOM}(\lambda)$  and  $a_p(\lambda)$ .

Particulate attenuation at 660 nm is plotted against Chl-*a*, TSM, POM and PIM to explore the contribution of each parameter to beam attenuation (Figure 4.3). There is a weak positive exponential relationship between  $c_p(660)$  and Chl-*a* ( $R^2=0.151$ ,  $p=0.0929$ ; Figure 4.3a). However, a much stronger correlation exists between  $c_p(660)$  and TSM ( $R^2=0.838$ ,  $p<0.001$ ), with 68% of the variability in  $c_p(660)$  explained by PIM as opposed to just 23% by POM (Figure 4.3c and d).

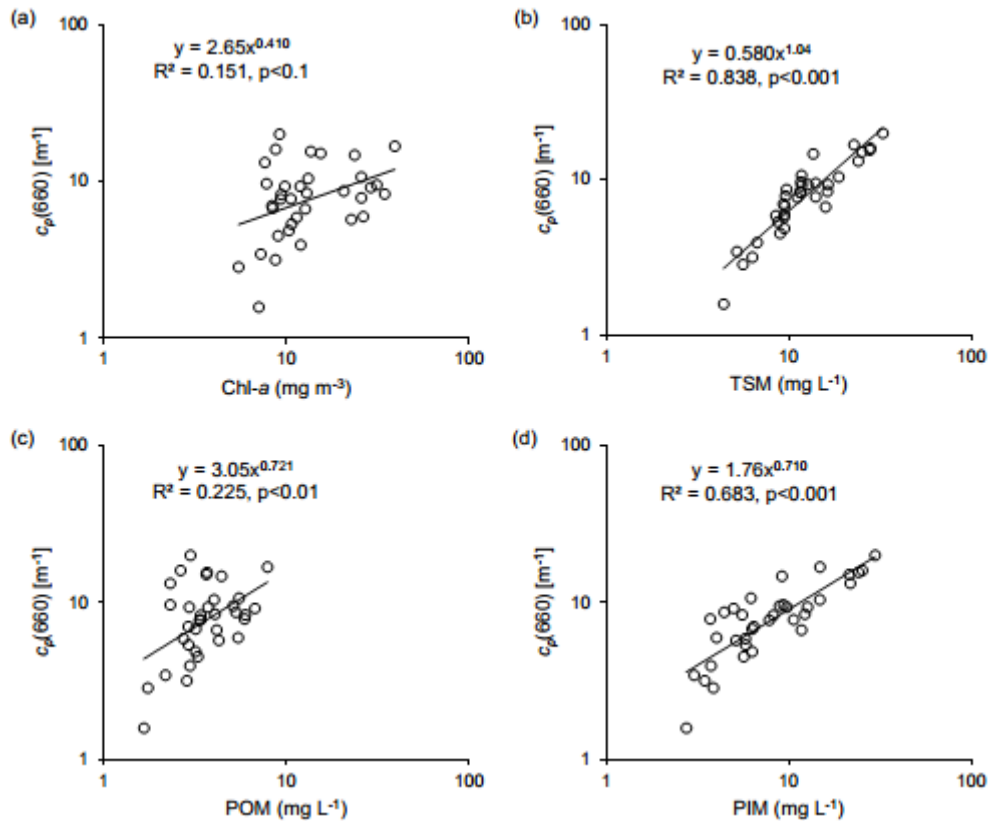


**Figure 4.3** Particulate attenuation at 660nm [ $c_p(660)$ ] plotted against (a) chlorophyll-*a* (Chl-*a*), (b) total suspended matter (TSM), (c) particulate organic matter (POM) and (d) particulate inorganic matter (PIM). Solid lines and equations represent best-fit power functions.

#### 4.3.3 Variability in scattering, backscattering and attenuation coefficients

Particulate backscattering [ $b_{bp}(\lambda)$ ] at 532 nm ranged from 0.0557 to 0.227  $m^{-1}$ , while mass specific backscattering [ $b^*_{bp}(\lambda)$ ] varied from 0.0104 to 0.0186  $m^2 g^{-1}$  in Basins 1-4 (Table 4.2). Particulate attenuation [ $c_p(660)$ ] measured by the AC-S ranged from 1.58 to 19.9  $m^{-1}$  (Table 4.2). Other studies have measured  $c_p$  at 650 nm, however it is noted there was minimal difference (<0.5%) between the values at either wavelength, therefore  $c_p(660)$  is used for analysis purposes here. Particulate scattering

$[b_p(531.3)]$ , as calculated from the difference of  $a_{pg}(\lambda)$  and  $c_{pg}(\lambda)$  measured by the AC-S, ranged from 1.58 to 20.46  $\text{m}^{-1}$ , and the mass specific scattering coefficient ranged from 0.36 to 1.14  $\text{m}^2 \text{g}^{-1}$  in Basins 1-4 (Table 4.2).

**Table 4.2** Summary of scattering, backscattering and attenuation coefficients for Lake Balaton.

<b>(S)IOP</b>	<b>n</b>	<b>Min</b>	<b>Median</b>	<b>Max</b>	<b>Mean</b>	<b>St Dev</b>	<b>Units</b>
$b_{bp}(532)$	29	0.0557	0.164	0.227	0.156	0.0500	$\text{m}^{-1}$
$b^*_{bp}(532)$	29	0.0104	0.0148	0.0186	0.0146	0.00199	$\text{m}^2 \text{g}^{-1}$
$b_p(531.3)$	35	1.58	8.96	20.46	9.35	4.45	$\text{m}^{-1}$
$b^*_p(531.3)$	35	0.36	0.69	1.14	0.71	0.17	$\text{m}^2 \text{g}^{-1}$
$\tilde{b}_{bp}(532)$	29	0.0146	0.0205	0.0352	0.0208	0.00369	-
$c_p(650)$	35	1.58	8.22	19.9	8.67	4.35	$\text{m}^{-1}$
$c_p(660)$	35	1.58	8.25	19.9	8.67	4.35	$\text{m}^{-1}$

The mean ratio of backscattering to scattering in Lake Balaton ( $\tilde{b}_{bp}$ ) was  $0.0208 \pm 0.00369$ , which is within the range reported for many coastal studies (Boss et al., 2004, Mckee & Cunningham, 2006, Loisel et al., 2007, Whitmire et al., 2007, Snyder et al., 2008). Compared to Lake Taihu,  $\tilde{b}_{bp}$  varied over a similar range (0.005-0.027) (Sun et al., 2009), although  $\tilde{b}_{bp}$  was notably higher in Lake Balaton. As previously stated, the backscattering ratio applied in the present study was calculated at 532 nm for consistency with the literature. However, it is important to note that this study found a sizeable difference in  $\tilde{b}_{bp}$  if calculated at either 470 or 650 nm (the other two wavelengths at which  $b_{bp}(\lambda)$  was measured), with mean percent differences of +31% and -48%, respectively (Figure 4.4). Wavelength dependency of  $\tilde{b}_{bp}$  was also recently reported in three Chinese lakes, with generally decreasing  $\tilde{b}_{bp}$  across increasing wavelength (Lyu Heng et al., 2015). This refutes the generally accepted concept that  $\tilde{b}_{bp}$  is spectrally independent, as found by Whitmire et al. (2007) in a range of inland (Crater Lake, USA), coastal (Southern California coast, Gulf of California, USA) and marine waters (mid-Atlantic Bight off New Jersey, USA). Whitmire et al. (2007) had a significantly larger sampling size (n=9,154), therefore the wavelength dependence of  $\tilde{b}_{bp}$  may be specific to the turbid, productive waters of Lake Balaton.

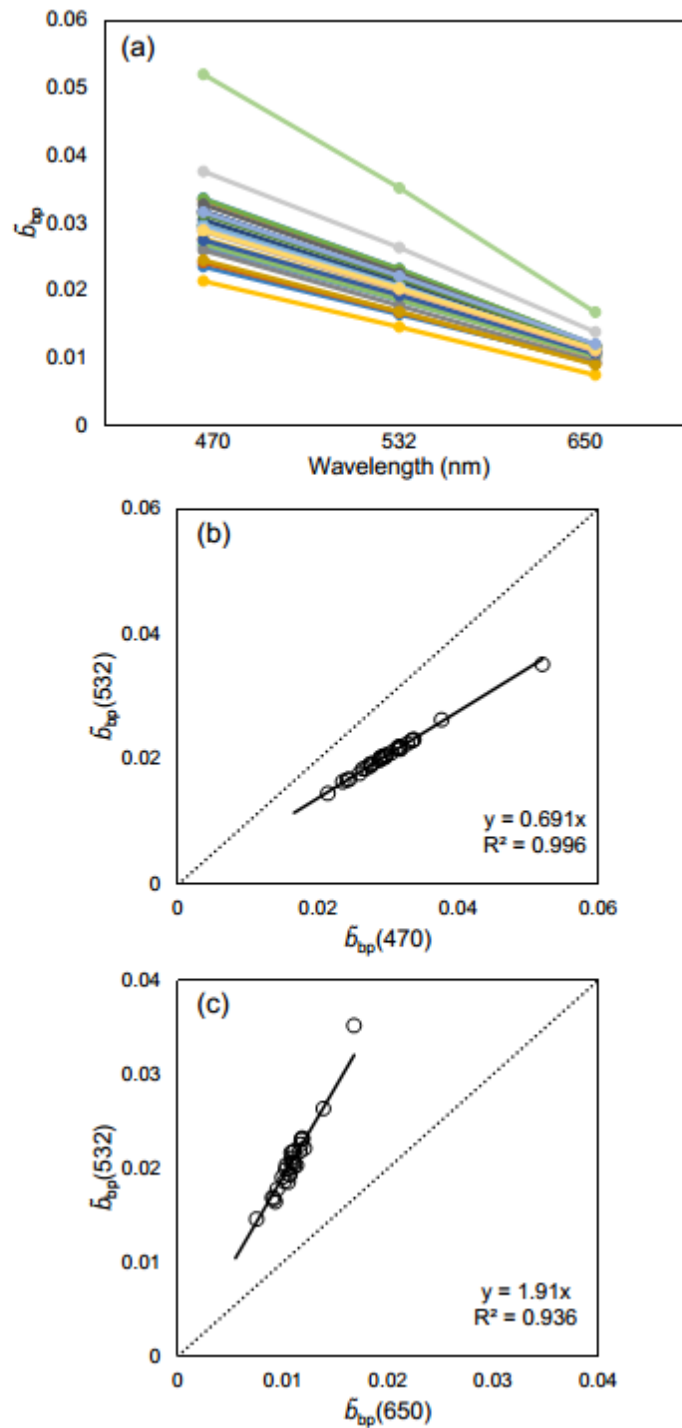


**Figure 4.4** (a) The particulate backscattering ratio ( $\tilde{b}_{bp}$ ) for each station ( $n=29$ ) over the three wavelengths at which *in situ*  $b_{bp}$  was measured, and linear regression plots for  $\tilde{b}_{bp}(532)$  as a function of (b)  $\tilde{b}_{bp}(470)$  and (c)  $\tilde{b}_{bp}(650)$ .

The mean  $b_{bp}(532)$  was highest in Basin 4 ( $0.174 \text{ m}^{-1}$ ), while the lowest  $b_{bp}(532)$  was recorded in Basin 3 ( $0.101 \text{ m}^{-1}$ ; Table 4.3). Mean  $b_{bp}(532)$  declined from west to east, across Basins 1 to 3. In contrast, the mean  $b^*_{bp}(532)$  was highest in Basin 2 ( $0.0157 \text{ m}^2 \text{ g}^{-1}$ ) and lowest in Basin 4 ( $0.0138 \text{ m}^2 \text{ g}^{-1}$ ). As observed with  $b_{bp}(532)$ ,

particulate scattering coefficients [ $b_p(531.3)$ ] declined from west to east (Basins 1 to 3), with the highest  $b_p(531.3)$  measured in Basin 1 ( $11.2 \text{ m}^{-1}$ ). Mass-specific scattering coefficients [ $b^*_p(531.3)$ ] were higher in the westerly basins (Basins 1 and 2;  $0.774\text{-}0.891 \text{ m}^2 \text{ g}^{-1}$ ), and lower in the east of the lake (Basins 3 and 4;  $0.626\text{-}0.638 \text{ m}^2 \text{ g}^{-1}$ ). Conversely, the mean backscattering ratio was lower in Basins 1 and 2 ( $0.0188$  and  $0.0180$ , respectively), and slightly higher in Basins 3 and 4 ( $0.0242$  and  $0.0214$ , respectively). Particulate attenuation coefficients [ $c_p(650)$  and  $c_p(660)$ ] were highest in Basin 1 ( $10.1 \text{ m}^{-1}$ ) with a decreasing gradient across Basins 1 to 3, producing a similar pattern to that observed in of  $b_{bp}(532)$ ,  $b_p(531.3)$ , Chl-a, PC, TSM, POM and total and cyanobacteria biomass.

**Table 4.3** Mean  $\pm$  standard deviation of backscattering and scattering coefficients in Lake Balaton by basin.

<b>(S)IOP</b>	<b>Basin 1 (n=4)*</b>		<b>Basin 2 (n=8)</b>		<b>Basin 3 (n=8)*</b>		<b>Basin 4 (n=15)</b>		<b>Units</b>
$b_{bp}(532)$	0.170	$\pm 0.0396$	0.164	$\pm 0.0371$	0.101	$\pm 0.0578$	0.174	$\pm 0.0397$	$m^{-1}$
$b^*_{bp}(532)$	0.0145	$\pm 0.000839$	0.0157	$\pm 0.00144$	0.0146	$\pm 0.00229$	0.0138	$\pm 0.00213$	$m^2 g^{-1}$
$b_p(531.3)$	11.2	$\pm 4.67$	9.43	$\pm 3.21$	7.95	$\pm 6.97$	9.57	$\pm 3.43$	$m^{-1}$
$b^*_p(531.3)$	0.774	$\pm 0.0351$	0.891	$\pm 0.164$	0.626	$\pm 0.150$	0.638	$\pm 0.11$	$m^2 g^{-1}$
$\tilde{b}_{bp}$	0.0188	$\pm 0.000450$	0.0180	$\pm 0.00237$	0.0242	$\pm 0.00579$	0.0214	$\pm 0.00138$	-
$c_p(650)$	10.1	$\pm 4.64$	8.49	$\pm 3.12$	7.56	$\pm 6.92$	8.96	$\pm 3.33$	$m^{-1}$
$c_p(660)$	10.1	$\pm 4.66$	8.49	$\pm 3.12$	7.56	$\pm 6.92$	8.97	$\pm 3.32$	$m^{-1}$

\* For  $b_{bp}(532)$ ,  $b^*_{bp}(532)$  and  $\tilde{b}_{bp}$ , outliers were removed where the ECO-BB3 saturated. For these parameters, n=3 for Basin 1 and n=3 for Basin 3.

#### 4.3.4 Relationships between scattering coefficients and biogeochemical parameters

When the ‘saturated’ stations were excluded (Stations 3, 31, 32, 33, 34 and 35),  $b_{bp}(532)$  measured by the BB3 agreed well with scattering coefficients [ $b_p(531.3)$ ] measured by the AC-S (Figure 4.5;  $R^2=0.85$ ,  $p<0.001$ ).

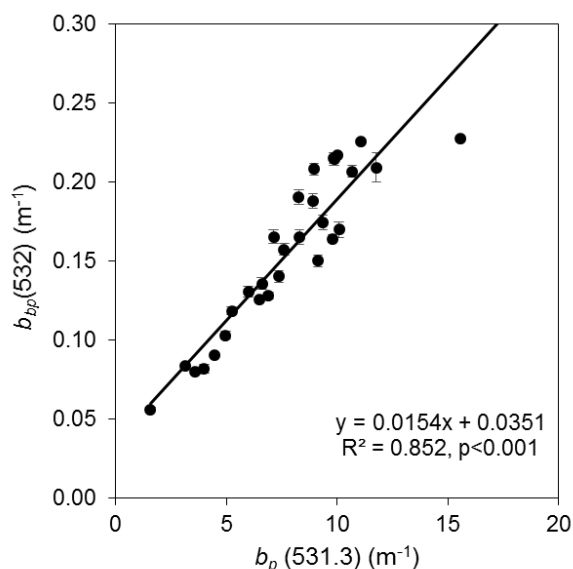


**Figure 4.5** Scatterplot of  $b_p(531.3)$  and  $b_{bp}(532)$  as measured by the AC-S and BB3, respectively. Solid line is a linear regression and vertical error bars are standard deviation of mean  $b_{bp}(532)$ .

$b_p(531.3)$  and  $b_{bp}(532)$  increased with increasing concentrations of TSM (Figure 4.6a,e), although only a weak negative relationship was found between  $\tilde{b}_{bp}$  and TSM (Figure 4.6i). However, a stronger positive relationship was found between  $\tilde{b}_{bp}$  and the proportion of PIM (Figure 4.6j). In fact, if the high  $\tilde{b}_{bp}$  value is removed from the figure (0.035; Station 30), the determination coefficient increases ( $R^2=0.391$ ) and there is strong evidence that the relationship is significant ( $p<0.001$ ). It is noted that Station 30 was sampled on 24 August when wind speeds were high (daily maximum of  $9.2 \text{ m s}^{-1}$ ), therefore this station may be considered an outlier from the dataset. Thus, future work (where backscattering measurements do not saturate under windy conditions) could include wind as a predictor in models for backscattering and scattering coefficients as a function of TSM, PIM and POM.

Particulate scattering and backscattering at 531.3 and 532 nm, respectively, increased significantly ( $p<0.001$ ) with greater concentrations of PIM (Figure 4.6b, f).

There was no significant correlation between  $\tilde{b}_{bp}$  and PIM, in contrast to that reported in Lake Taihu by Sun et al. (2009) (Figure 4.6j). However, it is expected that  $\tilde{b}_{bp}$  would exhibit a stronger relationship with an indicator of particle size and composition as opposed to concentration, and a stronger relationship was indeed found with PIM:TSM (Figure 4.6l). Additionally, no correlations were found between POM and  $b_p(531.3)$  or  $b_{bp}(532)$  (Figure 4.6c, g), which indicates a strong influence of PIM on scattering in Lake Balaton. Positive correlations were also found between  $b_p(531.3)$ ,  $b_{bp}(532)$  and the ratio of PIM (Figure 4.6d, h, l).

The backscattering ratio ( $\tilde{b}_{bp}$ ) showed a significant ( $R^2=0.556$ ,  $p<0.001$ ) decline with increasing concentration of organic particles (Figure 4.6k). Thus, with increasing POM there is a concurrent decrease in scattering efficiency. The particulate backscattering ratio has been similarly linked to the POM:TSM and the ratio of particulate organic carbon (POC) to TSM in ocean and coastal waters (Loisel et al., 2007, Neukermans et al., 2012).

Particulate scattering and backscattering coefficients and the ratio between these were also plotted against Chl-*a* concentrations.  $b_p(531.3)$  and  $b_{bp}(532)$  increased with increasing Chl-*a* concentration, although there was a lot of scatter around these relationships with low significance ( $p<0.05$ ; Figure 4.7a, b). However, the backscattering ratio significantly declined with increasing Chl-*a* concentrations ( $\tilde{b}_{bp} = 0.0355 [\text{Chl-a}]^{-0.213}$ ;  $R^2=0.472$ ,  $p<0.001$ ), following a similar pattern to that observed in Lake Taihu (Sun et al., 2009).

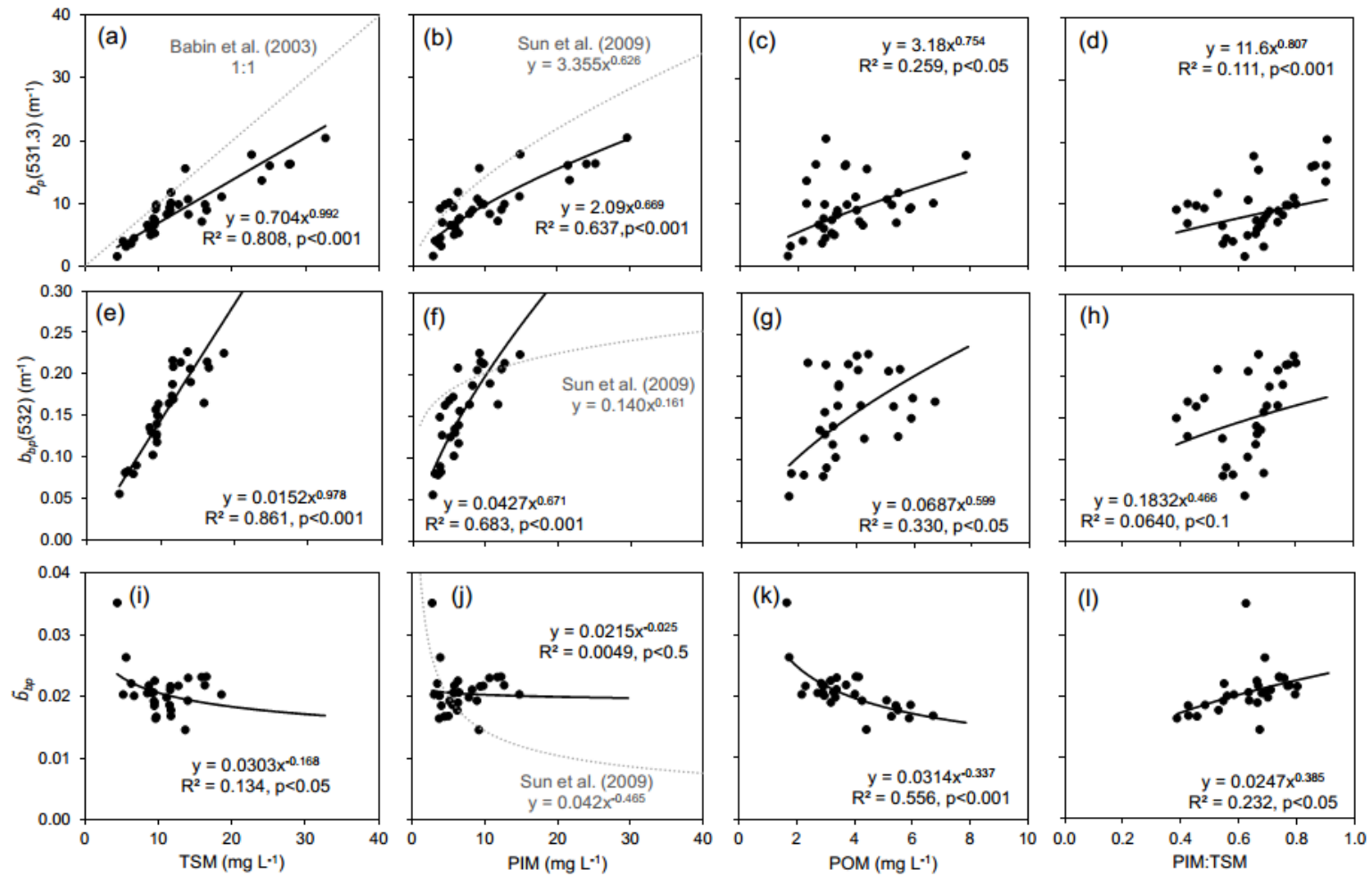


**Figure 4.6** Scatterplots of  $b_p(531.3)$ ,  $b_{bp}(532)$  and  $\tilde{b}_{bp}$  against concentrations of TSM (a, d, g), PIM (b, e, h) and POM (c, f, i). Solid lines and equations are for regression curves by least squares fit.

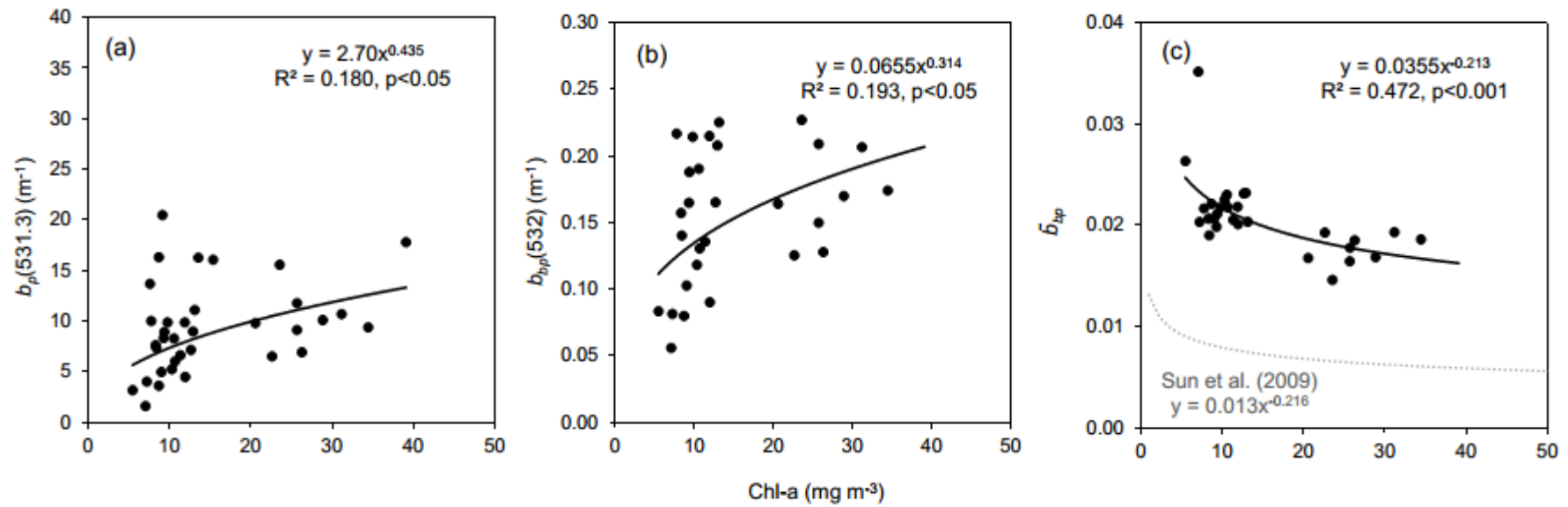


**Figure 4.7** Scatterplots of (a)  $b_p(531.3)$ , (b)  $b_{bp}(532)$  and (c)  $\tilde{b}_{bp}$  as a function of Chl-*a* concentration. Solid lines and equations are for regression by least squares fit, with the exponential fit from Lake Taihu shown as a dashed line (Sun et al., 2009).

Scattering efficiency was plotted as a function of phytoplankton and cyanobacteria biomass. As with Chl-*a* and POM,  $\tilde{b}_{bp}$  decreased over the increasing gradient of phytoplankton biomass (Figure 4.8a), with a particularly high determination coefficient for the relationship between  $\tilde{b}_{bp}$  and cyanobacteria biomass ( $R^2=0.727$ ;  $p<0.001$ ; Figure 4.8b). A similar relationship was found between  $\tilde{b}_{bp}$  and the ratio of cyanobacteria to total phytoplankton biomass (Figure 4.8c). However, these relationships between  $\tilde{b}_{bp}$  and biomass were driven by a single point with high backscattering efficiency (Station 30).

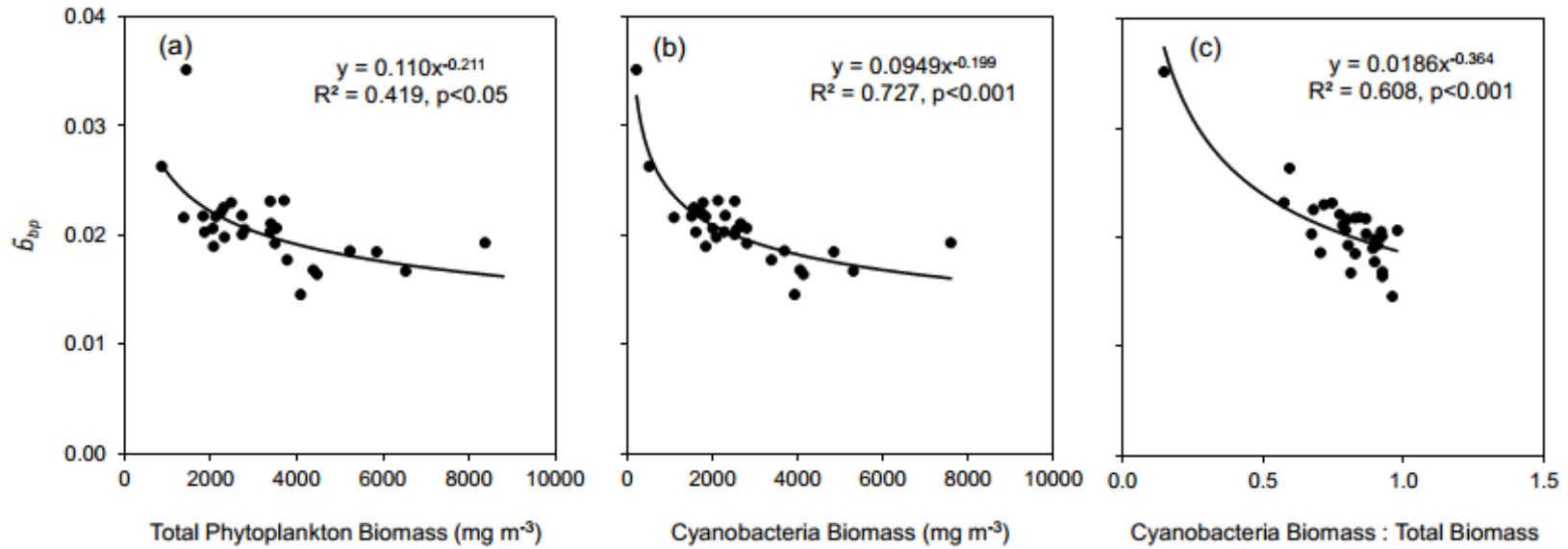


**Figure 4.8** Backscattering ratio ( $\tilde{b}_{bp}$ ) as a function of (a) total phytoplankton biomass, (b) cyanobacteria biomass and (c) ratio of cyanobacteria to total biomass. Solid lines are best-fit power functions.

$b^*_p(531.3)$  was significantly related with the ratio of PIM:TSM and POM:TSM (Figure 4.9a,b). However,  $b^*_p(531.3)$  was negatively correlated with PIM:TSM, in contrast to the positive relationship reported in three turbid Chinese lakes (Shi et al., 2014), likely driven by differences in particle size in Lake Balaton. Significant positive linear relationships were also found between  $b^*_p(531.3)$  and Chl-*a* and PC (Figure 4.9c,d).  $b^*_{bp}(532)$  varied from 0.0104 – 0.0186 m<sup>2</sup> g<sup>-1</sup> (Table 3.3), and no significant relationships were found between  $b^*_{bp}(532)$  and any measured biogeochemical parameter. For comparison,  $b^*_{bp}(532)$  in Lakes Taihu, Chaohu and Dianchi ranged from 0.0018-0.0206 m<sup>2</sup> g<sup>-1</sup>, a similar range to that reported for Lake Balaton.

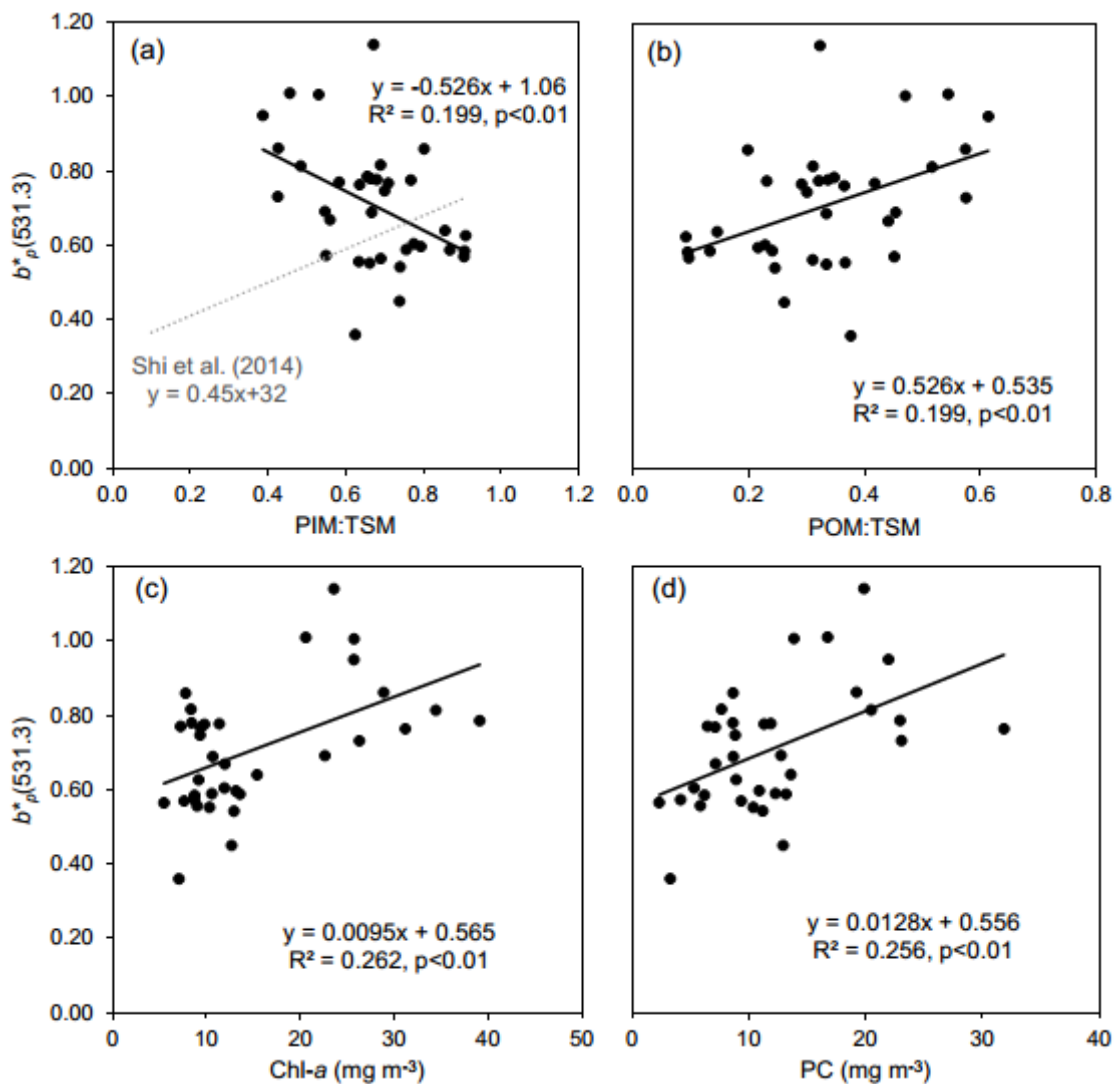


**Figure 4.9** The mass-specific scattering coefficient ( $b^*_p(531.3)$ ; m<sup>2</sup> g<sup>-1</sup>) as a function of (a) PIM:TSM, (b) POM:TSM, (c) Chl-*a* and (d) PC. Solid lines are best-fit linear regressions. Grey dashed line in (a) represents the linear relationship from 3 turbid Chinese lakes in Shi et al. (2014).

#### 4.3.5 Backscattering ratio, bulk refractive index and particle size distribution

The estimated slope of the particulate size distribution ( $\zeta$ ) was linearly related to  $\tilde{b}_{bp}$ . Using two models,  $\zeta$  was estimated as a function of  $\gamma$ , the hyperbolic slope of the  $c_p(\lambda)$  spectrum. When  $\zeta$  was estimated as  $\gamma+3$ , this relationship was  $\tilde{b}_{bp} = 0.0119 \zeta - 0.0200$  ( $R^2=0.261$ ,  $p<0.01$ ; Figure 4.10a), while estimation of  $\zeta$  as in Boss et al. (2001) generated a linear relationship of  $\tilde{b}_{bp} = 0.00877 \zeta - 0.00874$  ( $R^2=0.246$ ,  $p<0.01$ ; Figure 4.10b). When plotted over bulk refractive index ( $\bar{n}_p$ ) contours, the high  $\tilde{b}_{bp}$  observed in Lake Balaton are indicative of high PIM:TSM ratios across all basins. In this study,  $\bar{n}_p$  ranged from 1.15 to 1.24 (Figure 4.10), markedly higher values than that reported for Lake Taihu (1.02-1.17) (Sun et al., 2009). Mean  $\bar{n}_p$  values were higher in Basins 3 and 4 than Basins 1 and 2, corresponding to higher and lower PIM:TSM ratios, respectively (Table 4.4).

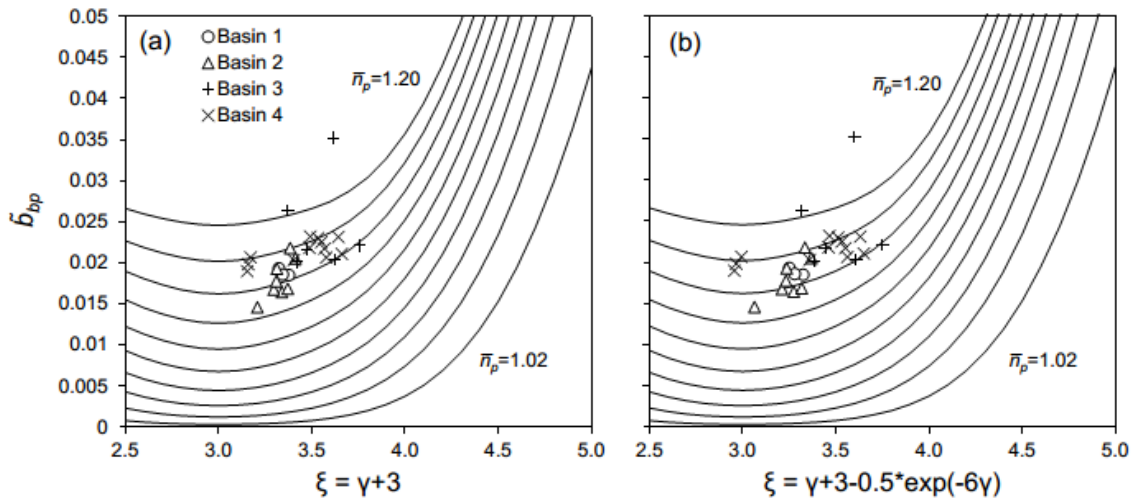


**Figure 4.10** Scatterplot of particulate backscattering ratio [ $\tilde{b}_{bp} = b_{bp}(532): b_p(531.3)$ ] against the PSD slope ( $\zeta$ ). Solid curves are overlaid to represent the refractive index contours ( $\bar{n}_p$ ) as calculated by Twardowski et al. (2001), ranging from 1.02 to 1.20 by increments of 0.02.

**Table 4.4** Mean  $\pm$  standard deviation of PIM ratios and refractive index ( $\bar{n}_p$ ) values, as calculated according to Twardowski et al. (2001).

<b>Basin</b>	$\bar{n}_p$	<b>PIM:TSM</b>
1	$1.17 \pm 0.0034$	$0.55 \pm 0.11$
2	$1.16 \pm 0.011$	$0.55 \pm 0.12$
3	$1.18 \pm 0.031$	$0.70 \pm 0.15$
4	$1.18 \pm 0.0065$	$0.75 \pm 0.079$
Lake Mean	$1.17 \pm 0.016$	$0.67 \pm 0.14$

## 4.4 Discussion

### 4.4.1 Contributions to particulate attenuation

In this study, particulate scattering was found to account for a very high percentage of total light attenuation (up to 85-99%; Figure 4.2), with a mean  $b_p(531.3)$  of  $9.35 \text{ m}^{-1}$ . Coastal studies have found much lower values of particulate scattering, with mean  $b_p(532)$  values of  $0.555 \pm 0.272 \text{ m}^{-1}$  in the English Channel (Martinez-Vicente et al., 2010) and  $0.959 \pm 0.739 \text{ m}^{-1}$  in the North Sea (Tilstone et al., 2012). The level of scattering in Lake Balaton is more consistent with a mineral-dominated water body. High mineral suspended sediment content was also reported in the Irish Sea (63% on average), and this study also found a broader range for  $b_p(555)$  of  $0.04\text{-}6.32 \text{ m}^{-1}$  (Bowers & Binding, 2006). Therefore scattering contributes greatly to the underwater light field in Lake Balaton, and thus has a large impact on the remote sensing signal [i.e.  $R_{rs}(\lambda)$ ] reflected from the lake surface.

The particulate attenuation coefficient in Lake Balaton was strongly correlated with TSM, particularly PIM (Figure 4.3). This contrasts with the strong relationship between  $c_p(660)$  and Chl-*a* found in open ocean waters ( $c_p(660) = 0.65[\text{Chl-}a]^{0.80}$ ) (Loisel & Morel, 1998). Suspended matter in ocean waters is dominated by phytoplankton, and the direct relationship between Chl-*a* (phytoplankton biomass) and the IOPs of the water column is well-documented. In Lake Balaton, however, there is a higher concentration of suspended minerals due to the presence of dolomite limestone bed sediments (Tyler et al., 2006), with lake mean PIM concentrations comprising over 70% of the mean TSM. In this study, nearly all of the variability in lake TSM concentrations was explained by PIM (96%). Algae have a low backscattering efficiency, so the mineral particles in Lake Balaton contribute more strongly than

phytoplankton to  $c_p(660)$ , resulting in a better correlation with TSM than Chl-*a*. The scatter caused by non-algal particles is not accounted for in the  $c_p(660)$  relationship to Chl-*a* in ocean waters.

#### 4.4.2 Variability in the scattering and backscattering properties, and relationships with optically active particles

The scattering properties in Lake Balaton generally indicate a gradient across the basins, from the eutrophic western portion to the oligotrophic eastern basins. This was observed most distinctly with a decline in particulate scattering [ $b_p(531.3)$ ] and particulate attenuation [ $c_p(660)$ ] coefficients alongside diminishing concentrations of Chl-*a*, TSM, POM and phytoplankton and cyanobacteria biomass (Table 4.1; Table 4.3). Similar spatial variability of absorption properties was also recorded across the lake in Chapter 3 (Riddick et al., 2015). However, only minimal differences in  $b_{bp}(532)$  were measured across the basins.

The inorganic particles in Lake Balaton are comprised mainly of dolomite limestone, which gives the lake its characteristic milky blue colour. Minerogenic particles in general have a higher relative refractive index and therefore tend to be more efficient backscatterers than organic particles [see Table 6 in Babin et al. (2003a)]. Specifically, the refractive index of dolomite is  $\sim 1.60$  ( $n_o=1.679-1.681$ ; www.mindat.org), markedly higher than the organic particles (e.g. phytoplankton and detritus) that comprise the majority of marine total suspended matter. Thus, in Lake Balaton it is unsurprising that a stronger relationship was found between  $b_p(531.3)$  or  $b_{bp}(532)$  and PIM as opposed to POM (Figure 4.6). In fact, in Lake Taihu, it was found that due to low ratios of POM:PIM, the impact of organic matter absorption on the scattering coefficient was negligible (Sun et al., 2009). In Lake Balaton, PIM typically comprises over 50% of the TSM, therefore it is likely that the effect of organic matter on the scattering coefficient is similarly low.

The mass-specific backscattering coefficient in this study showed a coefficient of variation of  $\sim 14\%$  across the lake ( $b^*_{bp}(532) = 0.0146 \pm 0.00199 \text{ m}^2 \text{ g}^{-1}$ ). This suggests that variability of  $b^*_{bp}$  in Lake Balaton is primarily driven by the consistently high percentage of PIM across the lake ( $>50\%$ ), therefore  $b^*_{bp}$  is correspondingly high across the lake. However, the mass-specific scattering coefficient varied over a larger range than that observed in studies of coastal waters ( $b^*_p(531.3) = 0.36-1.14 \text{ m}^2 \text{ g}^{-1}$ ; see Table 4.5 for comparison with other studies). This is likely due to

the broader range of Chl-*a* and TSM in Lake Balaton than coastal waters previously studied. However,  $b^*_p(555)$  in Lake Taihu varied over a much wider range than Lake Balaton (0.14-1.57 m<sup>2</sup> g<sup>-1</sup>), although this is likely accounted for by the markedly greater range of Chl-*a* and TSM in Lake Taihu (Chl-*a* = 40.59 ± 72.11 mg m<sup>-3</sup>; TSM = 33.92 ± 24.18 mg L<sup>-1</sup>) (Sun et al., 2009).

#### 4.4.3 Backscattering ratio, bulk refractive index and particle size distribution

The particulate backscattering ratio ( $\tilde{b}_{bp}$ ) represents the fraction of light scattered in the backwards direction. In Lake Balaton,  $\tilde{b}_{bp}$  was significantly related to POM, Chl-*a* and phytoplankton and cyanobacteria biomass, according to a declining power function. This is in contrast to Lake Taihu, where only a weak negative relationship was found between  $\tilde{b}_{bp}$  and Chl-*a*, and  $\tilde{b}_{bp}$  was significantly negatively correlated to PIM ( $R^2 = 0.757$ ) (Sun et al., 2009). In Lake Balaton, there were no significant differences in PIM concentrations across the four basins, while POM, Chl-*a* and phytoplankton and cyanobacteria biomass did vary significantly across the lake ( $p < 0.01$ , see Table 3.2 in Chapter 3; Riddick et al., 2015). Thus, the change in  $\tilde{b}_{bp}$  across Lake Balaton is likely related to the decreasing gradient in phytoplankton biomass from west to east. The scattering efficiency may also change in relation to phytoplankton cell size, as smaller cells are more efficient scatterers (Vaillancourt et al., 2004). In Lake Balaton, the phytoplankton community in the western basins was mainly composed of large N-fixing cyanobacteria cells (100-200 µm), comprising up 85% of the community at these stations (Riddick et al., 2015). However, the mesotrophic eastern basins had a more diverse community, with greater abundance of smaller celled phytoplankton such as chlorophytes and diatoms. Diatoms, for example, are more efficient scatterers than comparably sized cyanobacteria due to their siliceous cell walls.

The backscattering ratio was plotted as a function of the estimated hyperbolic slope of the PSD, or Junge coefficient ( $\xi$ ). There was little difference between the estimates of  $\xi$  using the two methods of calculation from the hyperbolic slope of the  $c_p$  spectrum ( $\gamma$ ). The Boss et al. (2004) correction is for more general cases of hyperbolic PSDs with finite limits, and is important for flat PSDs encountered in e.g. bottom boundary layers, which is likely not significant in Lake Balaton. In either case,  $\tilde{b}_{bp}$  was positively linearly correlated with  $\xi$  ( $R^2 > 0.25$ ,  $p < 0.01$ ; Figure 4.10). In contrast, no significant relationship between  $\tilde{b}_{bp}$  and  $\xi$  has been reported in other studies on inland

(Sun et al., 2009), coastal or ocean waters (Twardowski et al., 2001, Boss et al., 2004). This indicates a strong contribution of particle size on the scattering efficiency in Lake Balaton, where the higher relative abundance of finer mineral particles contribute more to scattering properties in the eastern basins, while the presence of larger algal cells contribute more to scattering properties in the western basins.

The bulk particle refractive index ( $\bar{n}_p$ ) reproduces the bulk scattering properties of a particle assemblage, and is equivalent to the mean of the individual refraction indices weighted by particle size (Twardowski et al., 2001). In seawater, typically  $\bar{n}_p$  values above 1.15 are waters dominated by inorganic sediments, while waters where  $\bar{n}_p \approx 1.04$  are dominated by phytoplankton (Boss et al., 2004). Relative to these guidelines for ocean waters,  $\bar{n}_p$  values in Lake Balaton were high, ranging from 1.15-1.23. This is markedly higher than the range of  $\bar{n}_p$  reported in Lake Taihu, where stations with high PIM:TSM ratios had a maximum  $\bar{n}_p$  of 1.17 and those with high POM:TSM ratios had a peak  $\bar{n}_p$  value of 1.11 (Sun et al., 2009). This is likely because Lake Balaton has a greater proportion of “hard” inorganic suspended matter than Lake Taihu, due to resuspension of the dolomite limestone sediments. This again indicates the significant contribution from the resuspended mineral particles to the scattering properties in Lake Balaton. Interestingly, the highest  $\bar{n}_p$  in Lake Balaton was recorded at Station 3 in Basin 3, the basin sampled under particularly windy conditions with notable resuspension of sediments in the water column. This indicates that sediment resuspension causes an increase in the mean refractive index of the particle assemblage, as a result of the higher proportion of suspended minerogenic particles.

**Table 4.5** Table of bulk and mass-specific scattering and backscattering coefficients and the backscattering ratio in other recent studies.

<b>(S)IOP</b>	<b>Min</b>	<b>Max</b>	<b>Mean</b>	<b>St Dev</b>	<b>Units</b>	<b>Study Area</b>	<b>Reference</b>
$b_p(532)$	3.32	48.09	20.17	9.35	$m^{-1}$	Lake Taihu	Sun et al. (2009)
$b_p(560)$	0.115	3.84	0.959	0.739	$m^{-1}$	North Sea	Tilstone et al. (2012)
$b_p(555)$	0.04	6.32	1.22	-	$m^{-1}$	Irish Sea	Bowers and Binding (2006)
$b_p(532)$	0.125	1.76	0.555	0.272	$m^{-1}$	English Channel	Martinez-Vicente et al. (2010)
$b_p(532)$	-	-	0.52- 5.08	0.31- 2.69	$m^{-1}$	US coastal waters	Snyder et al. (2008)
$b_p(532)$	2.23	44.21	19.55	10.61	$m^{-1}$	Lake Taihu	Lyu et al. (2015)
$b_p(532)$	12.04	55.63	28.66	12.13	$m^{-1}$	Lake Chaohu	Lyu et al. (2015)
$b_p(532)$	11.51	26.08	16.97	3.30	$m^{-1}$	Lake Dianchi	Lyu et al. (2015)
$b^*_p(555)$	0.14	1.57	0.67	0.22	$m^2g^{-1}$	Lake Taihu	Sun et al. (2009)
$b^*_p(532)$	0.29	0.79	0.58	0.08	$m^2g^{-1}$	Lakes Taihu, Chaohu, Dianchi	Shi et al. (2014)
$b^*_p(532)$	0.12	1.07	0.58	0.15	$m^2g^{-1}$	Lake Taihu	Lyu et al. (2015)
$b^*_p(532)$	0.50	1.01	0.66	0.10	$m^2g^{-1}$	Lake Chaohu	Lyu et al. (2015)
$b^*_p(532)$	0.21	0.82	0.40	0.13	$m^2g^{-1}$	Lake Dianchi	Lyu et al. (2015)
$b^*_p(555)$	-	-	0.51	1.9	$m^2g^{-1}$	European coastal waters	Babin et al. (2003a)
$b^*_p(555)$	-	-	0.97	1.9	$m^2g^{-1}$	Atlantic	Babin et al. (2003a)
$b^*_p(560)$	0.030	2.018	0.469	0.313	$m^2g^{-1}$	North Sea	Tilstone et al. (2012)
$b^*_p(555)$	-	-	0.22	0.02	$m^2g^{-1}$	Irish Sea	Bowers and Binding (2006)
$b^*_p(532)$	0.177	0.735	0.366	0.30	$m^2g^{-1}$	English Channel	Martinez-Vicente et al. (2010)
$b_{bp}(532)$	0.09	0.25	0.22	0.03	$m^{-1}$	Lake Taihu	Sun et al. (2009)
$b_{bp}(532)$	0.0955	0.1892	0.1780	0.0113	$m^{-1}$	Lake Taihu	Lyu et al. (2015)
$b_{bp}(532)$	0.1804	0.1879	0.1834	0.0020	$m^{-1}$	Lake Chaohu	Lyu et al. (2015)
$b_{bp}(532)$	0.1814	0.1883	0.1839	0.0014	$m^{-1}$	Lake Dianchi	Lyu et al. (2015)

<b>(S)IOP</b>	<b>Min</b>	<b>Max</b>	<b>Mean</b>	<b>St Dev</b>	<b>Units</b>	<b>Study Area</b>	<b>Reference</b>
$b_{bp}(532)$	-	-	0.008- 0.114	0.008- 0.078	$m^{-1}$	US coastal waters	Snyder et al. (2008)
$b^*_{bp}(532)$	0.0018	0.0206	0.0069	0.0036	$m^2g^{-1}$	Lake Taihu	Lyu et al. (2015)
$b^*_{bp}(532)$	0.0022	0.0117	0.0051	0.0025	$m^2g^{-1}$	Lake Chaohu	Lyu et al. (2015)
$b^*_{bp}(532)$	0.0027	0.0075	0.0043	0.0011	$m^2g^{-1}$	Lake Dianchi	Lyu et al. (2015)
$\tilde{b}_{bp}(532)$	0.005	0.027	0.013	0.005	-	Lake Taihu	Sun et al. (2009)
$\tilde{b}_{bp}(532)$	0.0042	0.0444	0.131	0.0092	-	Lake Taihu	Lyu et al. (2015)
$\tilde{b}_{bp}(532)$	0.0032	0.0152	0.0074	0.0033	-	Lake Chaohu	Lyu et al. (2015)
$\tilde{b}_{bp}(532)$	0.0072	0.0150	0.0109	0.0019	-	Lake Dianchi	Lyu et al. (2015)
$\tilde{b}_{bp}$	0.005	0.035	-	-	-	New Jersey coastal waters	Boss et al. (2004)
$\tilde{b}_{bp}$	0.005	0.050	-	-	-	Irish Sea	McKee and Cunningham (2006)
$\tilde{b}_{bp}$	0.0024	0.0417	-	-	-	English Channel and North Sea	Loisel et al. (2007)
$\tilde{b}_{bp}$	0.005	0.060	0.013	-	-	Gulf of California, Mid- Atlantic Bight and Crater Lake	Whitmire et al. (2007)
$\tilde{b}_{bp}$	0.005	0.060	0.008- 0.023	0.002- 0.008	-	US coastal waters	Snyder et al. (2008)

## 4.5 Conclusions

This study reported a higher contribution of particulate scattering to total light attenuation in Lake Balaton (over 85%) as compared to previous studies in coastal waters, findings that are consistent with a mineral- as opposed to phytoplankton-dominated water body. Furthermore,  $c_p(660)$  was strongly correlated to TSM, particularly PIM, in contrast to the well-documented relationship between  $c_p(660)$  and Chl-*a* reported in ocean waters, highlighting the distinct scattering properties in Lake Balaton.

The backscattering and scattering coefficients demonstrated variability across the four basins of Lake Balaton. In particular,  $b_p(531.3)$  and  $b_{bp}(532)$  declined across a decreasing gradient of optically active substances (including TSM, Chl-*a*, total phytoplankton biomass). However, little variation was observed in the mass-specific backscattering properties, indicating that  $b^*_{bp}(532)$  variability is primarily driven by the high concentrations of PIM across the lake.  $\tilde{b}_{bp}$  was significantly negatively related to the organic fraction of TSM, Chl-*a* and phytoplankton and cyanobacteria biomass, in contrast to previous studies where only a weak relationship was reported with Chl-*a*. This demonstrated a link between scattering efficiency and the decreasing gradient in phytoplankton biomass and changing phytoplankton community across Lake Balaton (west to east). High bulk refractive indices also indicated a significant contribution from dolomite particles to the scattering properties in Lake Balaton, with the highest  $\bar{n}_p$  values recorded during a period with significant wind-driven resuspension of sediments.

These findings quantify the scattering properties of Lake Balaton, and demonstrate the importance of fine mineral particles to the scattering and attenuation of light in inland waters. This has implications for the backscattering coefficients estimated by bio-optical models and semi-analytical algorithms, which can be a major source of error in the retrieval of water quality parameters (e.g. Chl-*a*). Given the prevalence of inorganic particles in inland water bodies such as Lake Balaton, these findings must be considered for the further improvement of Earth observation methods for inland waters.

## **5 Evaluation of algorithms for retrieval of cyanobacterial pigments in highly turbid, optically complex waters using MERIS data**

*This chapter is based on the following manuscript in review:*

Riddick, C.A.L., Hunter, P.D., Domínguez Gómez, J.A, Martinez-Vicente, V., Présing, M., Horváth, H., Kovács, A.W., Vörös, L., Zsigmond, E. and Tyler, A.N. (in review) Evaluation of algorithms for retrieval of cyanobacterial pigments in highly turbid, optically complex waters using MERIS data.

---

### **5.1 Introduction**

It has recently been estimated that there are as many as 117 million lakes on Earth covering approximately 3.7% of the planet's non-glaciated land surface (Verpoorter et al., 2014). While they comprise only a small fraction of the Earth's land surface, inland water bodies play a fundamental role in many global and regional biogeochemical processes (Cole et al., 2007, Bastviken et al., 2011). Lakes are also highly sensitive to environmental perturbation and change impacting their airsheds and watersheds. For example, inputs of nutrients derived from anthropogenic sources to lakes have increased in recent years, with freshwater eutrophication recognised as one of the most universally widespread ecological, economic and social issues affecting the quality of freshwaters globally (Smith, 2003).

More commonly known as blue-green algae, cyanobacteria are notorious bloom-forming prokaryotes that often dominate the phytoplankton community in nutrient-enriched freshwaters. Blooms of cyanobacteria can have profound and often highly adverse impacts on lake ecosystems (Paerl et al., 2011). Some species of cyanobacteria can fix dissolved dinitrogen gas into organic nitrogen thus allowing them to outcompete other phytoplankton species and thrive in conditions with a low nitrogen to phosphorus ratio (Schindler, 1977, Smith, 1983, Downing, 2001, Ferber, 2004, Horváth et al., 2013a). Other adaptations such as the ability to store excess nutrients such as phosphorus (Antenucci et al., 2005), low light requirements (Reynolds et al., 2002), increased growth rates at higher temperatures (Paerl & Huisman, 2009) and buoyancy regulation mechanisms (Wagner & Adrian, 2009) further allow cyanobacteria to prosper in warmer, nutrient enriched waters.

Cyanobacteria can also pose significant risks to animal and human health, as many species produce cyanotoxins with neurotoxic, hepatotoxic, cytotoxic, genotoxic, endotoxin and tumor-promoting properties (Codd et al., 2005a). It is therefore vital to that we develop methods for the accurate and rapid assessment and monitoring of cyanobacteria blooms in lakes. Earth-observing satellites can provide data at a spatial and temporal resolution to permit rapid detection and monitoring of cyanobacteria populations in lakes on an operational basis. To this end, this study aims to assess the capability of semi-analytical and inversion algorithms for retrieval of cyanobacterial pigments from inland waters using data from MERIS (the MEdium Resolution Imaging Spectrometer that was flown on the Envisat satellite) captured over the highly turbid, optically complex waters of Lake Balaton, Hungary. The ultimate aim of this research is to rigorously validate algorithms that can be used for near real-time operational detection and monitoring of cyanobacterial blooms in lakes.

### **5.1.1 Satellite remote sensing of cyanobacteria blooms**

Remote sensing is used operationally for monitoring phytoplankton in the global ocean, but remote sensing of inland waters has not progressed as rapidly due to the greater complexity in the atmospheric and in-water optical properties of lakes (Palmer et al., 2015b). Chlorophyll-*a* (Chl-*a*) can be retrieved with algorithms from remote sensing measurements as an indicator of total phytoplankton biomass (Gons et al., 2002, Kutser, 2004, Tyler et al., 2006). However, Chl-*a* does not provide information about the phytoplankton community composition or reliably indicate the presence of potentially toxic cyanobacteria blooms. More useful information can be acquired by also estimating the concentration of phycocyanin (PC), an indicator pigment for cyanobacteria (Simis et al., 2005, Kutser et al., 2006, Ruiz-Verdu et al., 2008, Kutser, 2009, Hunter et al., 2010, Li et al., 2012, Duan et al., 2012, Song et al., 2013). The unique optical properties of cyanobacteria mean that they can be distinguished from other phytoplankton using knowledge of the shape and magnitude of the remote-sensing reflectance [ $R_{rs}(0^+, \lambda)$ ] signal observed during blooms (Hunter et al., 2008b).

Chl-*a* and PC can be most simply estimated from  $R_{rs}(0^+, \lambda)$  using empirical algorithms incorporating [ $R_{rs}(0^+, \lambda)$ ] band-ratios or band-differences targeting the main absorption features for these pigments at ~665 nm and ~620 nm, respectively. The reflectance band-ratio  $R_{rs}(665)/R_{rs}(709)$  has been used effectively for retrieval of Chl-*a* absorption in eutrophic waters (Mittenzwey et al., 1992, Dekker, 1993, Gons et al.,

2002, Gurlin et al., 2011), while three-band empirical methods (Dall'Olmo et al., 2003, Gitelson et al., 2008) and semi-analytical methods (Gons, 1999, Gons et al., 2002, Gons et al., 2005) have also been developed for inland waters. Inversion models have been more commonly developed for Chl-*a* retrieval in ocean and coastal waters, e.g. the Quasi-Analytical Algorithm (QAA) (Lee et al., 2002), Garver–Siegel–Maritorena Model (GSM) (Maritorena et al., 2002) and the adaptive Linear Matrix Inversion Method (aLMI) (Brando et al., 2012), with some limited application of inversion methods to inland waters, e.g. Modular Image Processing system (MIP) (Heege & Fischer, 2004). Other models specifically developed for Chl-*a* retrieval from MERIS have included the Maximum Peak Height algorithm (MPH) (Matthews et al., 2012, Matthews & Odermatt, 2015), Maximum Chlorophyll Index (MCI) (Gower et al., 2005) and Fluorescence Line Height (FLH) (Gower et al., 1999). More recently, artificial neural network type approaches have been investigated and are available as plug-ins in the widely used BEAM software (Brockmann Consult), e.g. Case 2 Regional (Doerffer & Schiller, 2007), Free Universität Berlin (FUB/WeW) (Schroeder et al., 2007), Eutrophic Lake and Boreal Lake (Doerffer & Schiller, 2008) processors, although these were primarily developed for and validated in coastal waters.

PC has been estimated from  $R_{rs}(0^+, \lambda)$  with a semi-empirical baseline algorithm (Dekker, 1993), reflectance band differences or band ratios (Schalles & Yacobi, 2000, Vincent et al., 2004, Mishra et al., 2009, Dash et al., 2011, Ogashawara et al., 2013), a nested band ratio or semi-empirical algorithm (Simis et al., 2005), spectral shape algorithm (Wynne et al., 2008), three-band empirical algorithms (Hunter et al., 2008b, Hunter et al., 2010, Song et al., 2013, Mishra & Mishra, 2014), non-linear least-square fitting to total absorption derived from the quasi-analytical algorithm (QAA) (Becker et al., 2009), a four-band semi-analytical algorithm (Le et al., 2011), a three-band and baseline algorithm (Li et al., 2012), extension of the QAA for Chl-*a* retrieval (Mishra et al., 2013), a PC Index algorithm (Qi et al., 2014) and an inherent optical property (IOP) inversion model (Li et al., 2015).

However, the practical use of some of the algorithms developed for pigment retrieval, particularly for PC, is limited by the spectral coverage and resolution available with current satellite instruments (Ruiz-Verdu et al., 2008). While the MERIS sensor is no longer operational, the data archive remains immensely useful for algorithm development and validation studies, particularly because the OLCI instrument on the European Space Agency's recently launched Sentinel-3 satellite has a strong MERIS

heritage. Importantly, MERIS had a spectral band centered at 620 nm near the PC absorption maximum that could be used for PC retrieval (OLCI will also have this band).

The semi-empirical algorithm for PC estimation developed by Simis et al. (2005) (hereafter referred to as Simis05) and the related algorithm for Chl-*a* retrieval by Gons (1999) and adapted by Simis et al. (2005) (hereafter referred to as Gons05) were specifically tailored to the bands for MERIS. More recently, other MERIS- and (potentially) OLCI-compatible algorithms for PC retrieval have been developed and published, including the adapted quasi-analytical (QAA) algorithm developed by Mishra et al. (2013) and the IOP Inversion Model of Inland Waters (IIMIW) by Li et al. (2015), hereafter referred to as Mishra13 and Li15, respectively. These three algorithms were identified as the most relevant PC retrieval methods presently available for MERIS data, and were thus selected for this study.

### **5.1.2 MERIS phycocyanin algorithms**

Gons05 and Simis05 algorithms have proved effective for retrievals of phytoplankton pigments. The Gons05 algorithm is naturally considered here for Chl-*a* retrievals, as it was the foundation upon which the Simis05 PC algorithm evolved. Gons05 was calibrated in the shallow eutrophic freshwaters of IJssel Lagoon, Netherlands (Chl-*a* = 4-185 mg m<sup>-3</sup>), with initial validation in well-mixed and optically deep lakes in The Netherlands, the Scheldt Estuary (The Netherlands and Belgium), Lake Taihu (China), the Hudson/Raritan Estuary (USA) and the North Sea (Belgian coast) (Gons, 1999, Gons et al., 2000, Gons et al., 2002). As a progression of Gons05, Simis05 was initially calibrated in the well-mixed and eutrophic Lakes Loosdrecht (Chl-*a* = 48-98 mg m<sup>-3</sup>, PC = 22-80 mg m<sup>-3</sup>) and IJsselmeer (Chl-*a* = 23-92 mg m<sup>-3</sup>, PC = 0.8-65 mg m<sup>-3</sup>) in The Netherlands, and has subsequently obtained accurate PC retrievals in mostly eutrophic inland waters with moderate to high cyanobacterial biomass, including Spanish lakes and reservoirs (Simis et al., 2007), Indiana reservoirs (Randolph et al., 2008, Li et al., 2012, Song et al., 2013), Spanish and Dutch lakes and reservoirs (Ruiz-Verdu et al., 2008), shallow eutrophic UK lakes (Hunter et al., 2010) and eutrophic lakes in East China (Duan et al., 2012). The Simis05 algorithm in particular has undergone limited testing with independent datasets of inland waters, and there is a need for validation in waters with differing optical properties.

Inversion models work by first retrieving the inherent optical properties (IOPs) from an  $R_{rs}(\lambda)$  spectrum, including the estimation of the particulate backscattering coefficient [ $b_{bp}(\lambda)$ ] and the total absorption coefficient [ $a_t(\lambda)$ ] or non-water absorption coefficient [ $a_{t-w}(\lambda)$ ].  $a_t(\lambda)$  or  $a_{t-w}(\lambda)$  is then partitioned into the individual components related to absorption by pigments (Chl-*a* and PC), non-algal particles and coloured dissolved organic matter (CDOM). Chl-*a* and PC concentrations are subsequently estimated from the phytoplankton absorption [ $a_{ph}(\lambda)$ ] and phycocyanin absorption [ $a_{pc}(\lambda)$ ] coefficients, respectively, based on knowledge of the specific absorption coefficients for these pigments. As an inversion model, the Mishra13 algorithm builds upon the QAA algorithm for Chl-*a* retrieval (Lee et al., 2002), which was developed for oceans and has been widely validated in ocean, coastal and more recently inland waters. The Mishra13 model was calibrated for PC retrieval in turbid and highly productive aquaculture ponds (Mishra et al., 2013). Similarly, the Li15 inversion model extends the IIMIW algorithm for Chl-*a* retrieval (Li et al., 2013), and was calibrated using three central Indiana reservoirs (Li et al., 2015). However, to our knowledge at the time of writing the Mishra13 and Li15 algorithms have yet to be validated with independent datasets.

It is vital to investigate whether remote sensing algorithms are transferable to other lakes with differing optical and biogeochemical properties, and further understanding is required of the uncertainties over the full range of optical water types (Mouw et al., 2015, Palmer et al., 2015b). Many validation studies have also used *in situ* measurements of subsurface reflectance, however this ignores the differences in spectral and radiometric resolutions of satellite sensors and the potentially confounding effects of the atmosphere on retrievals. Moreover, to date there have simply been very few attempts to validate PC inversion algorithms using satellite data such as MERIS. To address this deficiency, this study aims to apply PC algorithms to a novel MERIS dataset on Lake Balaton (Hungary), a site with recurrent summer cyanobacteria blooms, a gradient of phytoplankton biomass and CDOM, and unique optical properties that are highly influenced by inorganic particulates.

More specifically, this study aims to test PC retrievals with the Simis05, Mishra13 and Li15 algorithms over a large optically complex shallow lake. PC retrievals within 1 day of *in situ* measurements are compared and the best-performing algorithm is investigated in greater detail over a range of matchup windows. Pigment retrievals from the best-performing algorithm are validated with a time series of

pigment and cell count data from 2007-2011. Finally, the sources of error are examined by validating retrievals of  $a_{ph}(\lambda)$  and  $b_b(\lambda)$  with a dataset of IOP measurements from August 2010.

## 5.2 Methods

### 5.2.1 Study site

Lake Balaton (46.8°N, 17.7°E; Figure 5.1) is the largest shallow lake in Europe by surface area (592 km<sup>2</sup>), with a mean depth of just 3.2 m. It has a large catchment, dominated by the Zala River, and a history of eutrophication and summer cyanobacteria blooms. The lake itself typically has a gradient in phytoplankton biomass and Chl-*a*, with the highest Chl-*a* concentrations occurring in the western Keszthely basin (~3-45 mg m<sup>-3</sup>), and lower phytoplankton biomass and Chl-*a* in the eastern Siófok basin (~3-20 mg m<sup>-3</sup>). Cyanobacteria biomass tends to peak in late summer (anywhere from June-October), with PC values up to ~60-100 mg m<sup>-3</sup> in the westernmost basins (Horváth et al., 2013a). In recent years, summer cyanobacteria populations in Lake Balaton are dominated by nitrogen-fixing species, including *Cylindrospermopsis raciborskii* [(Wolosz.) Seenayya et Subba Raju], *Aphanizomenon flos-aquae* [(L.) Ralfs], *Aphanizomenon issatschenkoi* [(Ussatzew.) Proschkina-Lawrenko], *Anabaena aphanizomenoides* and *Anabaena spiroides* (KLeb.). During a bloom, cyanobacteria often contribute to >70% of the total phytoplankton biomass (Horváth et al., 2013a). Kis-Balaton is a reservoir system on the Zala River to the west of the lake, consisting of an upper and lower reservoir, with generally very high phytoplankton biomass and Chl-*a* concentrations (typically ~50-250 mg m<sup>-3</sup>).

In spite of the often high concentrations of phytoplankton that occur in Lake Balaton during the summer, light attenuation is largely determined by the frequent resuspension of mineral particles from the lake bottom. Total suspended matter in the lake is mostly of inorganic origin, with concentrations are typically in the order of 18-28 mg L<sup>-1</sup> (2010 annual mean), but can exceed 100 mg L<sup>-1</sup> during windy periods. These high loads of mineral particles contribute significantly to light absorption and scattering; absorption by non-algal particles [ $a_{NAP}(440)$ ] is typically 0.2 m<sup>-1</sup> and particulate backscattering [ $b_{bp}(532)$ ] varies between 0.04-0.2 m<sup>-1</sup> (Chapter 3 and Chapter 4; Riddick et al., 2015)(Riddick et al., in review)(Riddick et al., in review)(Riddick et al., in review)(Riddick et al., in review). These fine particles have a

high backscattering efficiency ( $b_{bp}:b_p$  up to 0.03) and thus contribute strongly to the water-leaving radiative signal and impart the lake with its characteristic turquoise colour.

Lake Balaton also demonstrates highly localised concentrations of colour dissolved organic matter (CDOM), with CDOM absorption coefficients [ $a_{\text{CDOM}(440)}$ ] typically ranging from 0.09–1.4  $\text{m}^{-1}$  with the highest CDOM absorption observed at the mouth of the Zala River [ $a_{\text{CDOM}(440)}$  up to 9.5  $\text{m}^{-1}$ ] where water rich in dissolved organic carbon produced in Kis-Balaton is discharged into the lake. However, CDOM is rapidly diluted and bleached through photodegradation as water passes through the system.

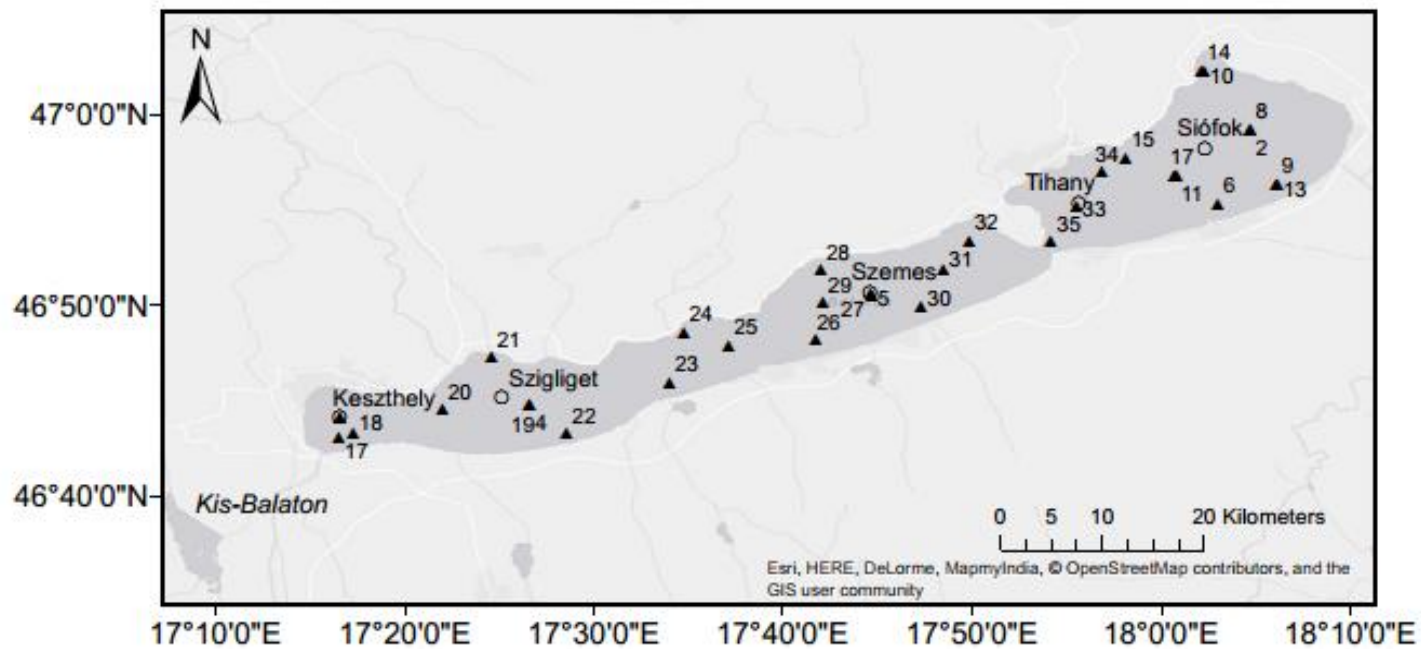


**Figure 5.1** Map of Lake Balaton, indicating the five regularly monitored stations (BLI) (Keszthely, Szigliget, Balatonszemes, Siófok and Tihany) and the 35 locations from the August 2010 field campaign.

## 5.2.2 Routine monitoring programmes

Lake Balaton is regularly monitored by Balaton Limnological Institute (BLI, MTA CER) at a bi-weekly to monthly frequency at up to 5 stations on the lake, thus it has an extensive archive of data for satellite validation studies. In this study, we compiled the routine Chl-*a* concentration and phytoplankton count data from the years 2007-2011 and more recent measurements of the PC concentrations from the years 2010-2011. In addition, further Chl-*a* data from 2007-2011 were obtained from the Central Transdanubian (Regional) Inspectorate for Environmental Protection, Nature Conservation and Water Management [Közép-dunántúli Környezetvédelmi, Természetvédelmi és Vízügyi Felügyelőség (KDT KTVF)]. However, for consistency with previous publications, the abbreviation KdKVI has been used throughout. The water sampling and Chl-*a* extraction methods of both BLI and KdKVI are detailed in Palmer et al. (2015c), and the two data sets show good agreement when the Chl-*a* concentration was measured on the same day and at the same station.

### 5.2.2.1 Chlorophyll-*a*

Water samples were collected as depth integrated over the water column at each station. A 5-litre sample was stored in the dark on ice before Chl-*a* extraction, within 24 hours. Samples were filtered under low vacuum pressure through GF/C (Whatman) filter papers and subsequently extracted in 90% hot methanol. Depending on the sample turbidity, between 500 and 1,500 mL was filtered. Sample absorbance was measured spectrophotometrically (Shimadzu UV-1601), as in Iwamura et al. (1970). The concentration ( $\text{mg m}^{-3}$ ) of Chl-*a* was then determined by the following equation, where  $A_x$  is the measured absorbance at wavelength  $x$  (nm):

$$[\text{Chl} - a] = 17.12(A_{666} - A_{750}) - 8.68(A_{653} - A_{750}) \quad (5.1)$$

KdKVI routine monitoring consists of water samples collected at the surface, followed by filtration under low vacuum pressure through GF/C (Whatman) filter papers. Chl-*a* was extracted in ethanol and measured spectrophotometrically, with concentration calculated as in Equation 5.1.

### 5.2.2.2 Phycocyanin

The samples collected for BLI routine monitoring were depth integrated over the first 2-3.5 metres of the water column, depending on the maximum sample depth at each station. A 5-litre sample was stored in the dark on ice before PC extraction, within

24 hours. Samples were filtered under low vacuum pressure through GF/C (Whatman) filter papers and subsequently extracted in a solution of 15 mL 0.05M phosphate buffer (pH=6.8). Depending on the sample turbidity, between 70 and 450 mL of water was filtered. Filter papers in the buffer solution underwent one freeze-thaw cycle as in Sarada et al. (1999), and phycocyanin was extracted by sonication over ice for 15 seconds (Ultrasonic Homogenizer 4710 Series, Cole-Palmer Instrument Co., USA), as detailed in Horváth et al. (2013a) (Method E). Finally, extracts were filtered (GF/C Whatman) and the absorption measured on a spectrophotometer (Shimadzu UV-1601, Shimadzu Co., Japan). Phycocyanin concentrations were calculated using the following equation (Siegelman & Kycia, 1978), where  $A_x$  is the measured absorbance at wavelength  $x$  (nm):

$$[PC] = (A_{615} - 0.474 \times A_{652})/5.34 \quad (5.2)$$

### 5.2.2.3 *Phytoplankton biomass*

Depth integrated water samples were collected in a 50 mL polyethylene container and preserved in Lugol's solution immediately after collection for analysis within 6 months. At least 25 cells (or filaments) of each species were measured to determine biomass and at least 400 were counted using an inverted plankton microscope (Utermöhl, 1958). The wet weight of each species was then calculated from cell volumes (Németh & Vörös, 1986).

## 5.2.3 **MERIS validation campaign**

In addition to the routine monitoring programmes, a separate sampling campaign for MERIS validation was conducted from 18-26<sup>th</sup> August 2010 to coincide with an Envisat MERIS overpass on 22<sup>nd</sup> August 2010. IOP measurements and water samples were collected at 35 stations during this campaign. Large volume water samples (5 L) were taken from the surface (~0.5 m) using an acid-rinsed wide-necked polyethylene carboy for subsequent analysis of pigments (Chl-*a* and PC), phytoplankton absorption and phytoplankton counts. Samples were stored on ice in the dark prior to analysis for pigments.

### 5.2.3.1 *Chlorophyll-a*

For the August 2010 sampling campaign, the following Chl-*a* extraction method was applied. A subsample of a 5 L surface water (0.5 m) sample was filtered on the boat immediately after sample collection under low vacuum pressure through GF/F

(Whatman) filter papers. Depending on the water clarity at the location (using Secchi depth), between 20 and 70 mL of sample water was filtered. Filter papers were then flash frozen in liquid nitrogen for <12 hours and placed in a -80°C freezer until analysis (no more than 6 months). Frozen GF/F filter papers were thawed in the dark from -80°C and chlorophyll-*a* was measured spectrophotometrically (Shimadzu UV-1601), as for the BLI routine monitoring programme above.

#### **5.2.3.2 *Phycocyanin***

For the August 2010 PC data, subsamples of a 5 L surface water (~0.5 m) sample were filtered on the boat immediately after sample collection under low vacuum pressure through GF/F (Whatman) filter papers. Depending on the water clarity at the location (using Secchi depth), between 20 and 70 mL of sample water was filtered. Filter papers were then flash frozen in liquid nitrogen for <12 hours and placed in a -80°C freezer until analysis (no more than 6 months). Frozen GF/F filter papers (2 replicates) were thawed from -80°C and the pigment concentration was obtained according to the method described above for BLI routine monitoring.

#### **5.2.3.3 *Phytoplankton biomass***

A subsample of a 5 L surface water sample was collected in a 50 mL polyethylene container and preserved in Lugol's solution immediately after collection for analysis within 6 months. Phytoplankton biomass was subsequently measured following the counting method from the BLI routine monitoring programme, detailed above.

#### **5.2.3.4 *Measurement of absorption and backscattering coefficients***

Particulate absorption measurements were made during the August 2010 campaign only. A subsample of a 5 L water sample was filtered on the boat immediately after sample collection under low vacuum pressure. Depending on the location, 20-70 mL of water was passed through GF/F (Whatman) filter papers and the filters were immediately flash frozen in liquid nitrogen for <12 hours prior to storage at -80°C. All samples were analyzed within 6 months of collection. Frozen GF/F filters were defrosted in the lab from -80°C in the dark. The absorbance of the material on the filter was measured from 350-750 nm using a dual beam spectrophotometer retro-fitted with Spectralon coated integrating spheres, according to the 'transmittance-reflectance' method of Tassan and Ferrari (1998). Absorption of the filter was measured to obtain

total absorption ( $a_T$ ), absorption by non-algal particles ( $a_{NAP}$ ) and absorption by phytoplankton ( $a_{ph}$ ) as in Chapter 3 and Riddick et al. (2015).

Particle backscattering coefficients [ $b_{bp}(\lambda)$ ] were derived from measurements collected with an ECO-BB3 backscatter meter (WET Labs). The calibration was performed by the manufacturer immediately prior to sampling, and it was assumed that there was no drift in the calibration coefficients and/or dark counts. The ECO-BB3 measures the total volume scattering function [ $\beta_t(\lambda, 124^\circ)$ ] from a centroid angle of scattering ( $124^\circ$ ) at 3 wavelengths ( $\lambda = 470, 532$  and  $650$  nm). The transformation of the raw counts into  $b_{bp}(\lambda)$  was done following the manufacturer's user guide (WET Labs, 2010) and the methods as in Slade and Boss (2015). Mean  $b_{bp}(\lambda)$  values were calculated over 1-5 min measurement periods. Detail on this method is provided in Chapter 4, Section 4.2.10.

#### 5.2.3.5 *In situ radiometry*

*In situ* radiometry was collected with a HyperSAS (Hyperspectral Surface Acquisition System; Satlantic) for validation of the atmospheric correction of MERIS data. Three radiometers were positioned at a height of 3.5 m from a pole at the bow of the boat. The boat was positioned on station to point radiance sensors at a relative azimuth angle of  $135^\circ$  from the sun. The three radiometers measured downwelling irradiance [ $E_s(\lambda)$ ], surface radiance of the water [ $L_t(\lambda)$ ] and sky radiance [ $L_{sky}(\lambda)$ ]. The latter two parameters are used to calculate the water-leaving radiance [ $L_w(\lambda)$ ] after correction for air-sea interface reflection using the following equation (Mueller et al., 2000):

$$L_w(\lambda) = L_t(\lambda) - \rho_{sky} L_{sky}(\lambda) \quad (5.3)$$

Where  $\rho_{sky}$ , the air-sea interface reflection coefficient, is estimated for sunny conditions as a function of wind speed ( $W$ ) in  $m\ s^{-1}$ :

$$\rho_{sky} = 0.0256 + 0.00039*W + 0.000034*W^2 \quad (5.4)$$

The HyperSAS raw data was processed to level 3a using Satlantic ProSoft software (v.7.7.10). After processing, all spectra underwent quality control for any outliers due to variable cloudiness or sun glint due to sea state. Remote sensing reflectance,  $R_{rs}(\lambda)$  ( $sr^{-1}$ ), was then calculated with the following equation:

$$R_{rs}(\lambda) = L_w(\lambda) / E_s(\lambda) \quad (5.5)$$

#### 5.2.4 MERIS data processing

MERIS full resolution full swath (FRS) 300 m Level-1b data for Lake Balaton were obtained for a period of 5 years (2007-2011) from the European Space Agency's Mercator system (<https://earth.esa.int/web/guest/data-access/online-archives>). The geolocation of the data was improved using the AMORGOS (Accurate MERIS Ortho-Rectified Geo-location Operational Software) v.4.0 processor. Images with high cloud cover were discarded, leaving 34 images with matching Chl-*a* data, 21 images with matching cell biomass data and 5 images with matching PC data (within 7 days of overpass date). The MERIS data were atmospherically corrected using the Self-Contained Atmospheric Parameters Estimation for MERIS data (SCAPE-M) automatic atmospheric correction processor developed by Guanter et al. (2010), following the SCAPE-M\_B2 implementation as in Domínguez Gómez et al. (2011). SCAPE-M\_B2 is an improved version of SCAPE-M, which corrects MERIS band 2 with an interpolation between the values of band 1 and band 3 (Domínguez Gómez et al., 2011). It is noted that this is the first implementation of the SCAPE-M\_B2 correction to MERIS FRS data, as opposed to FR (full resolution) data, and the intention is that SCAPE-M\_B2 will be adapted to OLCI data in the future. SCAPE-M and SCAPE-M\_B2 have been shown to compute accurate water-leaving reflectances for lakes, particularly for highly turbid waters (Yang et al., 2011a, Yang et al., 2011b, Agha et al., 2012, Jaelani et al., 2013, Medina-Cobo et al., 2014).

Following atmospheric correction with SCAPE-M\_B2, water-leaving reflectance [ $\rho_w(\lambda)$ ] was extracted from the MERIS images using BEAM VISAT v.4.11 (Brockmann Consult, v.4.11).  $\rho_w(\lambda)$  was converted to remote sensing reflectance [ $R_{rs}(\lambda)$ ] by the following equation:

$$R_{rs}(\lambda) = \rho_w(\lambda)/\pi \quad (5.6)$$

Each algorithm was then applied to the extracted remote sensing reflectances, and the best performing algorithm was implemented using the Graph Processing Framework in BEAM to produce mapped time-series products.

##### 5.2.4.1 Validation of atmospheric correction

The SCAPE-M\_B2 atmospheric correction was validated using the MERIS data from 22 August 2010 and the August 2010 MERIS validation campaign *in situ* data. Same-day ( $\pm 1$  day) matchups with *in situ*  $R_{rs}$  were considered (n=7), as this was considered a suitable approach for a validation over a dynamic lake system. However,

all available matchups of MERIS SCAPE-M\_B2 and *in situ*  $R_{rs}$  from the August 2010 campaign are presented here for completeness (n=30).  $R_{rs}$  was compared at all 15 MERIS bands with *in situ*  $R_{rs}$  collected by HyperSAS radiometry. HyperSAS  $R_{rs}$  data was simulated to the 12 MERIS bands using the spectral response functions, assuming a Gaussian distribution around the MERIS band center. At each station with coincident data,  $R_{rs}$  for each MERIS band was also plotted over the range of *in situ*  $R_{rs}$  measured by the HyperSAS at the respective station (n=30).

#### 5.2.4.2 Validation datasets and strategy

In August 2010, 35 PC and Chl-*a* measurements were collected specifically for matchup with MERIS overpasses. The mean PC or Chl-*a* retrieval for a 3x3 pixel kernel was extracted for matchup with *in situ* data. To reduce the effects of spatial variability on the validation, any retrieved pigments with a standard deviation >2 were removed, similar to the methods for spatial homogeneity employed in Goyens et al. (2013) and Jamet et al. (2011). Matchups were generally discarded due to cloud cover or where there was interference from land pixels (adjacency effect), leaving 29 Chl-*a* and 28 PC matchups. Following the same approach, an additional 52 Chl-*a* matchups were available from BLI routine monitoring campaigns from 2008-2011 at five lake sites (Keszthely, Szigliget, Szemes, Tihany and Siófok), as well as 113 matchups from KdKVI monitoring from 2007-2011 (Keszthely, Balatonszemes, Szigliget and Siófok), yielding a total of 194 *in situ* Chl-*a* concentrations were matched with MERIS retrievals. An additional 12 PC matchups were also available from BLI routine monitoring in 2011 (Keszthely, Szigliget, Szemes and Siófok), for a total of 40 *in situ* PC concentrations available for matchup with MERIS retrieved PC ( $\pm 7$  days). 29 matchups were available with  $a_{ph}(\lambda)$  and  $b_b(\lambda)$  data from the August 2010 campaign ( $\pm 7$  days), following the same approach as for pigment matchups. Algorithm retrievals were validated with field data for time constraints of  $\pm 1, 3$  and 7 days of a MERIS overpass, with duplicate matchups discarded (i.e. where more than one sampling date corresponded to the same MERIS image for a particular station).

The performance of Simis05, Mishra13 and Li15 algorithms were compared for PC retrievals from MERIS data, using matchups within 1 day of *in situ* PC measurements from 2010 and 2011 (n=22). The Gons05 and Simis05 algorithms were implemented for Chl-*a* and PC retrieval, respectively, as in Simis et al. (2005), using  $a^*_{chl(665)}=0.0139 \text{ m}^2 \text{ mg}^{-1}$  [Uncorrected Chl-*a*; (Gons et al., 2005)] and

$a_{pc}^*(620)=0.007 \text{ m}^2 \text{ mg}^{-1}$  (Simis et al., 2005). A constant spectral slope of  $a_{CDOM}(\lambda)$  ( $S_{CDOM} = 0.020 \text{ nm}^{-1}$ ) was applied in the Li15 model [See Table 3, Step 9 in Li et al. (2015) and Chapter 8 - Appendix], as this was the mean measured value for Lake Balaton in 2010. Additionally, the Mishra13 algorithm was applied using two different values of  $a_{pc}^*(620)$  from Simis et al. (2005) and Mishra et al. (2013) (0.007 and 0.0048  $\text{m}^2 \text{ mg}^{-1}$ , respectively).

The strength of the relationship between the algorithm estimated values and measured values was evaluated using least-squares regression analysis. The agreement (goodness of fit) is reported by the coefficient of determination ( $R^2$ ) and associated p value. Algorithm accuracy was quantified with measures of error, including the Root Mean Square Error (RMSE), Mean Absolute Percentage Error (MAPE) and Bias. RMSE and bias were also calculated in log space ( $RMSE_{\log}$  and  $Bias_{\log}$ , respectively).

## **5.3 Results**

### **5.3.1 Pigment and cell counts**

Inter-annual variations in cell counts are shown from 2007-2011 for total phytoplankton and cyanobacteria biomass, alongside Chl-*a* and PC pigments (Figure 5.2). Lake Balaton generally has a spring (January-March) diatom bloom, which is indicated by the smaller peaks in phytoplankton biomass and Chl-*a*. This is followed by a late summer (August-October) bloom in cyanobacteria, as indicated by the larger peaks in phytoplankton biomass and Chl-*a*. Keszthely is the westernmost basin, which has higher Chl-*a* concentrations than Tihany in the east. Both Keszthely and Tihany show the same timing of peaks in phytoplankton abundance, although the late summer cyanobacteria bloom is more prolific in Keszthely, with cyanobacteria biomass reaching nearly an order of magnitude higher than that in Tihany.

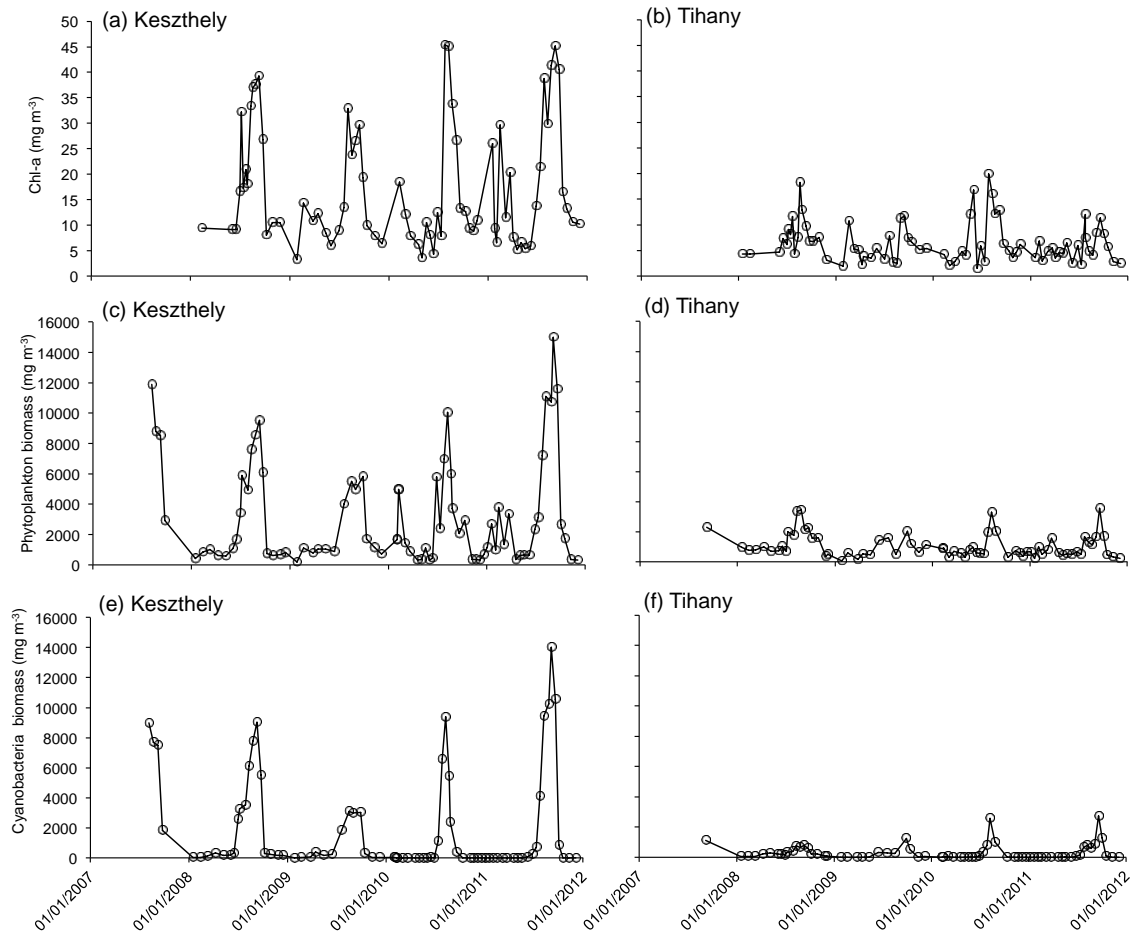


**Figure 5.2.** Inter-annual variations in (a,b) chlorophyll-*a*, (c,d) phytoplankton biomass and (e,f) cyanobacteria biomass at Keszthely and Tihany stations (BLI data).

Previous research over the same time period has shown that phycocyanin concentrations have a strong linear relationship to cyanobacteria biomass in field samples from Lake Balaton ( $R^2=0.94$ ,  $CV=1.7\%$ ) (Horváth et al., 2013a). This is important because it not only demonstrates that satellite retrieved PC concentrations can be used as an indicator of cyanobacterial biomass, but it also allows the use of cyanobacterial cell counts for partial-validation of the PC algorithms. Lake Balaton, like many other lakes, has longer and more complete data on phytoplankton cell counts than on PC measurements. However, it is important to note that this strong relationship between PC and cyanobacteria biomass may not be found in other lakes.

### 5.3.2 Validation of atmospheric correction

MERIS remote sensing reflectance spectra atmospherically corrected with SCAPE-M\_B2 were compared to *in situ* measurements made with a HyperSAS which

were convolved to the MERIS bands using spectral response functions. Scatterplots of data from the same day as the MERIS overpass (22 August 2010) showed good agreement at all 12 bands compared (RMSE<sub>log</sub><0.205, Bias<sub>log</sub><0.197, MAPE<58.7%, n=7; Figure 5.3). However, agreement was poorest over the NIR wavelengths (Bands 10-12) and blue portion of the spectrum (Band 1).

MERIS SCAPE-M\_B2  $R_{rs}(\lambda)$  spectra are presented alongside *in situ*  $R_{rs}(\lambda)$  for all stations in Figure 5.4 and Figure 5.5. For same-day matchups (stations 16-22), MERIS bands generally fell reasonably within the range of *in situ*  $R_{rs}(\lambda)$ . However, for matchups out with the  $\pm 1$  day matchup window,  $R_{rs}(\lambda)$  was frequently under- (stations 1-15) or over-estimated (e.g. stations 29-30). Note that the NIR range for stations 10, 14 and 24 shows high standard deviation for MERIS  $R_{rs}(\lambda)$  because these 3x3 pixel windows were impacted by the adjacency effect (i.e. were influenced by land pixels).

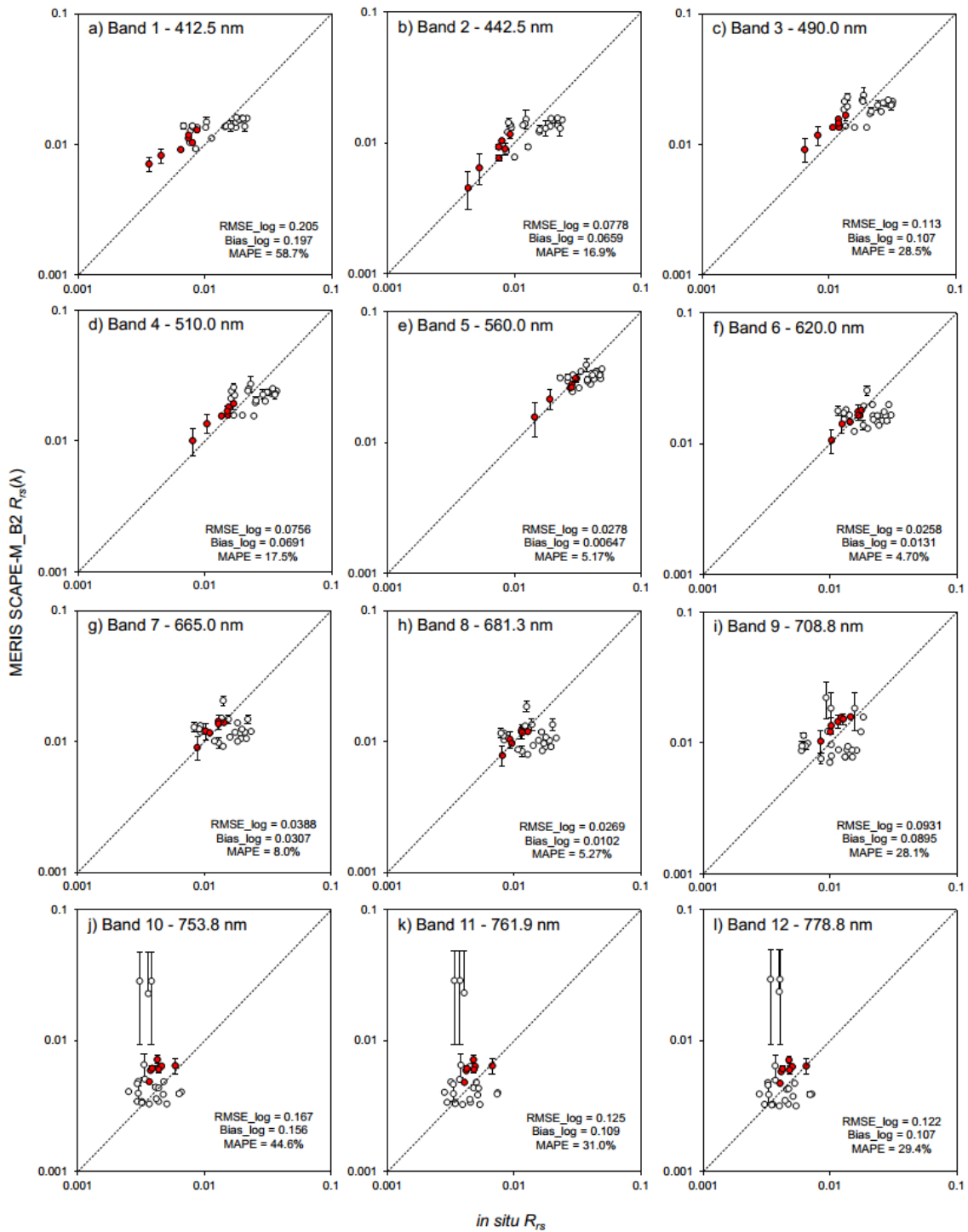


**Figure 5.3.** Validation of MERIS data atmospherically corrected with SCAPE-M\_B2 with *in situ* reflectance data, including scatter plots of  $R_{rs}(\lambda)$  at each band. Scatterplots include all stations with *in situ* data (n=30), with same day matchups shown in red (n=7). Statistics correspond to the same day matchups only.

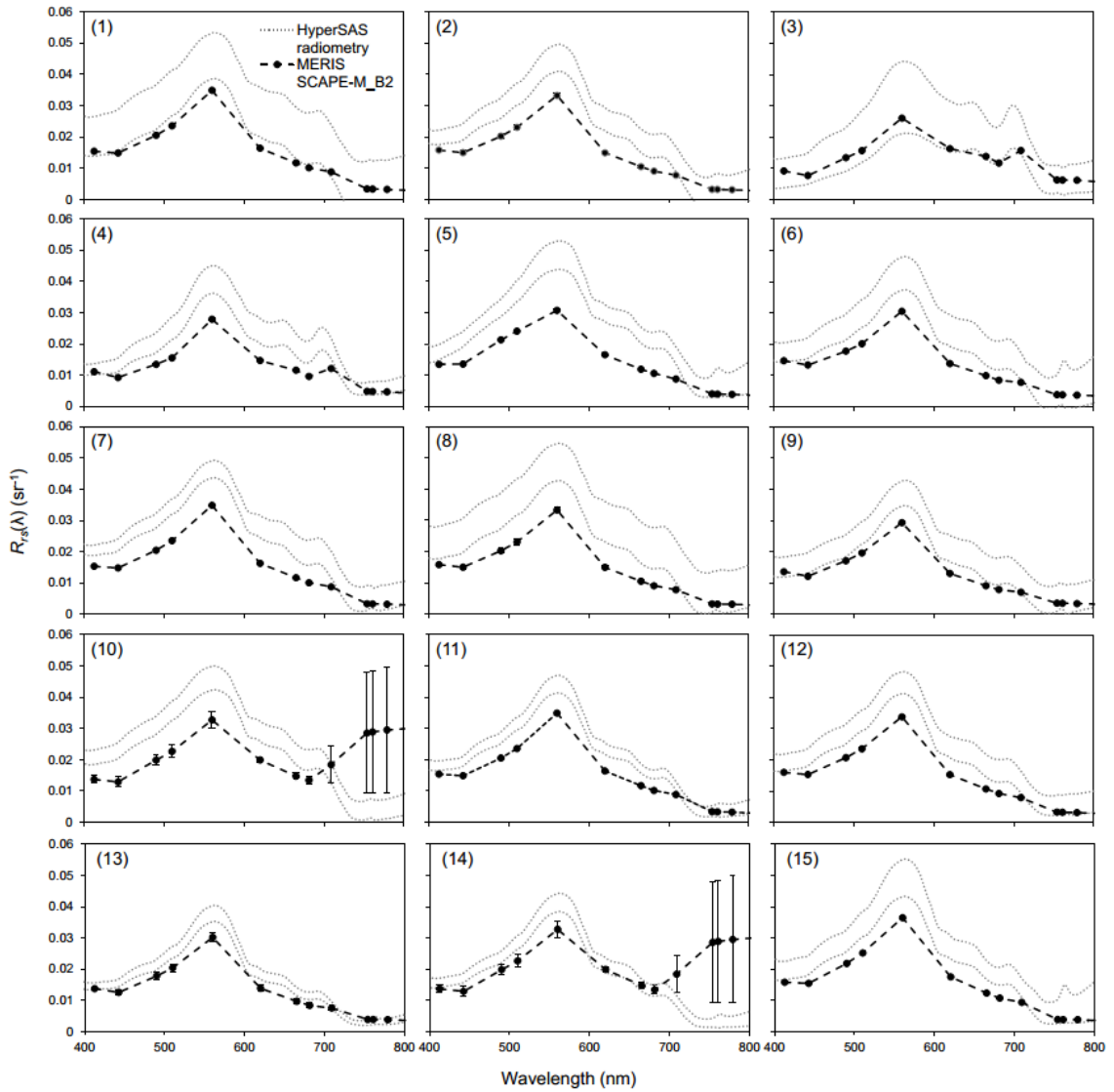


**Figure 5.4.** Validation MERIS data atmospherically corrected with SCAPE-M\_B2 with *in situ* HyperSAS reflectance data for stations 1-15. MERIS data is the mean of a 3x3 pixel window with error bars indicating standard deviation. HyperSAS radiometry is shown as a range of minimum to maximum recorded at each station.

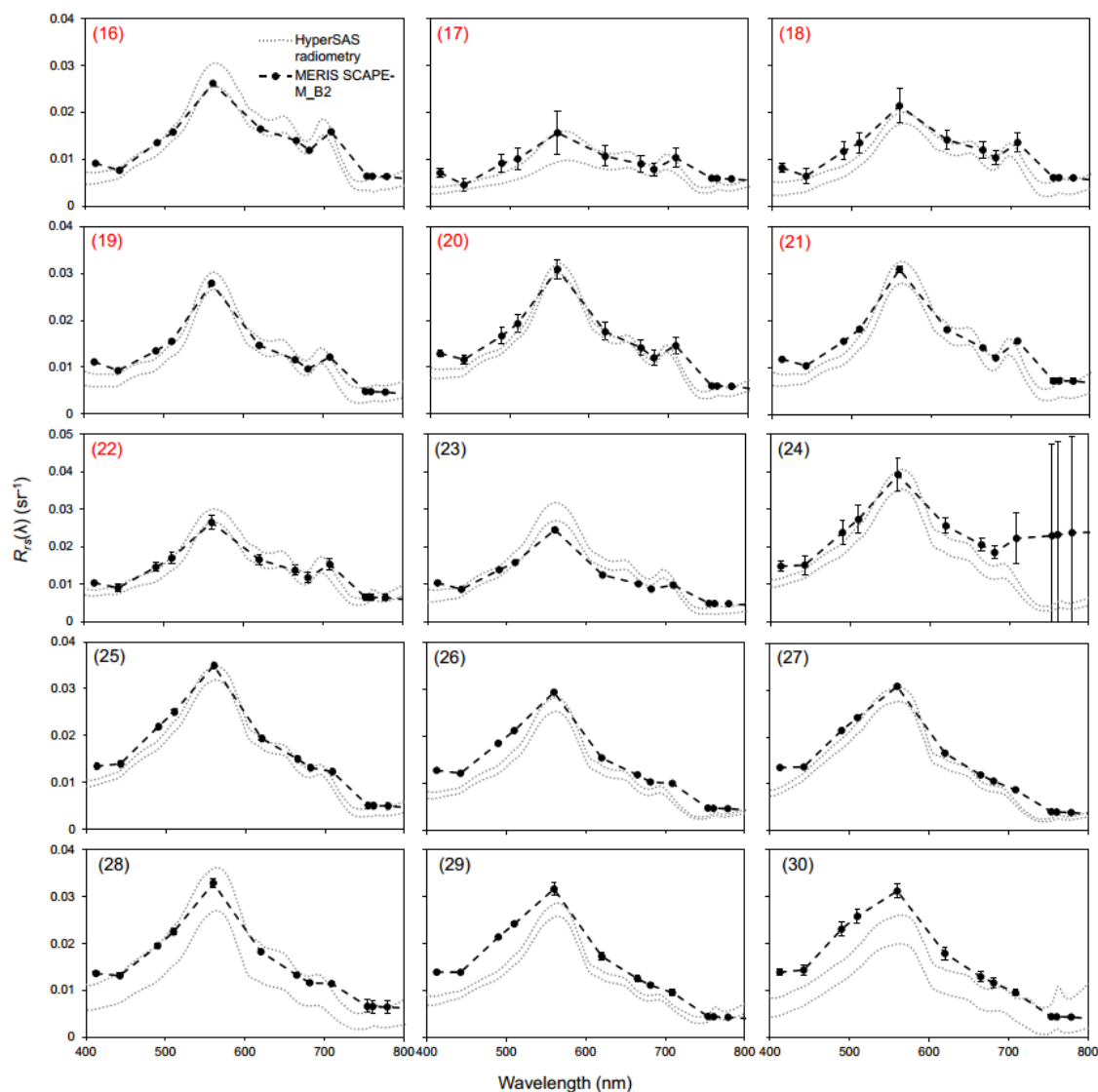


**Figure 5.5.** Validation MERIS data atmospherically corrected with SCAPE-M\_B2 with *in situ* HyperSAS reflectance data for stations 16-30. MERIS data is the mean of a 3x3 pixel window with error bars indicating standard deviation. HyperSAS radiometry is shown as a range of minimum to maximum recorded at each station. Same-day matchups include stations 16-22 only, shown in red (n=7). Note the different ranges for y-axis values.

### 5.3.3 Algorithm performance

The performance results for each algorithm tested (Simis05, Mishra13 and Li15) are provided in Figure 5.6, with associated details and measures of error in **Table 5.1**. The Simis05 algorithm retrieved PC concentrations with an RMSE of  $11.8 \text{ mg m}^{-3}$ , with a near 1:1 relationship with measured PC concentrations (MERIS Retrieved PC =  $0.722 \cdot \text{Measured PC} + 8.95$ ; Figure 5.6a). The Mishra13 algorithm had the poorest

relationship between retrieved and measured PC, with an  $R^2$  value of 0.00836 using  $a^*_{pc}(620)$  values from both Simis et al. (2005) and Mishra et al. (2013) (RMSE= 22.3 and 22.9  $\text{mg m}^{-3}$ , respectively). While PC retrievals with Li15 had a similar coefficient of determination ( $R^2=0.716$ ) as Simis05 retrievals, agreement was poor (MAPE=205%) with negative PC retrievals for *in situ* concentrations  $<10 \text{ mg m}^{-3}$ . Additionally, both Mishra13 and Li15 PC retrievals deteriorated markedly at high PC concentrations. In particular, a marked decrease in the RMSE was observed for Li15 retrievals for *in situ*  $\text{PC} < 50 \text{ mg m}^{-3}$  (RMSE = 20.2  $\text{mg m}^{-3}$ ). The Simis05 semi-analytical algorithm retrieved PC with higher accuracy and better agreement with *in situ* concentrations than either of the inversion models, therefore the performance of the Simis05 algorithm was investigated in further detail for the remainder of this study.

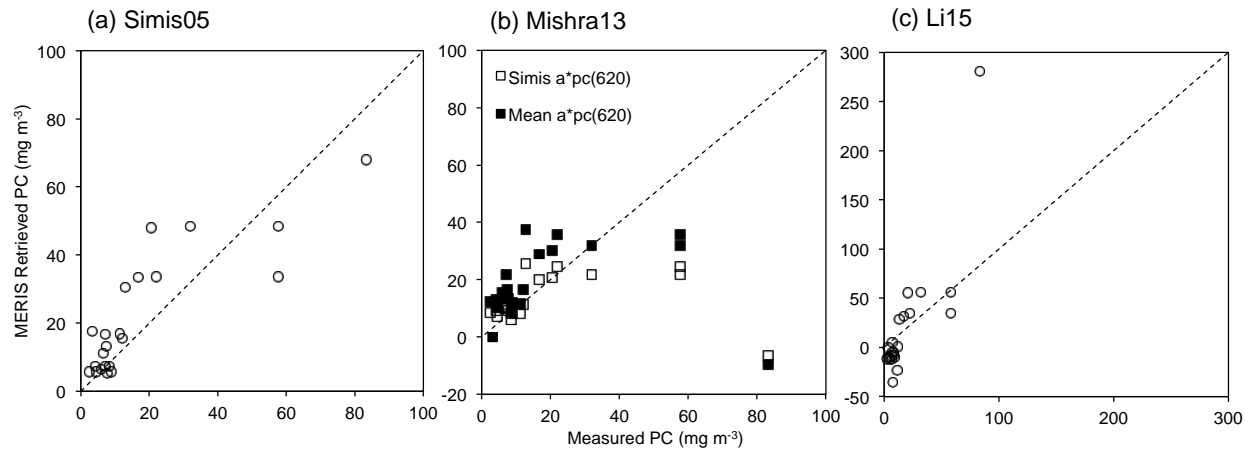


**Figure 5.6** Phycocyanin retrieval performance for a)Simis05, b)Mishra13 and c)Li15 algorithms using MERIS data from 2010-2011 (n=22). Matchups are within 1 day of *in situ* phycocyanin measurements. Mishra13 was applied using  $a^*_{pc}(620)=0.007 \text{ m}^2 \text{ mg}^{-1}$  from Simis et al. (2005) and  $a^*_{pc}(620)=0.0048 \text{ m}^2 \text{ mg}^{-1}$  from Mishra et al. (2013).

**Table 5.1** PC retrieval statistics for Simis05, Mishra13 and Li15 algorithms using MERIS data from 2010-2011 (n=22 unless specified otherwise). Matchups are within 1 day of *in situ* phycocyanin measurements.

<b>Model</b>	<b><i>B</i></b>	<b><i>m</i></b>	<b><math>R^2</math></b>	<b><i>p</i></b>	<b>RMSE mg m<sup>-3</sup></b>	<b>RMSE<sub>log</sub></b>	<b>Bias</b>	<b>Bias<sub>log</sub></b>	<b>MAPE %</b>
<b>Simis05</b>	8.95	0.722	0.710	<0.0001	11.8	0.272	3.92	0.147	77.0
<b>Mishra13</b> <sup>a</sup>	11.8	0.0358	0.00836	0.686	22.3	0.246	-5.62	0.0664	61.2
<b>Mishra13</b> <sup>b</sup>	17.3	0.0522	0.00836	0.686	22.9	0.330	0.0987	0.230	104
<b>Li15</b>	-26.2	2.55	0.716	<0.0001	46.3	0.503	1.84	0.0349	205
<b>Li15</b> <sup>c</sup>	-26.0	2.82	0.697	<0.0001	20.2	0.561	-6.90	0.00889	222

<sup>a</sup>  $a^*_{pc}(620) = 0.007 \text{ m}^2 \text{ mg}^{-1}$  as in Simis et al. (2005)

<sup>b</sup>  $a^*_{pc}(620) = 0.0048 \text{ m}^2 \text{ mg}^{-1}$  as in Mishra et al. (2013)

<sup>c</sup> for *in situ* PC < 50 mg m<sup>-3</sup> only (n=19).

### 5.3.4 Chlorophyll-*a* retrieval

As the performance of the Simis05 algorithm is partly based on that of its predecessor, the Gons05 algorithm was initially validated for chlorophyll-*a* retrieval. Chl-*a* was retrieved from MERIS after estimating the absorption coefficient of phytoplankton at 665 nm. At  $\pm 1$ , 3 and 7 day matchup intervals, the Gons05 algorithm retrieved Chl-*a* with high accuracy using all three datasets for validation ( $R^2 > 0.75$  and  $RMSE < 12 \text{ mg m}^{-3}$ ; Figure 5.7). However, there was increased scatter in the relationship at Chl-*a* concentrations  $< 10 \text{ mg m}^{-3}$  ( $\pm 7$  days:  $RMSE_{\log} = 0.476$ ,  $MAPE = 208\%$ ,  $n = 98$ ) compared to those stations with higher Chl-*a* concentrations,  $> 10 \text{ mg m}^{-3}$  ( $\pm 7$  days:  $RMSE_{\log} = 0.384$ ,  $MAPE = 142\%$ ,  $n = 159$ ). When Chl-*a* retrievals were restricted to those stations also used for PC validation, there was better agreement between MERIS retrieved and *in situ* Chl-*a* ( $R^2 = 0.866-0.910$ ,  $p < 0.0001$ ,  $RMSE = 8.47-10.4 \text{ mg m}^{-3}$ ; Figure 5.8). Furthermore, retrievals validated with surface samples from August 2010 only (Table 5.3) had higher  $R^2$  values ( $R^2 = 0.906-0.943$ ,  $p < 0.0001$ ) and were closer to the 1:1 line ( $MAPE = 50.0-58.9\%$ ) than those validated with integrated samples routinely taken by BLI ( $R^2 = 0.723-0.810$ ,  $p < 0.0001$ ,  $MAPE = 107-112\%$ ; Table 5.4) or surface samples from the KdKVI dataset ( $R^2 = 0.784-0.786$ ,  $p < 0.0001$ ,  $MAPE = 165-169\%$ ; Table 5.5).

Gons05 Chl-*a* retrievals were also partially-validated with phytoplankton counts (Figure 5.9). There was good agreement between the Chl-*a* values retrieved from MERIS and total phytoplankton biomass, with little difference in the  $R^2$  values for  $\pm 1$  ( $R^2 = 0.667$ ,  $p < 0.001$ ), 3 ( $R^2 = 0.698$ ,  $p < 0.001$ ) and 7 ( $R^2 = 0.636$ ,  $p < 0.001$ ) day matchups (Table 5.2). There was no noticeable difference for validation using surface (August 2010) versus integrated (BLI) samples (Table 5.3 and Table 5.4).

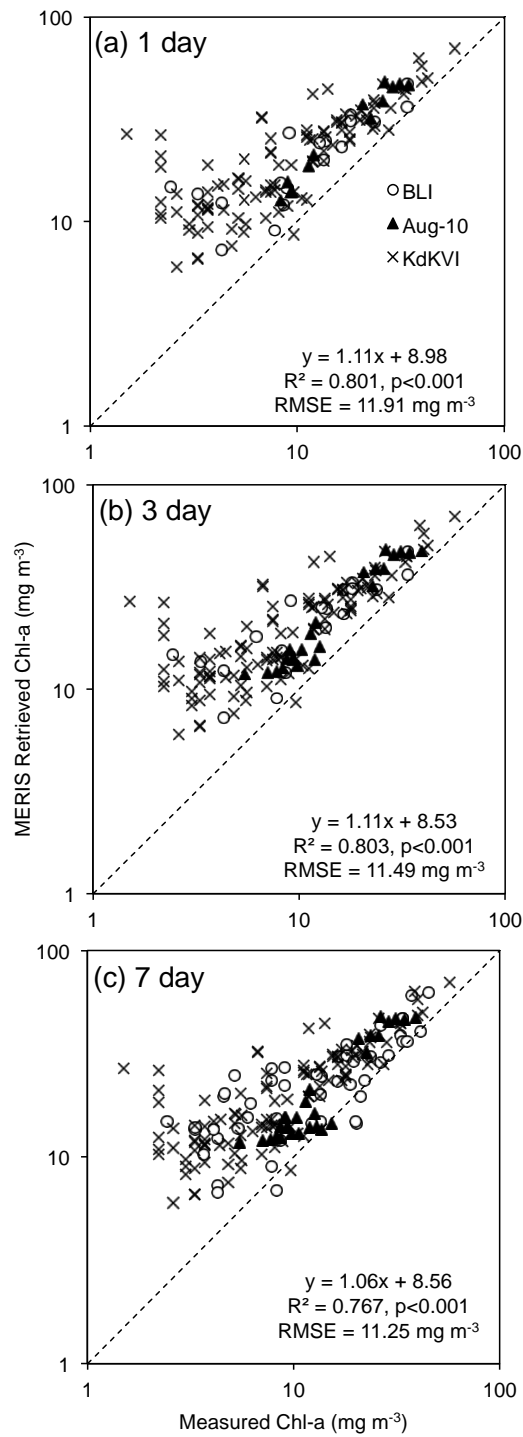


**Figure 5.7** Retrievals of Chl-*a* from MERIS at matchups with measured Chl-*a* within (a)  $\pm 1$  day, (b)  $\pm 3$  days and (c)  $\pm 7$  days. Retrievals shown are mean pixel values within 2 standard deviations. Linear regression results shown are for all data. Dashed line is 1:1.

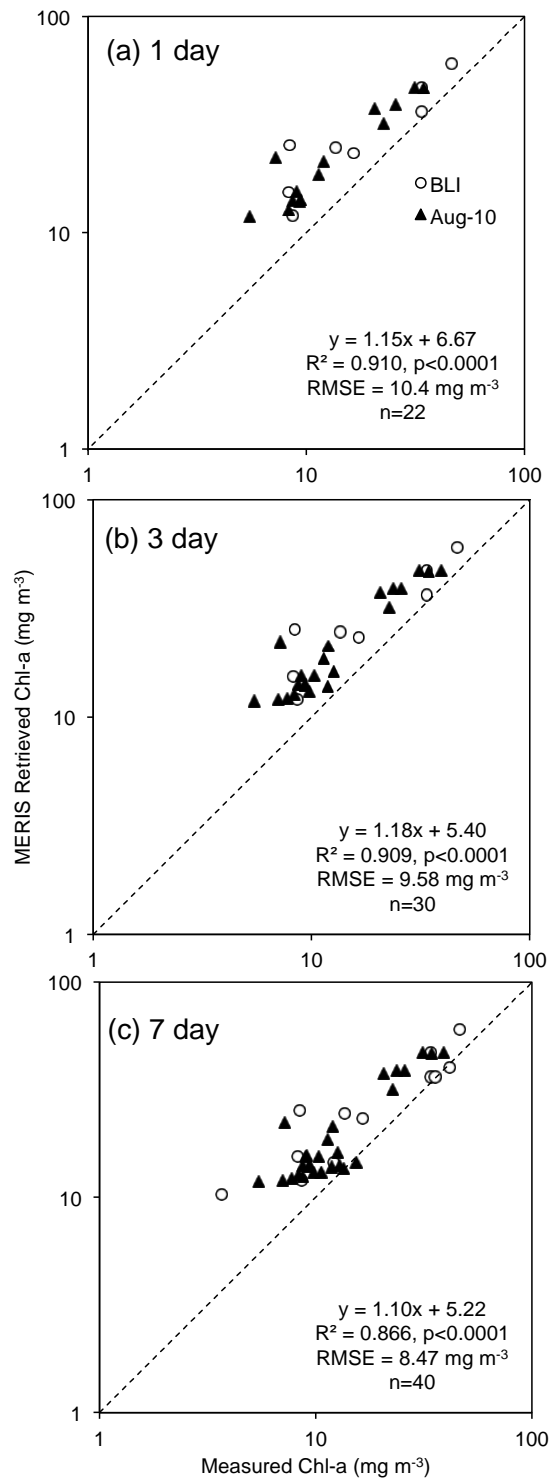


**Figure 5.8** Retrievals of Chl-*a* from MERIS at matchups with measured Chl-*a* within (a)  $\pm 1$  day, (b)  $\pm 3$  days and (c)  $\pm 7$  days, using only those matchups used for Simis05 retrievals of PC. Retrievals shown are mean pixel values within 2 standard deviations. Linear regression results shown are for all data. Dashed line is 1:1.

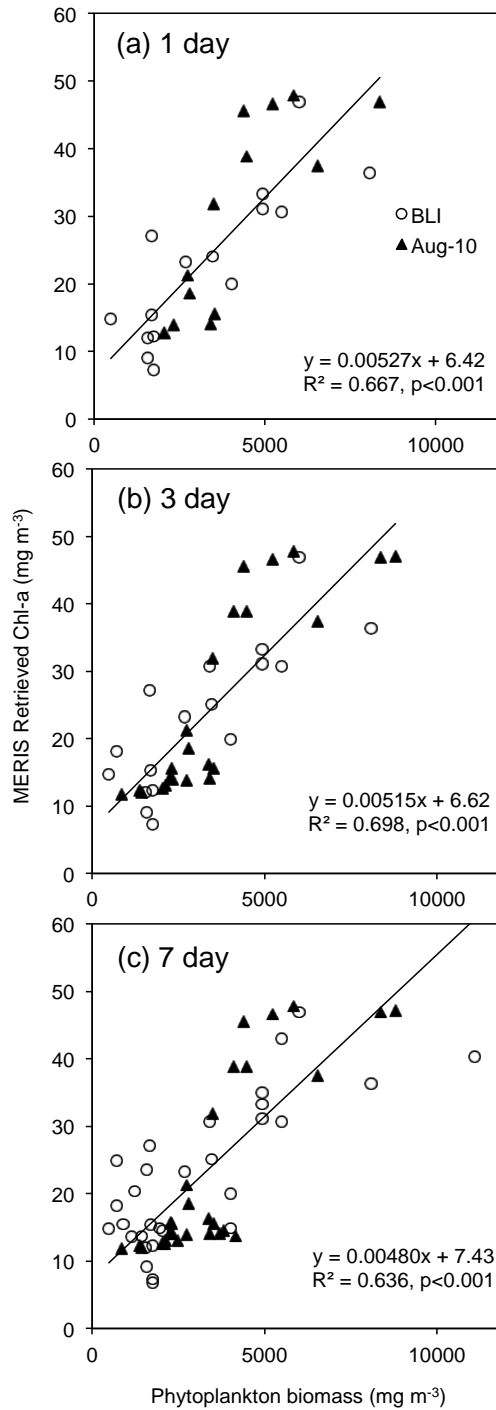


**Figure 5.9** Retrievals of Chl-*a* from MERIS at matchups with measured phytoplankton biomass from (a)  $\pm 1$  day, (b)  $\pm 3$  days and (c)  $\pm 7$  days. Retrievals shown are mean pixel values within 2 standard deviations. Solid line is a linear regression for all data.

### 5.3.5 Phycocyanin retrieval

Phycocyanin concentrations were retrieved from MERIS data after estimation of  $a_{pc}(620)$ , and were validated with measured concentrations from the August 2010 campaign and BLI routine monitoring data. The PC concentrations retrieved using Simis05 showed good agreement with the *in situ* data for matchups  $\pm 3$  days of the overpass ( $R^2=0.663-0.710$ ,  $p<0.0001$ ,  $RMSE <11.8 \text{ mg m}^{-3}$ ) (Figure 5.10 and Table 5.2). However, the agreement between the PC concentrations retrieved from MERIS and those measured *in situ* deteriorated markedly from the  $\pm 1$  to  $\pm 7$  day matchup windows, with  $R^2$  values decreasing from 0.710 ( $p<0.0001$ ) to 0.433 ( $p<0.0001$ ), and increasing RMSE ( $11.8 \text{ mg m}^{-3}$  to  $18.3 \text{ mg m}^{-3}$ ). At all three time intervals, retrievals validated with data taken from the surface samples during August 2010 (Table 5.3) showed higher  $R^2$  values for matchups  $\pm 7$  days ( $R^2=0.718$ ,  $p<0.0001$ ) than those validated with the integrated samples routinely taken by BLI ( $R^2=0.580$ ,  $p<0.01$ ; Table 5.4). Additionally, PC retrievals at all three time windows showed better agreement with the August 2010 surface samples ( $MAPE=59.3-71.6\%$ ) than the BLI integrated samples ( $MAPE=71.7-86.4\%$ ). As with Chl-*a* retrievals, the Simis05 algorithm did not accurately retrieve PC values below approximately  $5 \text{ mg m}^{-3}$ , and this was most noticeable with the greater matchup timeframe (e.g. at  $\pm 7$  days:  $MAPE=126\%$  for  $PC<5 \text{ mg m}^{-3}$ ,  $MAPE=52\%$  for  $PC>5 \text{ mg m}^{-3}$ ).

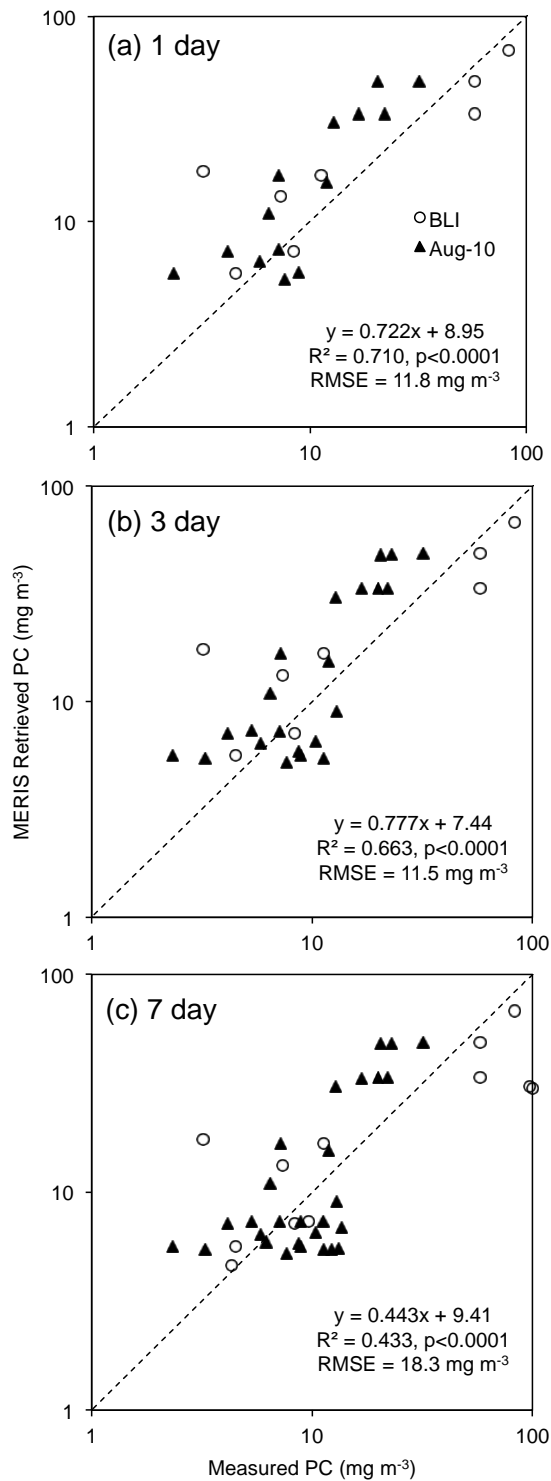


**Figure 5.10** Retrievals of PC from MERIS at matchups with measured PC from (a)  $\pm 1$  day, (b)  $\pm 3$  days and (c)  $\pm 7$  days. Retrievals shown are mean pixel values within 2 standard deviations. Linear regression results shown are for all data. Dashed line is 1:1.

Retrievals of PC from the Simis05 algorithm were also compared with measured cyanobacteria biomass (Figure 5.11). There was significant scatter around the linear regression, however PC estimates were still found to be significantly related to cyanobacteria counts with  $R^2$  values from 0.462 ( $p < 0.001$ ) to 0.525 ( $p < 0.001$ ) depending on the temporal window used for the matchups. There was no evidence of degradation in the relationship between PC retrievals and cyanobacteria biomass, with correlation coefficients actually improving from  $\pm 1$  to 7 days. Although, this is perhaps simply due to the greater number of matchups at  $\pm 3$  and  $\pm 7$  days and the increased data range as compared to  $\pm 1$  day. It should also be noted that determination coefficients improved very slightly when a linear regression was performed using PC estimates as a function of combined cyanobacteria and cryptophyte biomass ( $R^2 = 0.489-0.554$ ,  $p < 0.0001$ ). The relationship between retrieved Chl-*a* and phytoplankton biomass was stronger than the relationship between retrieved PC and cyanobacterial biomass at all three matchup intervals (see Table 5.2).

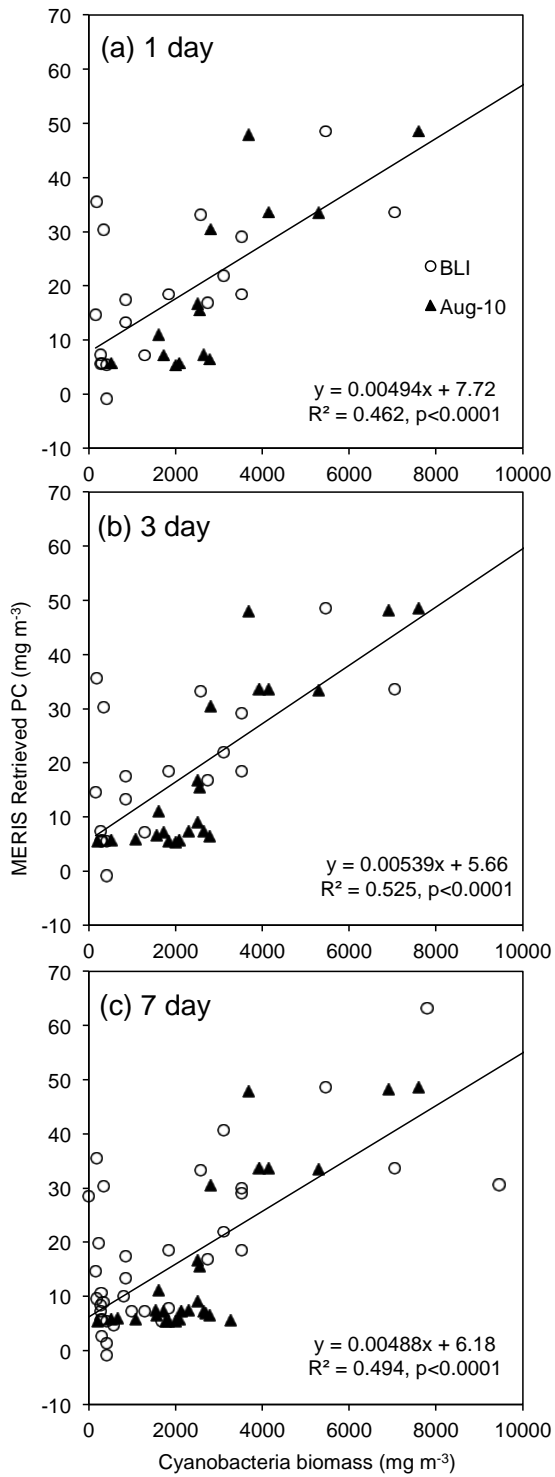


**Figure 5.11** Retrievals of PC from MERIS at matchups with measured cyanobacteria biomass from (a)  $\pm 1$  day, (b)  $\pm 3$  days and (c)  $\pm 7$  days. Retrievals shown are mean pixel values within 2 standard deviations. Solid line is a linear regression for all data.

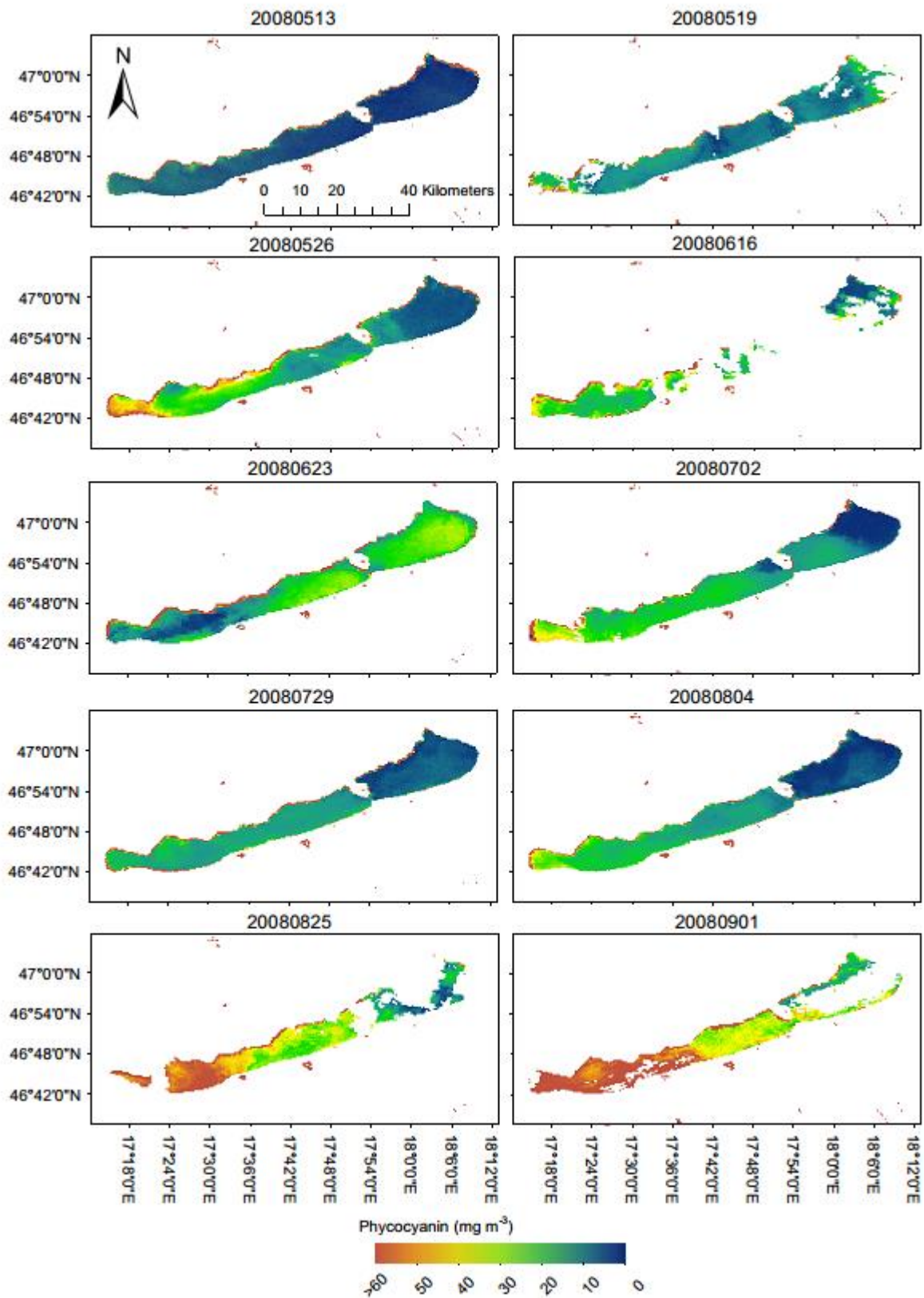


**Figure 5.12** Time series of estimated PC from MERIS (Simis05 algorithm) for May-September 2008.

An example time-series of the mapped PC products produced using the Simis05 algorithm is shown in Figure 5.12 for 2008. Retrieved PC concentrations show a significant peak in late summer during the cyanobacteria bloom, from mid-August into September. A gradient in PC is indicated across the lake, with the highest concentration generally in the western basins. It is also noted that a smaller spike in estimated PC is shown in western basins in the image for 26 May 2008 (Figure 5.12), however this is not mirrored by the cyanobacteria cell counts (Figure 5.2e-f). It is known that algae containing chlorophyll *b* or *c* (1+2) also have a reflectance minima (absorption peak) around the same wavelength as PC absorption (~640 nm). In particular, laboratory measurements of diatom cultures have reported a reflectance minima (absorption peak) around the same wavelength as PC absorption (~640nm), possibly related to the high concentrations of chlorophyll *c* (1+2) found in diatoms (Hunter et al., 2008b). Thus, it could be that in large enough numbers (i.e. a diatom bloom), the pigments of other algal groups are incorrectly interpreted by the Simis05 algorithm as phycocyanin. Indeed, increasing diatom abundance was recorded in Lake Balaton from May-June 2008, and this may be responsible for the false positive.

### 5.3.6 IOP retrievals

The Gons05 semi-analytical algorithm was deconstructed and the component parts were validated using the IOP measurements from the August 2010 sampling campaign on Lake Balaton. The Gons05 algorithm retrieves  $a_{ph}(665)$  based on the equation by Gons et al. (2005) using a correction factor,  $\gamma$ , introduced by Simis et al. (2005). This study compared the retrieved  $a_{ph}(665)$  against those determined using filter-pad absorption measurements. The retrieved values for  $a_{ph}(665)$  were found to over-estimate the measured  $a_{ph}(665)$  by a factor of 2 (Figure 5.13a). The coefficient of determination for least squares linear regression was 0.836, however the error was high ( $RMSE_{\log}=0.444$ ,  $Bias_{\log}=0.430$ ,  $MAPE=178\%$ ; Table 5.2). Summed absorption by Chl-*a* and PC at 620nm was also retrieved with Simis05 and compared to measured  $a_{ph}(620)$  from August 2010 (Figure 5.13b). Again, the coefficient of determination was high ( $R^2=0.834$ ) but the values retrieved with Simis05 were found to over-estimate measured pigment absorption by a factor of 3 ( $RMSE_{\log}=0.645$ ,  $Bias_{\log}=0.635$ ,  $MAPE=346\%$ ; Table 5.2). It is important to note, however, that filter-pad absorption measurements can be subject to significant errors due to unresolved issues with path-

length amplification (McKee et al., 2014), therefore some of this error may be a result of the method itself.

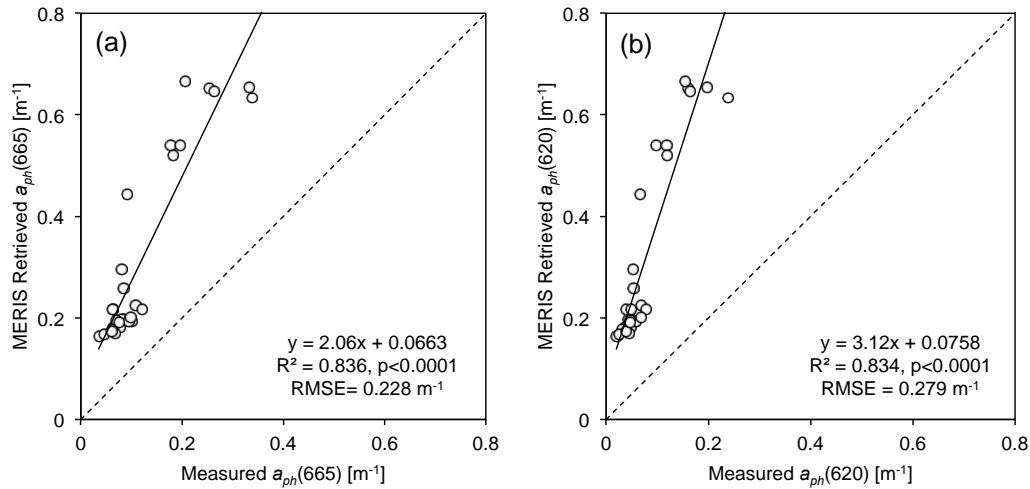


**Figure 5.13** Retrieval of (a)  $a_{ph}(665)$  and (b)  $a_{ph}(620)$  using Simis05 for 22 August 2010 with matchups  $\pm 7$  days ( $n=29$ ).

The Gons05 and Simis05 algorithms estimate  $b_b(\lambda)$  from reflectance at 778.75 nm based on the assumption that it is spectrally invariant over the wavelengths used in the algorithm (Gons, 1999). This assumption was tested using  $b_b(\lambda)$  coefficients measured at three wavelengths with an ECO-BB3 at 35 stations during the August 2010 sampling campaign (Figure 5.14a). Backscattering was highest at 470 nm, with lower coefficients at 532 and 650 nm. Measured  $b_b(\lambda)$  coefficients at 650 nm were then compared with the retrieved  $b_b(\lambda)$  coefficient from MERIS band 12 (778.75 nm) using the image from 22 August 2010 (Figure 5.14b).  $b_b(650)$  was chosen because it lies between the 620 nm and 665 nm bands used in the Gons05 and Simis05 algorithms. If backscattering was spectrally neutral and the algorithms were accurately retrieving the  $b_b(\lambda)$  coefficient a correlation between MERIS retrieved  $b_b(778.75)$  and measured  $b_b(650)$  may be expected. However, there was no linear relationship between the measured and retrieved  $b_b(\lambda)$  coefficients ( $R^2=0.0004$ ,  $p=0.9$ ; Table 5.2). The assumption of spectral neutrality may be reasonable based on the flat trend between 532 and 650 nm (Figure 5.14a), although it is unknown how  $b_b(\lambda)$  varies between 650 and 780 nm. In general, the retrieved  $b_b(\lambda)$  coefficients also showed significantly less variation across the stations sampled in Lake Balaton than was actually measured.

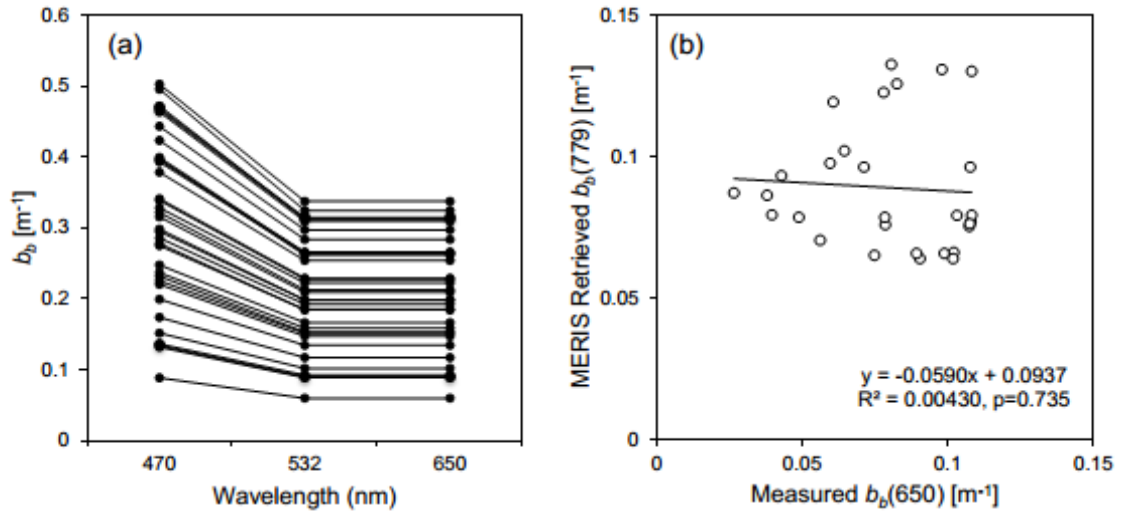


**Figure 5.14** (a) Spectra of backscattering at 3 wavelengths as measured by the ECO-BB3 during the August 2010 field campaign (n=35) and (b) linear regression of estimated  $b_b(779)$  from Simis05 and measured  $b_b(650)$  (n=29).

### 5.3.7 Time series analysis

The pigment concentrations retrieved from MERIS ( $\pm 7$  days) using Gons05 and Simis05 were compared alongside the available time series of pigment and cell biomass data (Figure 5.15). Generally, MERIS retrieved concentrations of Chl-*a* and PC followed the interannual patterns of peaks for *in situ* Chl-*a*, phytoplankton biomass and cyanobacteria biomass. However, retrieved pigments tended to match the variability better in Keszthely (Figure 5.15 a,c,e) than in Tihany (Figure 5.15 b,d,f).

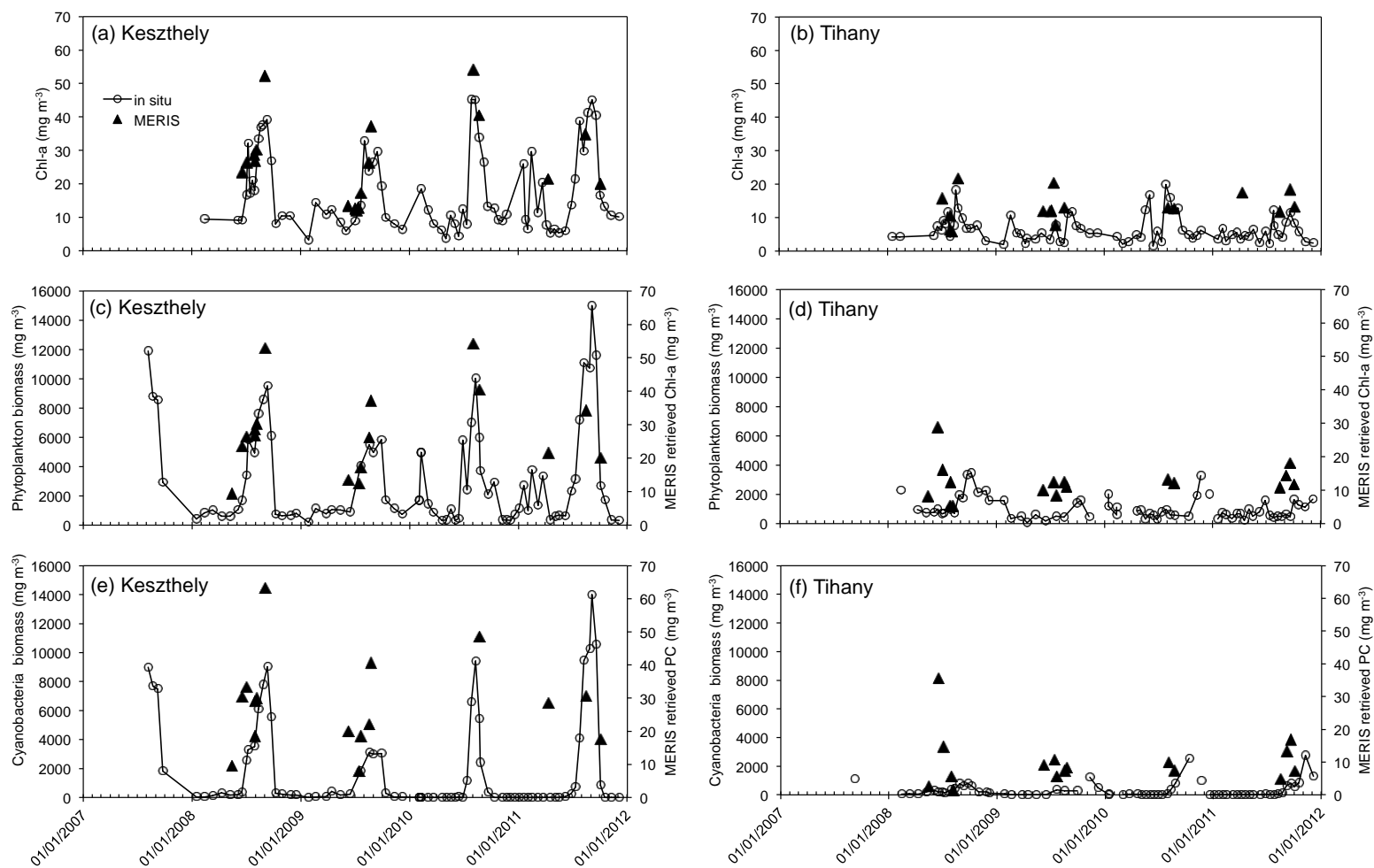


**Figure 5.15** MERIS retrieved concentrations of Chl-a (a-d) and PC (e-f) over the time series of *in situ* measurements of Chl-a (a-b), phytoplankton biomass (c-d) and cyanobacteria biomass (e-f) at Keszthely and Tihany.

**Table 5.2** Least squares linear regression results ( $y=mx+b$ ) for Chl-*a*, PC,  $a_{ph}$  and  $b_b$  using Gons05 and Simis05 algorithms for all data, including integrated and surface samples.

	Matchup interval	n	x	y	<i>B</i>	<i>m</i>	R <sup>2</sup>	p	RMSE mg m <sup>-3</sup>	RMSE <sub>log</sub>	Bias	Bias <sub>log</sub>	MAPE %
<b>PC</b>	1 day	22	Measured PC	MERIS Retrieved PC	8.95	0.722	0.710	<0.0001	11.8	0.272	3.92	0.147	77.0
	3 day	30	Measured PC	MERIS Retrieved PC	7.44	0.777	0.663	<0.0001	11.5	0.261	3.77	0.110	71.0
	7 day	40	Measured PC	MERIS Retrieved PC	9.41	0.443	0.433	<0.0001	18.1	0.269	-1.63	0.0191	61.7
	1 day	33	Cyanobacteria biomass	MERIS Retrieved PC	7.72	0.00494	0.462	<0.0001	-	-	-	-	-
	3 day	41	Cyanobacteria biomass	MERIS Retrieved PC	5.66	0.00539	0.525	<0.0001	-	-	-	-	-
	7 day	64	Cyanobacteria biomass	MERIS Retrieved PC	6.18	0.00488	0.494	<0.0001	-	-	-	-	-
<b>Chl-<i>a</i></b>	1 day	136	Measured Chl- <i>a</i>	MERIS Retrieved Chl- <i>a</i>	8.98	1.11	0.801	<0.0001	11.9	0.394	10.4	0.329	151
	3 day	156	Measured Chl- <i>a</i>	MERIS Retrieved Chl- <i>a</i>	8.53	1.11	0.803	<0.0001	11.5	0.382	9.97	0.319	143
	7 day	194	Measured Chl- <i>a</i>	MERIS Retrieved Chl- <i>a</i>	8.56	1.06	0.767	<0.0001	11.2	0.369	9.38	0.296	132
	1 day	28	Phytoplankton biomass	MERIS Retrieved Chl- <i>a</i>	6.42	0.00527	0.667	<0.0001	-	-	-	-	-
	3 day	40	Phytoplankton biomass	MERIS Retrieved Chl- <i>a</i>	6.62	0.00515	0.698	<0.0001	-	-	-	-	-
	7 day	61	Phytoplankton biomass	MERIS Retrieved Chl- <i>a</i>	7.43	0.00480	0.636	<0.0001	-	-	-	-	-

**Table 5.3** Least squares linear regression results ( $y=mx+b$ ) for Chl-*a*, PC,  $a_{ph}$  and  $b_b$  retrievals using Gons05 or Simis05 algorithms, validated with surface samples only (August 2010 only).

	Matchup interval	n	x	y	<i>b</i>	<i>m</i>	R <sup>2</sup>	p	RMSE mg m <sup>-3</sup> or m <sup>-1</sup>	RMSE <sub>log</sub>	Bias	Bias <sub>log</sub>	MAPE %
PC	1 day	14	Measured PC	MERIS Retrieved PC	-1.28	1.77	0.836	<0.0001	11.7	0.254	7.79	0.174	71.6
	3 day	22	Measured PC	MERIS Retrieved PC	-4.15	1.87	0.799	<0.0001	11.3	0.246	6.18	0.189	65.4
	7 day	28	Measured PC	MERIS Retrieved PC	-5.95	1.85	0.718	<0.0001	10.3	0.248	3.89	0.042	59.3
	1 day	14	Cyanobacteria biomass	MERIS Retrieved PC	-2.48	0.00737	0.660	<0.001	-	-	-	-	-
	3 day	22	Cyanobacteria biomass	MERIS Retrieved PC	-3.04	0.00743	0.745	<0.0001	-	-	-	-	-
	7 day	28	Cyanobacteria biomass	MERIS Retrieved PC	-3.88	0.00731	0.709	<0.0001	-	-	-	-	-
Chl- <i>a</i>	1 day	13	Measured Chl- <i>a</i>	MERIS Retrieved Chl- <i>a</i>	2.22	1.45	0.943	<0.0001	12.2	0.203	10.9	0.199	58.9
	3 day	23	Measured Chl- <i>a</i>	MERIS Retrieved Chl- <i>a</i>	2.38	1.38	0.930	<0.0001	10.2	0.198	8.71	0.189	55.9
	7 day	29	Measured Chl- <i>a</i>	MERIS Retrieved Chl- <i>a</i>	0.995	1.41	0.906	<0.0001	9.19	0.185	7.36	0.167	50
	1 day	13	Phytoplankton biomass	MERIS Retrieved Chl- <i>a</i>	3.24	0.00633	0.656	<0.001	-	-	-	-	-
	3 day	23	Phytoplankton biomass	MERIS Retrieved	3.88	0.00588	0.736	<0.0001	-	-	-	-	-

Matchup interval	n	x	y	<i>b</i>	<i>m</i>	R <sup>2</sup>	p	RMSE mg m <sup>-3</sup> or m <sup>-1</sup>	RMSE <sub>log</sub>	Bias	Bias <sub>log</sub>	MAPE %	
7 day	29	Phytoplankton biomass	Chl- <i>a</i> MERIS Retrieved Chl- <i>a</i>	2.22	0.00587	0.682	<0.0001	-	-	-	-	-	
<i>a<sub>ph</sub></i> (665)	7 day	29	Measured <i>a<sub>ph</sub></i> (665)	MERIS Retrieved <i>a<sub>ph</sub></i> (665)	0.0663	2.06	0.836	<0.0001	0.228	0.444	0.197	0.430	178
<i>a<sub>ph</sub></i> (620)	7 day	29	Measured <i>a<sub>ph</sub></i> (620)	MERIS Retrieved <i>a<sub>pc</sub></i> + <i>a<sub>Chl-a</sub></i> (620)	0.0758	3.12	0.834	<0.0001	0.279	0.645	0.242	0.635	346
<i>b<sub>b</sub></i> (λ)	7 day	29	Measured <i>b<sub>b</sub></i> (650)	MERIS Retrieved <i>b<sub>b</sub></i> (779)	0.0938	-0.0603	0.0043	0.734	-	-	-	-	-

**Table 5.4** Least squares linear regression results ( $y=mx+b$ ) for Chl-*a* and PC retrievals using Gons05 and Simis05 algorithms, respectively, validated with integrated samples only (BLI, 2007-2011).

	Matchup interval	n	x	y	<i>b</i>	<i>m</i>	R <sup>2</sup>	p	RMSE mg m <sup>-3</sup>	RMSE <sub>log</sub>	Bias	Bias <sub>log</sub>	MAPE %
PC	1 day	8	Measured PC	MERIS Retrieved PC	6.94	0.664	0.910	<0.001	12.1	0.301	-2.86	0.100	86.4
	3 day	8	Measured PC	MERIS Retrieved PC	6.94	0.664	0.910	<0.001	12.1	0.301	-2.86	0.100	86.4
	7 day	12	Measured PC	MERIS Retrieved PC	9.55	0.379	0.580	<0.01	29.5	0.324	-13.4	-0.026	71.7
	1 day	19	Cyanobacteria biomass	MERIS Retrieved PC	11.2	0.00421	0.405	<0.01	-	-	-	-	-
	3 day	19	Cyanobacteria biomass	MERIS Retrieved PC	11.2	0.00421	0.405	<0.01	-	-	-	-	-
	7 day	36	Cyanobacteria biomass	MERIS Retrieved PC	10.1	0.00430	0.474	<0.0001	-	-	-	-	-
	Chl- <i>a</i>	1 day	18	Measured Chl- <i>a</i>	MERIS Retrieved Chl- <i>a</i>	8.26	1.03	0.810	<0.0001	9.73	0.331	8.60	0.271
3 day		20	Measured Chl- <i>a</i>	MERIS Retrieved Chl- <i>a</i>	8.81	1.02	0.798	<0.0001	10.2	0.337	9.09	0.281	112
7 day		52	Measured Chl- <i>a</i>	MERIS Retrieved Chl- <i>a</i>	9.12	0.950	0.723	<0.0001	10.7	0.334	8.33	0.249	107
1 day		15	Phytoplankton biomass	MERIS Retrieved Chl- <i>a</i>	8.27	0.00438	0.692	<0.001	-	-	-	-	-
3 day		17	Phytoplankton biomass	MERIS Retrieved Chl- <i>a</i>	9.82	0.00417	0.660	<0.0001	-	-	-	-	-
7 day		37	Phytoplankton biomass	MERIS Retrieved Chl- <i>a</i>	10.3	0.00432	0.640	<0.0001	-	-	-	-	-

**Table 5.5** Least squares linear regression results ( $y=mx+b$ ) for Chl-*a* retrievals using the Gons05 algorithm, validated with KdKVI surface samples only (2007-2011).

	<b>Matchup interval</b>	<b>n</b>	<b>x</b>	<b>y</b>	<b><i>b</i></b>	<b><i>m</i></b>	<b>R<sup>2</sup></b>	<b>p</b>	<b>RMSE mg m<sup>-3</sup></b>	<b>RMSE<sub>log</sub></b>	<b>Bias</b>	<b>Bias<sub>log</sub></b>	<b>MAPE %</b>
Chl- <i>a</i>	1 day	105	Measured Chl- <i>a</i>	MERIS Retrieved Chl- <i>a</i>	9.52	1.09	0.784	<0.0001	12.22	0.421	10.6	0.355	169
	3 day	113	Measured Chl- <i>a</i>	MERIS Retrieved Chl- <i>a</i>	9.27	1.09	0.786	<0.0001	12.0	0.416	10.4	0.352	165
	7 day	113	Measured Chl- <i>a</i>	MERIS Retrieved Chl- <i>a</i>	9.27	1.09	0.786	<0.0001	12.0	0.416	10.4	0.352	165

## 5.4 Discussion

### 5.4.1 Algorithm performance for pigment retrievals at 1 day matchups

The Gons05 and Simis05 algorithms retrieved pigment concentrations (Chl-*a* and PC, respectively) in Lake Balaton with high accuracy (see Table 5.2 to Table 5.5 for a summary of retrieval parameters and errors). Chl-*a* concentrations were retrieved from MERIS using  $\pm 1$  day matchups with high accuracy ( $R^2=0.801$ ,  $p<0.0001$ ; RMSE=11.9 mg m<sup>-3</sup>). PC concentrations were also retrieved with high accuracy from MERIS with a  $\pm 1$  day temporal window ( $R^2=0.710$ ,  $p<0.0001$ ; RMSE=11.8 mg m<sup>-3</sup>). With same day matchups as the golden standard, this study can attest to the good performance of Gons05 and Simis05 algorithms for pigment retrievals in Lake Balaton.

We compared three models for PC retrieval from MERIS data in Lake Balaton, and of these Simis05 provided the most accurate retrievals. While a stronger linear relationship was found between MERIS retrieved and *in situ* PC using Li15, this model significantly underestimated PC values  $<10$  mg m<sup>-3</sup> and over-estimated for concentrations  $\sim 10$ -100 mg m<sup>-3</sup>. The Li15 model was developed using three reservoirs in Indiana (Eagle Creek, Geist and Morse Reservoirs), where PC concentrations ranged from 0.73-370 mg m<sup>-3</sup>, while the PC validation dataset for Lake Balaton varied over a narrower range (2.34-113 mg m<sup>-3</sup>). However, the discrepancy in performance using Li15 is more likely related to the high concentration of inorganic particles in Lake Balaton (in August 2010, 3-30 mg L<sup>-1</sup> and comprising up to 91% of the TSM), therefore the model coefficients developed for the reservoirs may not be appropriate in Lake Balaton. Although TSM concentrations were relatively similar between the Indiana reservoirs and Lake Balaton, we are unaware as to what fraction of the TSM in the Indiana reservoirs was comprised of organic or inorganic particles and cannot therefore compare. In contrast, PC retrievals from the Mishra13 algorithm had no significant relationship with *in situ* PC, although agreement with *in situ* PC improved greatly for lower PC concentrations ( $<50$  mg m<sup>-3</sup>). This is unexpected as Mishra13 was developed using a training set from hypereutrophic aquaculture ponds (Chl-*a* = 59.4-1376.6 mg m<sup>-3</sup>; PC = 68.1-3032.5 mg m<sup>-3</sup>). Both the Mishra13 and Li15 inversion algorithms were also developed using *in situ* reflectance measurements, and recommended different methods for conversion of above surface to below surface  $R_{rs}(\lambda)$ . Ultimately, the Simis05 algorithm was found to outperform these more complex inversion algorithms

over the range of PC concentrations found in Lake Balaton. Although there were also differences in the water chemistry and optical properties of the lakes used to calibrate Simis05, Lake Loosdrecht and Lake IJsselmeer are noted to have generally high absorption by non-algal particles (up to 50% of water constituents), not unlike Lake Balaton (up to 40%) [see Chapter 3 (Riddick et al., 2015)].

#### **5.4.2 Ability to retrieve biomass using Simis05 and Gons05**

The estimated PC and Chl-*a* concentrations from MERIS were also partially-validated using microscopy-based estimates of cyanobacteria and total phytoplankton biomass, respectively. PC and Chl-*a* retrievals with Gons05 and Simis05 did predict cell biomass with good accuracy, with ( $R^2 > 0.4$ ,  $p < 0.01$ ) with surface and/or integrated samples for  $\pm 1$ , 3 and 7 day temporal windows (Table 5.2, Table 5.3 and Table 5.4). The coefficients of determination were lower for the linear regressions between retrieved pigments and cell biomass ( $R^2 = 0.462-0.698$ ,  $p < 0.0001$ ) in contrast to measured pigments ( $R^2 = 0.433-0.803$ ,  $p < 0.0001$ ), when using the complete dataset for validation (Table 5.2). This was expected due to the variability in PC cell quotas among freshwater cyanobacteria taxa. The exception to this was for the  $\pm 7$  day PC matchups, where MERIS retrieved PC was explained marginally better by cyanobacteria biomass ( $R^2 = 0.494$ ,  $p < 0.0001$ ) than by measured PC ( $R^2 = 0.433$ ,  $p < 0.0001$ ).

It is particularly useful to retrieve cyanobacteria counts in the case that PC data is unavailable, but an archive of cyanobacteria biomass data exists. A previous study has demonstrated that phycocyanin concentrations have a strong linear relationship to cyanobacteria biomass in field samples from Lake Balaton ( $R^2 = 0.94$ ,  $CV = 1.7\%$ ) (Horváth et al., 2013a). Although, this may not be the case in other lakes, where intracellular PC content in cyanobacteria can vary in response to environmental stressors, such as nitrogen limitation or increased irradiance (photoacclimation). Recently, cell counts were successfully retrieved from numerous lakes in the eastern US, with a significant positive correlation between MERIS retrieved and *in situ* cyanobacteria cell counts for matchups within 7 days of MERIS overpass (Lunetta et al., 2015). Although both Lunetta et al. (2015) and the present study found significant scatter around this relationship, both studies confirm the capability of remote sensing for monitoring cyanobacteria cell counts in lakes.

Additionally, there was little variation in accuracy at the three matchup ranges when validating with cell counts, with no apparent degradation in PC or Chl-*a* retrieval capability within  $\pm 7$  days of image acquisition. It was noted, however, that the relationship between retrieved Chl-*a* and phytoplankton biomass was better than that for retrieved PC and cyanobacterial biomass. This is perhaps because PC may be more spatially variable within a pixel. Although in its time MERIS provided the best available resolution for satellite application to lakes, the pixel size (300 m) is still quite large given that cyanobacteria blooms can vary markedly over a few metres or hours (Hunter et al., 2008a). Therefore it is likely the time difference between *in situ* samples and MERIS overpass causes this discrepancy.

#### 5.4.3 Temporal windows for satellite validation

There was a notable impact on retrieval accuracy depending on the temporal window for validation matchups. When the complete *in situ* pigment dataset is considered, Chl-*a* retrievals deteriorated only slightly over the  $\pm 1$  to 7 day windows, with no noticeable difference at  $\pm 3$  days, and slightly lower  $R^2$  at  $\pm 7$  days.  $R^2$  values ranged from 0.767-0.801 ( $p < 0.0001$ ) and the RMSE ranged from 11.2-11.9 mg m<sup>-3</sup> for the three temporal windows, confirming the Gons05 algorithm can retrieve Chl-*a* concentrations in Lake Balaton within 7 days of MERIS overpass. When considering the KdKVI surface Chl-*a* dataset only, there was no notable decrease in retrieval accuracy (Table 5.5). This is simply due to the consistently large sample size for the KdKVI validation dataset, which varied little with increasing temporal windows ( $n=105$ , 113 and 113 for  $\pm 1$ , 3 and 7 days, respectively). In contrast, PC concentrations were retrieved at a matchup interval of  $\pm 7$  days with notably poorer agreement than same day matchups. Use of *in situ* Chl-*a* data collected within 1 day of the MERIS image yielded the best  $R^2$  of 0.710 ( $p < 0.0001$ ), while using data within 7 days of the image resulted in a  $R^2$  of 0.433 ( $p < 0.0001$ ) and the highest RMSE (18.3 mg m<sup>-3</sup>) (Table 5.2).

The difference in ability to retrieve Chl-*a* and PC at larger temporal windows may be twofold. First, simply the number of samples for Chl-*a* which matched to the satellite images is greater than the number of samples for *in situ* PC measurement, with  $n=136-194$  and  $n=22-40$  for Chl-*a* and PC, respectively (Table 5.2). It may be that further *in situ* PC data are required to obtain better validation with MERIS retrieved PC at a  $\pm 7$  day interval. Secondly, PC is mostly representative of cyanobacteria in Lake

Balaton, while Chl-*a* is a proxy for general phytoplankton abundance. It is well known that cyanobacteria form surface scums and migrate vertically in the water column, therefore these ephemeral spatial dynamics may not be captured by satellite remote sensing if the *in situ* sample is temporally distant from the time of image capture (Hunter et al., 2008a). This is likely to be the most important factor affecting PC retrievals, particularly when the time of data acquisition by the satellite is several days apart from the time of *in situ* data collection. For example, *Cylindrospermopsis raciborskii* typically form subsurface maxima or are found dispersed throughout the water column, rather than as a surface bloom (Fabbro & Duivenvoorden, 1996, Saker & Griffiths, 2001, Falconer, 2001, Everson et al., 2009, Antunes et al., 2015). Given that *C. raciborskii* commonly formed the majority of the phytoplankton community in Lake Balaton during August 2010 (which comprises 70% of the PC dataset), and given that the August 2010 field work was conducted during high solar irradiance, it is possible that the PC surface samples may not accurately represent the cyanobacteria present in the entire water column or alternatively, the subsurface population had less influence on the water-leaving radiative signal.

#### 5.4.4 Impact of dataset used and sampling methods

MERIS retrieved Chl-*a* from the Gons05 algorithm validated with the August 2010 surface samples only had the highest accuracy, with the highest  $R^2$  (0.943,  $p < 0.0001$ ) for  $\pm 1$  day matchups (Table 5.3). These Chl-*a* samples were intentionally collected at the surface during the 2010 field campaign for the purpose of satellite validation, and it is therefore unsurprising that these data align well with MERIS retrieved Chl-*a*. As signal penetration in turbid lakes can be very limited, it is expected that surface samples would be more comparable with satellite retrievals. However, PC was retrieved with the highest accuracy within  $\pm 1$  day when validated with integrated samples from BLI only ( $R^2 = 0.910$ ,  $p < 0.001$ ; Table 5.4), although this is based on a small sample size ( $n = 8$ ) and the error is higher (RMSE = 12.1 mg m<sup>-3</sup>, MAPE = 86.4%) than that for retrievals validated with surface samples only (RMSE = 11.7 mg m<sup>-3</sup>, MAPE = 71.6%).

#### 5.4.5 Sources of error in the retrieval of (S)IOPs

In the case of both Chl-*a* and PC pigment retrievals, concentrations were over-estimated by the models, and this is most notable for Chl-*a* retrievals. This can be explained, in part, due to the application of constant  $a^*_{ph}(665)$  and  $a^*_{pc}(620)$

coefficients for calculating Chl-*a* and PC concentrations, respectively. These coefficients are taken from previous studies (Gons et al., 2005, Simis et al., 2007) and may not be representative of the phytoplankton community in Lake Balaton during the period of analysis, which was often dominated by the subtropical cyanobacterium *C. raciborskii*. The specific absorption coefficient (or absorption efficiency) may also vary across the lake or between phytoplankton communities due to differences in pigmentation, physiology, cell size and pigment packaging effects (Bricaud et al., 1995). The mean measured  $a_{ph}^{*}(665)$  during August 2010 in Lake Balaton was  $0.0075 \text{ m}^2 \text{ mg}^{-1} \text{ Chl-}a$  ( $\pm 0.0015$ ), while Gons et al. (2005) employed a higher value of  $0.0139 \text{ m}^2 \text{ mg}^{-1} \text{ Chl-}a$ . If the lower  $a_{ph}^{*}(665)$  measured for Lake Balaton was used in the Gons05 algorithm to retrieve Chl-*a*, retrieved values of Chl-*a* would actually be overestimated and poorer representations of *in situ* Chl-*a*. Subsequent studies have also investigated measurement of  $a_{pc}^{*}(620)$  in laboratory algal cultures using a timed bleaching procedure, although this method was deemed unsuitable for mixed phytoplankton communities and thus it was not employed in this study (Simis & Kauko, 2012). More recently,  $a_{pc}^{*}(625)$  was estimated by subtracting the effect of chlorophylls at 625 nm, and  $a_{pc}^{*}(625)$  was found to vary widely for low PC concentrations ( $<10 \text{ mg m}^{-3}$ ) (Yacobi et al., 2015). The phycocyanin specific absorption coefficient published in Simis and Kauko (2012) was  $a_{pc}^{*}(622)=0.0071 \text{ m}^2 \text{ mg}^{-1} \text{ PC}$  and the range recommended by Yacobi et al. (2015) was  $a_{pc}^{*}(625)=0.007-0.008 \text{ m}^2 \text{ mg}^{-1}$ , which both agree with the value of  $0.007 \text{ m}^2 \text{ mg}^{-1}$  recommended in Simis et al. (2005, 2007) and which was adopted in this study. However, given the lower value of  $a_{ph}^{*}(665)$  measured in Lake Balaton, it is plausible that the published data for  $a_{pc}^{*}(620)$  may also misrepresent the phytoplankton community in Lake Balaton.

The error in the Gons05 and Simis05 algorithms is further illuminated by the retrieval of the phytoplankton absorption coefficients.  $a_{ph}(665)$  was over-estimated compared to the measured values from the August 2010 sampling campaign (Figure 5.13). However, because the standard algorithm uses a higher  $a_{ph}^{*}(665)$  coefficient than that measured in Lake Balaton, the errors effectively cancel out resulting in relatively good agreement between the measured and MERIS retrieved Chl-*a* concentrations. The  $a_{ph}^{*}(665)$  coefficient measured for the August 2010 dataset was lower ( $0.0075 \text{ m}^2 \text{ mg}^{-1}$ ), and substituting this into Gons05 actually results in greater errors, with Chl-*a* overestimated by a factor of 1.9 for matchups  $\pm 7$  days ( $R^2=0.730$ ,  $p<0.001$ ,  $\text{RMSE}_{\log}=0.621$ ,  $\text{Bias}_{\log}=0.579$ ,  $\text{MAPE}=347\%$ ; Compare with results in Table

5.2). In fact, for the August 2010 dataset only, substitution of the Balaton  $a^*_{ph}(665)$  results in an even greater over-estimate by a factor of 2.5. This suggests the errors within the application of the Simis05 algorithm to Lake Balaton lie within the estimate of the IOPs [ $a_{ph}(\lambda)$  and  $b_b(\lambda)$ ] rather than the SIOPs [ $a^*_{ph}(\lambda)$ ].

The  $b_b(\lambda)$  coefficient was estimated by the Simis05 algorithm at MERIS band 12, or 778.75 nm, as in Gons et al.(1999). During the August 2010 campaign backscattering was measured by an ECO-BB3, which does not measure explicitly at this wavelength (779 nm), however it is useful to examine the assumptions that are also employed in the Simis05 semi-analytical algorithm. From the *in situ* measurements, it was found that there was little difference in  $b_b(\lambda)$  across the 3 wavelengths measured (Figure 5.14a). It is therefore a valid assumption that backscattering is spectrally neutral across all wavelengths (Gons, 1999). However, it was also shown that there is no significant linear relationship ( $R^2=0.000446$ ,  $p=0.913$ ) between  $b_b(\lambda)$  measured *in situ* and that estimated with Simis05 (Figure 5.14b). Although the *in situ* backscattering coefficient is measured at a different wavelength, it is reasonable to expect to see a relationship between retrieved and measured  $b_b(\lambda)$ . As this is not the case, the  $b_b(\lambda)$  estimation by the Gons05 and Simis05 algorithms is a potential source of error to PC retrievals. Additionally, he measured particulate  $b_b(532)$  in Lake Balaton during August 2010 varied over a wide range from 0.06-0.34  $m^{-1}$ , with a high mean ratio of backscattering to total suspended matter ( $b_b(532):TSM = 0.016$ ). This was mainly due to the high percentage (~40-90%) of inorganic mineral sediments that were frequently resuspended in Lake Balaton (Chapter 4). The unique biogeochemical composition and distinctive optical properties in Lake Balaton may then explain why the backscattering coefficient is not estimated well by the Gons05 and Simis05 algorithms.

When measured  $b_b(650)$  is substituted into the Gons05 algorithm for each station in the August 2010 dataset, Chl-*a* is over-estimated by a factor of 2.8 for a  $\pm 7$  day matchup window ( $R^2=0.883$ ,  $p<0.0001$ ,  $RMSE_{log}=0.376$ ,  $Bias_{log}=-0.341$ ,  $MAPE=133\%$ ). Thus, as with substitution of  $a^*_{ph}(665)$ , applying the measured  $b_b(650)$  actually results in higher errors than Chl-*a* retrievals using estimated  $b_b$  at MERIS band 12 and does not improve the algorithm (see Table 5.3). In the case that  $b_b(\lambda)$  was measured at the same wavelength as MERIS band 12 (779 nm), the Chl-*a* retrievals would perhaps be more precisely compared. However, adjustment of the  $b_b(\lambda)$  coefficient does not seem to appreciably alter the Chl-*a* retrievals from Gons05, or at least not as significantly as with the modification of  $a^*_{ph}(665)$ .

#### 5.4.6 Applicability of algorithms

There was a distinct lower limit for MERIS retrieval of pigments (Figure 5.7; Figure 5.8 Figure 5.9; Figure 5.10; Figure 5.11). This is perhaps most noticeable on the PC plots, and especially in the figures for  $\pm 7$  day matchups. This may suggest differences in the water sampling methods, where the routine monitoring data for Chl-*a* is derived from to depth-integrated samples but the August 2010 Chl-*a* data were determined from surface samples. The effect is a much higher accuracy for the August 2010 samples as opposed to the routine monitoring (Figure 5.7). Additionally, the euphotic depth ( $Z_{eu}$ ) in Lake Balaton in August 2010 was typically less than 1.7 m. Thus, it not surprising that the water-leaving reflectance signal measured by MERIS shows stronger agreement with surface rather than depth-integrated samples.

Quite possibly this minimum in retrieved pigments is due to limitations of MERIS itself or the Gons05 and Simis05 algorithms. The pigment retrievals from Gons05 and Simis05 fit in with the interannual patterns of *in situ* Chl-*a*, phytoplankton biomass and cyanobacteria biomass (Figure 5.15). However, it was noted that the most accurate retrievals were in the western basin, where Chl-*a* is generally higher ( $<60 \text{ mg m}^{-3}$ ), than in the east of Lake Balaton (Tihany), where Chl-*a* levels are predominantly lower ( $<20 \text{ mg m}^{-3}$ ). The Gons05 algorithm may therefore not be appropriate for Chl-*a* retrieval in waters with low phytoplankton biomass (e.g. where Chl-*a*  $<10 \text{ mg m}^{-3}$ ). This is further supported by the poor accuracy and high scatter for retrievals when Chl-*a* is low (Figure 5.7). Gons et al. (2008) found that MERIS retrieved Chl-*a* values were poorly predicted by Gons05 at Chl-*a*  $<5 \text{ mg m}^{-3}$  in oligotrophic lakes, which was attributed to weak emerging light flux, masking of the red Chl-*a* absorption peak by absorption of water, and an increased influence of Chl-*a* fluorescence that is not taken into account by the algorithm. To address this issue, Domínguez Gómez et al. (2011) applied a different version of the Normalised Difference Chlorophyll Index (NDCI) for values of Chl-*a* greater or less than a threshold of  $17 \text{ mg m}^{-3}$ , as water-leaving reflectance is very low for Chl-*a*  $<17 \text{ mg m}^{-3}$ . This is further corroborated by a recent study, where the fluorescence line height (FLH) algorithm retrieved Chl-*a* from MERIS most accurately at higher Chl-*a* concentrations (Palmer et al., 2015c). It is therefore possible that Gons05 and Simis05 algorithms have limited applicability. These algorithms were designed for and perform optimally in eutrophic lakes as opposed to mesotrophic or oligotrophic waters, and are insensitive to changes in Chl-*a* below  $10 \text{ mg m}^{-3}$ . In addition, PC retrieval with Simis05 may also be limited by interference of

chlorophyll-b, particularly when cyanobacteria biomass is low and the community is dominated by other eukaryotic phytoplankton groups, which may be a factor in the overestimation of PC when Chl-*a* is low. It may be that the Simis05 and Gons05 algorithms are better considered as part of an ensemble approach, as a single algorithm is unlikely to work in all conditions, even within a single lake system.

## 5.5 Conclusions

With the recent launch of ESA's Sentinel-3 Ocean and Land Colour Instrument (OLCI), it is a crucial time to explore the historic archive of data from satellite instruments, such as MERIS, to investigate and improve retrievals of inland water quality. In recent years, there has been vast improvement to both the availability of ESA instrument data (with the MERCI system) and the tools for data analysis (e.g. Beam), and this has allowed for corresponding advances in the remote sensing of inland waters. There have also been developments in the atmospheric correction of MERIS data, including this study as the first instance of implementing SCAPE-M\_B2 for the correction of MERIS FRS data. Field data and research on the optical properties of water and the development of bio-optical models has also been furthered with the accessibility of and tools available for MERIS data.

Specific to this study, the Simis05 and Gons05 semi-analytical algorithms performed well to retrieve PC and Chl-*a* pigment concentrations in Lake Balaton, respectively. Phytoplankton and cyanobacteria biomass were also retrieved, albeit to a lesser degree of accuracy, demonstrating a critical step towards the monitoring of medium-term changes in cyanobacteria abundance in lakes. While accuracy for Chl-*a* retrieval was fairly consistent within  $\pm 7$  days of the MERIS overpass, PC retrievals deteriorated with increased time between the image acquisition and ground sampling. It is therefore imperative that samples for phycocyanin analysis are collected as temporally close as possible to the date and time of the MERIS overpass. Additionally, the retrievals from Gons05 and Simi05 algorithms matched the interannual patterns in Chl-*a* and biomass, although *in situ* data were better predicted in the more eutrophic western basin than the meso- to oligotrophic eastern basin of Lake Balaton. Although Gons05 and Simis05 perform well in Lake Balaton, the IOP measurements enabled this study to address the sources of error in estimates of  $a_{ph}(\lambda)$  and  $b_b(\lambda)$ . Estimated  $b_b(\lambda)$  was found to be unrelated to measured  $b_b(\lambda)$ , while  $a_{ph}$  at 665 and 620 nm was overestimated by the algorithms, then subsequently overcorrected by using a higher

$a^*_{ph}(665)$  than measured in Lake Balaton. While substituting Balaton specific IOPs into the algorithms did not improve Chl-*a* retrievals, knowledge of the IOPs did elucidate the sources of error within the Gons05 and Simis05 algorithms.

This study provides additional evidence for the success of Chl-*a* and PC retrieval algorithms using MERIS data in an emblematic European lake, with a view to facing new challenges for remote sensing of inland waters with the recently launched OLCI at match-up timescales of up to 7 days. Furthermore, this study proves the effectiveness of collecting IOP measurements alongside pigment and satellite data, in order to analyse the performance of pigment retrieval algorithms and the ability to tune a semi-analytical algorithm to the waterbody of interest. In this way, future work can generate more informed decisions on the parameterisation of models (e.g. via optical classification) in order to improve pigment retrievals and achieve model transferability among inland waters. There remains abundant opportunity for future work on the success of water quality algorithms for MERIS (and OLCI), and the ability to accurately retrieve parameters in a range of inland waters within the constraints (i.e. spatial and spectral resolution) of contemporary satellite instruments.

## 6 Multiscale remote sensing observations of water quality in a large, turbid shallow lake

---

### 6.1 Introduction

Phytoplankton blooms, often dominated by nuisance cyanobacteria, plague inland waters across the world. Blooms of potentially-toxic cyanobacteria can have an adverse impact on water quality, and it is suggested that warmer climates are increasing the dominance of cyanobacteria, especially in shallow lakes (Kosten, 2012). Harmful algal blooms can form surface scums with unpleasant odours, generate anoxic conditions in the water column and pose a risk to human health due to the production of toxins (Codd et al., 2005a). However, traditional methods for the detection of phytoplankton blooms are costly and do not provide the spatial information necessary to adequately capture the heterogeneity of phytoplankton populations.

Remote sensing has been widely applied for the monitoring of phytoplankton in oceans, with more recent progress in developing remote sensing for coastal and inland waters. Chlorophyll-*a* (Chl-*a*) is a commonly retrieved pigment from remotely sensed data in order to quantify total phytoplankton biomass in freshwaters (Mittenzwey et al., 1992, Gons, 1999, Schalles & Yacobi, 2000, George & Malthus, 2001, Gons et al., 2002, Dall'Olmo et al., 2003, Kutser, 2004, Gons et al., 2005, Gitelson et al., 2008, Hunter et al., 2008a, Gilerson et al., 2010, Hunter et al., 2010, Campbell et al., 2011, Duan et al., 2012). More recently, the accessory pigment phycocyanin (PC) has been successfully retrieved across a range of inland waters as a bio-marker for cyanobacteria (Dekker, 1993, Schalles & Yacobi, 2000, Vincent et al., 2004, Simis et al., 2005, Kutser et al., 2006, Randolph et al., 2008, Ruiz-Verdu et al., 2008, Hunter et al., 2008a, Hunter et al., 2008b, Hunter et al., 2010, Le et al., 2011, Duan et al., 2012, Li et al., 2012, Song et al., 2013, Riddick et al., in review). The retrieval of phytoplankton pigments can map the distribution of potentially toxic algal blooms, highlighting the potential of remote sensing as a real-time monitoring tool.

Lake observation by remote sensing can be conducted using a variety of different platforms, including satellite, airborne and *in situ* methods. Sensors on satellite platforms have accurately retrieved Chl-*a* over larger inland waters using ocean colour sensors, including SeaWiFS [e.g. (Vos et al., 2003)], Moderate resolution Imaging Spectroradiometer (MODIS) [e.g. (Wu et al., 2009)] and Medium Resolution

Imaging Spectrometer (MERIS) [e.g. (Giardino et al., 2005, Odermatt et al., 2008, Palmer et al., 2015c)]. However, the spatial resolution of ocean colour instruments is often too coarse (>300 m) and are often not appropriate or unable to capture the marked heterogeneity within inland waters. This is particularly acute for inland waters, where the combination of cyanobacteria buoyancy regulation and local climatic and hydrological conditions can lead to patchy distribution and the accumulation of surface scums (Hunter et al., 2008a). Alternatively, satellite instruments developed for terrestrial applications (e.g. Landsat) have been used to retrieve Chl-*a* concentrations in lakes [e.g. (Tyler et al., 2006, Duan et al., 2007, Tebbs et al., 2013)], however these sensors often have insufficient spectral and radiometric resolution for accurate retrieval of phytoplankton pigments. With the exception of MERIS and MODIS, most satellite sensors also do not measure over a large spectral region between 555 and 670 nm, which does not cover the PC absorption peak at ~620 nm (Mouw et al., 2015). Few instruments are available with a frequent revisit time in order to capture the ephemeral dynamics of phytoplankton populations in lakes. Furthermore, even instruments with high signal-to-noise (SNR) ratios tend to saturate over highly turbid waters (Mouw et al., 2015).

However, it is worth noting that there is an increasing availability of sensors with improved specifications for inland water remote sensing. For instance, the very recently launched Sentinel satellites have improved spatial (MCI onboard Sentinel-2) and spectral resolutions (OLCI onboard Sentinel-3), and together are anticipated to provide a useful tool for monitoring phytoplankton in inland waters. Other forthcoming missions, e.g. the Ocean Ecosystem Spectrometer/Radiometer onboard the Pre-Aerosols Clouds and ocean Ecosystems mission (PACE), the HyperSpectral Imager (HSI) onboard the Environmental Mapping and Analysis Program (EnMAP) and the VSWIR Imaging Spectrometer onboard the Hyperspectral Infrared Imager (HyspIRI), will provide marked improvements in spectral resolution for satellite based instruments, offering new opportunities for data inversion and potentially more accurate retrievals of phytoplankton pigment concentrations. Nonetheless, a gap remains between the capability and requirements of present satellite technology, and this has been widely acknowledged in recent literature as a major challenge to the remote sensing of inland waters (Mouw et al., 2015, Palmer et al., 2015b).

The capability of airborne remote sensing for the detection and study of phytoplankton blooms was first demonstrated by Wrigley and Horne (1974). Since

then, various studies have used airborne remote sensing to capture a high quality image over a short period of time for the detection and quantification of blooms. Airborne platforms allow for high spatial resolution data acquisition with flights directed over the water body of interest to achieve a desired pixel size. They additionally provide improved spectral and sometimes radiometric resolution over satellites or handheld sensors, particularly with modern hyperspectral instruments. The spectral range and band positions of airborne sensors can also normally be adjusted to suit the intended application (Matthews, 2011). Satellite based sensors have relatively fixed overpass times, which may not be sufficient to record the daily variations in phytoplankton distribution (e.g. diel vertical migrations). In contrast, airborne sensors can offer a flexible timescale for deployment to capture these dynamics. A few recent studies have successfully used airborne remote sensing to detect and quantify phytoplankton blooms in inland waters (Randolph et al., 2008, Hunter et al., 2008a, Hunter et al., 2010, Kudela et al., 2015), however the availability of these sensors is still rather limited. Airborne campaigns are also relatively expensive and therefore generally unsuitable for the collection of routine monitoring data. Most recently, airborne remote sensing has provided the capability of distinguishing cyanobacteria species in Lake Pinto, which may be a significant step towards early warning of toxic bloom-forming species (Kudela et al., 2015). Airborne studies like these can provide datasets with higher spatial resolution, which can be used to simulate the spectral and spatial capabilities of satellite sensors. As hyperspectral satellite missions are planned for the near future (e.g. HypSIRI and EnMAP), airborne campaigns provide a timely tool for testing the utility of high spatial resolution datasets alongside lower resolution satellite datasets.

*In situ* reflectance measurements can be used for testing of retrieval algorithms, however these are generally collected as point samples or transects. Studies have used systems including the ASD Field Spectroradiometer (Simis et al., 2007), PR-650 SpectraColorimeter (Gons et al., 2002) and TriOS-RAMSES radiometers (Ruddick et al., 2006). *in situ* sensors have value for calibration and validation purposes, especially ship- or buoy-mounted systems, as well as for deriving empirical algorithms e.g. (Gitelson et al., 1993b). However, point or transect measurements may not capture the patchiness of phytoplankton blooms in lakes.

Thus, with the increasing number of sensors available on satellite, airborne and *in situ* platforms, there is firstly a need to quantify the errors on pigment retrievals at a range of spatial resolutions in order to thoroughly understand the uncertainty in

satellite-retrieved parameters from inland waters. Secondly, there is a need to make synergistic use of instruments with differing capabilities, as the complementary spectral, spatial, radiometric and temporal resolutions could provide a more holistic approach for the monitoring of inland water quality.

Increasingly, multiscale and multisensor remote sensing approaches have been used for lakes, whether for cross-comparison of sensor performance or to increase the temporal coverage of a site. One of the first multiplatform studies was conducted on Lakes IJssel and Marken by Vos et al. (2003), which emphasised the importance of synoptic datasets at high sampling frequency for reliable water quality monitoring. Two airborne sensors (CASI-2 and AISA Eagle) were used by Hunter et al. (2010) to provide two seasons of hyperspectral data over Loch Leven in order to test retrieval algorithms for cyanobacteria pigments. Olmanson et al. (2011) evaluated Landsat, MERIS, MODIS and SeaWiFS satellite data for the ability to retrieve Secchi depth and Chl-*a* concentrations over Minnesota lakes. MERIS and QuickBird satellite data together were also previously used on Lake Champlain to provide information on the abundance and distribution of potentially toxic cyanobacteria (Wheeler et al., 2012). More recently, Torbick and Corbiere (2015) conducted a comparative study of the Landsat 8 Operational Land Imager (OLI), Proba Compact High Resolution Imaging Spectrometer (CHRIS) and RapidEye data for the detection of cyanobacteria blooms in Lake Champlain. However, of these studies, only Wheeler et al. (2012) investigated the ability of a satellite sensor to map the spatial heterogeneity of phytoplankton biomass. Wheeler et al. (2012) concluded that MERIS (300 m) and Quickbird (2.4 m) were both able to sufficiently distinguish the spatial structure of a cyanobacteria bloom, although no metrics to prove this conclusion were provided other than the mapped Chl-*a* and PC concentrations.

The present study aims to provide a case study of remote sensing at varying spatial scales for the detection of phytoplankton blooms over a large and optically-complex shallow lake, Lake Balaton, Hungary. Specifically, this study examines the use of multiple sensors on multiple platforms (satellite, airborne and *in situ*) and their ability to accurately capture spatial patterns in phytoplankton biomass. This is accomplished using a novel combination of two coincident satellite datasets [Landsat 5 Thematic Mapper (Landsat 5 TM) and MERIS], airborne hyperspectral imagery [Airborne Imaging Spectroradiometer for Applications (AISA) Eagle] and *in situ* radiometry [Hyperspectral Surface Acquisition System (HyperSAS)]. The multisensor

approach has been previously used to extend satellite time series (e.g. MERIS, MODIS and SeaWiFS), and Tyler et al. (2016) have recently identified that new and forthcoming satellites have the potential to provide synergistic multi-scale operational observations. Therefore this study is well placed to provide insight for future satellite observations of phytoplankton distribution in lakes. This study compares the performance of the Normalised Difference Chlorophyll Index (NDCI) approach for Chl-*a* retrieval at a range of spatial resolutions, and conducts a cross-comparison of Chl-*a* retrieval performance using four coincident spectral datasets. The *in situ* measured reflectances further allow for validation of the atmospheric corrections used for each remote sensing dataset. Finally, the finer resolution datasets (AISA Eagle and Landsat 5 TM) are resampled to a coarser spatial resolution akin to MERIS (300 m) in order to quantify the errors over the degradation in spatial resolution. This study has clear implications for the very recently launched Ocean and Land Colour Instrument (OLCI) onboard the Sentinel-3 satellite, which measures the same spectral bands and operates at the same spatial resolution as MERIS.

## **6.2 Methods**

### **6.2.1 Study area – Lake Balaton**

As the largest shallow lake in Central Europe, Lake Balaton (46.8°N, 17.7°E) has great socio-economic importance to the Transdanubian region of Hungary. Lake Balaton has a surface area of 592 km<sup>2</sup> and mean depth of just 3.2m, with a catchment dominated by the Zala River in the west. This riverine input provides approximately one third to half of the total external nutrient load to the lake (Szilagyi et al., 1990). The mineral-rich sediments (dolomite limestone) are frequently resuspended in the water column, giving Lake Balaton its unique milky blue appearance.

The study site also includes the Kis-Balaton wetland area adjacent to the western shore of Lake Balaton, which is comprised of an upper and lower reservoir. The Kis-Balaton Water Protection System was engineered in the 1980s-1990s in order to promote retention of phosphorus and nitrogen for eutrophication management (Pomogyi, 1993). Due to the range of hydro-morphology and function of the water bodies, there is significant variability in the water quality within Kis-Balaton (Horváth et al., 2013b). Therefore it is useful to include Kis-Balaton in a multi-scale study to

observe the ability of different platforms to adequately characterise the heterogeneity within this system as well as the lake itself.

Lake Balaton has frequent algal blooms with significant cyanobacteria populations. In recent years, cyanobacteria may comprise over 90% of the total phytoplankton biomass in western basins of the lake during a late summer bloom. Of these cyanobacteria blooms, nitrogen-fixing types often form the majority or even entirety of the bloom, including *Cylindrospermopsis raciborskii*, *Aphanizomenon* sp. and *Anabaena* sp. The lake also generally maintains a longitudinal gradient in phytoplankton biomass, with the highest concentrations in the westerly basins and decreasing to the northeastern basin. Additionally, the lake has a documented gradient in coloured dissolved organic matter (CDOM), with the highest concentrations in the west near the Zala River input (Balogh et al., 2003). It is this gradient in biogeochemical parameters and thus inherent optical properties (IOPs), which provides an interesting study site for remote sensing applications (Riddick et al., 2015).

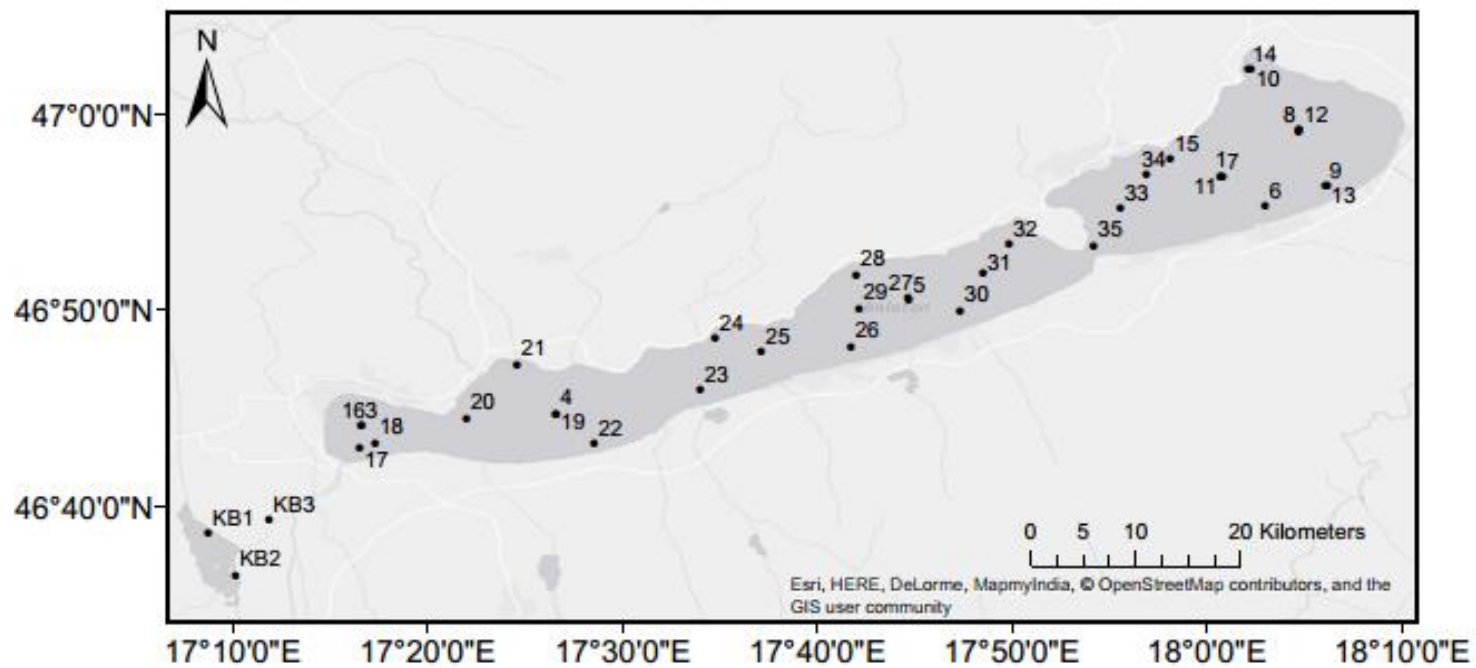


**Figure 6.1** Map of Lake Balaton, indicating the 38 sampling stations.

### **6.2.2 Water sampling**

Field measurements were collected in Lake Balaton and Kis-Balaton from 17-26 August 2010 at 38 stations (Figure 6.1). The ground campaign by boat collected *in situ* radiometric measurements and surface water samples, concurrent to the collection of airborne radiometric data. Surface water samples at each station were divided into aliquots for subsequent filtration or preservation.

### **6.2.3 Chlorophyll-*a* pigment analysis**

Subsamples for pigment analysis were filtered immediately on the boat (20-70ml, depending on location) using low vacuum pressure through GF/F (Whatman) filter papers. Filters were then flash frozen in liquid nitrogen and stored at -80°C for analysis within 6 months. Frozen GF/F filter papers were thawed in the dark prior to analysis. Chlorophyll-*a* (Chl-*a*) was measured in triplicate via spectrophotometry (Shimadzu UV-1601) after a hot 90% methanol extraction following Iwamura et al.(1970). The hot methanol method was used here as it has been previously found to provide the most complete extraction of Chl-*a* for the phytoplankton types found in Lake Balaton (Présing pers. comm.).

### **6.2.4 Phytoplankton biomass, total suspended matter and coloured dissolved organic matter**

One aliquot of surface water at each station was collected for enumeration of phytoplankton. 500-1500 ml of water was also filtered for analysis of total suspended matter (TSM) by gravimetric determination. Water samples for measurement of coloured dissolved organic matter (CDOM) were filtered into clean glassware through 0.2 µm nucleopore membrane filters (Whatman) and the absorbance was measured within 24 hours of collection. For further detail on these analyses for this specific campaign on Lake Balaton, see Chapter 3 and Riddick et al. (2015).

### **6.2.5 HyperSAS radiometry**

A Hyperspectral Surface Acquisition System (HyperSAS) collected irradiance and radiance measurements at a height of 3.5 m from a pole fixed to the bow of the boat. The HyperSAS data were collected at 30 stations in Lake Balaton only (Stations 1-30). During data collection, the boat was positioned on station to point radiance sensors at a relative azimuth angle of 135° from the sun. Three radiometers measured downwelling irradiance [ $E_s(\lambda)$ ], surface radiance of the water [ $L_r(\lambda)$ ] and sky radiance

$[L_{sky}(\lambda)]$ , where the latter two parameters are used to calculate the water-leaving radiance  $[L_w(\lambda)]$  after correction for air-sea interface reflection (Mueller et al., 2000):

$$L_w(\lambda) = L_t(\lambda) - \rho_{sky} L_{sky}(\lambda) \quad (6.1)$$

where  $\rho_{sky}$ , the air-sea interface reflection coefficient, is estimated for sunny conditions as a function of wind speed in m/s,  $W$ :

$$\rho_{sky} = 0.0256 + 0.00039 * W + 0.000034 * W^2 \quad (6.2)$$

The HyperSAS raw data were processed using Satlantic ProSoft software (v.7.7.10). After processing, all spectra underwent quality control for any outliers due to variable cloudiness or sun glint due to sea state. Remote sensing reflectance  $[R_{rs}(\lambda)]$  was then calculated as:

$$R_{rs}(\lambda) = L_w(\lambda) / E_s(\lambda) \quad (6.3)$$

For consistency with the satellite datasets,  $R_{rs}(\lambda)$  was converted to water-leaving reflectance as follows:

$$\rho_w(\lambda) = R_{rs}(\lambda) * \pi \quad (6.4)$$

### 6.2.6 Remote sensing datasets

There was an airborne remote sensing campaign conducted concurrent with the collection of *in situ* water samples and radiometry, with flights on 21, 22, 23 and 26 August 2010. Additionally, two satellite overpasses occurred on 22 August 2010, providing additional data from MERIS and Landsat 5 TM instruments. This unique collection of four coincident surface reflectance datasets collected between 19 and 26 August is summarised in Table 6.1.

**Table 6.1** Date (XX August 2010) and acquisition time (GMT) of *in situ* and remote sensing datasets collected at each station. Same-day match-ups are shown in bold, and same-day matchups across all datasets are additionally highlighted in gray ( $n=7$ ).

Station	<i>in situ</i> <sup>a</sup>		AISA Eagle		Landsat 5 TM		MERIS <sup>b</sup>	
	Date	Time	Date	Time	Date	Time	Date	Time
1	19	07:03	21	11:00	22	9:29	22	9:01
2	19	08:07	21	12:12	22	9:29	22	9:01
3	19	10:59	22	08:04	22	9:29	22	9:01
4	19	12:04	22	10:30	22	9:29	22	9:01
5	19	13:40	23	10:29	22	9:29	22	9:01
6	20	07:10	21	11:37	22	9:29	22	9:01
7	20	08:24	21	11:00	22	9:29	22	9:01
8	20	09:10	21	11:49	22	9:29	22	9:01
9	20	09:55	21	12:12	22	9:29	22	9:01
10	20	10:45	21	11:13	22	9:29	-	-
11	<b>21</b>	<b>10:43</b>	<b>21</b>	<b>11:00</b>	22	9:29	22	9:01
12	<b>21</b>	<b>11:45</b>	<b>21</b>	<b>12:12</b>	22	9:29	22	9:01
13	<b>21</b>	<b>12:37</b>	<b>21</b>	<b>12:45</b>	22	9:29	22	9:01
14	<b>21</b>	<b>13:32</b>	<b>21</b>	<b>11:13</b>	22	9:29	-	-
15	<b>21</b>	<b>14:18</b>	<b>21</b>	<b>13:21</b>	22	9:29	22	9:01
16	<b>22</b>	<b>08:37</b>	<b>22</b>	<b>09:09</b>	<b>22</b>	<b>9:29</b>	<b>22</b>	<b>9:01</b>
17	<b>22</b>	<b>09:38</b>	<b>22</b>	<b>09:09</b>	<b>22</b>	<b>9:29</b>	<b>22</b>	<b>9:01</b>
18	<b>22</b>	<b>10:10</b>	<b>22</b>	<b>09:09</b>	<b>22</b>	<b>9:29</b>	<b>22</b>	<b>9:01</b>
19	<b>22</b>	<b>10:55</b>	<b>22</b>	<b>10:50</b>	<b>22</b>	<b>9:29</b>	<b>22</b>	<b>9:01</b>
20	<b>22</b>	<b>11:35</b>	<b>22</b>	<b>11:17</b>	<b>22</b>	<b>9:29</b>	<b>22</b>	<b>9:01</b>
21	<b>22</b>	<b>12:15</b>	<b>22</b>	<b>10:39</b>	<b>22</b>	<b>9:29</b>	<b>22</b>	<b>9:01</b>
22	<b>22</b>	<b>13:03</b>	<b>22</b>	<b>10:50</b>	<b>22</b>	<b>9:29</b>	<b>22</b>	<b>9:01</b>
23	<b>23</b>	<b>07:43</b>	<b>23</b>	<b>08:42</b>	22	9:29	22	9:01
24	<b>23</b>	<b>08:21</b>	<b>23</b>	<b>08:42</b>	22	9:29	-	-
25	<b>23</b>	<b>09:00</b>	<b>23</b>	<b>08:58</b>	22	9:29	22	9:01
26	<b>23</b>	<b>09:39</b>	<b>23</b>	<b>09:33</b>	22	9:29	22	9:01
27	<b>23</b>	<b>10:19</b>	<b>23</b>	<b>10:48</b>	22	9:29	22	9:01
28	<b>23</b>	<b>11:00</b>	<b>23</b>	<b>09:33</b>	22	9:29	22	9:01
29	<b>23</b>	<b>11:41</b>	<b>23</b>	<b>09:51</b>	22	9:29	22	9:01
30	24	06:39	23	10:55	22	9:29	22	9:01
31	26 <sup>a</sup>	07:32	26	08:05	22	9:29	22	9:01
32	26 <sup>a</sup>	08:16	26	08:15	22	9:29	22	9:01
33	26 <sup>a</sup>	09:05	26	09:37	22	9:29	22	9:01
34	26 <sup>a</sup>	09:43	26	09:58	22	9:29	22	9:01
35	26 <sup>a</sup>	10:27	26	10:05	22	9:29	22	9:01

<sup>a</sup> *in situ* data includes water sampling and HyperSAS radiometric measurements. Note that HyperSAS data were not collected on 26 August.

<sup>b</sup> MERIS data were acquired for all of Lake Balaton, however stations 10, 14 and 24 were excluded from the dataset due to a high coefficient of variation in  $R_{rs}(709)$  (>20%) for a 3x3 pixel window at these stations.

#### **6.2.6.1 MERIS dataset: acquisition and correction**

MERIS full resolution full swath (FRS) 300 m Level-1b data for 22 August 2010 over Lake Balaton were obtained from the European Space Agency's MERCI repository (<https://earth.esa.int/web/guest/data-access/online-archives>). The standard geolocation of the data was improved using the AMORGOS (Accurate MERIS Ortho-Rectified Geo-location Operational Software) v.4.0 processor. Atmospheric correction was performed using the Self-Contained Atmospheric Parameters Estimation for MERIS data (SCAPE-M) automatic atmospheric correction processor developed by Guanter et al. (2010), following the SCAPE-M\_B2 implementation as in Domínguez et al. (2011). SCAPE-M and SCAPE-M\_B2 have been shown to compute accurate water-leaving reflectances for lakes, particularly for highly turbid waters (Yang et al., 2011a, Yang et al., 2011b, Agha et al., 2012, Jaelani et al., 2013, Medina-Cobo et al., 2014, Riddick et al., in review). Following atmospheric correction with SCAPE-M\_B2, water-leaving reflectance [ $\rho_w(\lambda)$ ] was extracted from the MERIS image using BEAM VISAT v.4.11 software (Brockmann Consult, v.4.11).

MERIS data were screened for those 3x3 pixel windows where  $R_{rs}(709)$  was <20% CV (i.e. standard deviation was within 20% of the mean  $R_{rs}(709)$  for the 9 pixels). This method for spatial homogeneity was previously employed in Goyens et al. (2013) and Jamet et al. (2011). The NDCI was then applied to the extracted water-leaving reflectances, and mapped products were produced using the Graph Processing Framework in BEAM.

#### **6.2.6.2 Landsat 5 TM dataset: acquisition and correction**

A 30-m resolution Landsat 5 Thematic Mapper (TM) Surface Reflectance Climate Data Record (CDR) product was acquired over Lake Balaton for 22 August 2010, using the U.S. Geological Survey (USGS) Earth Explorer tool (<http://earthexplorer.usgs.gov/>, courtesy of the USGS Earth Resources Observation and Science Center). The Surface Reflectance CDR product is radiometrically, geometrically and atmospherically corrected. The atmospheric correction of Level-1 Landsat TM data were conducted using the Moderate Resolution Imaging Spectroradiometer (MODIS) 6S atmospheric correction routine with the Landsat

Ecosystem Disturbance Adaptive Processing System (LEDAPS) (Masek et al., 2006). Although this atmospheric correction method was developed for use over land surfaces, it has been used successfully in other studies over inland waters for retrieval of biogeochemical parameters (Yeo et al., 2014, Chang et al., 2014a, Chang et al., 2014b). Atmospheric corrections designed for terrestrial applications are more likely to be effective over bright water bodies like Lake Balaton, and other land atmospheric corrections have been similarly adapted to lakes, e.g. SCAPE-M (Guanter et al., 2010). Atmospheric correction with the 6S radiative transfer code has also been validated with Landsat TM data for retrieval of water quality parameters (Torbick et al., 2013, Dona et al., 2015).

Landsat 5 TM data were screened for those 3x3 pixel windows where  $R_{rs}$  at band 3 and 4 was <20% CV (i.e. standard deviation was within 20% of the mean  $R_{rs}$  for the 9 pixels). However, it was noted there were no instances of a CV>20% for  $R_{rs}$  at either band. The NDCI was then applied to the extracted surface reflectances, or water-leaving reflectances, and mapped products were produced using the Graph Processing Framework in BEAM.

#### **6.2.6.3 AISA Eagle hyperspectral airborne dataset: acquisition and correction**

The AISA Eagle (Specim) is a 12-bit pushbroom hyperspectral radiometer, which measures over the visible and near infrared spectrum (400-970 nm). The instrument collected radiances at 253 wavelengths, with a spectral resolution of 2.44 nm. Flight altitude was such that the pixel size acquired was 5 meters. Under the operation of the UK's Natural Environmental Research Council Airborne Research and Survey Facility (NERC ARSF Project Code EU 10/03), flights were conducted within two hours of solar noon on cloud-free days on August 17, 21, 22, 23 and 26 of 2010. Level 1b processed imagery was provided by NERC ARSF, with radiometric calibration algorithms applied. All flight lines were geometrically corrected and atmospheric correction was applied by ARSF-DAN (Airborne Research and Survey Facility - Data Analysis Node) at Plymouth Marine Laboratory (Plymouth, UK) using the airborne Atmospheric and Topographic Correction model (ATCOR-4; ReSe Applications Schl pfer, <http://www.rese.ch/products/atcor/atcor4/>). ATCOR-4 perform atmospheric and topographic correction using look-up tables calculated with Modtran@ 5 radiative transfer code. Initial comparisons between the ATCOR-4 atmospherically corrected products and the *in situ* radiometry showed that ATCOR-4 provided more

accurate water-leaving reflectances than other processors such as FLAASH, and therefore it has been applied here (Plymouth Marine Laboratory, unpublished data).

Following atmospheric correction, the NDCI was applied to the extracted water-leaving reflectances, and mapped products were produced using the Graph Processing Framework in BEAM.

### **6.2.7 Validation of atmospheric correction routines**

The atmospheric correction routine for MERIS (SCAPE-M\_B2) was validated in Chapter 5 [Riddick et al. (in review)]. For the Landsat 5 TM and AISA Eagle datasets, the respective atmospheric corrections were validated with *in situ*  $R_{rs}(\lambda)$  data from the HyperSAS. The HyperSAS data were resampled to Landsat 5 TM spectral resolution using the spectral response functions, assuming a Gaussian distribution around each band centre using the full width half maximum of each Landsat 5 TM band. Simulated Landsat 5 TM data were produced using R (v. 3.2.1).  $R_{rs}(\lambda)$  at the nearest HyperSAS wavelength was used for comparison of HyperSAS reflectance with atmospherically corrected AISA Eagle reflectance. Atmospherically corrected products from each dataset were validated using same-day matchups only ( $n=7$  for Landsat 5 TM,  $n=19$  for AISA Eagle). As Lake Balaton exhibited large variations in total suspended matter over the sampling period,  $\pm 1$  day matchups with *in situ* data were deemed to provide the most accurate assessment of any errors due to the atmospheric correction.

The accuracy of the atmospheric correction water-leaving reflectance products was assessed using the determination coefficient ( $R^2$ ), root mean square error in log space ( $RMSE_{\log}$ ), bias in log space ( $Bias_{\log}$ ) and mean absolute percentage error (MAPE).

### **6.2.8 The Normalized Difference Chlorophyll Index (NDCI)**

The Normalized Difference Chlorophyll Index (NDCI) was proposed by Mishra and Mishra (2012) to estimate Chl-*a* concentration in turbid productive waters. NDCI was designed to use water-leaving reflectance at the MERIS bands centered at 665 nm and 708 nm. However, its general form is also easily adapted to Landsat 5 TM data, using bands 3 (630-690 nm) and 4 (760-900 nm). Thus, the NDCI was chosen for this multisensor study not because it is expected to be the best performing Chl-*a* retrieval algorithm for Lake Balaton, but because it was readily adapted to sensors of differing spectral resolution with bands in the red and near infrared. The NDCI uses the

reflectance peak at ~708 nm which is maximally sensitive to variations in Chl-*a*, as well as the spectral absorption peak of Chl-*a* at ~665-675 nm, via the following equation:

$$[Chl - a] \alpha \frac{[\rho_w(708) - \rho_w(665)]}{[\rho_w(708) + \rho_w(665)]} \quad (6.5)$$

The NDCI was implemented in this study as in the above equation for MERIS data. Water-leaving reflectance at Bands 3 and 4 were substituted this equation for Landsat 5 TM data, and  $\rho_w(709.52)$  and  $\rho_w(664.26)$  were employed for AISA Eagle data.

NDCI was subsequently fitted against measured Chl-*a* using an exponential equation of the form  $[Chl-a] = Ae^{b \cdot NDCI}$ , as this was found to be a better fit than linear or polynomial regressions. The resulting exponential fit was then applied to obtain retrieved Chl-*a* concentrations. For ease of comparison, a reduced dataset of the matchups common to all sensors ( $n=27$ ) was used for assessment of algorithm performance across the different sensors. This excluded stations 10, 14, 24, 31-35 and the three Kis-Balaton stations.

### 6.2.9 Method for resampling resolution of Landsat 5 TM and AISA Eagle datasets

Table 8.1 provides a summary of the three sensor capabilities. The Landsat 5 TM and AISA Eagle datasets were each resampled to approximately match MERIS resolution (300 m), while the AISA Eagle data were also degraded to Landsat 5 TM resolution (30 m). For all mapped products, water-leaving reflectances were first spatially resampled to the lower resolution (MERIS resolution, ~300 m) using BEAM VISAT software (Brockmann Consult, v.5.0). The NDCI was then applied to the resampled water-leaving reflectances, and mapped products were produced using the Graph Processing Framework in BEAM.

Retrieved Chl-*a* values from the NDCI were acquired by first extracting water-leaving reflectances at the desired pixel window size in BEAM. To ensure the station was located at the center of the pixel window, the nearest odd number of pixels were used for the dimensions. For example, a window size of 11 x 11 (330 m) and 61 x 61 (305 m) was applied for Landsat 5 TM and AISA Eagle data, respectively, for comparison with MERIS data. The NDCI was applied to the mean  $\rho_w(\lambda)$  value of the pixel window, and errors from the resampled dataset were quantified (RMSE<sub>log</sub>, Bias<sub>log</sub> and MAPE). Within pixel variability was also established with calculation of standard deviation and the coefficient of variation.

**Table 6.2** Details of sensors investigated in this study.

<b>Sensor</b>	<b>No. of Bands</b>	<b>Spectral range (nm)</b>	<b>Spatial resolution (m)</b>	<b>Radiometric Resolution (bits)</b>
AISA Eagle	253	400-970	5	12
Landsat 5 TM	6 <sup>a</sup>	450-2350	30	8
MERIS	15	390-1040	300	16

<sup>a</sup> Landsat 5 TM images consist of 7 bands, however Band 6 is a thermal band sampled at 120 m resolution.

## **6.3 Results**

### **6.3.1 Summary of biogeochemical parameters and biomass**

A summary of the biogeochemical constituents in Lake Balaton during the August 2010 campaign is shown in Table 6.3. Chapter 3, Chapter 4 and Riddick et al. (2015) provide further detail on the optical properties alongside the biogeochemistry and phytoplankton biomass of Lake Balaton during August 2010. During the August 2010 field campaign Chl-*a* concentrations ranged from 5.45-253 mg m<sup>-3</sup>, with a decreasing gradient from Kis-Balaton (west) to Siofók (east). CDOM absorption ranged from 0.093-2.93 m<sup>-1</sup> and also followed a decreasing gradient from west to east, with the highest lake concentrations reported near the mouth of the Zala River. Total suspended matter concentrations varied from 4.40-50.6 mg L<sup>-1</sup>, with particularly high TSM concentrations observed on the windiest sampling date (26 August 2010) due to resuspension of bottom sediments [see Chapter 3 (Riddick et al., 2015)].

**Table 6.3** Summary of biogeochemical parameters in August 2010 in Lake Balaton and Kis-Balaton, including Chlorophyll-*a* (Chl-*a*), Total phytoplankton biomass, Total Suspended Matter (TSM), Particulate Inorganic Matter (PIM), Particulate Organic Matter (POM) and absorption of Coloured Dissolved Organic Matter at 440 nm [ $a_{\text{CDOM}}(440)$ ].

		<b>Chl-<i>a</i></b> ( <b>mg m<sup>-3</sup></b> )	<b>Biomass</b> ( <b>mg m<sup>-3</sup></b> )	<b>TSM</b> ( <b>mg L<sup>-1</sup></b> )	<b>PIM</b> ( <b>mg L<sup>-1</sup></b> )	<b>POM</b> ( <b>mg L<sup>-1</sup></b> )	<b><math>a_{\text{CDOM}}</math></b> <b>(440)</b> <b>(m<sup>-1</sup>)</b>
Lake (n=35)	Mean	15.08	3348	13.47	9.69	3.78	0.39
	StDev	8.90	1832	7.01	6.98	1.43	0.30
	Min	5.45	859	4.40	2.75	1.65	0.093
	Max	39.09	8794	32.65	29.68	7.86	1.35
Kis- Balato n (n=3)	Mean	166.51	70839	40.98	13.44	27.53	2.82
	StDev	83.15	53637	13.28	11.54	8.63	0.12
	Min	87.68	20662	25.83	2.03	21.40	2.69
	Max	253.40	127370	50.60	25.10	37.40	2.93
All Data (n=38)	Mean	27.04	8676	15.64	9.98	5.66	0.58
	StDev	46.46	22333	10.54	7.28	6.93	0.72
	Min	5.45	859	4.40	2.03	1.65	0.093
	Max	253.40	127370	50.60	29.68	37.40	2.93

## 6.3.2 Validation of atmospheric corrections

### 6.3.2.1 SCAPE-M\_B2 atmospheric correction for MERIS

The SCAPE-M\_B2 atmospheric correction for MERIS data were fully validated in Chapter 5 and Riddick et al. (in review). Scatterplots of same-day matchups of MERIS data and HyperSAS *in situ* reflectance spectra showed good agreement (n=7,  $\text{RMSE}_{\log} < 0.205$ ,  $\text{Bias}_{\log} < 0.197$ ,  $\text{MAPE} < 58.7\%$ ; see Figure 5.3, Figure 5.4 and Figure 5.5).

### 6.3.2.2 MODIS/6S atmospheric correction for Landsat 5 TM CDR product

The MODIS/6S atmospheric correction for the Landsat 5 TM CDR product has been mainly validated over land (Masek et al., 2006). However, the 6S radiative transfer model has been used for atmospheric correction of MERIS data over Lake Omodeo, Italy (Bresciani et al., 2012), Lake Idro, Italy (Bresciani et al., 2011) and the small hypereutrophic Lake Zeekoevlei, South Africa (Matthews et al., 2010), and also Landsat data over Bung Boraphet, Thailand (Sriwongsitanon et al., 2011) and Lake Taihu, China (Gong et al., 2008). To our knowledge the Landsat 5 TM CDR product

has not been validated over inland waters, therefore this is presented below in Figure 6.2 and Figure 6.3 for Landsat 5 TM bands 1, 2 and 3 (blue, green and red wavelengths). Bands 4, 5 and 7 were unable to be validated, as the *in situ* hyperspectral radiometers have a calibrated spectral range of 350-800 nm which does not cover these Landsat 5 TM bands. For bands 1-3, the coefficient of determination was high ( $R^2 > 0.789$ ,  $p < 0.01$ ) and errors were low ( $RMSE_{\log} < 0.0721$ ,  $Bias_{\log} < 0.0630$ ,  $MAPE < 16.0\%$ ; Figure 6.2). The highest errors were in the blue wavelengths (Band 1), while the lowest errors were reported in the red portion of the spectrum (Band 3). For stations with same-day matchups, bands 1, 2 and 3 typically fell within the range of the *in situ* HyperSAS  $R_{rs}(\lambda)$  (Figure 6.3).

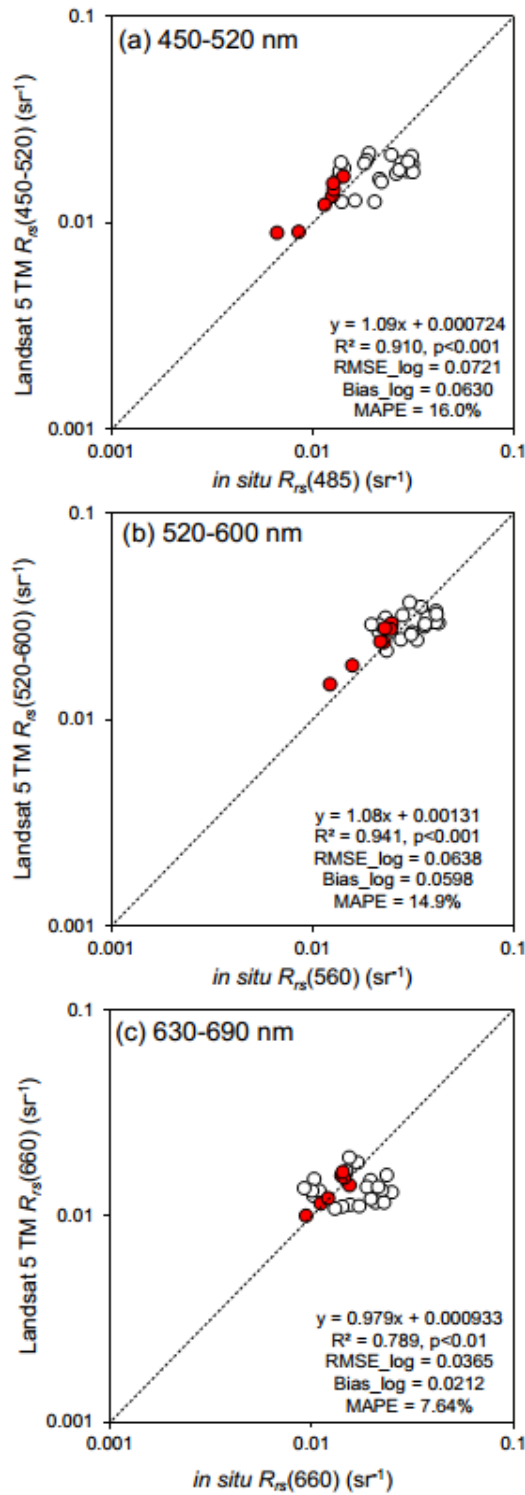


**Figure 6.2** Validation of Landsat 5 TM atmospheric correction with *in situ*  $R_{rs}$  at Landsat bands (a) 1 (450-520 nm), (b) 2 (520-600 nm) and (c) 3 (630-690 nm). *In situ*  $R_{rs}$  was resampled to the respective Landsat 5 TM bands, using the Landsat 5 TM band center and full width half maximum, assuming a Gaussian distribution. Same-day matchups are presented for validation (red points), with equations and errors corresponding to these points only (n=7).

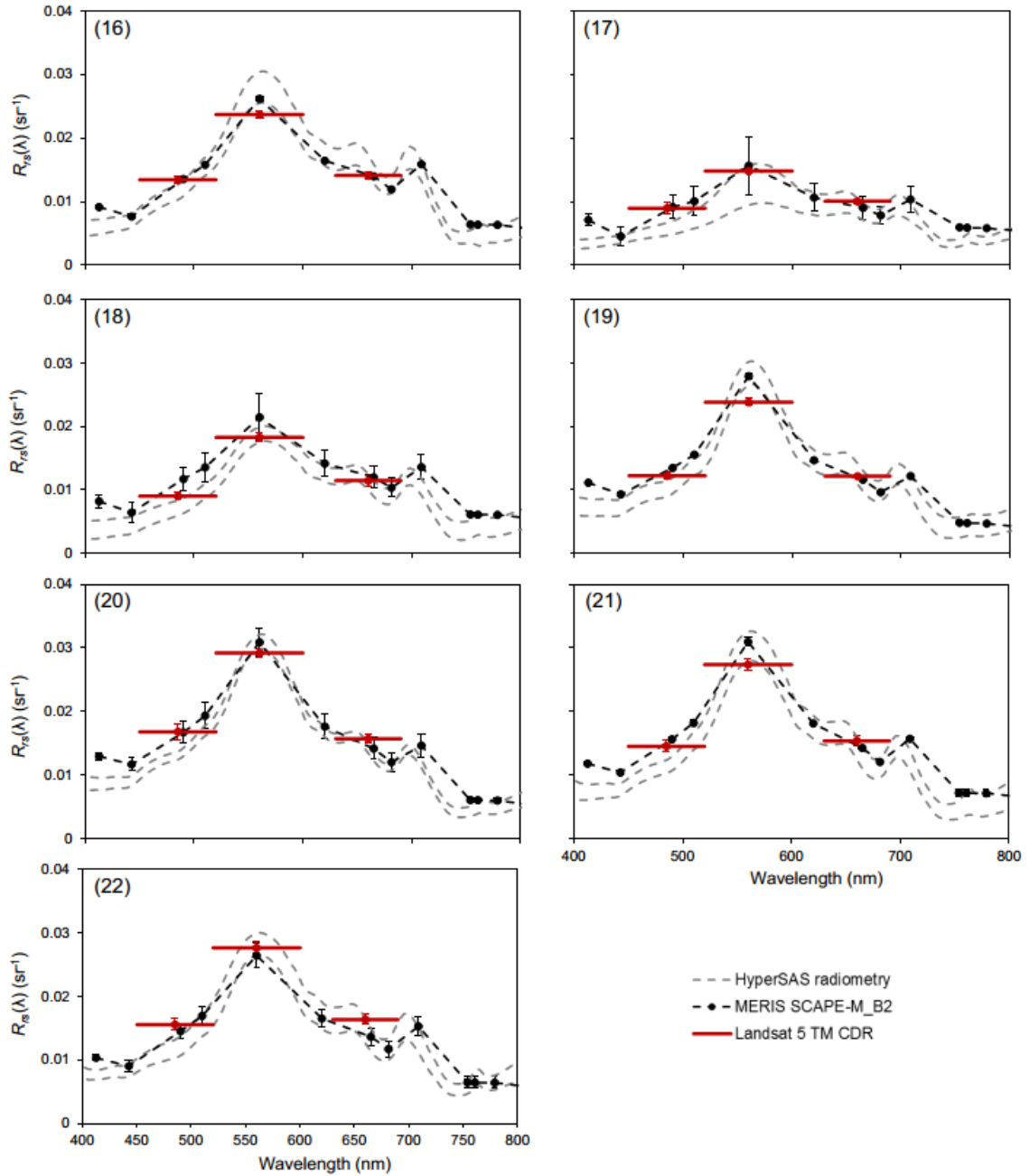


**Figure 6.3** Validation of atmospheric correction of Landsat 5 TM with *in situ*  $R_{rs}(\lambda)$  for same day matchups ( $n=7$ ). *in situ*  $R_{rs}(\lambda)$  is shown as two dashed grey lines, indicating the minimum and maximum  $R_{rs}(\lambda)$  measured by HyperSAS radiometry. MERIS SCAPE-M\_B2  $R_{rs}(\lambda)$  data also shown for comparison. Error bars indicate standard deviation.

### 6.3.2.3 ATCOR-4 atmospheric correction for AISA Eagle product

Preliminary testing of the ATCOR-4 atmospheric correction method for AISA Eagle data has shown performance comparable or better than other atmospheric models (e.g. FLAASH) (Plymouth Marine Laboratory, unpublished data). In this study, the AISA Eagle data atmospherically corrected with ATCOR-4 is validated with *in situ*  $R_{rs}(\lambda)$  spectra for same-day matchups only (Figure 6.4; Figure 6.5). Four wavelengths were chosen to represent the CDOM and chlorophyll-*a* absorption peak (442 nm), phycocyanin-containing cyanobacteria absorption peak (620 nm), chlorophyll-*a* absorption peak (665 nm) and the chlorophyll-*a* absorption minima in the near infrared (708 nm). At all four wavelengths assessed, scatterplots of AISA Eagle and *in situ*  $R_{rs}(\lambda)$  showed good agreement, with high determination coefficients ( $R^2 > 0.894$ ,  $p < 0.001$ ) and low errors ( $RMSE_{\log} < 0.120$ ,  $Bias_{\log} < 0.0966$ ,  $MAPE < 28.3\%$ ; Figure 6.4). The poorest agreement was observed for 442.5 nm, with atmospherically corrected AISA Eagle data typically over-estimating *in situ* reflectance, while the lowest errors were reported at 620 nm. Other atmospheric correction validation studies have also reported poor agreement in the blue due to greater Rayleigh and aerosol scattering, e.g. (Goyens et al., 2013). However, for the purposes of this study, it is important to note that there was good agreement in the red (665 nm) and NIR (708 nm), the wavelengths used for the NDCI (Figure 6.4c and d). At stations with same-day matchups, the AISA Eagle spectra typically fell within the range of *in situ*  $R_{rs}(\lambda)$  measured by the HyperSAS (Figure 6.5). Where poorer agreement was observed, there was typically a larger time difference between acquisition of the airborne and *in situ* datasets (e.g. stations 22, 28, 29; see Table 6.1).

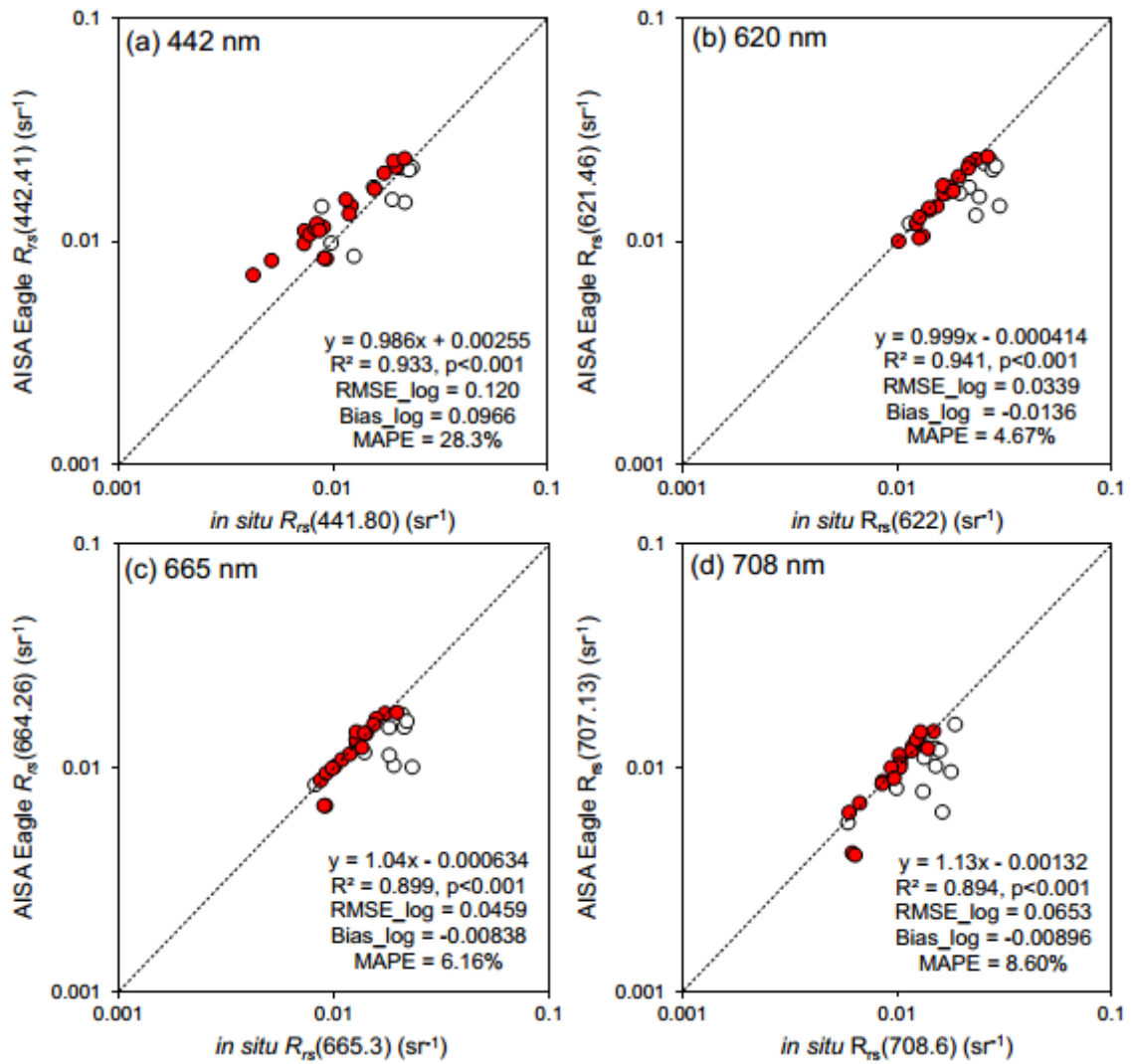


**Figure 6.4** Validation of ATCOR4 atmospheric correction of AISA Eagle data with *in situ*  $R_{rs}$  at (a) 442, (b) 620, (c) 665 and (d) 708 nm. The *in situ* wavelength which was closest to the center of the respective AISA Eagle band was used for validation. Only same-day matchups are presented for validation (red points), with equations and errors corresponding to these points only (n=19).

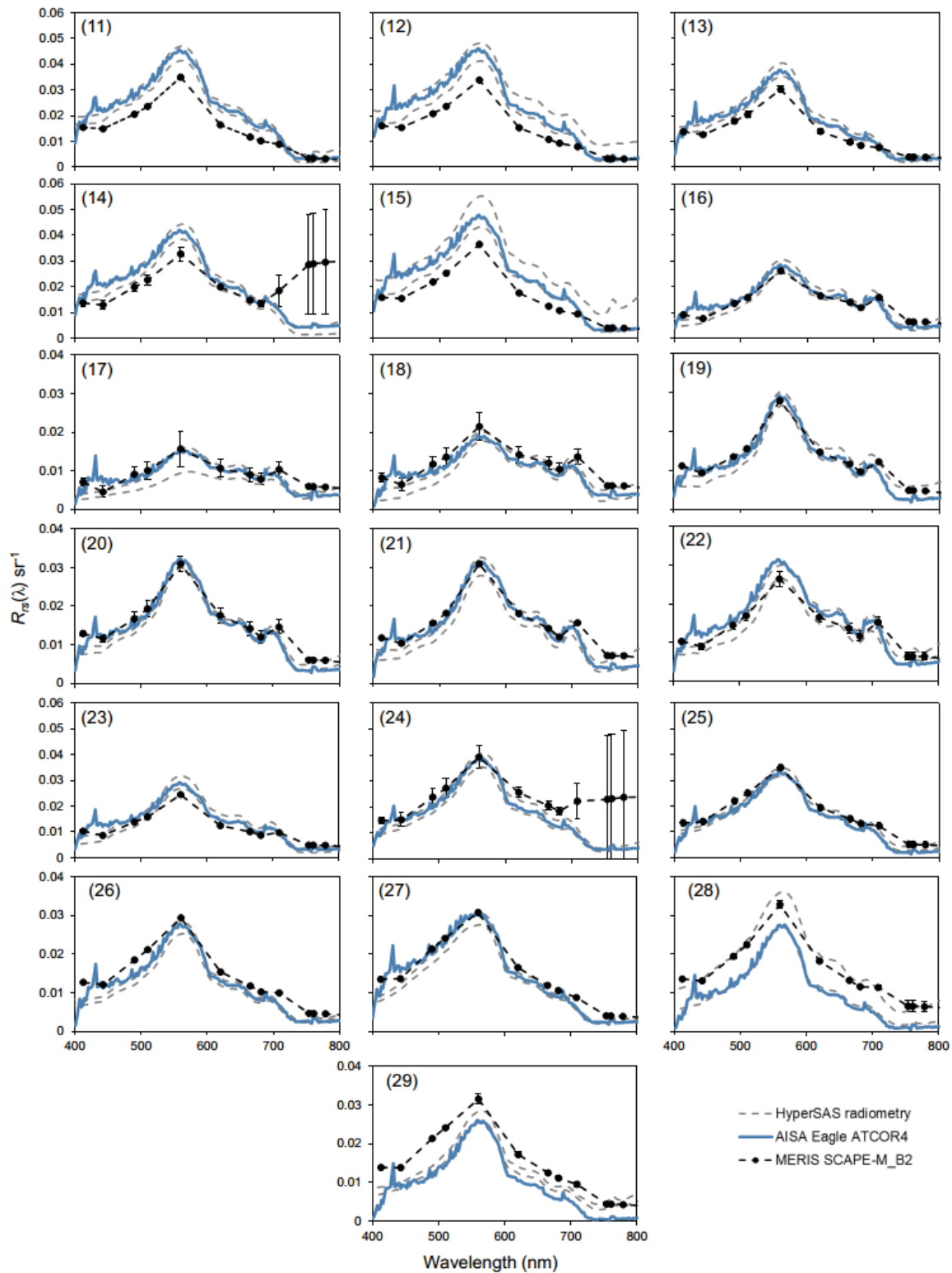


**Figure 6.5** Validation of ATCOR4 atmospheric correction of AISA Eagle data with *in situ*  $R_{rs}(\lambda)$  for same day matchups ( $n=19$ ). *in situ*  $R_{rs}(\lambda)$  is shown as two dashed grey lines, indicating the minimum and maximum  $R_{rs}(\lambda)$  measured by HyperSAS radiometry. MERIS SCAPE-M\_B2  $R_{rs}(\lambda)$  data also shown, with error bars indicating standard deviation. Note different y-axis ranges.

### 6.3.3 Algorithm performance

#### 6.3.3.1 Chl-*a* retrieval with NDCI

Chl-*a* was retrieved using the NDCI for MERIS, Landsat 5 TM, AISA Eagle and HyperSAS datasets (Figure 6.6; Figure 6.7). Using 3x3 pixel windows, all datasets showed good agreement with *in situ* Chl-*a* concentrations ( $R^2 > 0.268$ ,  $p < 0.01$ ,  $RMSE_{\log} < 0.198$ ,  $Bias_{\log} < 0.0171$ ,  $MAPE < 42.8\%$ ). Retrieved concentrations from the airborne AISA Eagle data demonstrated the best agreement, with the lowest errors overall. Chl-*a* retrievals from AISA Eagle, HyperSAS and MERIS data had low  $RMSE_{\log}$  ( $< 0.09$ ),  $Bias_{\log}$  ( $< 0.007$ ) and  $MAPE$  ( $< 16\%$ ), although markedly higher errors were reported for retrievals from Landsat 5 TM ( $RMSE_{\log} = 0.198$ ,  $Bias_{\log} = 0.0171$ ,  $MAPE = 42.8\%$ ). As was also noted in other investigations using MERIS data, e.g. [Chapter 5; Riddick et al. (in review)], a lower limit of  $\sim 10 \text{ mg m}^{-3}$  was reported for retrieved Chl-*a* concentrations (Figure 6.6a). All sensors indicated higher relative errors at Chl-*a*  $< 10 \text{ mg m}^{-3}$  (e.g. for MERIS, APE for Chl-*a*  $< 10 \text{ mg m}^{-3}$  ranged from 1.62-77.7%). This is possibly because at low concentrations it is radiometrically challenging to resolve changes in  $R_{rs}(\lambda)$  due to constraints of the sensor signal to noise ratio.

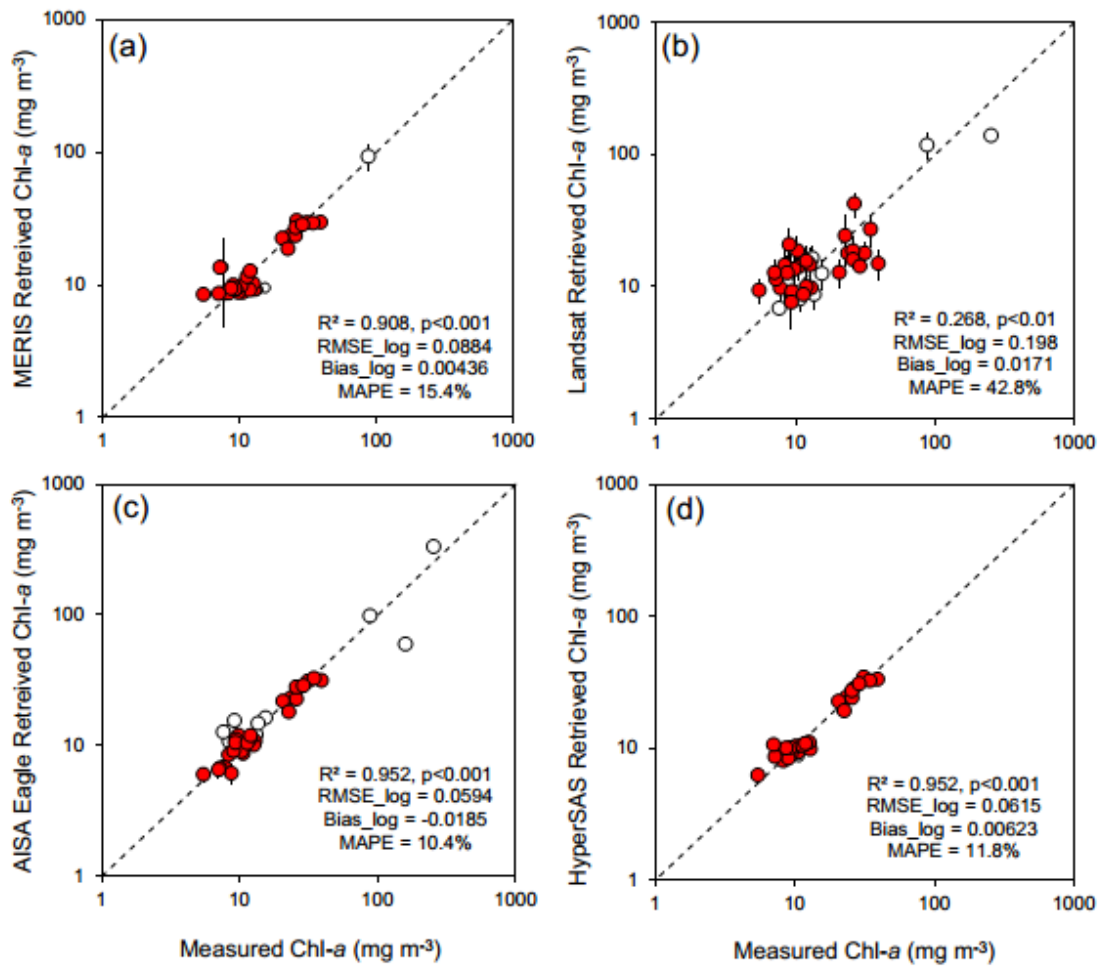


**Figure 6.6** Scatterplots of retrieved Chl-*a* against measured Chl-*a* using the NDCI with (a) MERIS (b) Landsat 5 TM, (c) AISA Eagle and (d) HyperSAS datasets. Pixel window of 3x3 applied for each dataset. Statistics are for common dataset, shown in red, with any additional matchups shown as open circles. Determination coefficients ( $R^2$ ) represent linear regressions of common dataset. Dashed line represents 1:1 relationship.

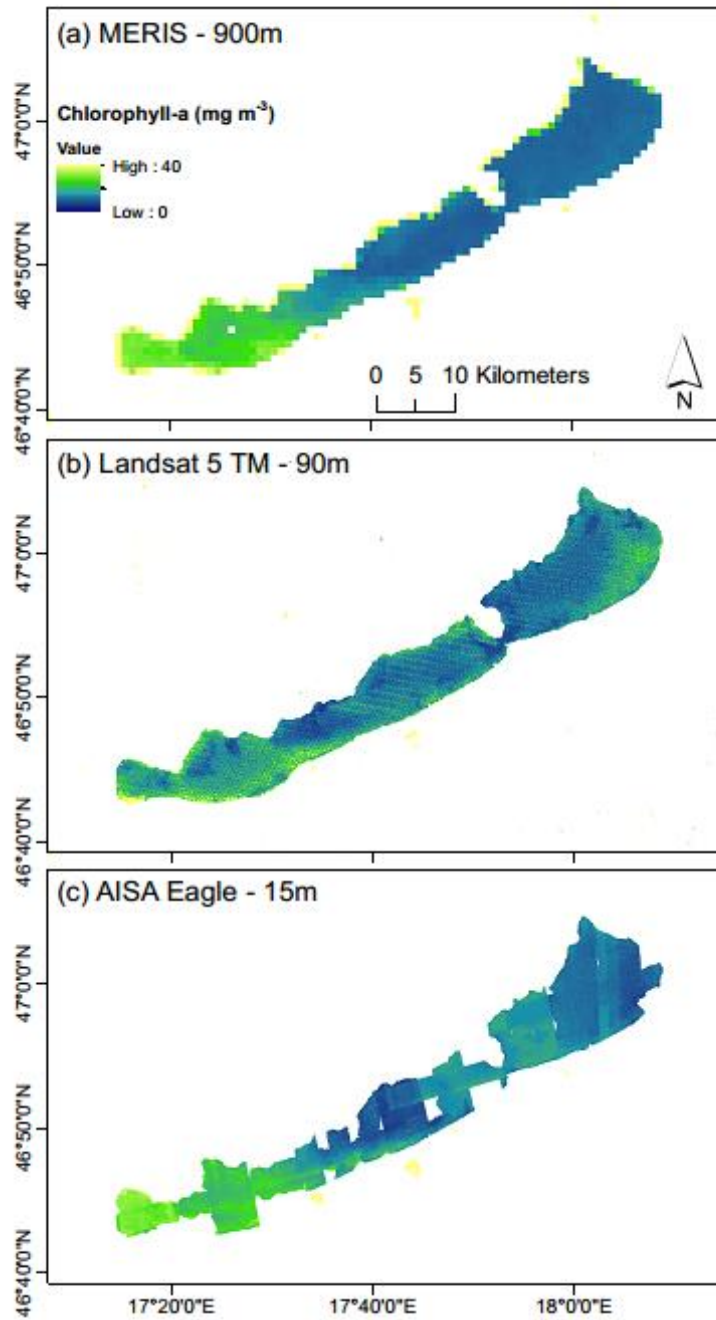


**Figure 6.7** Maps of Chl-*a* retrievals using the NDCI applied to the (a) MERIS (b) Landsat 5 TM and (c) AISA Eagle datasets. Pixel window of 3x3 applied for each dataset, i.e. maps shown at (a) 900 m, (b) 90 m and (c) 15 m resolutions.

### 6.3.4 Degradation of AISA Eagle and Landsat 5 TM datasets

#### 6.3.4.1 Chl-*a* retrieval with NDCI

The Landsat 5 TM (30 m) and hyperspectral AISA Eagle (5 m) datasets were degraded to match the resolution of MERIS and the forthcoming OLCI (300 m) (Table 6.4). The minimum errors (standard deviation and coefficient of variation) increased slightly from 15 to 35 m resolution for the AISA Eagle dataset. However, the errors increased markedly when AISA Eagle data were degraded to 305 m resolution, with a coefficient of variation of up to 544% and standard deviation of up to 104 mg m<sup>-3</sup>. In contrast, Landsat 5 TM data showed little change in errors between the 90 and 330 m resolution datasets, with a slight increase in the standard deviation (1.24-11.1 mg m<sup>-3</sup>), but a lower maximum coefficient of variation (35.9%).

**Table 6.4** Table of errors (Coefficient of Variation, %; Standard Deviation) within the resampled pixel windows for Chl-*a* retrieved by NDCI from AISA Eagle and Landsat 5 TM data. Sample size is for a common dataset ( $n=27$ ).

Sensor	Pixel Window Size ( $n$ )	Spatial Resolution (m)	To Compare With	Min SD (mg m <sup>-3</sup> )	Max SD (mg m <sup>-3</sup> )	Min CV (%)	Max CV (%)
AISA Eagle	3x3 ( $n=9$ )	15	-	0.224	2.38	1.87	17.5
	7x7 ( $n=49$ )	35	Landsat 5 TM	0.390	2.02	3.21	15.2
	61x61 ( $n=3721$ )	305	MERIS	0.505	104	4.24	544
Landsat 5 TM	3x3 ( $n=9$ )	90	-	0.854	10.5	9.22	48.2
	11x11 ( $n=121$ )	330	MERIS	1.24	11.1	12.1	35.9

Chl-*a* was retrieved using the NDCI with relatively low errors for all datasets at all resolutions (RMSE<sub>log</sub> = 0.06-0.21, Bias<sub>log</sub> = -0.019-0.019, MAPE = 10-43%; Table 6.5). For the AISA Eagle dataset, lower errors and a higher determination coefficient were observed for the 15 m resolution as compared to a single pixel extraction (5 m), while the largest pixel window (61x61; 305 m) was associated with the highest errors. The errors for AISA Eagle Chl-*a* retrievals at 5, 15 and 35 m resolutions were comparable with those reported for the *in situ* HyperSAS data. The Landsat 5 TM

dataset showed fairly consistent agreement with *in situ* Chl-*a* concentrations at all three resolutions, although MAPE and Bias<sub>log</sub> were slightly higher for 3x3 (90 m) and 11x11 (330 m) pixel windows. The errors for Landsat 5 TM retrievals were the highest of the four datasets compared in this study, with RMSE<sub>log</sub> ranging from 0.194-0.210 and MAPE = 40.8-42.8%. For MERIS, marginally better agreement was observed for Chl-*a* retrievals from a single pixel (300 m) as compared with a 3x3 pixel window (900 m).

**Table 6.5** Comparison of errors for Chl-*a* retrievals from AISA Eagle, Landsat 5 TM and MERIS data using the NDCI. Sample size is for the common dataset ( $n=27$ ).

Sensor	Pixel Window Size ( $n$ )	Spatial Resolution (m)	For comparison with	Range of Retrieved Chl- <i>a</i> ( $\text{mg m}^{-3}$ )	Median Retrieved Chl- <i>a</i> ( $\text{mg m}^{-3}$ )	$R^2$ ( $p$ -value)	$\text{RMSE}_{\log}$	$\text{Bias}_{\log}$	MAPE (%)
AISA Eagle	1x1	5	-	5.23 – 32.5	11.1	0.941 (<0.001)	0.0601	-0.0161	11.5
	3x3 ( $n=9$ )	15	-	6.03 – 32.8	11.2	0.952 (<0.001)	0.0594	-0.0185	10.4
	7x7 ( $n=49$ )	35	Landsat 5 TM	5.93 – 32.4	11.0	0.953 (<0.001)	0.0588	-0.0191	10.8
	61x61 ( $n=3721$ )	305	MERIS	6.18 – 32.6	11.0	0.910 (<0.001)	0.0692	-0.00417	12.6
Landsat 5 TM	1x1	30	-	6.45 – 35.4	13.6	0.255 (<0.01)	0.210	-0.00784	40.8
	3x3 ( $n=9$ )	90	-	7.67 - 42.7	14.4	0.268 (<0.01)	0.198	0.0171	42.8
	11x11 ( $n=121$ )	330	MERIS	8.68 - 47.0	13.3	0.268 (<0.01)	0.194	0.0185	41.8
MERIS	1x1 ( $n=1$ )	300	-	8.07 - 31.3	10.3	0.919 (<0.001)	0.0825	0.00388	14.6
	3x3 ( $n=9$ )	900	-	8.55 - 30.7	10.3	0.908 (<0.001)	0.0884	0.00436	15.4
HyperSAS ( <i>in situ</i> )	N/A ( $n=1$ )	N/A	-	6.28 - 34.6	10.7	0.952 (<0.001)	0.0615	0.00623	11.8

Histograms showed that the range and distribution of retrieved Chl-*a* values from all sensors were remarkably similar, with less than 10% difference between the median values for each sensor at the varying spatial resolutions (Figure 6.8; Table 6.5). However, fewer low Chl-*a* values (<10 mg m<sup>-3</sup>) were retrieved from Landsat data as compared to the AISA Eagle and MERIS datasets (Figure 6.8). Furthermore, the range of retrieved Chl-*a* concentrations notably increased with increasing resolution for the Landsat 5 TM dataset, with minimum concentrations increasing from 6.45 to 8.68 mg m<sup>-3</sup> and the maximum from 35.4 to 47.0 mg m<sup>-3</sup> (Table 6.5; Figure 6.8). However, a similar trend was absent for Chl-*a* retrievals from AISA Eagle and MERIS data, with histograms indicating relatively similar distributions over all spatial resolutions. Maps of Chl-*a* retrievals from the NDCI show this increase particularly on the shorelines of the westernmost basin (Keszthely) and the eastern edge of the easternmost basin (Siofók) (Figure 6.9).

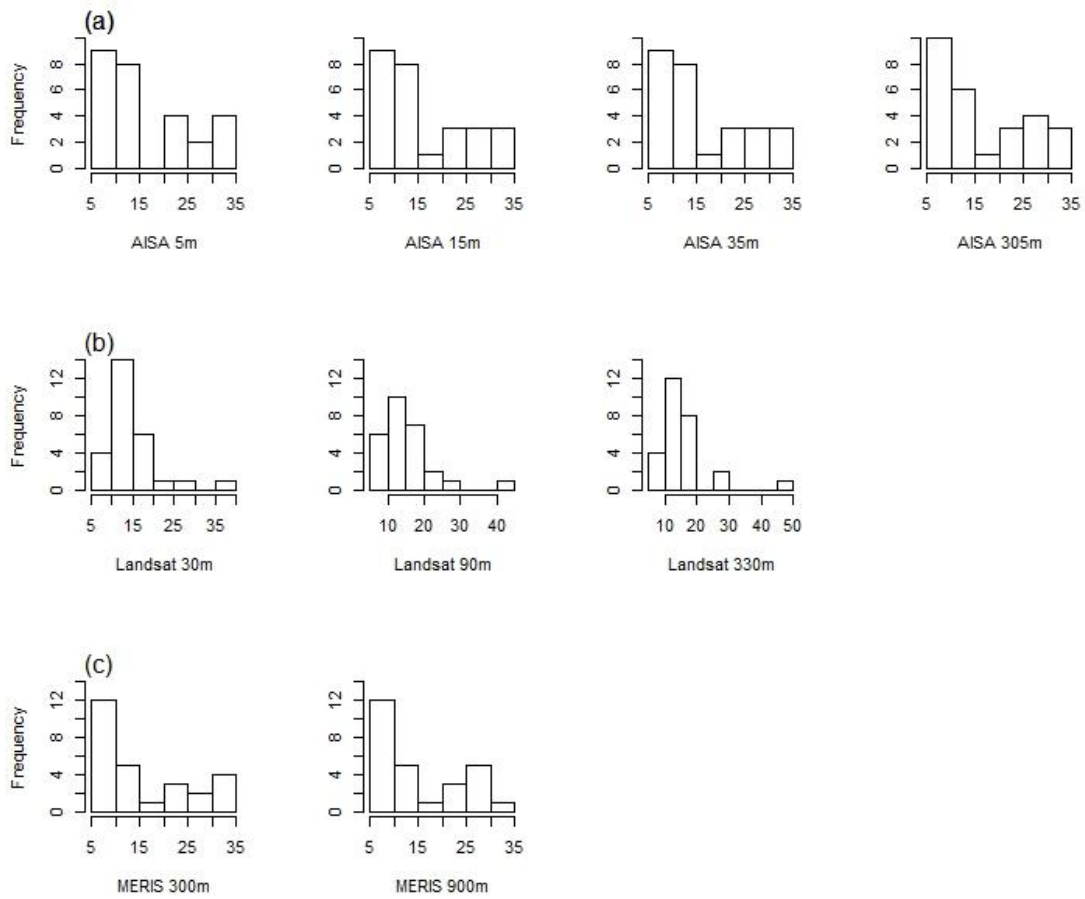


**Figure 6.8** Histograms of Chl-*a* concentrations (mg m<sup>-3</sup>) retrieved using the NDCI from (a) AISA Eagle, (b) Landsat 5 TM and (c) MERIS at variable spatial resolutions, as indicated.

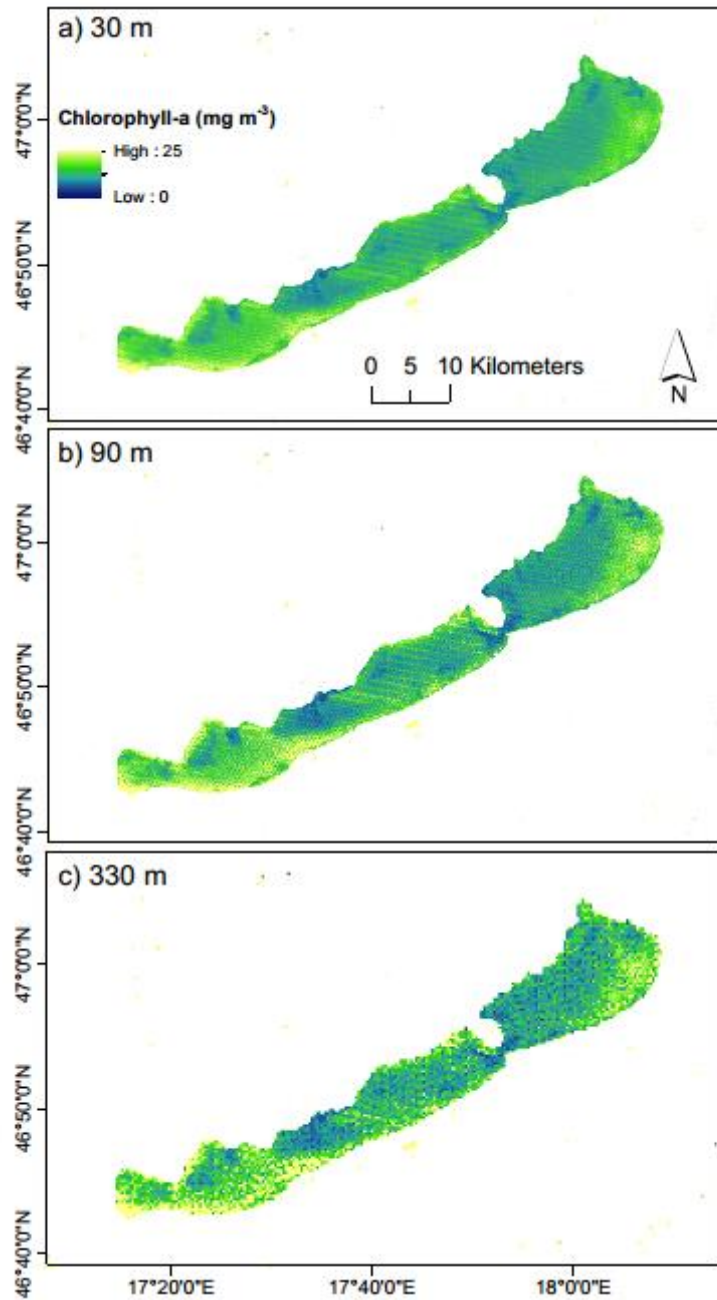


**Figure 6.9** Maps of Chl-*a* retrievals using the NDCI applied to the Landsat 5 TM data at (a) 30 m (1 pixel), (b) 90 m (3 x 3 pixel window) and (c) 330 m (11 x 11 pixel window) resolutions.

Chl-*a* retrievals from AISA Eagle data showed no marked change in the Chl-*a* concentration range from 5 to 305 m resolutions (Table 6.5; Figure 6.10). However, images with resolution higher than 5 m demonstrated a lack of ability to capture the heterogeneity in Chl-*a* concentrations (Figure 6.11). For example, this is particularly

evident on the eastern edge of the Tihany peninsula (top left in Figure 6.11), where the pattern in Chl-*a* distribution lost clarity along with the degradation in spatial resolution. It was additionally noted that Chl-*a* concentrations appear higher in the linear features to the south of the Tihany peninsula (Figure 6.11). These lines are presumed to be boat wakes, therefore higher Chl-*a* concentrations may be a result of ships causing mixing of the water column and/or resuspending subsurface phytoplankton.

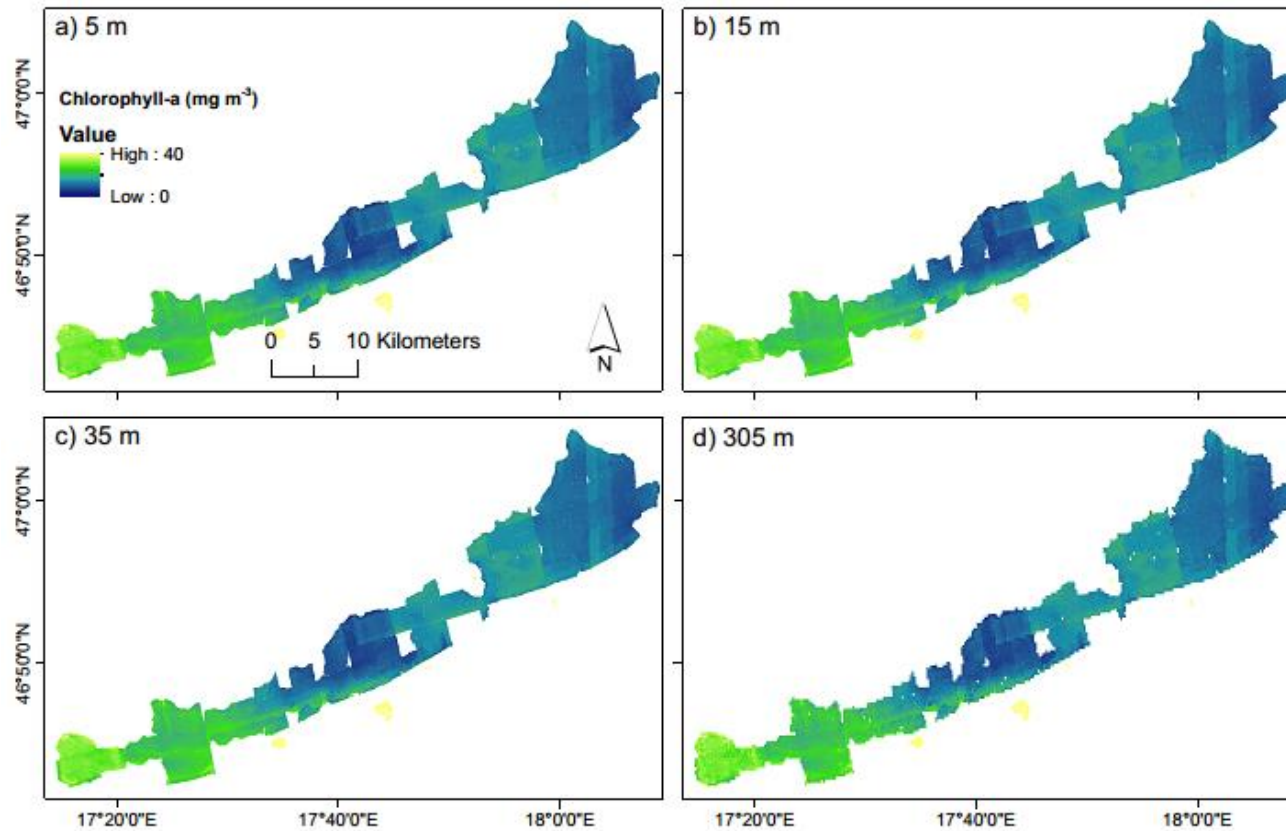


**Figure 6.10** Maps of Chl-*a* retrievals using the NDCI applied to the AISA Eagle data at (a) 5 m (1 pixel), (b) 15 m (3 x 3 pixel window), (c) 35 m (7 x 7 pixel window) and (d) 305 m (61 x 61 pixel window) resolutions.

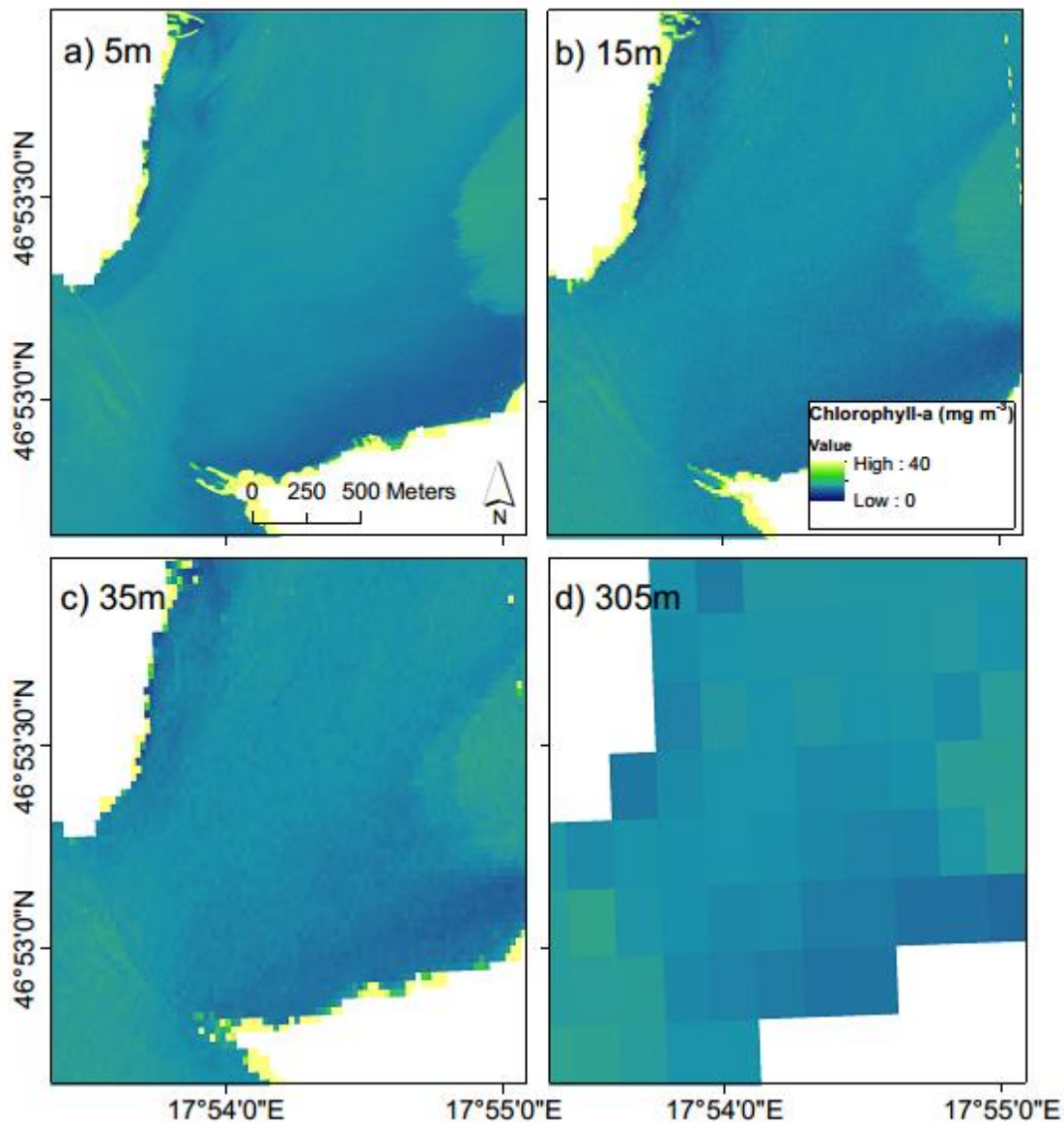


**Figure 6.11** Maps of Chl-*a* retrievals using the NDCI applied to the AISA Eagle data for the Tihany peninsula at a) 5 m (1 pixel), (b) 15 m (3 x 3 pixel window), (c) 35 m (7 x 7 pixel window) and (d) 305 m (61 x 61 pixel window) resolutions.

Chl-*a* retrieved from each satellite dataset was compared at the native spatial resolution alongside the AISA Eagle data of equivalent resolution acquired on the same day over the Keszthely basin. Landsat 5 TM predicted lower Chl-*a* values in the Keszthely basin than that retrieved from AISA Eagle data (Figure 6.12 a,b). Chl-*a* retrieved from MERIS data showed less inter-pixel variability than the equivalent resolution AISA Eagle data, indicating some loss in capturing the heterogeneity of phytoplankton distribution with MERIS data (Figure 6.12 c,d).

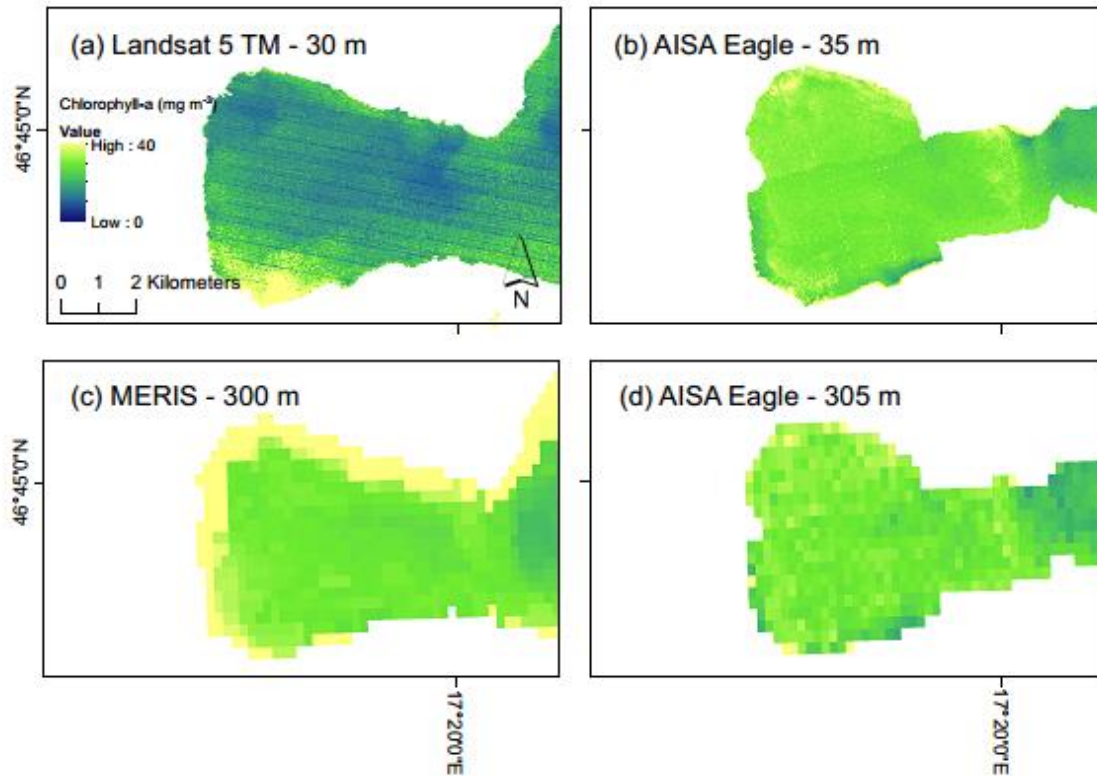


**Figure 6.12** Maps of Chl-*a* retrievals using the NDCI applied to (a) Landsat 5 TM data at the native 30 m resolution, (b) AISA Eagle data at 35 m resolution, (c) MERIS data at the native 300 m resolution and (d) AISA Eagle data at 305 m resolution for the Keszthely basin (Stations 16, 17 18). Data shown were acquired from 09:01-09:29 GMT on 22 August 2010.

It is worth noting the presence of high Chl-*a* values around the edge of the lake in the Chl-*a* retrieval maps (e.g. Figure 6.12c). This is possibly a result of the masking technique used (land/water mask processor in Beam), as well as the presence of emergent vegetation (e.g. macrophytes such as *Phragmites australis*). Future presentation of retrieval maps requires more efficient marking of land and emerging vegetation, particularly for MERIS and OLCI data which have coarser spatial resolution.

## 6.4 Discussion

### 6.4.1 Atmospheric corrections

Two atmospheric corrections were validated for their respective datasets in this study. ATCOR4 performed well for the AISA Eagle data, although poorer agreement

was observed in the blue wavelengths (412 nm). This trend has also been reported in validation studies of other atmospheric corrections over coastal waters due to greater Rayleigh and aerosol scattering at these wavelengths, e.g. Goyens et al. (2013). However, the NDCI was used in this study, which does not employ the blue wavelengths, so any impact on Chl-*a* retrievals due to atmospheric correction with ATCOR4 is likely to be minimal. The MODIS/6S atmospheric correction performed well for correction of Landsat 5 TM data, although Landsat 5 TM  $R_{rs}$  was over-estimated in the blue and NIR wavelength ranges. This could contribute to some of the error observed in NDCI retrievals, as band 4 (NIR) is used for this index.

#### **6.4.2 Chlorophyll-*a* retrieval with NDCI**

Chl-*a* was retrieved with relatively low errors for all datasets at all resolutions, indicating the usefulness of the NDCI for Chl-*a* retrieval over a range of multi- and hyperspectral datasets (Table 6.4; Table 6.5). As expected, Chl-*a* retrievals with NDCI showed the strongest agreement with *in situ* concentrations for the highest resolution datasets (HyperSAS and AISA Eagle). However, MERIS retrieved Chl-*a* more accurately than Landsat 5 TM, and this is likely a factor of the wavelengths available for the computation of NDCI. NDCI was calculated using bands 7 ( $665 \pm 10$  nm) and 9 ( $708.75 \pm 10$  nm) for MERIS data, while for Landsat 5 TM data bands 3 (630-690 nm) and 4 (760-900 nm) were substituted into the NDCI equation. The poorer agreement for Landsat 5 TM Chl-*a* retrievals may be due to the broader wavelength range or could also be a result of differences in radiometric resolution (MERIS is 16-bit while Landsat 5 TM is 8-bit).

#### **6.4.3 Resampling of Landsat 5 TM and AISA Eagle datasets**

While there was no apparent increase in errors when resampling the AISA Eagle data to 15 m or 35 m resolution, there was a marked increase in errors when the resolution was degraded to 300 m. However, there was no significant increase in errors when the Landsat 5 TM dataset was resampled to 90 m or 330 m resolution. This disparity may be a result of the greater errors caused by the large bandwidth for Landsat 5 TM bands, which overshadows the differences due to changes in spatial resolution.

Analysis of true colour images also provides visual detection of any degradation in data quality with decreased resolution. With the true colour AISA Eagle images, no apparent loss of detail is observed between 5 and 35 m, while the heterogeneity is clearly indistinguishable at 305 m (Figure 6.13). Similarly, no marked difference is

noticeable in true colour Landsat 5 TM images from 30 to 90 m resolution, however the loss of detail is apparent at 330 m (Figure 6.14).

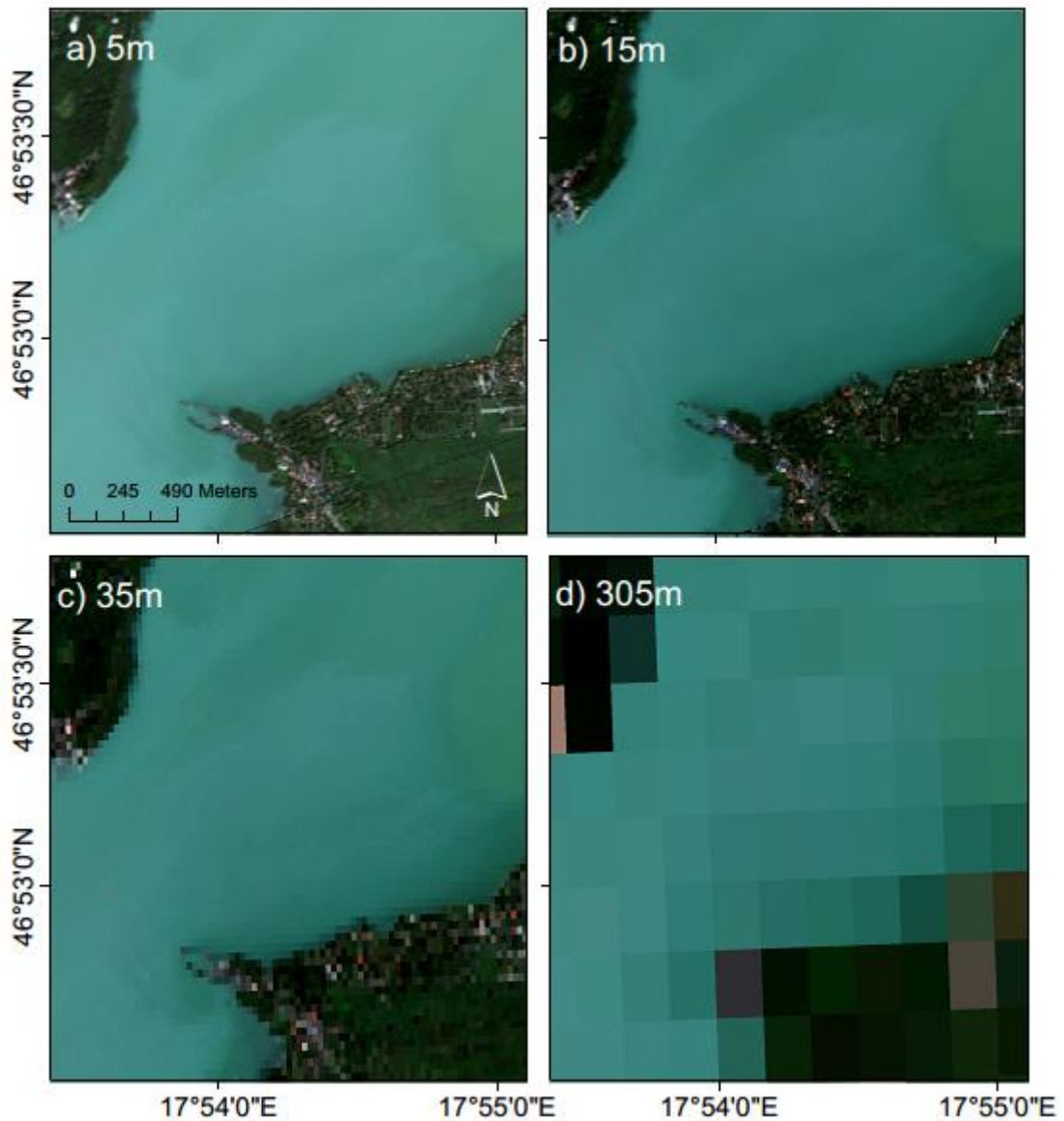


**Figure 6.13** True colour AISA Eagle images of the Tihany peninsula (Station 35) at (a) 5 m, (b) 15 m, (c) 35 m and (d) 305 m.

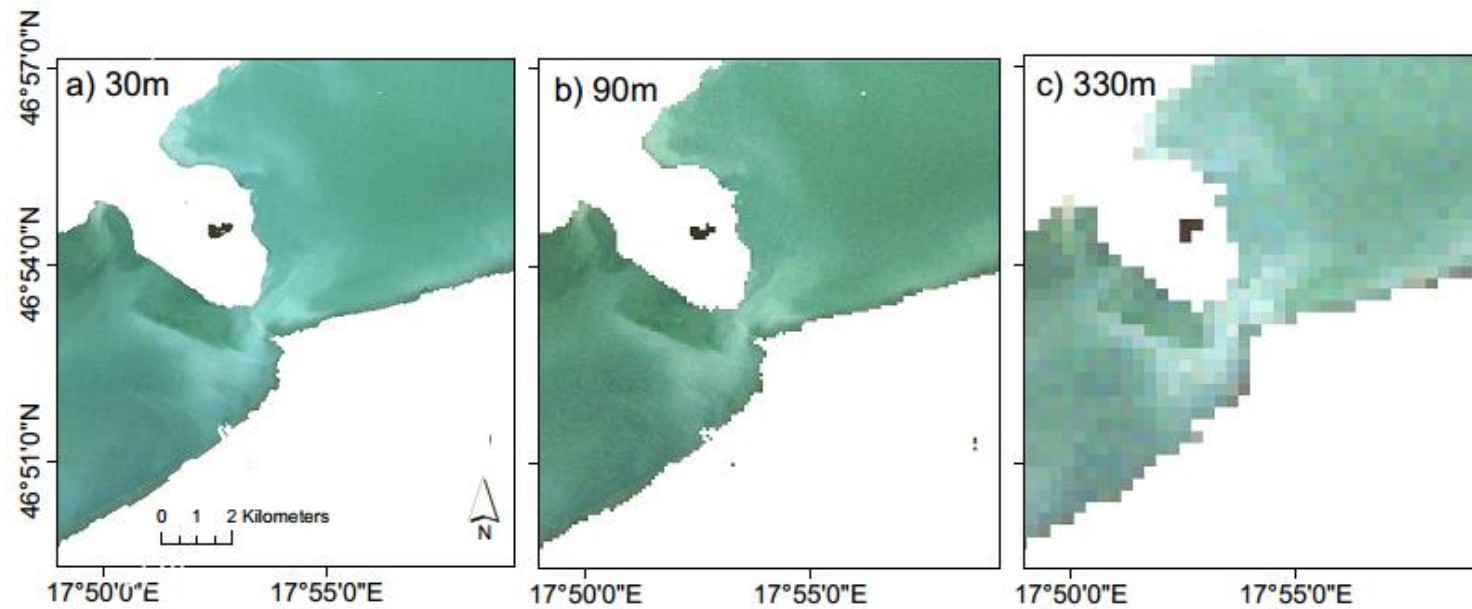


**Figure 6.14** True colour Landsat 5 TM images of the Tihany peninsula (Station 35) at (a) 30 m, (b) 90 m, (c) 330 m.

For the Landsat 5 TM dataset, the range of retrieved Chl-*a* concentrations increased by over 30% in response to the degradation of spatial resolution, although this trend was not reported for retrievals from AISA Eagle and MERIS data (Table 6.5; Figure 6.8). Chl-*a* maps highlight the increased concentrations particularly on the shorelines (Figure 6.9). This could be due to the greater concentrations of suspended matter along the shore and the influence of bottom and/or submerged vegetation. Concentrations of TSM are particularly variable in Lake Balaton given the high propensity for wind-induced resuspension, with concentrations ranging from ~5-50 mg L<sup>-1</sup> over the sampling period. With the increase in pixel window size, subtle spatial variations in suspended matter would not be detected and therefore lower reflectance would be recorded at Band 4 (760-900 nm). Given Equation 6.7 for the calculation of NDCI, this would then be misinterpreted as a greater concentration of Chl-*a* for such pixels. Additionally, Landsat 5 TM collects data over a broad wavelength range for each band, therefore this instrument may be less able to distinguish between Chl-*a* and TSM.

MERIS data also demonstrated a lack of ability to capture the heterogeneity of Chl-*a* concentrations across the Keszthely basin (Figure 6.12 c,d). Chl-*a* retrieved from AISA Eagle data (305 m resolution) showed greater inter-pixel variability than Chl-*a* retrieved from MERIS data, suggesting that sensors with higher spatial resolution can provide better detail on phytoplankton distribution than those with lower resolution. However, MERIS still produced a similar range of Chl-*a* values, therefore it remains a useful monitoring tool for the purpose of identifying the abundance of phytoplankton biomass present. This was confirmed by the histograms of retrieved Chl-*a* values, which demonstrate a remarkable consistency in the range and distribution of Chl-*a* retrieved by all sensors (Figure 6.8; Table 6.5). This suggests that for this study site, high spatial resolution data (e.g. AISA Eagle) may not really be necessary in order to accurately capture the range of Chl-*a* values, although it does remain useful for detecting variability in the finer spatial patterns of phytoplankton distribution (see Figure 6.11 and Figure 6.13).

## **6.5 Conclusions**

This study assessed the ability of NDCI to retrieve Chl-*a* concentrations in four coincident spectral datasets over Lake Balaton, including *in situ* HyperSAS radiometry, hyperspectral airborne AISA Eagle data, and multi-spectral satellite data from Landsat

5 TM and MERIS. The atmospheric corrections investigated here, including ATCOR4, SCAPE-M\_B2 and MODIS/6S, proved successful in creating accurate water-leaving reflectance spectra compared to the *in situ* data for the respective remote sensing dataset. All four remote sensing datasets were able to accurately retrieve Chl-*a* concentrations, confirming the NDCI is a useful approach for estimation of Chl-*a* from satellites, airborne and *in situ* reflectance data. In resampling the AISA Eagle and Landsat 5 TM data, greater errors were associated with retrieved Chl-*a* concentrations at  $\geq 300$  m as compared to the higher resolution datasets (5-30 m). Additionally, there was a marked loss in the ability to detect the subtle heterogeneity of Chl-*a* distribution with spatial resolutions above 5 m. This was particularly noted in the region near of the Tihany peninsula, where phytoplankton spatial dynamics are more complex. However, this study demonstrated there was minimal (<10%) difference in median retrieved Chl-*a* values at the different resolutions, therefore it may be concluded that there is little gain in using high spatial resolution data for the purpose of Chl-*a* retrieval, except the ability to resolve the finer spatial structures of phytoplankton distribution in dynamic large lakes.

This ultimately has implications for monitoring phytoplankton spatial distribution in large lakes with presently available satellite instruments, such as the recently launched OLCI onboard Sentinel-3 that has a spatial resolution akin to MERIS (300 m). For instance, the results of this study suggest that Sentinel-3/MERIS spatial resolution is adequate for retrieving the range and distribution of Chl-*a* values (i.e. phytoplankton abundance), however finer resolution datasets (e.g. Landsat-8 or MSI onboard Sentinel-2) could be used synergistically in order to better characterise the complex spatial patterns of phytoplankton in large lakes. The results of this study emphasise the utility of a coordinated approach to remote sensing of large inland water bodies, such as Lake Balaton, whereby the combination of variable spatial, spectral and temporal resolution datasets can both effectively quantify phytoplankton abundance and capture the subtleties of phytoplankton spatial dynamics.

## 7 Discussion, conclusions and future research

---

### 7.1 Contributions of this research

The research within this thesis has examined the use of *in situ* optics, radiometry, airborne and satellite platforms for the remote sensing of phytoplankton biomass. The observations were used, where possible concomitantly, to better understand the factors influencing the retrieval of phytoplankton pigments Chl-*a* and PC as indicators of total phytoplankton and cyanobacteria biomass, respectively. The results in this thesis have demonstrated the value of coincident *in situ* bio-geo-optical data, validated current phytoplankton pigment retrieval algorithms and shown how the use of multiple platforms and sensors can accurately map phytoplankton biomass and spatial distribution in inland waters. Lake Balaton was chosen as a complex case study in which to investigate the remote sensing of phytoplankton, as it is a large shallow water body with a gradient in biogeochemical properties. The specific research aims (as stated in Chapters 1 and 2) are outlined below, with a summary of how these were addressed by the research in this thesis:

*Aim 1: To increase the present understanding of within-lake variations in bio-geo-optical properties and investigate the relationships between (S)IOPs and biogeochemical parameters in context of those reported in ocean, coastal and inland waters.*

The research detailed in this thesis firstly demonstrated the fundamental importance of characterising the bio-geo-optical properties of inland waters, providing the first characterisation of the underwater light climate in Lake Balaton. This research has shown that the (S)IOPs of an optically complex lake can indeed vary significantly across a single water body, particularly as a function of distance from riverine inputs of particulate and dissolved organic matter (Chapter 3). Furthermore, the study of optical properties in Lake Balaton highlighted the distinct relationships between the (S)IOPs and biogeochemical parameters in inland waters, as compared to those reported in coastal and ocean waters. In particular, this research found that particulate inorganic matter is a main driver of the variability in optical properties in this lake (Chapters 3 and 4). Variations in the bio-geo-optical properties are of great significance, as they

were shown in this thesis to have a major impact on the accuracy of phytoplankton pigment concentrations retrieved from semi-analytical and analytical algorithms, through the over-estimation of phytoplankton absorption and under-estimation of Chl-*a* specific absorption coefficients (Chapter 5).

*Aim 2: To investigate the use of satellite remote sensing for retrieval of phytoplankton and cyanobacterial pigments in highly turbid waters by validation of existing algorithms.*

Secondly, the research in this thesis presented the first remote sensing assessment of cyanobacteria biomass in Lake Balaton, using the satellite-based instrument MERIS to retrieve PC concentrations (Chapter 5). This work provided a valuable validation study of the Gons05 algorithm for Chl-*a* retrieval and the Simis05, Mishra13 and Li15 PC retrieval algorithms. Using prior knowledge of the (S)IOPs (Chapters 3 and 4), the research in this thesis elucidated the errors in a semi-analytical algorithm (Gons05), further emphasizing the importance of correctly characterizing the Chl-*a* specific absorption coefficient for accurate pigment retrievals.

*Aim 3: Conduct a multi-scale comparison of coincident remote sensing datasets over a range of spectral and spatial resolutions for the retrieval of phytoplankton biomass in order to understand algorithm transferability between sensors with different capabilities and how this influences the efficacy of the retrieved products.*

Finally, the research in this thesis is the first study to combine four coincident datasets for a comparative study of remote sensing of phytoplankton biomass in an optically complex shallow lake (Chapter 6). The Normalised Difference Chlorophyll Index was successfully implemented for the retrieval of Chl-*a* using four sensors on different platforms (*in situ*, airborne and satellite). This study demonstrated there was minimal difference in median retrieved Chl-*a* values at the different spatial resolutions, therefore there may be little gain in using high spatial resolution data for the purpose of Chl-*a* retrieval, except the ability to resolve the finer spatial structures of phytoplankton distribution in dynamic large lakes. These results underlined the value of using a

“constellation” of sensors at multiple scales for a complete characterisation of the spatial patterns in phytoplankton biomass.

## 7.2 Summary of conclusions

The research presented in this thesis has drawn the following fundamental conclusions, as outlined below for each chapter:

### *Chapter 3 – Spatial variability of absorption coefficients over a biogeochemical gradient in a large and optically complex shallow lake*

- A novel comparison of *in situ* (AC-S and AC-9) and laboratory methods was presented for the measurement of particulate absorption, demonstrating that there was good agreement between laboratory and *in situ*  $a(\lambda)$ .
- Ternary plots identified the relative contribution of phytoplankton, NAP and CDOM to the absorption budget, and these indicated greater variations in the contributions to non-water absorption than reported for ocean waters. The contribution of NAP to non-water absorption in Lake Balaton was higher than that for ocean waters, and the high contribution of NAP and CDOM at 620 and 675 nm (PC and Chl-*a* absorption peaks, respectively) must be considered in bio-optical models for pigment retrieval. NAP and CDOM absorption extends into the red portion of the spectrum, which may cause errors in pigment retrieval if the absorption contributions are not accurately decomposed at these wavelengths.
- The gradient in CDOM, phytoplankton and mineral particles across Lake Balaton was associated with gradients in IOPs, including particulate [ $a_p(\lambda)$ ] and phytoplankton absorption [ $a_{ph}(\lambda)$ ].
- Lower mean  $S_{CDOM}$  values near the inflow of the Zala River indicate the pool of DOC is likely to be dominated by allochthonous material (i.e. terrestrial-influenced).
- Phytoplankton absorption at 620 nm was confirmed to be associated with cyanobacteria biomass, providing evidence for future application of this wavelength in phycocyanin retrieval algorithms.

- There was greater  $a_{ph}(440)$  per unit Chl-*a* than found in ocean waters, and this may be due to the presence of larger celled phytoplankton (microplankton) in Lake Balaton.
- A large amount of scatter in the relationship between  $a_{ph}(440)$  and Chl-*a* was likely associated with a more diverse phytoplankton community, as this relationship is more dependent upon species composition and photophysiology than that at 665 nm.
- The Chl-*a* specific absorption coefficient [ $a^*_{ph}(\lambda)$ ] ranged from 0.017-0.023 m<sup>2</sup> mg<sup>-1</sup> at 440 nm and 0.0088 – 0.011 m<sup>2</sup> mg<sup>-1</sup> at 675 nm, and there was no clear indication of the ‘pigment package effect’ at either absorption maximum (i.e. decreasing  $a^*_{ph}(\lambda)$  over increasing Chl-*a*) as observed in ocean waters.
- The UV peak in phytoplankton absorption in the eastern basins corresponded with decreased CDOM absorption, indicating that cyanobacteria in these basins may compensate for this decrease in CDOM by producing photo-protective pigments, such as MAAs.
- The data showed systematic trends in SIOPs across the basins, with significant differences in  $a^*_{ph}(350)$  and  $S_{CDOM}$  as a function of distance from the Zala River inflow. This is likely to be linked to the variable production of photo-protective pigments.
- The proportion of  $a_{NAP}(\lambda)$  was significantly correlated with PIM, demonstrating the large contribution from inorganic matter to non-algal particulate absorption.
- The differing nature of organic particles which make up the NAP pool in Lake Balaton contributed to the observed variations in  $S_{NAP}$ , particularly for low levels of TSM (<10 mg L<sup>-1</sup>) and  $a_{NAP}(440)$  (<0.1 m<sup>-1</sup>).
- Substantial wind-driven resuspension of sediment was observed on one sampling day, with this process one of the key drivers behind the observed variability in the (S)IOPs in Lake Balaton.

*Chapter 4 – Scattering and backscattering of suspended matter in an optically complex, shallow lake*

- Particulate scattering [ $b_p(\lambda)$ ] was found to account for a very high percentage of the total attenuated light due to particles (maximum of 85-99%), which is consistent with a mineral-dominated water body.

- In contrast with the strong relationship between the particulate attenuation coefficient [ $c_p(660)$ ] and Chl-*a* found in ocean waters,  $c_p(660)$  was strongly correlated to TSM and particularly PIM in Lake Balaton. As most of the variability in lake TSM concentrations was explained by PIM, this again emphasises the strong contribution of the mineral particles to particulate attenuation.
- There was a decline in particulate scattering [ $b_p(531.3)$ ] and particulate attenuation [ $c_p(660)$ ] coefficients alongside diminishing concentrations of Chl-*a*, TSM, POM and phytoplankton and cyanobacteria biomass, although only minimal differences in  $b_{bp}(532)$  were measured across the basins.
- A stronger relationship between particulate scattering and backscattering properties was found with PIM, as opposed to POM. This was a result of the high percentage of minerogenic particles (>50% PIM) across the lake, which have a higher relative refractive index and therefore are more efficient backscatterers than organic particles (e.g. phytoplankton).
- The range of  $b^*_{bp}(532)$  was similar to that recorded in other inland waters (mean =  $0.0146 \pm 0.00199 \text{ m}^2 \text{ g}^{-1}$ , CV=14%), suggesting mass-specific backscattering is driven by the consistently high PIM:TSM ratio across the lake.
- The significant relationship between the particulate backscattering ratio ( $\tilde{b}_{bp}$ ) and POM, Chl-*a* and phytoplankton and cyanobacteria biomass is likely due to the significant variations in organic matter across the basins. Thus, scattering efficiency is driven by changes in the organic particles in Lake Balaton and possibly changes in cell size and composition. For example, small cells are more efficient scatterers than larger cells, and diatoms are more efficient at scattering light than cyanobacteria.
- The significant relationship between  $\tilde{b}_{bp}$  and the Junge coefficient ( $\xi$ ) indicates the strong contribution of particle size on scattering efficiency in Lake Balaton.
- The bulk particle refractive index ( $\bar{n}_p$ ) values in Lake Balaton were higher than other studies on oceans and eutrophic lakes, ranging from 1.15-1.23, and this is likely due to the greater proportion of “hard” inorganic suspended matter (e.g. dolomite) than found in other water bodies.
- The highest  $\bar{n}_p$  values were recorded during a period with significant wind-driven resuspension of sediments, indicating that sediment resuspension causes

an increase in the mean refractive index of the particle assemblage as a result of the higher proportion of suspended minerogenic particles.

- These findings have implications to the accuracy of bio-optical and semi-analytical retrieval algorithms that estimate backscattering coefficients in turbid mineral-dominated waters.

*Chapter 5 – Evaluation of algorithms for retrieval of cyanobacterial pigments in highly turbid, optically complex waters using MERIS data*

- The SCAPE-M\_B2 atmospheric correction was validated with coincident *in situ* water-leaving reflectance data over Lake Balaton.
- Simis05 provided more accurate PC retrievals than more complex bio-optical inversion models (Mishra13 and Li15), which is likely related to the higher concentration of PIM in Lake Balaton than in the calibration datasets used to develop the Mishra13 and Li15 algorithms.
- The Gons05 and Simis05 algorithms retrieved pigment concentrations from MERIS data in Lake Balaton with high accuracy ( $\pm 1$  day:  $RMSE_{\log} < 0.39$ ,  $Bias_{\log} < 0.33$ ,  $MAPE < 151\%$ ).
- Estimated Chl-*a* and PC concentrations from Gons05 and Simis05 could also be partially-validated with total phytoplankton and cyanobacteria biomass, respectively ( $\pm 1$  day:  $R^2 > 0.462$ ,  $p < 0.0001$ ). The latter is likely due to the fact that cyanobacteria biomass is related to PC concentrations in Lake Balaton.
- The ability to retrieve Chl-*a* with Gons05 deteriorated only slightly over the  $\pm 1$  to 7 day temporal window for validation matchups, while a more marked decline in accuracy was noted for PC retrievals with Simis05. This is possibly because the ephemeral spatial dynamics of cyanobacteria (e.g. vertical migration and subsurface maxima) may not be captured by satellite remote sensing if the *in situ* sample is temporally distant from the time of image capture.
- Same-day purpose-collected *in situ* data (August 2010 campaign) unsurprisingly showed the best agreement with MERIS retrieved Chl-*a* and PC concentrations, highlighting the importance of collecting dedicated *in situ* data for validation.
- Mean measured  $a^*_{ph}(665)$  in Lake Balaton was actually lower than the value used in the Gons05 algorithm to retrieve Chl-*a*; however, use of the measured  $a^*_{ph}(665)$  overestimated Chl-*a* by a factor of  $\sim 2$  and was a poorer representation of *in situ* concentrations. This suggests that algorithms need to be tuned

regionally or to different water optical types, including model coefficients for estimation of  $a_{ph}(665)$  and  $a^*_{ph}(665)$  for accurate conversion to Chl-*a*.

- The Gons05 algorithm also over-estimated  $a_{ph}(665)$  compared to the measured values from the August 2010 sampling campaign; however, because the standard algorithm uses a higher  $a^*_{ph}(665)$ , the errors effectively cancelled out and resulted in good agreement between MERIS-retrieved and *in situ* Chl-*a*.
- *In situ* measurements of the  $b_b(\lambda)$  coefficient showed little variation in  $b_b(\lambda)$  between 532 and 650 nm, although  $b_b(\lambda)$  was up to ~30% higher in the blue wavelengths (470 nm). This suggests the assumption of spectrally neutral backscattering for the Gons05 algorithm may be valid in Lake Balaton, however multi- or hyperspectral backscattering measurements would provide improved assessment of this assumption.
- No relationship was found between MERIS retrieved  $b_b(778.75)$  and *in situ*  $b_b(650)$ , suggesting the estimation of  $b_b(778.75)$  by the Gons05 and Simis05 algorithms is a potential source of error to pigment retrievals. However, substitution of the measured  $b_b(650)$  does not appreciably alter the accuracy of Chl-*a* retrievals from Gons05.
- Poor accuracy and high scatter was noted for retrieval of low Chl-*a* concentrations (<10 mg m<sup>-3</sup>) using Gons05. Similar results have been confirmed with other Chl-*a* retrieval algorithms (e.g. NDCI and FLH).
- The Simis05 and Gons05 algorithms may be better considered as part of an ensemble approach, as a single algorithm is unlikely to work in all conditions, even within a single lake system.
- This study proves the effectiveness of collecting IOP measurements alongside pigment and satellite data in order to better analyse and possibly tune the performance of semi-analytical and analytical inversion algorithms.

#### *Chapter 6 – Multi-scale remote sensing observations of water quality in a large, turbid shallow lake*

- The ATCOR4 and MODIS/6S atmospheric corrections were validated with coincident *in situ* water-leaving reflectance data over Lake Balaton for AISA Eagle and Landsat 5 TM data, respectively.
- Chl-*a* was retrieved with low errors using the Normalised Difference Chlorophyll Index (NDCI) for all multi- and hyperspectral datasets, indicating

the utility of the NDCI approach for multiple datasets for monitoring phytoplankton biomass in optically complex lakes. The best agreement with *in situ* concentrations were for the hyperspectral datasets (HyperSAS and AISA Eagle).

- MERIS retrieved Chl-*a* more accurately than Landsat 5 TM, however this is likely due to the fact that Landsat 5 TM has broader spectral bands and is therefore less able to resolve the Chl-*a* absorption feature. Landsat 5 TM also has poorer radiometric resolution than MERIS (8-bit vs. 16-bit) and is thus less capable of distinguishing differences in incoming reflectance.
- There was a marked increase in errors when AISA Eagle data was degraded from 35 to 300 m resolution, while no significant increase in errors was shown for degradation of the Landsat 5 TM data from 30 to 330 m resolution. This may be due to the large bandwidths for Landsat 5 TM, which outweighs differences due to changes in spatial resolution.
- The range of retrieved Chl-*a* concentrations (for match-up with *in situ* stations) increased by over 30% with the degradation of spatial resolution for the Landsat 5 TM dataset (Table 6.5). This may be due to a misinterpretation of shoreline pixels or pixels with high TSM as greater concentrations of Chl-*a*. This exemplifies the loss of ability to detect the subtle heterogeneity in Chl-*a* distribution at coarser spatial resolution.
- All four water-leaving reflectance datasets retrieved Chl-*a* concentrations with high accuracy. Therefore, it may be that high spatial resolution allows for detection of fine structures and heterogeneity in a system, but is not as important as spectral and temporal resolution with regard to more general water quality monitoring purposes in large lakes.

### **7.3 The future of remote sensing for monitoring freshwater phytoplankton**

The operational use of remote sensing for inland waters is becoming a reality, as an increasing number of studies collect bio-geo-optical and remote sensing data over a range of complex water bodies. Recently launched satellite sensors will continue to progress the ability to monitor lakes, particularly the Multispectral Imager (MSI) on board Sentinel-2 and the Ocean and Land Colour Instrument (OLCI) on board Sentinel-3. A list of recently launched and forthcoming instruments relevant to inland water

remote sensing is provided in Table 7.1 [adapted from Tyler et al. (2016)]. The research in this thesis has shown the utility of previous sensors with similar spatial and spectral resolution (e.g. Landsat 5 TM and MERIS) for the retrieval of both bulk phytoplankton (Chl-*a*) and cyanobacteria biomass (PC) from an optically complex lake. Although no longer active, the long-term archives of Landsat and MERIS have proved valuable towards validating and improving in-water algorithms for retrieval of lake water quality parameters, and this work will no doubt continue as more datasets become available for contemporary satellite-based instruments.

**Table 7.1** List of relevant recently launched or forthcoming satellite-based instruments for the remote sensing of inland waters [adapted from Tyler et al. (2016)]. Italicised entries indicate satellite instruments that are not yet launched.

Sensor	Satellite	Spectral Resolution (nm)		Spatial Resolution (m)	Temporal Resolution (days)	Radiometric Resolution
		Spectral range	Number of bands			
ETM	Landsat 7	450-2350	8	10	16	8-bit
Aster	Terra	520-1165	14	15	16	8-bit
OLI	Landsat 8	435-2294	9	15	16	12-bit
CHRIS	Proba-1	415-1050	19	18	7	12-bit
Hyperion	EO-1	400-2500	220	30	16	12-bit
HICO	International Space Station	300-1000	87	100	3	14-bit
VIIRS	NPP and JPSS	402-11,800	22	370	1	12-bit
AVHRR 3	NOAA-18	580-1250	6	1100	1	12-bit
MCI	Sentinel-2	425-1405	13	10, 20 and 60	5	12-bit
OLCI	Sentinel-3	400-1020	21	300	~2	16-bit
<i>HSI</i>	<i>EnMAP</i>	<i>420-1000</i>	<i>89 (VNIR)</i>	<i>30</i>	<i>4</i>	<i>14-bit</i>
<i>Ocean Ecosystem Spectrometer/Radiometer</i>	<i>PACE</i>	<i>350-800, 865,940-2250</i>	<i>5 nm resolution (350-800)</i>	<i>1000</i>	<i>2</i>	<i>?</i>
<i>VSWIR Imaging Spectrometer</i>	<i>HypIRI</i>	<i>380-2500</i>	<i>212 (VSWIR)</i>	<i>60</i>	<i>19</i>	<i>14-bit</i>
<i>Not yet selected</i>	<i>GEO-CAPE</i>	<i>Possibly hyperspectral</i>		<i>375</i>	<i>Geostationary (95°-100°W)</i>	<i>?</i>

However, there remain significant challenges to the development of accurate remote sensing products from inland waters, and future research should focus on these elements. Firstly, there continues to be a need for further characterisation of the bio-geo-optical properties, with respect to seasonal and spatial differences between and within water bodies. The full range of (S)IOP values must be considered in bio-optical models for the inversion of phytoplankton pigments in order to avoid significant uncertainties in retrieved values. The research in this thesis highlighted that the (S)IOPs can vary significantly within a large lake, as well as quantified the differences in (S)IOPs in lakes as compared to marine waters (Chapters 3 and 4). This research further identified the impact (S)IOP estimates have in a semi-analytical model for pigment retrieval, emphasizing the importance of correctly parameterising these coefficients in order to obtain accurate phytoplankton pigment products (Chapter 5). However, Lake Balaton is a case study for a water body in which optical properties are primarily driven by resuspended inorganic particulates, therefore it is pertinent to continue to characterise the spatio-temporal differences in (S)IOPs across and within other optically complex inland waters. This research contributes towards the progression of analytical algorithms that use estimates of absorption and scattering coefficients for pigment retrieval in optically complex waters, although it has recently been acknowledged that a comprehensive understanding of the sources and magnitude of the variability in (S)IOPs for inland waters is still required (Mouw et al., 2015, Palmer et al., 2015b, Tyler et al., 2016). Ultimately, improved knowledge of the variability in the bio-geo-optical properties of inland waters can both: 1) reduce the associated errors for pigment retrieval using semi-analytical and analytical algorithms and 2) assist with the algorithm selection process, in order to facilitate the most appropriate choice for a water body with a specified range of optical properties.

Secondly, there needs to be a more unified and systematic approach for the remote sensing of inland waters. There has been a large increase in the number of algorithms developed for lakes and coastal waters since the designation of this research area as a priority by the International Ocean Colour Coordinating Group (IOCCG, 2000). However, many algorithms are site-specific or have yet to be tested independently on other inland water types or with other satellite datasets. In fact, the research presented in this thesis has implications for algorithm application in large shallow lakes with biogeochemical gradients (e.g. Lake Balaton), and calls into question whether a sole algorithm for constituent extraction is even suitable across a

single lake. For example, large lakes with variable biogeochemistry may require basin-specific remote sensing algorithms for accurate parameter retrieval (Campbell et al., 2011). It has been recently recommended that a “menu” style approach may prove useful, where the most appropriate algorithm(s) can be selected for retrieval in certain lake types with specific ranges of (S)IOPs and biogeochemical parameters (Mouw et al., 2015). In this case, a more coordinated algorithm comparison effort is required to clearly identify the strengths and limitations of each model. Alongside coincident collection of bio-geo-optical properties, such work would help establish the applicability and quantify uncertainties of each algorithm within each optical water type or class. The research in this thesis confirmed the effectiveness of collecting IOP measurements alongside pigment and satellite data in order to analyse the performance of analytical algorithms (Chapter 5). However, there remain abundant opportunities for similar work to enable more informed decisions on the parameterisation of models (e.g. via optical classification) in order to improve the accuracy of pigment retrieval and achieve model transferability among inland waters. There is a need for future work to determine the ability for current algorithms to accurately retrieve water quality parameters using both the past satellite data archive (e.g. Landsat and MERIS) and present and recently launched instruments (e.g. MSI and OLCI) in a range of inland waters, given the technological constraints of contemporary satellite instruments (i.e. spatial, spectral, radiometric and temporal resolutions).

Lastly, this research highlights the value of cross-comparisons of remote sensing instruments, algorithms and correction procedures. It has been widely recognised that there is a need for further validation of atmospheric and adjacency corrections over inland waters, as these can form a major source of uncertainty in the retrieval of water quality parameters, as also demonstrated by Palmer et al. (2015b). This thesis validates novel atmospheric corrections for MERIS (Chapter 5), Landsat 5 TM and AISA Eagle (Chapter 6) data. However, many atmospheric corrections have been developed for use over land or oceans and have yet to be proven useful over inland waters. Additionally, the comparative research in this thesis highlights that phytoplankton pigment retrieval algorithms may be instrument-specific and do not retrieve pigment concentrations as accurately when applied to other instruments (e.g. NDCI and Landsat 5 TM; Chapter 6). Further studies investigating multi-scale observations may also help to address the needs of future satellite missions. For example, in this thesis it was observed that all four water-leaving reflectance datasets (MERIS, Landsat 5 TM, AISA Eagle and *in situ*

radiometry) could retrieve Chl-*a* concentrations with high accuracy. It may be that high spatial resolution data allow for detection of fine structures and heterogeneity in a system, but are not vital with regard to more general water quality monitoring purposes (i.e. monitoring lake median Chl-*a* concentration). Therefore, perhaps more emphasis should be placed on appropriate spectral resolutions to capture the phytoplankton pigment absorption features (e.g. 620 nm for PC) and high temporal resolution datasets to capture the ephemeral nature of cyanobacteria blooms in inland waters. Such studies are needed to help resolve the optimal capabilities for future coastal and inland satellite missions and prioritise future investments.

Although there remain challenges to the accurate remote sensing of inland waters, these shortcomings are already being addressed within the research community. New earth observation missions are in place to continue to provide data for use over inland waters, such as the European Space Agency's Copernicus programme. In fact, the Sentinel-3A satellite was very recently launched on 6 February 2016. This satellite is the first of two that will carry the Ocean and Land Color Instrument (OLCI), which continues the 300 m resolution global coverage for inland waters that began with the MERIS instrument on-board Envisat (active from 2002-2013). Future missions are planned for the launch of hyperspectral and/or high spatial resolution satellite instruments (e.g. EnMap, PACE, HypSPIRI, GEO-CAPE), which will improve the capacity to detect and map the dynamic distribution of phytoplankton in lakes. Furthermore, many planned and recently launched satellite sensors have bands in the near infrared, specifically aimed at improving atmospheric correction over inland water bodies (Tyler et al., 2016). Advancements are also occurring in the testing and development of atmospheric correction of satellite data over turbid waters, e.g. (Jaelani et al. 2015). Additionally, there are ongoing validation efforts of current Chl-*a* retrieval algorithms (Dalu et al., 2015, Lyu et al., 2015, Feng et al., 2015, Palmer et al., 2015c, Lesht et al., 2016, Ali & Ortiz, 2016) and an increasing number of studies testing and developing PC algorithms over inland waters (Duan et al., 2012, Lyu et al., 2013, Sun et al., 2013, Qi et al., 2014, Torbick & Corbiere, 2015, Kudela et al., 2015, Sun et al., 2015, Li et al., 2015). Coordinated efforts are also emerging to further data availability and establish a strategy for implementing global water quality monitoring. For example, LIMNADES (Lake Bio-optical Measurements and Matchup Data for Remote Sensing; [www.globolakes.ac.uk/limnades](http://www.globolakes.ac.uk/limnades)) is a recently launched online database of (S)IOP and biogeochemical data which aims to increase access to matchup data for

algorithm development and validation over lakes. Thus, advancements in spaceborne technology, improved atmospheric corrections, continued validation of phytoplankton pigment retrieval algorithms and a coordinated effort to collect bio-geo-optical information will assist the inland water remote sensing community towards the goal of operational monitoring. Despite the challenges that remain, the future of inland water remote sensing is positive and the potential for operational monitoring is real.

## 8 Appendix – Supplementary Methods

---

### 8.1 August 2010 field campaign on Lake Balaton

#### 8.1.1 Details of the campaign

The August 2010 field campaign on Lake Balaton forms the fundamental dataset applied in this thesis for investigation of bio-geo-optical properties and remote sensing of inland waters [funded by the National Environmental Research Council (NERC) Airborne Research and Survey Facility (ARSF) with *in situ* optics provided by an equipment grant from NERC Field Spectroscopy Facility (FSF) (Loan ref EU10-03)]. The work presented in this thesis is built on the campaign in August 2010 aimed at collecting a coincident dataset of multi-spectral satellite, hyperspectral airborne, and *in situ* radiometric, bio-optical and biogeochemical data for the purposes of testing and developing remote sensing retrieval algorithms on Lake Balaton.

Coincident with this project, the European Facility for Airborne Research (EUFAR) funded collection of laser scanning (LiDAR) altimetry point-cloud data over the lake and shoreline. These LiDAR and airborne hyperspectral data (AISA) have been recently used for the mapping of aquatic vegetation (Zlinszky et al., 2012), monitoring wetland vegetation health and species type (Stratoulas et al., 2015a) and assessment of simulated Sentinel-2 data for lakeshore habitat mapping (Stratoulas et al., 2015b).

#### 8.1.2 Instrument specifications

The sensors applied in this PhD thesis include the satellite-based instruments MERIS and Landsat 5 TM (Thematic Mapper) (Table 8.1). Although no longer operational, these instruments have a strong heritage in inland water remote sensing and provide continuity with current and forthcoming instruments. The MERIS data archive remains immensely useful for algorithm development and validation studies, particularly because the Ocean and Land Colour Instrument (OLCI) on the European Space Agency's recently launched Sentinel-3 satellite will continue the global coverage at 300 m resolution and has a strong MERIS heritage. Fundamental to the study of freshwater cyanobacteria blooms, MERIS also had a spectral band centered at 620 nm near the PC absorption maximum, and OLCI will additionally have this band.

The Landsat series of satellite-based instruments were first launched in 1972 and are still in operation today, thus providing a longstanding chronicle of data. A Landsat 5 TM overpass corresponded to the August 2010 survey of Lake Balaton, although the Ocean and Land Instrument (OLI) onboard Landsat 8 is the most recently launched of the Landsat series (2013). In addition to the large archive, the higher spatial resolution (30 m pixel size) is a benefit to using Landsat data. However, as Landsat instruments were developed for terrestrial applications, these advantages are offset by the lower spectral resolution. Regardless, Landsat has been used to successfully retrieve water clarity (McCullough et al., 2013), total suspended matter (Torbick et al., 2013, Wu et al., 2015), Chl-*a* (Tebbs et al., 2013), phytoplankton group indicators (Torbick et al., 2013) and estimates of CDOM (Kutser, 2012, Brezonik et al., 2015).

Additionally, this thesis includes an airborne survey conducted with the Airborne Imaging Spectrometer for Applications (AISA) Eagle sensor, as this was the available hyperspectral sensor onboard the NERC ARSF aircraft at the time of the survey (August 2010; Table 8.1). However, it is noted that NERC ARSF have now replaced AISA Eagle with the AisaFENIX. The AISA Eagle is a hyperspectral 12-bit pushbroom sensor, with a spectral range of 400-970 nm and maximum spectral resolution of 2.9 nm. The use of this sensor enables acquisition of high spatial resolution, hyperspectral data, which is invaluable to testing and developing retrieval algorithms for inland waters. These data may better capture the heterogeneity in shallow waters, which satellite instruments may not adequately characterise.

Lastly, *in situ* radiometry was performed using the HyperSAS, a system comprised of three hyperspectral radiometers. The radiometers measure downwelling irradiance [ $E_s(\lambda)$ ], surface radiance of the water [ $L_t(\lambda)$ ] and sky radiance [ $L_{sky}(\lambda)$ ], from which water-leaving radiance [ $L_w(\lambda)$ ] and remote sensing reflectance [ $R_{rs}(\lambda)$ ] can be calculated. These *in situ* reflectance data were primarily measured in order to validate the atmospheric correction algorithms for satellite and airborne instruments.

**Table 8.1** Details of sensors investigated in this study.

Sensor	Sensor Type	No. of Bands	Spectral range (nm)	Spatial resolution (m)	Revisit time (days)
AISA Eagle	Airborne	253	400-970	5	N/A
Landsat 5 TM	Satellite	6 <sup>a</sup>	450-2350	30	16
MERIS	Satellite	15	390-1040	300	3
HyperSAS	<i>in situ</i> radiometry	137	350-800	N/A	N/A

<sup>a</sup> Landsat 5 TM images consist of 7 bands, however Band 6 is a thermal band sampled at 120 m resolution.

The *in situ* optics used in this thesis included a WET Labs AC-S, AC-9 and ECO-BB3 (Table 8.2). The AC-9 and AC-S are spectrophotometers which measure spectral absorption and attenuation at 9 and 84 wavelengths, respectively. These *in situ* measurements are used to supplement the laboratory measurements of absorption, and a comparison of *in situ* and laboratory methods is provided in Chapter 3. Combined with laboratory measurements of particulate and CDOM absorption, the total non-water attenuation can also be attributed to the relative contributions from  $b_p(\lambda)$ ,  $a_{CDOM}(\lambda)$  and  $a_p(\lambda)$  (see Chapter 4).

Measurement of optical backscattering was conducted with a WET Labs ECO-BB3 (Table 8.2). These *in situ* data provided the basis for the results in Chapter 4. The ECO-BB3 measures backscattering at the key wavelength of 532 nm, at which the literature typically reports the particulate backscattering and scattering coefficients and backscattering ratio. However, it is noted that the latest instrument from WET Labs, the ECO-BB9, measures at 9 wavelengths to allow for measurement of backscattering over a wider spectral range.

**Table 8.2** Details of *in situ* optical sensors investigated in this study.

Sensor	Type	No. of bands	Spectral range (nm)
AC-S	Absorption and Attenuation Spectrometer	84	400-730
AC-9	Absorption and Attenuation Spectrometer	9	412-715
ECO-BB3	Backscattering	3	470, 532, 650

## 8.2 Algorithms examined in Chapters 5 and 6

### 8.2.1 Gons05 (Chlorophyll-*a*)

Using a commonly acknowledged relationship between inherent optical properties and reflectance (Gordon et al., 1975), backscattering is assumed to be spectrally neutral and is derived from a single wavelength in the near infra-red (NIR) (Gons, 1999), as detailed in Gons et al. (2005):

$$b_b(779) = \frac{1.61 \times R_{rs}(779)}{0.082 - 0.6 \times R_{rs}(779)} \quad (8.1)$$

Total absorption at a particular wavelength can then be calculated from a reflectance ratio [ $R_{rs}(\lambda_1)/R_{rs}(\lambda_2)$ ],  $b_b$  and absorption at  $\lambda_2$  [ $a(\lambda_2)$ ]:

$$a(\lambda_1) = \frac{R_{rs}(\lambda_2)}{R_{rs}(\lambda_1)} \times [a(\lambda_2) + b_b] - b_b \quad (8.2)$$

where the reflectance ratio of  $\lambda_1=665$  nm and  $\lambda_2=709$  nm is effective for retrieval of Chl-*a* (Mittenzwey et al., 1992, Dekker, 1993, Gons et al., 2002). A correction factor,  $\gamma$ , was introduced by Simis et al. (2005) to relate the  $R_{rs}$  ratio to measured pigment absorption, thus obtaining the Gons05 algorithm for Chl-*a* absorption, modified from Gons et al. (2002, 2005):

$$a_{Chla}(665) = \left[ \left( \frac{R_{rs}(709)}{R_{rs}(665)} \times (a_w(709) + b_b) - b_b - a_w(665) \right) \right] \times \gamma^{-1} \quad (8.3)$$

where  $a_w(709)=0.727$  m<sup>-1</sup>,  $a_w(665) = 0.401$  m<sup>-1</sup> and  $\gamma=0.68$ .

Finally, the concentration of Chl-*a* can then be calculated by dividing the solutions to equation (8.3) by the specific absorption coefficient,  $a^*_{Chla}(665)$ :

$$[Chl - a] = \frac{a_{Chla}(665)}{a^*_{Chla}(665)} \quad (8.4)$$

where  $a^*_{Chla}(665)$  is 0.0139 m<sup>2</sup>mg<sup>-1</sup> for uncorrected Chl-*a* (Gons et al., 2005).

### 8.2.2 Simis05 (Phycocyanin)

The semi-empirical, nested band-ratio algorithm developed by Simis et al. (2005, 2007) evolved from the Chl-*a* retrieval algorithm initially presented by Gons (1999) with updated coefficients in Gons et al. (2002, 2005). As in the Gons05 algorithm, the backscattering coefficient is estimated in the NIR (Equation 8.1). However, for PC retrieval,  $\lambda_1=620$  nm and  $\lambda_2=709$  nm is applied for the reflectance ratio in Equation 8.2 (Simis et al., 2005).

It is assumed that PC and Chl-*a* comprise absorption at 620 nm, as apparent from reflectance spectra of cyanobacteria-dominated waters. Thus, in order to estimate PC absorption alone at this wavelength, summative pigment absorption at 620 nm is calculated first. A factor  $\delta$  is introduced for the correction of  $a(620)$ , and the summed absorption of PC and Chl-*a* at 620 nm is estimated as:

$$a_{chl-a}(620) + a_{pc}(620) = \left[ \frac{R_{rs}(709)}{R_{rs}(620)} \times (a_w(709) + b_b) - b_b - a_w(620) \right] \times \delta^{-1} \quad (8.5)$$

where  $a_w(620)=0.281 \text{ m}^{-1}$  and  $\delta=0.84$ .

Absorption by PC can then be derived by subtracting the absorption by Chl-*a* at 620 nm, using a conversion factor  $\varepsilon$ , which relates *in vivo* absorption by Chl-*a* at 665 nm to its absorption at 620 nm:

$$a_{pc}(620) = \left[ \frac{R_{rs}(709)}{R_{rs}(620)} \times (a_w(709) + b_b) - b_b - a_w(620) \right] \times \delta^{-1} - (\varepsilon \times a_{chl-a}(665)) \quad (8.6)$$

where  $\varepsilon = 0.24$ .

Finally, the concentration of pigment can then be calculated by dividing the solution to equation (8.6) by the specific absorption coefficient,  $a^*_{pc}(620)$ :

$$[PC] = \frac{a_{pc}(620)}{a^*_{pc}(620)} \quad (8.7)$$

where  $a^*_{pc}(620)$  is  $0.007 \text{ m}^2\text{mg}^{-1}$ , respectively (Simis et al., 2007).

### 8.2.3 Mishra13 (Phycocyanin)

The Mishra13 inversion algorithm was applied for PC retrieval as in Mishra et al. (2013), which is an extension of the quasi-analytical (QAA) for Chl-*a* retrieval developed by Lee et al. (2002). However, the wavelengths used were adapted to coincide with MERIS band centers. The steps for retrieval of PC concentration using the Mishra13 algorithm as applied in this thesis are summarised below.

Above surface remote sensing reflectance ( $R_{rs}$ ) is first converted to subsurface remote sensing reflectance ( $r_{rs}$ ) using the following equation:

$$r_{rs} = R_{rs} / (0.52 + 1.7R_{rs}) \quad (8.8)$$

$r_{rs}$  is a function of  $u$ , which is defined as the ratio of the backscattering coefficient ( $b_b$ ) to the sum of total absorption ( $a$ ) and backscattering coefficients:

$$u(\lambda) = \frac{b_b(\lambda)}{a(\lambda) + b_b(\lambda)} \quad (8.9)$$

$u$  is then empirically derived from  $r_{rs}$  as in Gordon et al. (1988):

$$u(\lambda) = \frac{-g_0 + \sqrt{(g_0)^2 + 4g_1 r_{rs}(\lambda)}}{2g_1} \quad (8.10)$$

where  $g_0=0.089$  and  $g_1=0.125$ .

Total absorption coefficients can then be estimated at a reference wavelength ( $\lambda_0$ ) as a function of the absorption coefficient of water [ $a_w(709)$ ]:

$$a(\lambda_0) = a_w(709) + 10^{-0.8125 - 2.3404\chi + 1.24\chi^2} \quad (8.11)$$

where  $\lambda_0=708$  nm, as parameterised for turbid and productive waters in Mishra et al. (2014),  $a_w(709)=0.7204$  and

$$\chi = \log_{10} \left( \frac{0.01 * r_{rs}(442.5) + r_{rs}(620)}{r_{rs}(708.75) + 0.005 * \frac{r_{rs}(620)}{r_{rs}(442.5)} * r_{rs}(620)} \right) \quad (8.12)$$

Next, the particulate backscattering coefficient at the reference wavelength [ $b_{bp}(\lambda_0)$ ] is retrieved as follows:

$$b_{bp}(\lambda_0) = \frac{u(\lambda_0)a(\lambda_0)}{1-u(\lambda_0)} - b_{bw}(\lambda_0) \quad (8.13)$$

The particulate backscattering coefficients at other wavelengths [ $b_{bp}(\lambda)$ ] are then estimated from  $b_{bp}(\lambda_0)$ :

$$b_{bp}(\lambda) = b_{bp}(\lambda_0) \left( \frac{\lambda_0}{\lambda} \right)^\eta \quad (8.14)$$

where the spectral power,  $\eta$ , is empirically estimated as:

$$\eta = 2.0 \left\{ 1 - 1.2 \exp \left[ -0.9 \frac{r_{rs}(442.5)}{r_{rs}(560)} \right] \right\} \quad (8.15)$$

The total absorption coefficient [ $a(\lambda)$ ] can thus be calculated as:

$$a(\lambda) = \frac{(1-u(\lambda))(b_{bw}(\lambda) + b_{bp}(\lambda))}{u(\lambda)} \quad (8.16)$$

The total absorption coefficient is then further decomposed into the combined absorption by coloured dissolved organic matter (CDOM) and detrital matter [ $a_{CDM}(\lambda)$ ] and phytoplankton absorption [ $a_{ph}(\lambda)$ ]:

$$a_{CDM}(443) = \frac{[a(412.5) - \zeta a(442.5)] - [a_w(411) - \zeta a_w(411)]}{\xi - \zeta} \quad (8.17)$$

where

$$\zeta = \frac{a_{ph}(411)}{a_{ph}(443)} = 0.74 + \frac{0.2}{0.8 + r_{rs}(442.5)/r_{rs}(560)}, \quad (8.18)$$

$$\xi = \frac{a_{CDM}(411)}{a_{CDM}(443)} = e^{S(443-411)} \quad (8.19)$$

and  $a_w(411)=0.0068$ .

$a_{CDM}(\lambda)$  can then be calculated using the exponential function:

$$a_{CDM}(\lambda) = a_{CDM}(443) e^{-S(\lambda-443)} \quad (8.20)$$

where the slope  $S$  is 0.02.  $a_{ph}(\lambda)$  is subsequently calculated by subtraction of  $a_w(\lambda)$  and  $a_{CDM}(\lambda)$  from total absorption:

$$a_{ph}(\lambda) = a(\lambda) - a_w(\lambda) - a_{CDM}(\lambda) \quad (8.21)$$

It is assumed that  $a_{ph}(\lambda)$  is approximately equal to absorption by chlorophyll- $a$  and phycocyanin [ $a_{ph}(\lambda) \approx a_{chl}(\lambda) + a_{pc}(\lambda)$ ] at  $\lambda=665$  and 620 nm, and  $a_{pc}(620)$  is retrieved as:

$$a_{pc}(620) = \frac{\psi_1 a_{ph}(620) - a_{ph}(665)}{\psi_1 - \psi_2} \quad (8.22)$$

where  $\psi_1 = a_{chl}(665)/a_{chl}(620)$  and  $\psi_2 = a_{pc}(665)/a_{pc}(620)$ .

Finally, PC concentrations are calculated by dividing  $a_{pc}(620)$  by the specific absorption coefficient of PC,  $a^*_{pc}(620)$ :

$$PC(mg\ m^{-3}) = \frac{a_{pc}(620)}{a^*_{pc}(620)} \quad (8.23)$$

For the application of Mishra13 in this thesis (Chapter 5), PC concentration was calculated using two different values of  $a^*_{pc}(620)$  from Simis et al. (2005) and Mishra et al. (2013) (0.007 and 0.0048  $m^2\ mg^{-1}$ , respectively).

#### 8.2.4 Li15 (Chlorophyll- $a$ )

The Li15 algorithm is an extension of the IIMIW model presented in Li et al. (2013) for the retrieval of Chl- $a$ . The steps for the application of the Li15 algorithm used in this thesis are as in Table 3 of Li et al. (2015), with wavelengths adapted to correspond with MERIS band centers, and are summarised below.

Above surface remote sensing reflectance ( $R_{rs}$ ) is first converted to subsurface remote sensing reflectance ( $r_{rs}$ ) using the following equation, as in Li et al. (2015):

$$r_{rs} = R_{rs}/0.54 \quad (8.24)$$

The backscattering coefficient at MERIS band 12 [ $b_b(778.75)$ ] is then estimated as a function of  $r_{rs}(778)$  and absorption by pure water [ $a_w(778)$ ]:

$$b_b(778.75) = \frac{r_{rs}(778.75)a_w(778)}{0.082 - r_{rs}(778.75)} \quad (8.25)$$

The spectral power,  $\eta$ , is empirically estimated as:

$$\eta = 2.0 \left\{ 1 - 1.2 \exp \left[ -0.9 \frac{r_{rs}(442.5)}{r_{rs}(560)} \right] \right\} \quad (8.26)$$

The particulate backscattering coefficient at 560 nm [ $b_{bp}(560)$ ] can then be retrieved as follows:

$$b_{bp}(560) = [b_{bp}(778.75) - b_{bw}(778.75)]/(0.7198)^\eta \quad (8.27)$$

and the backscattering coefficients at other wavelengths [ $b_b(\lambda)$ ] are then estimated from  $b_{bp}(560)$ :

$$b_b(\lambda) = b_{bp}(560) \left(\frac{560}{\lambda}\right)^\eta + b_{bw}(\lambda) \quad (8.28)$$

Subsequently, total minus water absorption [ $a_{t-w}(\lambda)$ ], or absorption of particulate ( $p$ ) and dissolved ( $g$ ) matter [ $a_{pg}(\lambda)$ ], can be calculated as:

$$a_{t-w}(\lambda) = \frac{r_{rs}(708.75)b_b(\lambda)[a_w(708.75)+b_b(708.75)]}{r_{rs}(\lambda)b_b(708.75)} - b_b(\lambda) - a_w(\lambda) \quad (8.29)$$

At this point in the algorithm steps, Chl- $a$  concentration can be estimated using three different approaches, as outlined in Li et al. (2013). Total absorption is further partitioned into  $a_{CDM}(\lambda)$  and  $a_{ph}(\lambda)$  by first calculating the *in vivo* phytoplankton absorption without the contribution from PC [ $a_{ph-pc}(\lambda)$ ]:

$$a_{ph-pc}(\lambda) = 1.1872C1(\lambda)a_{t-w}(665) + C2(\lambda) \quad (8.30)$$

where C1 and C2 are the wavelength dependent regression coefficients outlined in Table B1 of Appendix B in Li et al. (2015).

The combined absorption of CDOM, NAP and PC [ $a_{CDM+pc}(\lambda)$ ] is then calculated by subtraction:

$$a_{CDM+pc}(\lambda) = a_{t-w}(\lambda) - a_{ph-pc}(\lambda) \quad (8.31)$$

Absorption by CDM [ $a_{CDM}(\lambda)$ ] can then be calculated using the spectral slope of CDM ( $S_{CDM}$ ):

$$a_{CDM}(\lambda) = a_{CDM}(412.5)\exp[-S_{CDM} \times (\lambda - 412.5)] \quad (8.32)$$

where it is assumed  $a_{CDM}(412.5)=a_{CDM+pc}(412.5)$  and  $S_{CDM}$  is set to  $0.020 \text{ nm}^{-1}$ , the mean measured value of  $S_{CDM}$  for Lake Balaton in 2010.  $a_{CDM}(708.75)$  is set to 0, with  $a_{CDM}(\lambda)$  values adjusted accordingly.

The phytoplankton absorption coefficients [ $a_{ph}(\lambda)$ ] can then be calculated by subtraction:

$$a_{ph}(\lambda) = a_{t-w}(\lambda) - a_{CDM}(\lambda) \quad (8.33)$$

The phycocyanin absorption coefficient [ $a_{pc}(620)$ ] is then calculated as the difference between phytoplankton absorption and non-PC phytoplankton absorption at 620 nm:

$$a_{pc}(620) = a_{ph}(620) - a_{ph-pc}(620) \quad (8.34)$$

Finally, PC concentration is calculated by division of  $a_{pc}(620)$  by the PC specific absorption coefficient [ $a^*_{pc}(620)$ ]:

$$PC (mg m^{-3}) = a_{pc}(620)/a^*_{pc}(620) \quad (8.35)$$

where  $a^*_{pe}(620)$  is set to either  $0.0046 \text{ m}^2\text{mg}^{-1}$  as in Li et al. (2015) or  $0.007 \text{ m}^2\text{mg}^{-1}$  as in Simis et al. (2005).

### 8.2.5 Normalized Difference Chlorophyll Index, NDCI (Chlorophyll-*a*)

The Normalized Difference Chlorophyll Index (NDCI) was proposed by Mishra and Mishra (2012) to estimate Chl-*a* concentration in turbid productive waters. NDCI was designed to use water-leaving reflectance at the MERIS bands centered at 665 nm and 708 nm. However, it is also easily employed for Landsat 5 TM data, using bands 3 (630-690 nm) and 4 (760-900 nm), which is why it was chosen for use in this comparative study. Thus, the NDCI uses the reflectance peak at ~708 nm which is maximally sensitive to variations in Chl-*a*, as well as the spectral absorption peak of Chl-*a* at ~665-675 nm, via the following equation:

$$[Chl - a] \propto \frac{[\rho_w(708) - \rho_w(665)]}{[\rho_w(708) + \rho_w(665)]} \quad (8.36)$$

NDCI was subsequently fit against measured Chl-*a* using an exponential equation as this was found to be a better fit than linear or polynomial regressions:

$$[Chl-a] = A e^{b \cdot NDCI} \quad (8.37)$$

The resulting exponential fit was then applied to obtain retrieved Chl-*a* concentrations.

### 8.3 Definitions of error metrics

Where  $\hat{C}_i$  is the measured concentration and  $C_i$  is the estimated concentration, the following error metrics are defined as:

**Root Mean Square Error (RMSE):**

$$RMSE = \sqrt{\frac{1}{N} \sum_{i=1}^N (\hat{C}_i - C_i)^2}$$

**Log Root Mean Square Error (RMSE<sub>log</sub>):**

$$RMSE_{log} = \sqrt{\frac{1}{N} \sum_{i=1}^N (\log \hat{C}_i - \log C_i)^2}$$

**Mean Average Percent Error (MAPE):**

$$MAPE(\%) = \frac{1}{N} \sum_{i=1}^N \left| \frac{\hat{C}_i - C_i}{\hat{C}_i} \right| \times 100$$

**Bias:**

$$Bias = \frac{1}{N} \sum_{i=1}^N (\hat{C}_i - C_i)$$

**Log of Bias (Bias<sub>log</sub>):**

$$Bias_{log} = \frac{1}{N} \sum_{i=1}^N (\log \hat{C}_i - \log C_i)$$

**Mean ( $\mu$ ):**

$$\mu = \frac{1}{N} \sum_{i=1}^N C_i$$

**Standard Deviation ( $\sigma$ ):**

$$\sigma = \sqrt{\frac{1}{N} \sum_{i=1}^N (C_i - \mu)^2}$$

**Coefficient of Variation (CV):**

$$CV(\%) = \left( \frac{\sigma}{\mu} \right) \times 100$$

## 9 References

---

- Adrian, R., O'Reilly, C.M., Zagarese, H., Baines, S.B., Hessen, D.O., Keller, W., et al. (2009). Lakes as sentinels of climate change. *Limnology and Oceanography*, *54*, 2283-2297
- Agha, R., Cirés, S., Wörmer, L., Antonio Domínguez, J., & Quesada, A. (2012). Multi-scale strategies for the monitoring of freshwater cyanobacteria: Reducing the sources of uncertainty. *Water research*, *46*, 3043-3053
- Ali, K.A., & Ortiz, J.D. (2016). Multivariate approach for chlorophyll-a and suspended matter retrievals in Case II type waters using hyperspectral data. *Hydrological Sciences Journal-Journal Des Sciences Hydrologiques*, *61*, 200-213
- Ammenberg, P., Flink, P., Lindell, T., Pierson, D., & Strombeck, N. (2002). Bio-optical modelling combined with remote sensing to assess water quality. *International Journal of Remote Sensing*, *23*, 1621-1638
- Anderson, D.M., Glibert, P.M., & Burkholder, J.M. (2002). Harmful algal blooms and eutrophication: Nutrient sources, composition, and consequences. *Estuaries*, *25*, 704-726
- Antenucci, J., Ghadouani, A., Burford, M., & Romero, J. (2005). The long-term effect of artificial destratification on phytoplankton species composition in a subtropical reservoir. *Freshwater Biology*, *50*, 1081-1093
- Antunes, J.T., Leao, P.N., & Vasconcelos, V.M. (2015). *Cylindrospermopsis raciborskii*: review of the distribution, phylogeography, and ecophysiology of a global invasive species. *Frontiers in Microbiology*, *6*, 473
- Aplin, P. (2005). Remote sensing: ecology. *Progress in Physical Geography*, *29*, 104-113
- Astoreca, R., Doxaran, D., Ruddick, K., Rousseau, V., & Lancelot, C. (2012). Influence of suspended particle concentration, composition and size on the variability of

- inherent optical properties of the Southern North Sea. *Continental Shelf Research*, 35, 117-128
- Aurin, D.A., Dierssen, H.M., Twardowski, M.S., & Roesler, C.S. (2010). Optical complexity in Long Island Sound and implications for coastal ocean color remote sensing. *Journal of Geophysical Research-Oceans*, 115, C07011
- Aurin, D., Mannino, A., & Franz, B. (2013). Spatially resolving ocean color and sediment dispersion in river plumes, coastal systems, and continental shelf waters. *Remote Sensing of Environment*, 137, 212-225
- Ayoub, L.M., Hallock, P., Coble, P.G., & Bell, S.S. (2012). MAA-like absorbing substances in Florida Keys phytoplankton vary with distance from shore and CDOM: Implications for coral reefs. *Journal of experimental marine biology and ecology*, 420, 91-98
- Baban, S. (1993). Detecting Water-Quality Parameters in the Norfolk Broads, Uk, using Landsat Imagery. *International Journal of Remote Sensing*, 14, 1247-1267
- Babin, M., Morel, A., Fournier-Sicre, V., Fell, F., & Stramski, D. (2003a). Light scattering properties of marine particles in coastal and open ocean waters as related to the particle mass concentration. *Limnology and Oceanography*, 48, 843-859
- Babin, M., Stramski, D., Ferrari, G., Claustre, H., Bricaud, A., Obolensky, G., et al. (2003b). Variations in the light absorption coefficients of phytoplankton, nonalgal particles, and dissolved organic matter in coastal waters around Europe. *Journal of Geophysical Research-Oceans*, 108, 3211
- Balogh, K., Voros, L., Toth, N., & Bokros, M. (2003). Changes of organic matter quality along the longitudinal axis of a large shallow lake (Lake Balaton). *Hydrobiologia*, 506, 67-74
- Barlow, R., Cummings, D., & Gibb, S. (1997). Improved resolution of mono- and divinyl chlorophylls a and b and zeaxanthin and lutein in phytoplankton extracts using reverse phase C-8 HPLC. *Marine Ecology Progress Series*, 161, 303-307

- Baron, J.S., Poff, N.L., Angermeier, P.L., Dahm, C.N., Gleick, P.H., Hairston, N.G., et al. (2002). Meeting ecological and societal needs for freshwater. *Ecological Applications*, *12*, 1247-1260
- Bastviken, D., Tranvik, L.J., Downing, J.A., Crill, P.M., & Enrich-Prast, A. (2011). Freshwater Methane Emissions Offset the Continental Carbon Sink. *Science*, *331*, 50-50
- Becker, R.H., Sultan, M.I., Boyer, G.L., Twiss, M.R., & Konopko, E. (2009). Mapping cyanobacterial blooms in the Great Lakes using MODIS. *Journal of Great Lakes Research*, *35*, 447-453
- Beeri, O., & Phillips, R.L. (2007). Tracking palustrine water seasonal and annual variability in agricultural wetland landscapes using Landsat from 1997 to 2005. *Global Change Biology*, *13*, 897-912
- Bertilsson, S., & Tranvik, L. (2000). Photochemical transformation of dissolved organic matter in lakes. *Limnology and Oceanography*, *45*, 753-762
- Binding, C.E., Jerome, J.H., Bukata, R.P., & Booty, W.G. (2010). Suspended particulate matter in Lake Erie derived from MODIS aquatic colour imagery. *International Journal of Remote Sensing*, *31*, 5239-5255
- Binding, C.E., Jerome, J.H., Bukata, R.P., & Booty, W.G. (2008). Spectral absorption properties of dissolved and particulate matter in Lake Erie. *Remote Sensing of Environment*, *112*, 1702-1711
- Binding, C.E., Greenberg, T.A., Watson, S.B., Rastin, S., & Gould, J. (2015). Long term water clarity changes in North America's Great Lakes from multi-sensor satellite observations. *Limnology and Oceanography*, *60*, 1976-1995
- Binding, C., Bowers, D., & Mitchelson-Jacob, E. (2005). Estimating suspended sediment concentrations from ocean colour measurements in moderately turbid waters; the impact of variable particle scattering properties. *Remote Sensing of Environment*, *94*, 373-383

- Blache, U., Jakob, T., Su, W., & Wilhelm, C. (2011). The impact of cell-specific absorption properties on the correlation of electron transport rates measured by chlorophyll fluorescence and photosynthetic oxygen production in planktonic algae. *Plant Physiology and Biochemistry*, *49*, 801-808
- Boss, E., Twardowski, M., & Herring, S. (2001). Shape of the particulate beam attenuation spectrum and its inversion to obtain the shape of the particulate size distribution. *Applied Optics*, *40*, 4885-4893
- Boss, E., Pegau, W., Lee, M., Twardowski, M., Shybanov, E., Korotaev, G., et al. (2004). Particulate backscattering ratio at LEO 15 and its use to study particle composition and distribution. *Journal of Geophysical Research-Oceans*, *109*, C01014
- Boss, E., Taylor, L., Gilbert, S., Gundersen, K., Hawley, N., Janzen, C., et al. (2009). Comparison of inherent optical properties as a surrogate for particulate matter concentration in coastal waters. *Limnology and Oceanography-Methods*, *7*, 803-810
- Bowers, D., & Binding, C. (2006). The optical properties of mineral suspended particles: A review and synthesis. *Estuarine Coastal and Shelf Science*, *67*, 219-230
- Brando, V.E., Dekker, A.G., Park, Y.J., & Schroeder, T. (2012). Adaptive semianalytical inversion of ocean color radiometry in optically complex waters. *Applied Optics*, *51*, 2808-2833
- Bresciani, M., Vascellari, M., Giardino, C., & Matta, E. (2012). Remote sensing supports the definition of the water quality status of Lake Omodeo (Italy). *European Journal of Remote Sensing*, *45*, 349-360
- Bresciani, M., Giardino, C., Bartoli, M., Tavernini, S., Bolpagni, R., & Nizzoli, D. (2011). Recognizing harmful algal bloom based on remote sensing reflectance band ratio. *Journal of Applied Remote Sensing*, *5*, 053556

- Brezonik, P.L., Olmanson, L.G., Finlay, J.C., & Bauer, M.E. (2015). Factors affecting the measurement of CDOM by remote sensing of optically complex inland waters. *Remote Sensing of Environment*, 157, 199-215
- Bricaud, A. (2004). Natural variability of phytoplanktonic absorption in oceanic waters: Influence of the size structure of algal populations. *Journal of Geophysical Research - Oceans*, 109
- Bricaud, A., Morel, A., & Prieur, L. (1981). Absorption by dissolved organic-matter of the sea (yellow substance) in the UV and visible domains. *Limnology and Oceanography*, 26, 43-53
- Bricaud, A., Babin, M., Morel, A., & Claustre, H. (1995). Variability in the Chlorophyll-Specific Absorption-Coefficients of Natural Phytoplankton - Analysis and Parameterization. *Journal of Geophysical Research-Oceans*, 100, 13321-13332
- Bricaud, A., Morel, A., Babin, M., Allali, K., & Claustre, H. (1998). Variations of light absorption by suspended particles with chlorophyll a concentration in oceanic (case 1) waters: Analysis and implications for bio-optical models. *Journal of Geophysical Research-Oceans*, 103, 31033-31044
- Bricaud, A., Babin, M., Claustre, H., Ras, J., & Tieche, F. (2010). Light absorption properties and absorption budget of Southeast Pacific waters. *Journal of Geophysical Research-Oceans*, 115, C08009
- Brockmann Consult. (2014). DUE Coastcolour Final Report. , V 1, 1-93
- Bryant, R., Tyler, A., Gilvear, D., McDonald, P., Teasdale, I., Brown, J., et al. (1996). A preliminary investigation into the spectral characteristics of inter-tidal estuarine sediments. *International Journal of Remote Sensing*, 17, 405-412
- Burrage, D., Wesson, J., Martinez, C., Perez, T., Moller, O., Jr., & Piola, A. (2008). Patos Lagoon outflow within the Rio de la Plata plume using an airborne salinity mapper: Observing an embedded plume. *Continental Shelf Research*, 28, 1625-1638

- Buttner, G., Korandi, M., Gyomorei, A., Kote, Z., & Szabo, G. (1987). Satellite Remote-Sensing of Inland Waters - Lake Balaton and Reservoir Kiskore. *Acta Astronautica*, 15, 305-311
- Campbell, J.B. (2006). *Introduction to Remote Sensing*. (pp. 626). London: Taylor and Francis
- Campbell, G., Phinn, S.R., Dekker, A.G., & Brando, V.E. (2011). Remote sensing of water quality in an Australian tropical freshwater impoundment using matrix inversion and MERIS images RID A-1321-2008. *Remote Sensing of Environment*, 115, 2402-2414
- Carmichael, W.W., Azevedo, S.M.F.O., An, J.S., Molica, R.J.R., Jochimsen, E.M., Lau, S., et al. (2001). Human fatalities from cyanobacteria: Chemical and biological evidence for cyanotoxins. *Environmental health perspectives*, 109, 663-668
- Carvalho, L., Miller nee (Ferguson), C.A., Scott, E.M., Codd, G.A., Davies, P.S., & Tyler, A.N. (2011). Cyanobacterial blooms: Statistical models describing risk factors for national-scale lake assessment and lake management. *Science of the Total Environment*, 409, 5353-5358
- Chang, N., Vannah, B., & Yang, Y.J. (2014a). Comparative Sensor Fusion Between Hyperspectral and Multispectral Satellite Sensors for Monitoring Microcystin Distribution in Lake Erie. *Ieee Journal of Selected Topics in Applied Earth Observations and Remote Sensing*, 7, 2426-2442
- Chang, N., Vannah, B.W., Yang, Y.J., & Elovitz, M. (2014b). Integrated data fusion and mining techniques for monitoring total organic carbon concentrations in a lake. *International Journal of Remote Sensing*, 35, 1064-1093
- Choubey, V., & Subramanian, V. (1992). Estimation of Suspended-Solids using Indian Remote-Sensing Satellite-1a Data - a Case-Study from Central India. *International Journal of Remote Sensing*, 13, 1473-1486

- Ciavatta, S., Torres, R., Martinez-Vicente, V., Smyth, T., Dall'Olmo, G., Polimene, L., et al. (2014). Assimilation of remotely-sensed optical properties to improve marine biogeochemistry modelling. *Progress in Oceanography*, *127*, 74-95
- Ciotti, A., Lewis, M., & Cullen, J. (2002). Assessment of the relationships between dominant cell size in natural phytoplankton communities and the spectral shape of the absorption coefficient. *Limnology and Oceanography*, *47*, 404-417
- Cockell, C.S., & Knowland, J. (1999). Ultraviolet radiation screening compounds. *Biological reviews of the Cambridge Philosophical Society*, *74*, 311-345
- Codd, G.A., Morrison, L.F., & Metcalf, J.S. (2005a). Cyanobacterial toxins: risk management for health protection. *Toxicology and applied pharmacology*, *203*, 264-272
- Codd, G.A., Azevedo, S.M.F.O., Bagchi, S.N., Burch, M.D., Carmichael, W.W., Harding, W.R., et al. (2005b). CyanoNet: A global network for cyanobacterial bloom and toxin risk management.
- Cole, J.J., Prairie, Y.T., Caraco, N.F., McDowell, W.H., Tranvik, L.J., Striegl, R.G., et al. (2007). Plumbing the global carbon cycle: Integrating inland waters into the terrestrial carbon budget. *Ecosystems*, *10*, 171-184
- Dall'Olmo, G., & Gitelson, A. (2005). Effect of bio-optical parameter variability on the remote estimation of chlorophyll-a concentration in turbid productive waters: experimental results. *Applied Optics*, *44*, 412-422
- Dall'Olmo, G., Gitelson, A., & Rundquist, D. (2003). Towards a unified approach for remote estimation of chlorophyll-a in both terrestrial vegetation and turbid productive waters. *Geophysical Research Letters*, *30*, 1938
- Dall'Olmo, G., Westberry, T.K., Behrenfeld, M.J., Boss, E., & Slade, W.H. (2009). Significant contribution of large particles to optical backscattering in the open ocean. *Biogeosciences*, *6*, 947-967

- Dall'Olmo, G., & Gitelson, A.A. (2006). Effect of bio-optical parameter variability and uncertainties in reflectance measurements on the remote estimation of chlorophyll-a concentration in turbid productive waters: modeling results. *Applied Optics*, 45, 3577-3592
- Dalu, T., Dube, T., Froneman, P.W., Sachikonye, M.T.B., Clegg, B.W., & Nhiwatiwa, T. (2015). An assessment of chlorophyll-a concentration spatio-temporal variation using Landsat satellite data, in a small tropical reservoir. *Geocarto International*, 30, 1130-1143
- Darecki, M., & Stramski, D. (2004). An evaluation of MODIS and SeaWiFS bio-optical algorithms in the Baltic Sea. *Remote Sensing of Environment*, 89, 326-350
- Dash, P., Walker, N.D., Mishra, D.R., Hu, C., Pinckney, J.L., & D'Sa, E.J. (2011). Estimation of cyanobacterial pigments in a freshwater lake using OCM satellite data. *Remote Sensing of Environment*, 115, 3409-3423
- Dekker, A.G. (1993). Detection of optical water quality parameters for eutrophic waters by high resolution remote sensing. , *Vrije Univ. Amsterdam*
- Dekker, A., Vos, R., & Peters, S. (2001). Comparison of remote sensing data, model results and in situ data for total suspended matter (TSM) in the southern Frisian lakes. *Science of the Total Environment*, 268, 197-214
- Dera, J., & Wozniak, B. (2010). Solar radiation in the Baltic Sea. *Oceanologia*, 52, 533-582
- Dierberg, F., & Carriker, N. (1994). Field Testing 2 Instruments for Remotely Sensing Water-Quality in the Tennessee Valley. *Environmental science & technology*, 28, 16-25
- Doerffer, R., & Schiller, H. (2008). MERIS Lake Water Algorithm for BEAM. , *VI.0*, 1-17
- Doerffer, R., & Schiller, H. (2007). The MERIS case 2 water algorithm. *International Journal of Remote Sensing*, 28, 517-535

- Dokulil, M., & Teubner, K. (2000). Cyanobacterial dominance in lakes. *Hydrobiologia*, 438, 1-12
- Domínguez Gómez, J.A., Alonso Alonso, C., & Alonso García, A. (2011). Remote sensing as a tool for monitoring water quality parameters for Mediterranean Lakes of European Union water framework directive (WFD) and as a system of surveillance of cyanobacterial harmful algae blooms (SCyanoHABs). *Environmental monitoring and assessment*, 181, 317-334
- Dömötörfy, Z., Reeder, D., & Pomogyi, P. (2003). Changes in the macro-vegetation of the Kis-Balaton Wetlands over the last two centuries: a GIS perspective. *Hydrobiologia*, 506, 671-679
- Dona, C., Chang, N., Caselles, V., Sanchez, J.M., Camacho, A., Delegido, J., et al. (2015). Integrated satellite data fusion and mining for monitoring lake water quality status of the Albufera de Valencia in Spain. *Journal of environmental management*, 151, 416-426
- Downing, J.A. (2001). Predicting Cyanobacteria dominance in lakes. *Canadian Journal of Fisheries and Aquatic Sciences*, 58, 1905-1908
- Duan, H., Ma, R., & Hu, C. (2012). Evaluation of remote sensing algorithms for cyanobacterial pigment retrievals during spring bloom formation in several lakes of East China. *Remote Sensing of Environment*, 126, 126-135
- Duan, H., Zhang, Y., Zhan, B., Song, K., & Wang, Z. (2007). Assessment of chlorophyll-a concentration and trophic state for Lake Chagan using Landsat TM and field spectral data. *Environmental monitoring and assessment*, 129, 295-308
- Effler, S.W., Strait, C.M., Perkins, M., & O'Donnell, D.M. (2012). Optical characterization and tests of closure for Oneida Lake, New York, USA. *Inland Waters*, 2, 211-228
- Effler, S.W., Perkins, M., Peng, F., Strait, C., Weidemann, A.D., & Auer, M.T. (2010). Light-absorbing components in Lake Superior. *Journal of Great Lakes Research*, 36, 656-665

- European Commission. (2006). Directive 2006/7/EC of the European Parliament and of the Council of 15 February 2006 concerning the management of bathing water quality and repealing Directive 76/160/EEC. , *L64*, 37-51
- European Commission. (2000). Directive 2000/60/EC of the European Parliament and of the Council of 23 October 2000 establishing a framework for Community action in the field of water policy. , *L327*, 1-73
- European Commission. (1992). Council Directive 92/43/EEC of 21 May 1992 on the conservation of natural habitats and of wild fauna and flora. , *L206*, 7-50
- Everson, S., Fabbro, L., Kinnear, S., Eaglesham, G., & Wright, P. (2009). Distribution of the cyanobacterial toxins cylindrospermopsin and deoxycylindrospermopsin in a stratified lake in north-eastern New South Wales, Australia. *Marine and Freshwater Research*, *60*, 25-33
- Fabbro, L., & Duivenvoorden, L. (1996). Profile of a bloom of the cyanobacterium *Cylindrospermopsis raciborskii* (Woloszynska) Seenaya and Subba Raju in the Fitzroy River in tropical central Queensland. *Marine and Freshwater Research*, *47*, 685-694
- Falconer, I. (2001). Toxic cyanobacterial bloom problems in Australian waters: risks and impacts on human health. *Phycologia*, *40*, 228-233
- Feng, Q., Gong, J., Wang, Y., Liu, J., Li, Y., Ibrahim, A.N., et al. (2015). Estimating chlorophyll-a concentration based on a four-band model using field spectral measurements and HJ-1A hyperspectral data of Qiandao Lake, China. *Remote Sensing Letters*, *6*, 735-744
- Ferber, L. (2004). Do cyanobacteria dominate in eutrophic lakes because they fix atmospheric nitrogen? *Freshwater Biology*, *49*, 690-708
- Fichot, C.G., & Benner, R. (2012). The spectral slope coefficient of chromophoric dissolved organic matter (S<sub>275-295</sub>) as a tracer of terrigenous dissolved organic carbon in river-influenced ocean margins. *Limnology and Oceanography*, *57*, 1453-1466

- Finlayson, C.M., & Vandervalk, A.G. (1995). Wetland Classification and Inventory - a Summary. *Vegetatio*, 118, 185-192
- Flink, P., Lindell, T., & Ostlund, C. (2001). Statistical analysis of hyperspectral data from two Swedish lakes. *Science of the Total Environment*, 268, 155-169
- Fraser, R. (1998). Hyperspectral remote sensing of turbidity and chlorophyll a among Nebraska sand hills lakes. *International Journal of Remote Sensing*, 19, 1579-1589
- Galat, D., & Verdin, J. (1989). Patchiness, Collapse and Succession of a Cyanobacterial Bloom Evaluated by Synoptic Sampling and Remote-Sensing. *Journal of Plankton Research*, 11, 925-948
- Gallegos, C.L., Davies-Colley, R.J., & Gall, M. (2008). Optical closure in lakes with contrasting extremes of reflectance. *Limnology and Oceanography*, 53, 2021-2034
- Gallinaro, N., Tavernini, S., & Cantoni, F. (2013). European Lakes under Environmental Stressors: Supporting lake governance to mitigate the impact of climate change - Final Report. , *Ref. Nr. 2CE243P3*, 1-149
- Gege, P. (1998). Characterization of the phytoplankton in Lake Constance for classification by remote sensing. *Advances in Limnology*, 53, 179-193
- George, D. (1993). Physical and Chemical-Scales of Pattern in Fresh-Water Lakes and Reservoirs. *Science of the Total Environment*, 135, 1-15
- George, D., & Malthus, T. (2001). Using a compact airborne spectrographic imager to monitor phytoplankton biomass in a series of lakes in north Wales. *Science of the Total Environment*, 268, 215-226
- Giardino, C., Candiani, G., & Zilioli, E. (2005). Detecting chlorophyll-a in Lake Garda using TOA MERIS radiances. *Photogrammetric Engineering and Remote Sensing*, 71, 1045-1051
- Gilerson, A., Zhou, J., Hlaing, S., Ioannou, I., Schalles, J., Gross, B., et al. (2007). Fluorescence component in the reflectance spectra from coastal waters. Dependence on water composition. *Optics Express*, 15, 15702-15721

- Gilerson, A.A., Gitelson, A.A., Zhou, J., Gurlin, D., Moses, W., Ioannou, I., et al. (2010). Algorithms for remote estimation of chlorophyll-a in coastal and inland waters using red and near infrared bands. *Optics Express*, *18*, 24109-24125
- Gitelson, A. (1993). Algorithms for Remote-Sensing of Phytoplankton Pigments in Inland Waters. *Advances in Space Research*, *13*, 197-201
- Gitelson, A., Szilagyi, F., & Mittenzwey, K. (1993a). Improving Quantitative Remote-Sensing for Monitoring of Inland Water-Quality. *Water research*, *27*, 1185-1194
- Gitelson, A., Garbuzov, G., Szilagyi, F., Mittenzwey, K., Karnieli, A., & Kaiser, A. (1993b). Quantitative Remote-Sensing Methods for Real-Time Monitoring of Inland Waters Quality. *International Journal of Remote Sensing*, *14*, 1269-1295
- Gitelson, A.A., Gurlin, D., Moses, W.J., & Barrow, T. (2009). A bio-optical algorithm for the remote estimation of the chlorophyll-a concentration in case 2 waters. *Environmental Research Letters*, *4*, 045003
- Gitelson, A.A., Dall'Olmo, G., Moses, W., Rundquist, D.C., Barrow, T., Fisher, T.R., et al. (2008). A simple semi-analytical model for remote estimation of chlorophyll-a in turbid waters: Validation. *Remote Sensing of Environment*, *112*, 3582-3593
- Glibert, P.M., Anderson, D.M., Gentien, P., Graneli, E., & Sellner, K.G. (2005a). The global, complex phenomena of harmful algal blooms. *Oceanography*, *18*, 136-147
- Glibert, P.M., Seitzinger, S., Heil, C.A., Burkholder, J.M., Parrow, M.W., Codispoti, L.A., et al. (2005b). The role of eutrophication in the global proliferation of harmful algal blooms: New perspectives and new approaches. *Oceanography*, *18*, 198-209
- Gong, S., Huang, J., Li, Y., & Wang, H. (2008). Comparison of atmospheric correction algorithms for TM image in inland waters. *International Journal of Remote Sensing*, *29*, 2199-2210
- Gons, H. (1999). Optical teledetection of chlorophyll a in turbid inland waters. *Environmental science & technology*, *33*, 1127-1132

- Gons, H., Auer, M., & Effler, S. (2008). MERIS satellite chlorophyll mapping of oligotrophic and eutrophic waters in the Laurentian Great Lakes. *Remote Sensing of Environment*, *112*, 4098-4106
- Gons, H., Rijkeboer, M., & Ruddick, K. (2005). Effect of a waveband shift on chlorophyll retrieval from MERIS imagery of inland and coastal waters. *Journal of Plankton Research*, *27*, 125-127
- Gons, H., Rijkeboer, M., & Ruddick, K. (2002). A chlorophyll-retrieval algorithm for satellite imagery (Medium Resolution Imaging Spectrometer) of inland and coastal waters. *Journal of Plankton Research*, *24*, 947-951
- Gons, H., Rijkeboer, M., Bagheri, S., & Ruddick, K. (2000). Optical teledetection of chlorophyll a in estuarine and coastal waters. *Environmental science & technology*, *34*, 5189-5192
- Gonzalez Vilas, L., Spyarakos, E., & Torres Palenzuela, J.M. (2011). Neural network estimation of chlorophyll a from MERIS full resolution data for the coastal waters of Galician rias (NW Spain). *Remote Sensing of Environment*, *115*, 524-535
- Gordon, H. (1997). Atmospheric correction of ocean color imagery in the Earth Observing System era. *Journal of Geophysical Research-Atmospheres*, *102*, 17081-17106
- Gordon, H., & Wang, M. (1994). Retrieval of Water-Leaving Radiance and Aerosol Optical-Thickness Over the Oceans with Seawifs - a Preliminary Algorithm. *Applied Optics*, *33*, 443-452
- Gordon, H., Brown, O., & Jacobs, M. (1975). Computed relationships between inherent and apparent optical-properties of a flat homogeneous ocean. *Applied Optics*, *14*, 417-427
- Gordon, H., Brown, O., Evans, R., Brown, J., Smith, R., Baker, K., et al. (1988). A Semianalytic Radiance Model of Ocean Color. *Journal of Geophysical Research-Atmospheres*, *93*, 10909-10924

- Gower, J., King, S., Borstad, G., & Brown, L. (2005). Detection of intense plankton blooms using the 709 nm band of the MERIS imaging spectrometer. *International Journal of Remote Sensing*, 26, 2005-2012
- Gower, J., Doerffer, R., & Borstad, G. (1999). Interpretation of the 685 nm peak in water-leaving radiance spectra in terms of fluorescence, absorption and scattering, and its observation by MERIS. *International Journal of Remote Sensing*, 20, 1771-1786
- Goyens, C., Jamet, C., & Schroeder, T. (2013). Evaluation of four atmospheric correction algorithms for MODIS-Aqua images over contrasted coastal waters. *Remote Sensing of Environment*, 131, 63-75
- Grim, J.A., Kniewel, J.C., & Crosman, E.T. (2013). Techniques for Using MODIS Data to Remotely Sense Lake Water Surface Temperatures. *Journal of Atmospheric and Oceanic Technology*, 30, 2434-2451
- Guanter, L., Ruiz-Verdú, A., Odermatt, D., Giardino, C., Simis, S., Víctor Estellés, V., et al. (2010). Atmospheric correction of ENVISAT/MERIS data over inland waters: Validation for European lakes. *Remote Sensing of Environment*, 114, 467-480
- Gurlin, D., Gitelson, A.A., & Moses, W.J. (2011). Remote estimation of chl-a concentration in turbid productive waters - Return to a simple two-band NIR-red model? *Remote Sensing of Environment*, 115, 3479-3490
- Hajnal, E., & Padisak, J. (2008). Analysis of long-term ecological status of Lake Balaton based on the ALMOBAL phytoplankton database. *Hydrobiologia*, 599, 227-237
- Han, L., & Rundquist, D. (1997). Comparison of NIR/RED ratio and first derivative of reflectance in estimating algal-chlorophyll concentration: A case study in a turbid reservoir. *Remote Sensing of Environment*, 62, 253-261

- Harma, P., Vepsäläinen, J., Hannonen, T., Pyhälä, T., Kamari, J., Kallio, K., et al. (2001). Detection of water quality using simulated satellite data and semi-empirical algorithms in Finland. *Science of the Total Environment*, 268, 107-121
- Harrington, J., Schiebe, F., & Nix, J. (1992). Remote-Sensing of Lake Chicot, Arkansas - Monitoring Suspended Sediments, Turbidity, and Secchi Depth with Landsat Mss Data. *Remote Sensing of Environment*, 39, 15-27
- Heege, T., & Fischer, J. (2004). Mapping of water constituents in Lake Constance using multispectral airborne scanner data and a physically based processing scheme. *Canadian Journal of Remote Sensing*, 30, 77-86
- Herodek, S. (1986). Phytoplankton changes during eutrophication and P and N metabolism. In L. Somlyódy, & G. van Straten (Eds.), *Modeling and Managing Shallow Lake Eutrophication: With Application to Lake Balaton* (pp. 183-204). Berlin: Springer Verlag
- Herodek, S., Istvanovics, V., Jolankai, G., Csatho, P., Nemeth, T., & Varallyay, G. (1995). P-cycle in the Balaton catchment - a Hungarian case study. In H. Thiessen (Ed.), *Phosphorus in the Global Environment* (pp. 275-300). : Wiley
- Hoepffner, N., & Sathyendranath, S. (1991). Effect of Pigment Composition on Absorption Properties of Phytoplankton. *Marine Ecology Progress Series*, 73, 11-23
- Horváth, H., Kovács, A.W., Riddick, C., & Présing, M. (2013a). Extraction methods for phycocyanin determination in freshwater filamentous cyanobacteria and their application in a shallow lake. *European Journal of Phycology*, 48, 278-286
- Horváth, H., Mátyás, K., Suele, G., & Présing, M. (2013b). Contribution of nitrogen fixation to the external nitrogen load of a water quality control reservoir (Kis-Balaton Water Protection System, Hungary). *Hydrobiologia*, 702, 255-265
- Hu, C., & Feng, L. (2014). GOES Imager Shows Diurnal Changes of a *Trichodesmium erythraeum* Bloom on the West Florida Shelf. *Ieee Geoscience and Remote Sensing Letters*, 11, 1428-1432

- Hu, C., Feng, L., & Lee, Z. (2013). Uncertainties of SeaWiFS and MODIS remote sensing reflectance: Implications from clear water measurements. *Remote Sensing of Environment*, 133, 168-182
- Huang, C., Li, Y., Yang, H., Li, J., Chen, X., Sun, D., et al. (2014a). Assessment of water constituents in highly turbid productive water by optimization bio-optical retrieval model after optical classification. *Journal of Hydrology*, 519, 1572-1583
- Huang, C., Chen, X., Li, Y., Yang, H., Sun, D., Li, J., et al. (2015). Specific inherent optical properties of highly turbid productive water for retrieval of water quality after optical classification. *Environmental Earth Sciences*, 73, 1961-1973
- Huang, J., Chen, L., Chen, X., Tian, L., Feng, L., Yesou, H., et al. (2014b). Modification and validation of a quasi-analytical algorithm for inherent optical properties in the turbid waters of Poyang Lake, China. *Journal of Applied Remote Sensing*, 8, 083643
- Huang, W., & Lou, X. (2003). AVHRR detection of red tides with neural networks. *International Journal of Remote Sensing*, 24, 1991-1996
- Hunter, P.D., Tyler, A.N., Willby, N.J., & Gilvear, D.J. (2008a). The spatial dynamics of vertical migration by *Microcystis aeruginosa* in a eutrophic shallow lake: A case study using high spatial resolution time-series airborne remote sensing. *Limnology and Oceanography*, 53, 2391-2406
- Hunter, P.D., Tyler, A.N., Gilvear, D.J., & Willby, N.J. (2009). Using Remote Sensing to Aid the Assessment of Human Health Risks from Blooms of Potentially Toxic Cyanobacteria. *Environmental science & technology*, 43, 2627-2633
- Hunter, P.D., Tyler, A.N., Carvalho, L., Codd, G.A., & Maberly, S.C. (2010). Hyperspectral remote sensing of cyanobacterial pigments as indicators for cell populations and toxins in eutrophic lakes. *Remote Sensing of Environment*, 114, 2705-2718
- Hunter, P.D., Tyler, A.N., Presing, M., Kovacs, A.W., & Preston, T. (2008b). Spectral discrimination of phytoplankton colour groups: The effect of suspended particulate

- matter and sensor spectral resolution. *Remote Sensing of Environment*, 112, 1527-1544
- Ioannou, I., Gilerson, A., Gross, B., Moshary, F., & Ahmed, S. (2013). Deriving ocean color products using neural networks. *Remote Sensing of Environment*, 134, 78-91
- IOCCG. (2010). Atmospheric correction for remotely-sensed ocean-colour products. *Reports of the International Ocean-Colour Coordinating Group*, 10, 1
- IOCCG. (2000). Remote sensing of ocean colour in coastal, and other optically-complex, waters. , No. 3
- Iwamura, T., Nagai, H., & Ichimura, S. (1970). Improved Methods for Determining Contents of Chlorophyll, Protein, Ribonucleic Acid, and Deoxyribonucleic Acid in Planktonic Populations. *Internationale Revue der gesamten Hydrobiologie und Hydrographie*, 55, 131-147
- Jaelani, L.M., Matsushita, B., Yang, W., & Fukushima, T. (2013). Evaluation of four MERIS atmospheric correction algorithms in Lake Kasumigaura, Japan. *International Journal of Remote Sensing*, 34, 8967-8985
- Jamet, C., Loisel, H., Kuchinke, C.P., Ruddick, K., Zibordi, G., & Feng, H. (2011). Comparison of three SeaWiFS atmospheric correction algorithms for turbid waters using AERONET-OC measurements. *Remote Sensing of Environment*, 115, 1955-1965
- Jeffrey, S., Vesk, M., & Mantoura, R. (1997). Phytoplankton pigments: windows into the pastures of the sea. *Nature & Resources*, 33, 14-29
- Jiao, H.B., Zha, Y., Gao, J., Li, Y.M., Wei, Y.C., & Huang, J.Z. (2006). Estimation of chlorophyll-a concentration in Lake Tai, China using in situ hyperspectral data. *International Journal of Remote Sensing*, 27, 4267-4276
- Johnk, K.D., Huisman, J., Sharples, J., Sommeijer, B., Visser, P.M., & Stroom, J.M. (2008). Summer heatwaves promote blooms of harmful cyanobacteria. *Global Change Biology*, 14, 495-512

- Jolliff, J.K., Kindle, J.C., Penta, B., Helber, R., Lee, Z., Shulman, I., et al. (2008). On the relationship between satellite-estimated bio-optical and thermal properties in the Gulf of Mexico. *Journal of Geophysical Research-Biogeosciences*, *113*, G01024
- Jonasz, M., & Fournier, G.R. (2007). Chapter 4 - Measurements of light scattering by particles in water. In M.J.R. Fournier (Ed.), *Light Scattering by Particles in Water* (pp. 145-265). Amsterdam: Academic Press
- Kahru, M., & Mitchell, B. (2000). Influence of the 1997-98 El Nino on the surface chlorophyll in the California Current. *Geophysical Research Letters*, *27*, 2937-2940
- Kahru, M., Leppanen, J., & Rud, O. (1993). Cyanobacterial Blooms Cause Heating of the Sea-Surface. *Marine Ecology Progress Series*, *101*, 1-7
- Kallio, K., Koponen, S., & Pulliainen, J. (2003). Feasibility of airborne imaging spectrometry for lake monitoring - a case study of spatial chlorophyll alpha distribution in two meso-eutrophic lakes. *International Journal of Remote Sensing*, *24*, 3771-3790
- Kallio, K., Kutser, T., Hannonen, T., Koponen, S., Pulliainen, J., Vepsalainen, J., et al. (2001). Retrieval of water quality from airborne imaging spectrometry of various lake types in different seasons. *Science of the Total Environment*, *268*, 59-77
- Kay, J., Kampf, S., Handcock, R., Cherkauer, K., Gillespie, A., & Burges, S. (2005). Accuracy of lake and stream temperatures estimated from thermal infrared images. *Journal of the American Water Resources Association*, *41*, 1161-1175
- Kirk, J. (1994). *Light and Photosynthesis in Aquatic Ecosystems*. Cambridge, UK: Cambridge University Press
- Kiselev, V., Bulgarelli, B., & Heege, T. (2015). Sensor independent adjacency correction algorithm for coastal and inland water systems. *Remote Sensing of Environment*, *157*, 85-95

- Klemas, V. (2011). Remote Sensing Techniques for Studying Coastal Ecosystems: An Overview. *Journal of Coastal Research*, 27, 2-17
- Koponen, S., Pulliainen, J., Kallio, K., & Hallikainen, M. (2002). Lake water quality classification with airborne hyperspectral spectrometer and simulated MERIS data. *Remote Sensing of Environment*, 79, 51-59
- Kosten, S. (2012). Warmer climates boost cyanobacterial dominance in shallow lakes. *Global Change Biology*, 18, 118-126
- Kudela, R.M., Palacios, S.L., Austerberry, D.C., Accorsi, E.K., Guild, L.S., & Torres-Perez, J. (2015). Application of hyperspectral remote sensing to cyanobacterial blooms in inland waters. *Remote Sensing of Environment*, 167, 196-205
- Kutser, T. (2009). Passive optical remote sensing of cyanobacteria and other intense phytoplankton blooms in coastal and inland waters. *International Journal of Remote Sensing*, 30, 4401-4425
- Kutser, T. (2004). Quantitative detection of chlorophyll in cyanobacterial blooms by satellite remote sensing. *Limnology and Oceanography*, 49, 2179-2189
- Kutser, T., Metsamaa, L., Strombeck, N., & Vahtmae, E. (2006). Monitoring cyanobacterial blooms by satellite remote sensing. *Estuarine Coastal and Shelf Science*, 67, 303-312
- Kutser, T., Pierson, D., Kallio, K., Reinart, A., & Sobek, S. (2005a). Mapping lake CDOM by satellite remote sensing. *Remote Sensing of Environment*, 94, 535-540
- Kutser, T., Pierson, D., Tranvik, L., Reinart, A., Sobek, S., & Kallio, K. (2005b). Using satellite remote sensing to estimate the colored dissolved organic matter absorption coefficient in lakes. *Ecosystems*, 8, 709-720
- Kutser, T. (2012). The possibility of using the Landsat image archive for monitoring long time trends in coloured dissolved organic matter concentration in lake waters. *Remote Sensing of Environment*, 123, 334-338

- Kutser, T., Verpoorter, C., Paavel, B., & Tranvik, L.J. (2015). Estimating lake carbon fractions from remote sensing data. *Remote Sensing of Environment*, *157*, 138-146
- Landsberg, J.H. (2002). The effects of harmful algal blooms on aquatic organisms. *Reviews in Fisheries Science*, *10*, 113-390
- Lathrop, R., Lillesand, T., & Yandell, B. (1991). Testing the Utility of Simple Multi-Date Thematic Mapper Calibration Algorithms for Monitoring Turbid Inland Waters. *International Journal of Remote Sensing*, *12*, 2045-2063
- Le, C.F., Li, Y.M., Zha, Y., Sun, D., & Yin, B. (2009a). Validation of a Quasi-Analytical Algorithm for Highly Turbid Eutrophic Water of Meiliang Bay in Taihu Lake, China. *IEEE Transactions on Geoscience and Remote Sensing*, *47*, 2492-2500
- Le, C., Li, Y., Zha, Y., Wang, Q., Zhang, H., & Yin, B. (2011). Remote sensing of phycocyanin pigment in highly turbid inland waters in Lake Taihu, China. *International Journal of Remote Sensing*, *32*, 8253-8269
- Le, C., Li, Y., Zha, Y., Sun, D., Huang, C., & Lu, H. (2009b). A four-band semi-analytical model for estimating chlorophyll a in highly turbid lakes: The case of Taihu Lake, China. *Remote Sensing of Environment*, *113*, 1175-1182
- Lee, Z.P., Lance, V.P., Shang, S., Vaillancourt, R., Freeman, S., Lubac, B., et al. (2011). An assessment of optical properties and primary production derived from remote sensing in the Southern Ocean (SO GasEx). *Journal of Geophysical Research-Oceans*, *116*, C00F03
- Lee, Z.P., Carder, K.L., & Arnone, R.A. (2002). Deriving inherent optical properties from water color: a multiband quasi-analytical algorithm for optically deep waters. *Applied Optics*, *41*, 5755-5772
- Lee, Z., Carder, K., Mobley, C., Steward, R., & Patch, J. (1998). Hyperspectral remote sensing for shallow waters. I. A semianalytical model. *Applied Optics*, *37*, 6329-6338

- Lee, Z., Carder, K., Hawes, S., Steward, R., Peacock, T., & Davis, C. (1994). Model for the Interpretation of Hyperspectral Remote-Sensing Reflectance. *Applied Optics*, 33, 5721-5732
- Lesht, B.M., Barbiero, R.P., & Warren, G.J. (2016). Verification of a simple band ratio algorithm for retrieving Great Lakes open water surface chlorophyll concentrations from satellite observations. *Journal of Great Lakes Research*, 42, 448-454
- Leymarie, E., Doxaran, D., & Babin, M. (2010). Uncertainties associated to measurements of inherent optical properties in natural waters. *Applied Optics*, 49, 5415-5436
- Li, L., Li, L., & Song, K. (2015). Remote sensing of freshwater cyanobacteria: An extended IOP Inversion Model of Inland Waters (IIMIWI) for partitioning absorption coefficient and estimating phycocyanin. *Remote Sensing of Environment*, 157, 9-23
- Li, L., Li, L., Shi, K., Li, Z., & Song, K. (2012). A semi-analytical algorithm for remote estimation of phycocyanin in inland waters. *Science of the Total Environment*, 435, 141-150
- Li, L., Li, L., Song, K., Li, Y., Tedesco, L.P., Shi, K., et al. (2013). An inversion model for deriving inherent optical properties of inland waters: Establishment, validation and application. *Remote Sensing of Environment*, 135, 150-166
- Lindell, T., Pierson, D., Premazzi, G., & Zilioli, E. (1999). *Manual for Monitoring European Lakes Using Remote Sensing Techniques*. Ispra, Italy: Joint Research Centre
- Liu, X., Zhang, Y., Wang, M., & Zhou, Y. (2014). High-frequency optical measurements in shallow Lake Taihu, China: determining the relationships between hydrodynamic processes and inherent optical properties. *Hydrobiologia*, 724, 187-201

- Liu, Z., Hader, D., & Sommaruga, R. (2004). Occurrence of mycosporine-like amino acids (MAAs) in the bloom-forming cyanobacterium *Microcystis aeruginosa*. *Journal of Plankton Research*, *26*, 963-966
- Llewellyn, C., Fishwick, J., & Blackford, J. (2005). Phytoplankton community assemblage in the English Channel: a comparison using chlorophyll a derived from HPLC-CHEMTAX and carbon derived from microscopy cell counts. *Journal of Plankton Research*, *27*, 103-119
- Loisel, H., & Morel, A. (1998). Light scattering and chlorophyll concentration in case 1 waters: A reexamination. *Limnology and Oceanography*, *43*, 847-858
- Loisel, H., Meriaux, X., Berthon, J., & Poteau, A. (2007). Investigation of the optical backscattering to scattering ratio of marine particles in relation to their biogeochemical composition in the eastern English Channel and southern North Sea. *Limnology and Oceanography*, *52*, 739-752
- Loisel, H., Nicolas, J., Sciandra, A., Stramski, D., & Poteau, A. (2006). Spectral dependency of optical backscattering by marine particles from satellite remote sensing of the global ocean. *Journal of Geophysical Research-Oceans*, *111*, C09024
- Lubac, B., & Loisel, H. (2007). Variability and classification of remote sensing reflectance spectra in the eastern English Channel and southern North Sea. *Remote Sensing of Environment*, *110*, 45-58
- Luis Perez, G., Eugenia Llamas, M., Lagomarsino, L., & Zagarese, H. (2011). Seasonal variability of optical properties in a highly turbid lake (Laguna Chascomus, Argentina). *Photochemistry and photobiology*, *87*, 659-670
- Lunetta, R.S., Schaeffer, B.A., Stumpf, R.P., Keith, D., Jacobs, S.A., & Murphy, M.S. (2015). Evaluation of cyanobacteria cell count detection derived from MERIS imagery across the eastern USA. *Remote Sensing of Environment*, *157*, 24-34
- Lyu Heng, Wang Qiao, Wu Chuanqing, Zhu Li, Li Yunmei, & Huang Jiazhu. (2015). Variations in Optical Scattering and Backscattering by Organic and Inorganic

- Particulates in Chinese Lakes of Taihu, Chaohu and Dianchi. *Chinese Geographical Science*, 25, 26-38
- Lyu, H., Li, X., Wang, Y., Jin, Q., Cao, K., Wang, Q., et al. (2015). Evaluation of chlorophyll-a retrieval algorithms based on MERIS bands for optically varying eutrophic inland lakes. *Science of the Total Environment*, 530, 373-382
- Lyu, H., Wang, Q., Wu, C., Zhu, L., Yin, B., Li, Y., et al. (2013). Retrieval of phycocyanin concentration from remote-sensing reflectance using a semi-analytic model in eutrophic lakes. *Ecological Informatics*, 18, 178-187
- MacCallum, S.N., & Merchant, C.J. (2012). Surface water temperature observations of large lakes by optimal estimation. *Canadian Journal of Remote Sensing*, 38, 25-45
- Malthus, T., & Dekker, A. (1995). First Derivative Indexes for the Remote-Sensing of Inland Water-Quality using High-Spectral-Resolution Reflectance. *Environment international*, 21, 221-232
- Maritorena, S., Siegel, D., & Peterson, A. (2002). Optimization of a semianalytical ocean color model for global-scale applications. *Applied Optics*, 41, 2705-2714
- Maritorena, S., Morel, A., & Gentili, B. (1994). Diffuse-Reflectance of Oceanic Shallow Waters - Influence of Water Depth and Bottom Albedo. *Limnology and Oceanography*, 39, 1689-1703
- Martinez-Vicente, V., Land, P.E., Tilstone, G.H., Widdicombe, C., & Fishwick, J.R. (2010). Particulate scattering and backscattering related to water constituents and seasonal changes in the Western English Channel. *Journal of Plankton Research*, 32, 603-619
- Masek, J., Vermote, E., Saleous, N., Wolfe, R., Hall, F., Huemmrich, K., et al. (2006). A Landsat surface reflectance dataset for North America, 1990-2000. *Ieee Geoscience and Remote Sensing Letters*, 3, 68-72

- Matthews, M.W., Bernard, S., & Winter, K. (2010). Remote sensing of cyanobacteria-dominant algal blooms and water quality parameters in Zeekoevlei, a small hypertrophic lake, using MERIS. *Remote Sensing of Environment*, 114, 2070-2087
- Matthews, M.W. (2011). A current review of empirical procedures of remote sensing in inland and near-coastal transitional waters. *International Journal of Remote Sensing*, 32, 6855-6899
- Matthews, M.W., & Odermatt, D. (2015). Improved algorithm for routine monitoring of cyanobacteria and eutrophication in inland and near-coastal waters. *Remote Sensing of Environment*, 156, 374-382
- Matthews, M.W., & Bernard, S. (2013). Characterizing the absorption properties for remote sensing of three small optically-diverse South African reservoirs. *Remote Sensing*, 5, 4370-4404
- Matthews, M.W., Bernard, S., & Robertson, L. (2012). An algorithm for detecting trophic status (chlorophyll-a), cyanobacterial-dominance, surface scums and floating vegetation in inland and coastal waters. *Remote Sensing of Environment*, 124, 637-652
- McCullough, I.M., Loftin, C.S., & Sader, S.A. (2013). Landsat imagery reveals declining clarity of Maine's lakes during 1995-2010. *Freshwater Science*, 32, 741-752
- McCusker, E.M., Ostrom, P.H., Ostrom, N.E., Jeremiason, J.D., & Baker, J.E. (1999). Seasonal variation in the biogeochemical cycling of seston in Grand Traverse Bay, Lake Michigan. *Organic Geochemistry*, 30, 1543-1557
- Mckee, D., & Cunningham, A. (2006). Identification and characterisation of two optical water types in the Irish Sea from in situ inherent optical properties and seawater constituents. *Estuarine Coastal and Shelf Science*, 68, 305-316
- Mckee, D., Piskozub, J., & Brown, I. (2008). Scattering error corrections for in situ absorption and attenuation measurements. *Optics Express*, 16, 19480-19492

- McKee, D., Cunningham, A., Wright, D., & Hay, L. (2007). Potential impacts of nonalgal materials on water-leaving Sun induced chlorophyll fluorescence signals in coastal waters. *Applied Optics*, *46*, 7720-7729
- McKee, D., Roettgers, R., Neukermans, G., Calzado, V.S., Trees, C., Ampolo-Rella, M., et al. (2014). Impact of measurement uncertainties on determination of chlorophyll-specific absorption coefficient for marine phytoplankton. *Journal of Geophysical Research-Oceans*, *119*, 9013-9025
- McKillop, R.J., & Clague, J.J. (2007). Statistical, remote sensing-based approach for estimating the probability of catastrophic drainage from moraine-dammed lakes in Southwestern British Columbia. *Global and Planetary Change*, *56*, 153-171
- Medina-Cobo, M., Domínguez, J.A., Quesada, A., & de Hoyos, C. (2014). Estimation of cyanobacteria biovolume in water reservoirs by MERIS sensor. *Water research*, *63*, 10-20
- Meister, G., & McClain, C.R. (2010). Point-spread function of the ocean color bands of the Moderate Resolution Imaging Spectroradiometer on Aqua. *Applied Optics*, *49*, 6276-6285
- Menken, K.D., & Brezonik, P.L. (2006). Influence of chlorophyll and colored dissolved organic matter (CDOM) on lake reflectance spectra: Implications for measuring lake properties by remote sensing. *Lake and Reservoir Management*, *22*, 179-190
- Mishra, S., & Mishra, D.R. (2014). A novel remote sensing algorithm to quantify phycocyanin in cyanobacterial algal blooms. *Environmental Research Letters*, *9*, 114003
- Mishra, S., & Mishra, D.R. (2012). Normalized difference chlorophyll index: A novel model for remote estimation of chlorophyll-a concentration in turbid productive waters. *Remote Sensing of Environment*, *117*, 394-406
- Mishra, S., Mishra, D.R., & Lee, Z. (2014). Bio-Optical Inversion in Highly Turbid and Cyanobacteria-Dominated Waters. *IEEE Transactions on Geoscience and Remote Sensing*, *52*, 375-388

- Mishra, S., Mishra, D.R., & Schluchter, W.M. (2009). A Novel Algorithm for Predicting Phycocyanin Concentrations in Cyanobacteria: A Proximal Hyperspectral Remote Sensing Approach. *Remote Sensing*, 1, 758-775
- Mishra, S., Mishra, D.R., Lee, Z., & Tucker, C.S. (2013). Quantifying cyanobacterial phycocyanin concentration in turbid productive waters: A quasi-analytical approach. *Remote Sensing of Environment*, 133, 141-151
- Mittenzwey, K.H., Gitelson, A.A., & Kondratiev, K.Y. (1992). Determination of Chlorophyll-a of Inland Waters on the Basis of Spectral Reflectance. *Limnology and Oceanography*, 37, 147-149
- Mittenzwey, K., Breitwieser, S., Penig, J., Gitelson, A., Dubovitzkii, G., Garbusov, G., et al. (1991). Fluorescence and Reflectance for the Insitu Determination of some Quality Parameters of Surface Waters. *Acta Hydrochimica et Hydrobiologica*, 19, 3-15
- Mobley, C.D., Boss, E., & Roesler, C.S. (2016). Ocean Optics Web Book. , 2016
- Mobley, C.D. (1994). *Light and Water: Radiative Transfer in Natural Waters*. (pp. 592). San Diego, California: Academic
- Mobley, C., Sundman, L., & Boss, E. (2002). Phase function effects on oceanic light fields. *Applied Optics*, 41, 1035-1050
- Moran, M.A., & Zepp, R.G. (1997). Role of photoreactions in the formation of biologically labile compounds from dissolved organic matter. *Limnology and Oceanography*, 42, 1307-1316
- Morel, A., & Maritorena, S. (2001). Bio-optical properties of oceanic waters: A reappraisal. *Journal of Geophysical Research-Oceans*, 106, 7163-7180
- Morel, A., & Gentili, B. (1991). Diffuse reflectance of oceanic waters - its dependence on sun angle as influenced by the molecular-scattering contribution. *Applied Optics*, 30, 4427-4438

- Morel, A., & Prieur, L. (1977). Analysis of variations in ocean color. *Limnology and Oceanography*, 22, 709-722
- Morel, A., Gentili, B., Claustre, H., Babin, M., Bricaud, A., Ras, J., et al. (2007). Optical properties of the "clearest" natural waters. *Limnology and Oceanography*, 52, 217-229
- Moses, W.J., Gitelson, A.A., Berdnikov, S., & Povazhnyy, V. (2009). Satellite Estimation of Chlorophyll-a Concentration Using the Red and NIR Bands of MERIS-The Azov Sea Case Study. *Ieee Geoscience and Remote Sensing Letters*, 6, 845-849
- Mouw, C.B., Greb, S., Aurin, D., DiGiacomo, P.M., Lee, Z., Twardowski, M., et al. (2015). Aquatic color radiometry remote sensing of coastal and inland waters: Challenges and recommendations for future satellite missions. *Remote Sensing of Environment*, 160, 15-30
- Mozes, A., Presing, M., & Voros, L. (2006). Seasonal dynamics of picocyanobacteria and picoeukaryotes in a large shallow lake (Lake Balaton, Hungary). *International Review of Hydrobiology*, 91, 38-50
- Mueller, J.L., Davis, C., Arnone, R., Frouin, R., Carder, K., Lee, Z.P., et al. (2000). Above-water radiance and remote sensing reflectance measurements and analysis protocols. , *Revision 2*, 98-107
- Mueller, J.L., Morel, A., Frouin, R., Davis, C., Arnone, R., Carder, K., et al. (2003). Ocean Optics Protocols For Satellite Ocean Color Sensor Validation, Revision 4, Volume III: Radiometric Measurements and Data Analysis Protocols. *National Aeronautical and Space Administration, NASA/TM-2003-21621/Rev-Vol III*, 1-78
- Nellis, M., Harrington, J., & Wu, J. (1998). Remote sensing of temporal and spatial variations in pool size, suspended sediment, turbidity, and Secchi depth in Tuttle Creek Reservoir, Kansas: 1993. *Geomorphology*, 21, 281-293
- Németh, J., & Vörös, L. (1986). Konceptió és módszertan felszíni vizek algológiai monitoringjához.

- Neukermans, G., Loisel, H., Meriaux, X., Astoreca, R., & McKee, D. (2012). In situ variability of mass-specific beam attenuation and backscattering of marine particles with respect to particle size, density, and composition. *Limnology and Oceanography*, *57*, 124-144
- Odermatt, D., Gitelson, A., Brando, V.E., & Schaepman, M. (2012). Review of constituent retrieval in optically deep and complex waters from satellite imagery. *Remote Sensing of Environment*, *118*, 116-126
- Odermatt, D., Heege, T., Nieke, J., Kneubuehler, M., & Itten, K. (2008). Water quality monitoring for lake constance with a physically based algorithm for MERIS data. *Sensors*, *8*, 4582-4599
- O'Donnell, D.M., Effler, S.W., Perkins, M., & Strait, C. (2013). Optical characterization of Lake Champlain: Spatial heterogeneity and closure. *Journal of Great Lakes Research*, *39*, 247-258
- O'Donnell, D.M., Effler, S.W., Strait, C.M., & Leshkevich, G.A. (2010). Optical characterizations and pursuit of optical closure for the western basin of Lake Erie through in situ measurements. *Journal of Great Lakes Research*, *36*, 736-746
- Ogashawara, I., Mishra, D.R., Mishra, S., Curtarelli, M.P., & Stech, J.L. (2013). A Performance Review of Reflectance Based Algorithms for Predicting Phycocyanin Concentrations in Inland Waters. *Remote Sensing*, *5*, 4774-4798
- Olmanson, L.G., Brezonik, P.L., & Bauer, M.E. (2011). Evaluation of medium to low resolution satellite imagery for regional lake water quality assessments. *Water Resources Research*, *47*, W09515
- O'Reilly, J., Maritorena, S., Mitchell, B., Siegel, D., Carder, K., Garver, S., et al. (1998). Ocean color chlorophyll algorithms for SeaWiFS. *Journal of Geophysical Research-Oceans*, *103*, 24937-24953
- Ostrom, B. (1976). Fertilization of the Baltic by Nitrogen Fixation in the Blue-Green Alga *Nodularia-Spumigena*. *Remote Sensing of Environment*, *4*, 305-310

- Paavel, B., & Arst, H. (2009). *Bio-optical properties of North-European turbid lakes: Attenuation of solar light in the water*. Saarbrücken, Germany: VDM Verlag Dr. Müller
- Paavel, B., Arst, H., & Reinart, A. (2008). Variability of bio-optical parameters in two North-European large lakes. *Hydrobiologia*, 599, 201-211
- Paerl, H.W., & Huisman, J. (2009). Climate change: a catalyst for global expansion of harmful cyanobacterial blooms. *Environmental Microbiology Reports*, 1, 27-37
- Paerl, H.W., & Huisman, J. (2008). Climate - Blooms like it hot. *Science*, 320, 57-58
- Paerl, H.W., Hall, N.S., & Calandrino, E.S. (2011). Controlling harmful cyanobacterial blooms in a world experiencing anthropogenic and climatic-induced change. *Science of the Total Environment*, 409, 1739-1745
- Palmer, S.C.J. (2015). Spatiotemporal phytoplankton dynamics of the optically complex Lake Balaton. , 194
- Palmer, S.C.J., Odermatt, D., Hunter, P.D., Brockmann, C., Presing, M., Balzter, H., et al. (2015a). Satellite remote sensing of phytoplankton phenology in Lake Balaton using 10 years of MERIS observations. *Remote Sensing of Environment*, 158, 441-452
- Palmer, S.C.J., Kutser, T., & Hunter, P.D. (2015b). Remote sensing of inland waters: Challenges, progress and future directions. *Remote Sensing of Environment*, 157, 1-8
- Palmer, S.C.J., Hunter, P.D., Lankester, T., Hubbard, S., Spyarakos, E., Tyler, A.N., et al. (2015c). Validation of Envisat MERIS algorithms for chlorophyll retrieval in a large, turbid and optically-complex shallow lake. *Remote Sensing of Environment*, 157, 158-169
- Pegau, W., Gray, D., & Zaneveld, J. (1997). Absorption and attenuation of visible and near-infrared light in water: dependence on temperature and salinity. *Applied Optics*, 36, 6035-6046

- Peng, F., & Effler, S.W. (2016). Advancing two-component partitioning of light scattering in Cayuga Lake, New York. *Limnology and Oceanography*, *61*, 298-315
- Peng, F., & Effler, S.W. (2013). Spectral absorption properties of mineral particles in western Lake Erie: Insights from individual particle analysis. *Limnology and Oceanography*, *58*, 1775-1789
- Peng, F., & Effler, S.W. (2012). Mass-specific scattering coefficient for natural minerogenic particle populations: particle size distribution effect and closure analyses. *Applied Optics*, *51*, 2236-2249
- Peng, F., Effler, S.W., O'Donnell, D., Weidemann, A.D., & Auer, M.T. (2009). Characterizations of minerogenic particles in support of modeling light scattering in Lake Superior through a two-component approach. *Limnology and Oceanography*, *54*, 1369-1381
- Peng, F., Effler, S.W., O'Donnell, D., Perkins, M.G., & Weidemann, A. (2007). Role of minerogenic particles in light scattering in lakes and a river in central New York. *Applied Optics*, *46*, 6577-6596
- Perkins, M., Effler, S.W., & Strait, C.M. (2014). Phytoplankton absorption and the chlorophyll a-specific absorption coefficient in dynamic Onondaga Lake. *Inland Waters*, *4*, 133-146
- Perkins, M., Effler, S.W., Strait, C., & Zhang, L. (2009). Light absorbing components in the Finger Lakes of New York. *Fundamental and Applied Limnology*, *173*, 305-320
- Perkins, M., Effler, S.W., Peng, F., O'Donnell, D.M., & Strait, C. (2013). Light-absorbing components in the Great Lakes. *Journal of Great Lakes Research*, *39*, 123-136
- Pierson, D., & Strombeck, N. (2001). Estimation of radiance reflectance and the concentrations of optically active substances in Lake Malaren, Sweden, based on direct and inverse solutions of a simple model. *Science of the Total Environment*, *268*, 171-188

- Politi, E., Cutler, M.E.J., & Rowan, J.S. (2012). Using the NOAA Advanced Very High Resolution Radiometer to characterise temporal and spatial trends in water temperature of large European lakes. *Remote Sensing of Environment*, 126, 1-11
- Pomogyi, P. (1993). Nutrient Retention by the Kis-Balaton Water Protection System. *Hydrobiologia*, 251, 309-320
- Pozdnyakov, D., Shuchman, R., Korosov, A., & Hatt, C. (2005). Operational algorithm for the retrieval of water quality in the Great Lakes. *Remote Sensing of Environment*, 97, 352-370
- Preisendorfer, R.W. (1976). *Hydrologic Optics*. , 1
- Présing, M., Herodek, S., Preston, T., & Vörös, L. (2001). Nitrogen uptake and the importance of internal nitrogen loading in Lake Balaton. *Freshwater Biology*, 46, 125-139
- Présing, M., Herodek, S., Vörös, L., & Kobor, I. (1996). Nitrogen fixation, ammonium and nitrate uptake during a bloom of *Cylindrospermopsis raciborskii* in Lake Balaton. *Archiv Fur Hydrobiologie*, 136, 553-562
- Prieur, L., & Sathyendranath, S. (1981). An optical classification of coastal and oceanic waters based on the specific spectral absorption curves of phytoplankton pigments, dissolved organic-matter, and other particulate materials. *Limnology and Oceanography*, 26, 671-689
- Ptacnik, R., Lepisto, L., Willen, E., Brettum, P., Andersen, T., Rekolainen, S., et al. (2008). Quantitative responses of lake phytoplankton to eutrophication in Northern Europe. *Aquatic Ecology*, 42, 227-236
- Qi, L., Hu, C., Duan, H., Zhang, Y., & Ma, R. (2015). Influence of Particle Composition on Remote Sensing Reflectance and MERIS Maximum Chlorophyll Index Algorithm: Examples From Taihu Lake and Chaohu Lake. *Ieee Geoscience and Remote Sensing Letters*, 12, 1170-1174

- Qi, L., Hu, C., Duan, H., Cannizzaro, J., & Ma, R. (2014). A novel MERIS algorithm to derive cyanobacterial phycocyanin pigment concentrations in a eutrophic lake: Theoretical basis and practical considerations. *Remote Sensing of Environment*, *154*, 298-317
- Quincey, D.J., Richardson, S.D., Luckman, A., Lucas, R.M., Reynolds, J.M., Hambrey, M.J., et al. (2007). Early recognition of glacial lake hazards in the Himalaya using remote sensing datasets. *Global and Planetary Change*, *56*, 137-152
- Rainey, M., Tyler, A., Gilvear, D., Bryant, R., & McDonald, P. (2003). Mapping intertidal estuarine sediment grain size distributions through airborne remote sensing RID C-7737-2009. *Remote Sensing of Environment*, *86*, 480-490
- Randolph, K., Wilson, J., Tedesco, L., Li, L., Pascual, D.L., & Soyeux, E. (2008). Hyperspectral remote sensing of cyanobacteria in turbid productive water using optically active pigments, chlorophyll a and phycocyanin. *Remote Sensing of Environment*, *112*, 4009-4019
- Rantajarvi, E., Olsonen, R., Hallfors, S., Leppanen, J.M., & Raateoja, M. (1998). Effect of sampling frequency on detection of natural variability in phytoplankton: unattended high-frequency measurements on board ferries in the Baltic Sea. *ICES Journal of Marine Science*, *55*, 697-704
- Reinart, A., & Kutser, T. (2006). Comparison of different satellite sensors in detecting cyanobacterial bloom events in the Baltic Sea. *Remote Sensing of Environment*, *102*, 74-85
- Reynolds, C.S. (2006). *The Ecology of Freshwater Phytoplankton*. Cambridge: Cambridge University Press
- Reynolds, C.S., Huszar, V., Kruk, C., Naselli-Flores, L., & Melo, S. (2002). Towards a functional classification of the freshwater phytoplankton. *Journal of Plankton Research*, *24*, 417-428
- Richardson, L. (1996). Remote sensing of algal bloom dynamics. *Bioscience*, *46*, 492-501

- Riddick, C.A.L., Hunter, P.D., Tyler, A.N., Martinez-Vicente, V., Horváth, H., Kovács, A.W., et al. (2015). Spatial variability of absorption coefficients over a biogeochemical gradient in a large and optically complex shallow lake. *Journal of Geophysical Research: Oceans*, 120, 7040-7066
- Riddick, C.A.L., Hunter, P.D., Domínguez Gómez, J.A., Martinez-Vicente, V., Présing, M., Horváth, H., et al. (in review). Evaluation of algorithms for retrieval of cyanobacterial pigments in highly turbid, optically complex waters using MERIS data.
- Röttgers, R., McKee, D., & Woźniak, S.B. (2013). Evaluation of scatter corrections for ac-9 absorption measurements in coastal waters. *Methods in Oceanography*, 7, 21-39
- Rowan, K.S. (1989). *Photosynthetic pigments of algae*. (pp. 334). Cambridge, UK: Cambridge University Press
- Ruddick, K., De Cauwer, V., Park, Y., & Moore, G. (2006). Seaborne measurements of near infrared water-leaving reflectance: The similarity spectrum for turbid waters. *Limnology and Oceanography*, 51, 1167-1179
- Ruiz-Verdu, A., Simis, S.G.H., de Hoyos, C., Gons, H.J., & Pena-Martinez, R. (2008). An evaluation of algorithms for the remote sensing of cyanobacterial biomass. *Remote Sensing of Environment*, 112, 3996-4008
- Rundquist, D., Han, L., Schalles, J., & Peake, J. (1996). Remote measurement of algal chlorophyll in surface waters: The case for the first derivative of reflectance near 690 nm. *Photogrammetric Engineering and Remote Sensing*, 62, 195-200
- Saker, M., & Griffiths, D. (2001). Occurrence of blooms of the cyanobacterium *Cylindrospermopsis raciborskii* (Woloszynska) Seenayya and Subba Raju in a north Queensland domestic water supply. *Marine and Freshwater Research*, 52, 907-915
- Santer, R., & Schmechtig, C. (2000). Adjacency effects on water surfaces: primary scattering approximation and sensitivity study. *Applied Optics*, 39, 361-375

- Sarada, R., Pillai, M., & Ravishankar, G. (1999). Phycocyanin from *Spirulina* sp: influence of processing of biomass on phycocyanin yield, analysis of efficacy of extraction methods and stability studies on phycocyanin. *Process Biochemistry*, *34*, 795-801
- Sathyendranath, S., Lazzara, L., & Prieur, L. (1987). Variations in the Spectral Values of Specific Absorption of Phytoplankton. *Limnology and Oceanography*, *32*, 403-415
- Sathyendranath, S., Watts, L., Devred, E., Platt, T., Caverhill, C., & Maass, H. (2004). Discrimination of diatoms from other phytoplankton using ocean-colour data. *Marine Ecology Progress Series*, *272*, 59-68
- Sathyendranath, S., Stuart, V., Irwin, B.D., Maass, H., Savidge, G., Gilpin, L., et al. (1999). Seasonal variations in bio-optical properties of phytoplankton in the Arabian Sea. *Deep-Sea Research Part II-Topical Studies in Oceanography*, *46*, 633-653
- Schalles, J., Gitelson, A., Yacobi, Y., & Kroenke, A. (1998). Estimation of chlorophyll a from time series measurements of high spectral resolution reflectance in an eutrophic lake. *Journal of Phycology*, *34*, 383-390
- Schalles, J.F., & Yacobi, Y.Z. (2000). Remote detection and seasonal patterns of phycocyanin, carotenoid and chlorophyll pigments in eutrophic waters. *Ergebnisse der Limnologie*, 153-168
- Scheffer, M. (2001). *Ecology of Shallow Lakes*. Dordrecht: Kluwer Academic Press
- Schiebe, F., Harrington, J., & Ritchie, J. (1992). Remote-Sensing of Suspended Sediments - the Lake Chicot, Arkansas Project. *International Journal of Remote Sensing*, *13*, 1487-1509
- Schiller, H., & Doerffer, R. (1999). Neural network for emulation of an inverse model - operational derivation of Case II water properties from MERIS data. *International Journal of Remote Sensing*, *20*, 1735-1746

- Schindler, D.W. (2009). Lakes as sentinels and integrators for the effects of climate change on watersheds, airsheds, and landscapes. *Limnology and Oceanography*, 54, 2349-2358
- Schindler, D.W. (1977). Evolution of Phosphorus Limitation in Lakes. *Science*, 195, 260-262
- Schmid, H., Bauer, F., & Stich, H. (1998). Determination of algal biomass with HPLC pigment analysis from lakes of different trophic state in comparison to microscopically measured biomass. *Journal of Plankton Research*, 20, 1651-1661
- Schroeder, T., Schaale, M., & Fischer, J. (2007). Retrieval of atmospheric and oceanic properties from MERIS measurements: A new Case-2 water processor for BEAM. *International Journal of Remote Sensing*, 28, 5627-5632
- Scottish Executive. (2002). Blue-Green Algae (Cyanobacteria) in Inland Waters.
- Shi, K., Li, Y., Li, L., & Lu, H. (2013). Absorption characteristics of optically complex inland waters: Implications for water optical classification. *Journal of Geophysical Research-Biogeosciences*, 118, 860-874
- Shi, K., Li, Y., Zhang, Y., Li, L., Lv, H., & Song, K. (2014). Optical scattering properties of organic-rich and inorganic-rich particles in inland waters. *Journal of Great Lakes Research*, 40, 308-316
- Shiklomanov, I. (1993). World Fresh Water Resources. In P.H. Gleick (Ed.), *Water in Crisis: A Guide to the World's Fresh Water Resources* (pp. 13-24). New York: Oxford University Press
- Siegel, D., Wang, M., Maritorena, S., & Robinson, W. (2000). Atmospheric correction of satellite ocean color imagery: the black pixel assumption. *Applied Optics*, 39, 3582-3591
- Siegelman, H., & Kycia, J.H. (1978). Algal biliproteins. In J.A. Hellebust, & J.S. Craigie (Eds.), *Handbook of Phycological Methods* (pp. 71-79). New York: Cambridge University Press

- Simis, S., Peters, S., & Gons, H. (2005). Remote sensing of the cyanobacterial pigment phycocyanin in turbid inland water. *Limnology and Oceanography*, *50*, 237-245
- Simis, S., & Kauko, H.M. (2012). In vivo mass-specific absorption spectra of phycobilipigments through selective bleaching. *Limnology and Oceanography-Methods*, *10*, 214-226
- Simis, S., Ruiz-Verdú, A., Domínguez-Gómez, J.A., Peña-Martinez, R., Peters, S.W.M., & Gons, H.J. (2007). Influence of phytoplankton pigment composition on remote sensing of cyanobacterial biomass. *Remote Sensing of Environment*, *106*, 414-427
- Sinha, R.P., Singh, S.P., & Häder, D. (2007). Database on mycosporines and mycosporine-like amino acids (MAAs) in fungi, cyanobacteria, macroalgae, phytoplankton and animals. *Journal of Photochemistry and Photobiology B: Biology*, *89*, 29-35
- Slade, W.H., Boss, E., Dall'Olmo, G., Langner, M.R., Loftin, J., Behrenfeld, M.J., et al. (2010). Underway and moored methods for improving accuracy in measurement of spectral particulate absorption and attenuation. *Journal of Atmospheric and Oceanic Technology*, *27*, 1733-1746
- Slade, W.H., & Boss, E. (2015). Spectral attenuation and backscattering as indicators of average particle size. *Applied Optics*, *54*, 7264-7277
- Smayda, T.J. (1997). Harmful algal blooms: Their ecophysiology and general relevance to phytoplankton blooms in the sea. *Limnology and Oceanography*, *42*, 1137-1153
- Smith, V.H. (2003). Eutrophication of freshwater and coastal marine ecosystems - A global problem. *Environmental Science and Pollution Research*, *10*, 126-139
- Smith, V.H. (1983). Low Nitrogen to Phosphorus Ratios Favor Dominance by Blue-Green-Algae in Lake Phytoplankton. *Science*, *221*, 669-671

- Snyder, W.A., Arnone, R.A., Davis, C.O., Goode, W., Gould, R.W., Ladner, S., et al. (2008). Optical scattering and backscattering by organic and inorganic particulates in US coastal waters. *Applied Optics*, 47, 666-677
- Somlyódy, L., Herodek, S., Aradi, C., Clement, A., Dévai, G., Istvánovics, V., et al. (1997). Revision of the Lower Kis-Balaton Reservoir, Synthesis Report.
- Song, K.S., Li, L., Tedesco, L., Duan, H.T., Li, L.H., & Du, J. (2014). Remote Quantification of Total Suspended Matter through Empirical Approaches for Inland Waters. *Journal of Environmental Informatics*, 23, 23-36
- Song, K., Li, L., Tedesco, L., Clercin, N., Hall, B., Li, S., et al. (2013). Remote estimation of phycocyanin (PC) for inland waters coupled with YSI PC fluorescence probe. *Environmental Science and Pollution Research*, 20, 5330-5340
- Spyrakos, E., Gonzalez Vilas, L., Torres Palenzuela, J.M., & Desmond Barton, E. (2011). Remote sensing chlorophyll a of optically complex waters (rias Baixas, NW Spain): Application of a regionally specific chlorophyll a algorithm for MERIS full resolution data during an upwelling cycle. *Remote Sensing of Environment*, 115, 2471-2485
- Sriwongsitanon, N., Surakit, K., & Thianpopirug, S. (2011). Influence of atmospheric correction and number of sampling points on the accuracy of water clarity assessment using remote sensing application. *Journal of Hydrology*, 401, 203-220
- Sterckx, S., Knaeps, S., Kratzer, S., & Ruddick, K. (2015). SIMilarity Environment Correction (SIMEC) applied to MERIS data over inland and coastal waters. *Remote Sensing of Environment*, 157, 96-110
- Stramski, D., Bricaud, A., & Morel, A. (2001). Modeling the inherent optical properties of the ocean based on the detailed composition of the planktonic community. *Applied Optics*, 40, 2929-2945
- Stramski, D., Reynolds, R.A., Babin, M., Kaczmarek, S., Lewis, M.R., Roettgers, R., et al. (2008). Relationships between the surface concentration of particulate organic

- carbon and optical properties in the eastern South Pacific and eastern Atlantic Oceans. *Biogeosciences*, 5, 171-201
- Stramski, D., Babin, M., & Wozniak, S.B. (2007). Variations in the optical properties of terrigenous mineral-rich particulate matter suspended in seawater. *Limnology and Oceanography*, 52, 2418-2433
- Stratoulas, D., Balzter, H., Zlinszky, A., & Toth, V.R. (2015a). Assessment of ecophysiology of lake shore reed vegetation based on chlorophyll fluorescence, field spectroscopy and hyperspectral airborne imagery. *Remote Sensing of Environment*, 157, 72-84
- Stratoulas, D., Balzter, H., Sykioti, O., Zlinszky, A., & Toth, V.R. (2015b). Evaluating Sentinel-2 for Lakeshore Habitat Mapping Based on Airborne Hyperspectral Data. *Sensors*, 15, 22956-22969
- Subramaniam, A., Brown, C., Hood, R., Carpenter, E., & Capone, D. (2002). Detecting Trichodesmium blooms in SeaWiFS imagery. *Deep-Sea Research Part II-Topical Studies in Oceanography*, 49, 107-121
- Sullivan, J.M., Twardowski, M.S., Zaneveld, J.R.V., & Moore, C.C. (2013). Measuring optical backscattering in water. In A.A. Kokhanovsky (Ed.), *Light Scattering Reviews 7: Radiative Transfer and Optical Properties of Atmosphere and Underlying Surface* (pp. 189-224). Berlin: Springer-Verlag
- Sullivan, J., Twardowski, M., Donaghay, P., & Freeman, S. (2005). Use of optical scattering to discriminate particle types in coastal waters. *Applied Optics*, 44, 1667-1680
- Sun, D., Hu, C., Qiu, Z., & Shi, K. (2015). Estimating phycocyanin pigment concentration in productive inland waters using Landsat measurements: A case study in Lake Dianchi. *Optics Express*, 23, 3055-3074
- Sun, D., Li, Y., Wang, Q., Gao, J., Le, C., Huang, C., et al. (2013). Hyperspectral Remote Sensing of the Pigment C-Phycocyanin in Turbid Inland Waters, Based on

- Optical Classification. *IEEE Transactions on Geoscience and Remote Sensing*, 51, 3871-3884
- Sun, D., Li, Y., Wang, Q., Lv, H., Le, C., Huang, C., et al. (2010). Partitioning particulate scattering and absorption into contributions of phytoplankton and non-algal particles in winter in Lake Taihu (China). *Hydrobiologia*, 644, 337-349
- Sun, D., Li, Y., Wang, Q., Gao, J., Lv, H., Le, C., et al. (2009). Light scattering properties and their relation to the biogeochemical composition of turbid productive waters: a case study of Lake Taihu. *Applied Optics*, 48, 1979-1989
- Svab, E., Tyler, A., Preston, T., Presing, M., & Balogh, K. (2005). Characterizing the spectral reflectance of algae in lake waters with high suspended sediment concentrations. *International Journal of Remote Sensing*, 26, 919-928
- Szilagyi, F., Somlyody, L., & Koncsos, L. (1990). Operation of the Kis-Balaton Reservoir - Evaluation of Nutrient Removal Rates. *Hydrobiologia*, 191, 297-306
- Tassan, S., & Ferrari, G. (1998). Measurement of light absorption by aquatic particles retained on filters: determination of the optical pathlength amplification by the 'transmittance-reflectance' method. *Journal of Plankton Research*, 20, 1699-1709
- Tebbs, E.J., Remedios, J.J., & Harper, D.M. (2013). Remote sensing of chlorophyll-a as a measure of cyanobacterial biomass in Lake Bogoria, a hypertrophic, saline-alkaline, flamingo lake, using Landsat ETM. *Remote Sensing of Environment*, 135, 92-106
- Tilstone, G.H., & Martinez-Vicente, V. (2012). ISECA Protocols for the Validation of Ocean Colour Satellite Data in Case 2 European Waters. *INTERREG IVA 2 Mers Seas Zeeen Cross-border Cooperation Programme 2007 – 2013, 07-027-FR-ISECA*, 1-45
- Tilstone, G.H., Smyth, T., Gowen, R., Martinez-Vicente, V., & Groom, S. (2005). Inherent optical properties of the Irish Sea and their effect on satellite primary production algorithms. *Journal of Plankton Research*, 27, 1127-1148

- Tilstone, G.H., Moore, G.F., Sorensen, K., Doerffer, R., Rottgers, R., Ruddick, K.G., et al. (2002). Regional validation of MERIS chlorophyll products in North Sea coastal waters. , *EVG1 - CT - 2001 - 00049*, 1-77
- Tilstone, G.H., Peters, S.W.M., van der Woerd, H.J., Eleveld, M.A., Ruddick, K., Schoenfeld, W., et al. (2012). Variability in specific-absorption properties and their use in a semi-analytical ocean colour algorithm for MERIS in North Sea and Western English Channel Coastal Waters. *Remote Sensing of Environment*, *118*, 320-338
- Torbick, N., & Corbiere, M. (2015). A Multiscale Mapping Assessment of Lake Champlain Cyanobacterial Harmful Algal Blooms. *International Journal of Environmental Research and Public Health*, *12*, 11560-11578
- Torbick, N., Hession, S., Hagen, S., Wiangwang, N., Becker, B., & Qi, J. (2013). Mapping inland lake water quality across the Lower Peninsula of Michigan using Landsat TM imagery. *International Journal of Remote Sensing*, *34*, 7607-7624
- Tranvik, L.J., Downing, J.A., Cotner, J.B., Loiselle, S.A., Striegl, R.G., Ballatore, T.J., et al. (2009). Lakes and reservoirs as regulators of carbon cycling and climate. *Limnology and Oceanography*, *54*, 2298-2314
- Twardowski, M., Zhang, X., Vagle, S., Sullivan, J., Freeman, S., Czerski, H., et al. (2012). The optical volume scattering function in a surf zone inverted to derive sediment and bubble particle subpopulations. *Journal of Geophysical Research-Oceans*, *117*, C00H17
- Twardowski, M., Boss, E., Sullivan, J., & Donaghay, P. (2004). Modeling the spectral shape of absorption by chromophoric dissolved organic matter. *Marine Chemistry*, *89*, 69-88
- Twardowski, M., Boss, E., Macdonald, J., Pegau, W., Barnard, A., & Zaneveld, J. (2001). A model for estimating bulk refractive index from the optical backscattering ratio and the implications for understanding particle composition in case I and case II waters. *Journal of Geophysical Research-Oceans*, *106*, 14129-14142

- Tyler, A.N., Hunter, P.D., Spyrakos, E., Groom, S., Constantinescu, A.M., & Kitchen, J. (2016). Developments in Earth observation for the assessment and monitoring of inland, transitional, coastal and shelf-sea waters.
- Tyler, A., Svab, E., Preston, T., Présing, M., & Kovács, A.W. (2006). Remote sensing of the water quality of shallow lakes: A mixture modelling approach to quantifying phytoplankton in water characterized by high-suspended sediment. *International Journal of Remote Sensing*, 27, 1521-1537
- Tzortziou, M., Herman, J.R., Cede, A., Loughner, C.P., Abuhassan, N., & Naik, S. (2015). Spatial and temporal variability of ozone and nitrogen dioxide over a major urban estuarine ecosystem. *Journal of Atmospheric Chemistry*, 72, 287-309
- Ulloa, O., Sathyendranath, S., & Platt, T. (1994). Effect of the Particle-Size Distribution on the Backscattering Ratio in Seawater. *Applied Optics*, 33, 7070-7077
- Utermöhl, H. (1958). Zur Vervollkommnung der quantitativen Phytoplankton-Methodik. , 9, 1-38
- Vaillancourt, R., Brown, C., Guillard, R., & Balch, W. (2004). Light backscattering properties of marine phytoplankton: relationships to cell size, chemical composition and taxonomy. *Journal of Plankton Research*, 26, 191-212
- Verpoorter, C., Kutser, T., Seekell, D.A., & Tranvik, L.J. (2014). A global inventory of lakes based on high-resolution satellite imagery. *Geophysical Research Letters*, - 2014GL060641
- Verspecht, F., & Pattiaratchi, C. (2010). On the significance of wind event frequency for particulate resuspension and light attenuation in coastal waters. *Continental Shelf Research*, 30, 1971-1982
- Vincent, R., Qin, X., McKay, R., Miner, J., Czajkowski, K., Savino, J., et al. (2004). Phycocyanin detection from LANDSAT TM data for mapping cyanobacterial blooms in Lake Erie. *Remote Sensing of Environment*, 89, 381-392

- Vos, R., Hakvoort, J., Jordans, R., & Ibelings, B. (2003). Multiplatform optical monitoring of eutrophication in temporally and spatially variable lakes. *Science of the Total Environment*, 312, 221-243
- Wagner, C., & Adrian, R. (2009). Cyanobacteria dominance: Quantifying the effects of climate change. *Limnology and Oceanography*, 54, 2460-2468
- Wang, Y., Liu, D., Song, K., Du, J., Wang, Z., Zhang, B., et al. (2011). Characterization of water constituents spectra absorption in Chagan Lake of Jilin Province, Northeast China. *Chinese Geographical Science*, 21, 334-345
- Wang, M., & Shi, W. (2007). The NIR-SWIR combined atmospheric correction approach for MODIS ocean color data processing. *Optics Express*, 15, 15722-15733
- WET Labs. (2010). ECO BB User's Guide. , 26 pp
- Wheeler, S.M., Morrissey, L.A., Levine, S.N., Livingston, G.P., & Vincent, W.F. (2012). Mapping cyanobacterial blooms in Lake Champlain's Missisquoi Bay using QuickBird and MERIS satellite data. *Journal of Great Lakes Research*, 38, 68-75
- Whitmire, A.L., Boss, E., Cowles, T.J., & Pegau, W.S. (2007). Spectral variability of the particulate backscattering ratio. *Optics Express*, 15, 7019-7031
- WHO. (2004). Guidelines for Drinking-water Quality.
- WHO. (2003). Guidelines for safe recreational water environments.
- Williams, R., Gingrich, J., & Glazer, A. (1980). Cyanobacterial Phycobilisomes - Particles from *Synechocystis*-6701 and 2 Pigment Mutants. *Journal of Cell Biology*, 85, 558-566
- Wrigley, R.C., & Horne, A.J. (1974). Remote-Sensing and Lake Eutrophication. *Nature*, 250, 213-214

- Wu, G., Cui, L., Duan, H., Fei, T., & Liu, Y. (2013). Specific absorption and backscattering coefficients of the main water constituents in Poyang Lake, China. *Environmental monitoring and assessment*, 185, 4191-4206
- Wu, G., Cui, L., Liu, L., Chen, F., Fei, T., & Liu, Y. (2015). Statistical model development and estimation of suspended particulate matter concentrations with Landsat 8 OLI images of Dongting Lake, China. *International Journal of Remote Sensing*, 36, 343-360
- Wu, M., Zhang, W., Wang, X., & Luo, D. (2009). Application of MODIS satellite data in monitoring water quality parameters of Chaohu Lake in China. *Environmental monitoring and assessment*, 148, 255-264
- Wynne, T.T., Stumpf, R.P., Tomlinson, M.C., Warner, R.A., Tester, P.A., Dyble, J., et al. (2008). Relating spectral shape to cyanobacterial blooms in the Laurentian Great Lakes. *International Journal of Remote Sensing*, 29, 3665-3672
- Xi, H. (2015). Beam attenuation, scattering and backscattering of marine particles in relation to particle size distribution and composition in Hudson Bay (Canada). *Journal of Geophysical Research - Oceans*, 120, 3286-3300
- Yacobi, Y.Z., Köhler, J., Leunert, F., & Gitelson, A. (2015). Phycocyanin-specific absorption coefficient: Eliminating the effect of chlorophylls absorption. *Limnology and Oceanography: Methods*, 13, 157-168
- Yacobi, Y., Gitelson, A., & Mayo, M. (1995). Remote-Sensing of Chlorophyll in Lake Kinneret using High-Spectral-Resolution Radiometer and Landsat-Tm - Spectral Features of Reflectance and Algorithm Development. *Journal of Plankton Research*, 17, 2155-2173
- Yang, W., Matsushita, B., Chen, J., & Fukushima, T. (2011a). A Relaxed Matrix Inversion Method for Retrieving Water Constituent Concentrations in Case II Waters: The Case of Lake Kasumigaura, Japan. *IEEE Transactions on Geoscience and Remote Sensing*, 49, 3381-3392

- Yang, W., Matsushita, B., Chen, J., & Fukushima, T. (2011b). Estimating constituent concentrations in case II waters from MERIS satellite data by semi-analytical model optimizing and look-up tables. *Remote Sensing of Environment*, *115*, 1247-1259
- Yeo, I., Lang, M., & Vermote, E. (2014). Improved Understanding of Suspended Sediment Transport Process Using Multi-Temporal Landsat Data: A Case Study From the Old Woman Creek Estuary (Ohio). *Ieee Journal of Selected Topics in Applied Earth Observations and Remote Sensing*, *7*, 636-647
- Ylöstalo, P., Kallio, K., & Seppälä, J. (2014). Absorption properties of in-water constituents and their variation among various lake types in the boreal region. *Remote Sensing of Environment*, *148*, 190-205
- Yoshimura, K., Zaitso, N., Sekimura, Y., Matsushita, B., Fukushima, T., & Imai, A. (2012). Parameterization of chlorophyll a-specific absorption coefficients and effects of their variations in a highly eutrophic lake: a case study at Lake Kasumigaura, Japan. *Hydrobiologia*, *691*, 157-169
- Zaneveld, J. (1995). A Theoretical Derivation of the Dependence of the Remotely-Sensed Reflectance of the Ocean on the Inherent Optical-Properties. *Journal of Geophysical Research-Oceans*, *100*, 13135-13142
- Zaneveld, R., Kitchen, J., & Moore, C. (1994). *The Scattering Error Correction of Reflecting-Tube Absorption Meters*. (pp. 55). Bellingham, WA: SPIE - Int. Soc. Optical Engineering
- Zhang, Y., Qin, B., Zhu, G., Gao, G., Luo, L., & Chen, W. (2006). Effect of sediment resuspension on underwater light field in shallow lakes in the middle and lower reaches of the Yangtze River: A case study in Longgan Lake and Taihu Lake. *Science in China Series D-Earth Sciences*, *49*, 114-125
- Zhang, X., Hu, L., & He, M. (2009). Scattering by pure seawater: Effect of salinity. *Optics Express*, *17*, 5698-5710

- Zhang, Y., Yin, Y., Wang, M., & Liu, X. (2012). Effect of phytoplankton community composition and cell size on absorption properties in eutrophic shallow lakes: field and experimental evidence. *Optics Express*, 20, 11882-11898
- Zhang, Y., Qin, B., Zhu, G., Zhang, L., & Yang, L. (2007). Chromophoric dissolved organic matter (CDOM) absorption characteristics in relation to fluorescence in Lake Taihu, China, a large shallow subtropical lake. *Hydrobiologia*, 581, 43-52
- Zhang, Y., Feng, L., Li, J., Luo, L., Yin, Y., Liu, M., et al. (2010). Seasonal-spatial variation and remote sensing of phytoplankton absorption in Lake Taihu, a large eutrophic and shallow lake in China. *Journal of Plankton Research*, 32, 1023-1037
- Zhang, Y., Yin, Y., Liu, X., Shi, Z., Feng, L., Liu, M., et al. (2011). Spatial-seasonal dynamics of chromophoric dissolved organic matter in Lake Taihu, a large eutrophic, shallow lake in China. *Organic Geochemistry*, 42, 510-519
- Zibordi, G., Holben, B., Slutsker, I., Giles, D., D'Alimonte, D., Melin, F., et al. (2009). AERONET-OC: A Network for the Validation of Ocean Color Primary Products. *Journal of Atmospheric and Oceanic Technology*, 26, 1634-1651
- Zimba, P., & Gitelson, A. (2006). Remote estimation of chlorophyll concentration in hyper-eutrophic aquatic systems: Model tuning and accuracy optimization. *Aquaculture*, 256, 272-286
- Zlinszky, A., Muecke, W., Lehner, H., Briese, C., & Pfeifer, N. (2012). Categorizing Wetland Vegetation by Airborne Laser Scanning on Lake Balaton and Kis-Balaton, Hungary. *Remote Sensing*, 4, 1617-1650